January, 1959
Vol. 47 No. 1

Proceedings of the IRE

Poles and Zeros

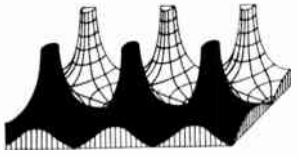

Is There an Engine in Engineer? Conversations resulting from our September piece on engineering education lead to a conviction that there are many images produced by the word "engineer," and that we are in some difficulty until our semantic troubles are overcome.

To the lay public an engineer frequently is still a man who directs a locomotive, operates a power shovel, or installs a TV antenna. By title at least, an engineer may also be the man who repairs the shower head in your hotel room. While we are somewhat unsure of our past practices, it seems reasonable to guess that no engineer, in a professional sense, ever operated a locomotive except on a test basis. It also seems reasonable, however, that such operation of an engine did lead to the operator's designation as an engineer. Therefore, the locomotive and power shovel engineer has a real and logical claim to the name, and we as professional engineers may be the usurpers. In any case, we are not going to reverse that usage of the name.

We also have many hundreds of thousands of men who are college trained and practiced in the design of structures or machines, the layout of highway systems or production lines, or in new applications of power. Many such men are employed in day-to-day operation in manufacturing industries or in the sale of technical apparatus. There seems almost universal agreement that these men are engineers in the professional sense.

But now our major industries and our research laboratories have realized that we are entering a new scientific world—into which the door was opened perhaps by electronics. In this new world, education which trains only to make big things bigger may not be sufficient; education which teaches us only to utilize the materials and forces as nature gave them may not be enough for solution of tomorrow's problems. It begins to appear that men are needed who know how to improve on nature's materials—pure metals or semiconductors—who know how to improve on nature's forces on this earth—hydrogen fusion—and who know how to design not just a single machine or a single process but who can put many machines, many processes, and man, into a *system*.

Education which provides a basic knowledge of the science of nature, plus mathematics, plus analysis, plus synthesis, is needed to build this new world (and would have helped in the old one, in our opinion). A person so educated may be lacking in knowledge of today's (more likely yesterday's) techniques and hardware, and we hear it said that these men will not be useful to our highway departments, our consultants, or our electric utilities as examples, although no proof has yet been offered. On the other side, we already have proof in the booming increase in electrical engineering enrollments that such scientifically-oriented programs appeal to our good students.

If this new engineering-science education does not produce the traditional engineer, let us debate only the applicability of the title and not the need for men so fundamentally science-educated. The field of engineering is already so broad that technical communication between the extremes is impossible, and perhaps the semantic debate further supports a thesis that a new name should be selected for the devotees of this new variety of applied science. Could we then avoid semantic conflict, and get on with the job of devising appropriate colleges and college curriculums?

But would such devising then be a duty of colleges of engineering? Or does the engineer continue to run his engines or to design his highways, while electronics, magnetohydrodynamics, thermodynamics, and the other areas of applied classical physics take to space with their engineer-scientists?

Atlanta Is Captured, IRE Style. The Board of Directors, further developing its technique in how-to-get-away-from-New York, invaded Atlanta in November and was met with warm and enervating Southern weather and bombarded with Region Three-brand Southern hospitality. Following a practice instituted a year ago, the newly-elected Regional Directors, to take office in January, were in attendance for aid in getting a running start on their 1959–1960 jobs, and heard the Board tackle a number of problems.

One was the discussion centering on a revised Constitution in preparation for submission to a vote of the membership. The revision, necessitated by certain changes in the New York State membership corporations law, was complicated by the attempt to describe our present organization in the language of the law and still retain intelligibility. In fact, we are led to conclude that legal language was devised solely for transmission through a very narrow frequency channel!

Consideration is also being given to revision of certain of the criteria for the Senior Member grade, in the hope that the grade will be raised in stature and will be more clearly representative of high professional standing. Time was also given to discussion of the place of the NATIONAL CONVENTION RECORD in our publication program.

A day was devoted to analysis of the Professional Group system, one aspect being its growth pattern. Now numbering 28 Groups, the most recent additions are Education, Radio Frequency Interference, Engineering Writing and Speech, and Human Factors in Electronics. These Groups seem to cut horizontally across the 24 preceding areas which were largely concerned with fields of technical interest. While not desiring to greatly increase the number of Groups, the Board felt that expansion should continue to be possible as new areas of electrical technology arise.

Greetings, Tokyo! Our Tokyo Section has taken the initiative and formed the first Professional Group Chapter outside the U. S. and Canadian Sections. This Chapter in Microwave Theory and Techniques clearly indicates the interest of the Tokyo Section in this important technical field.—J.D.R.

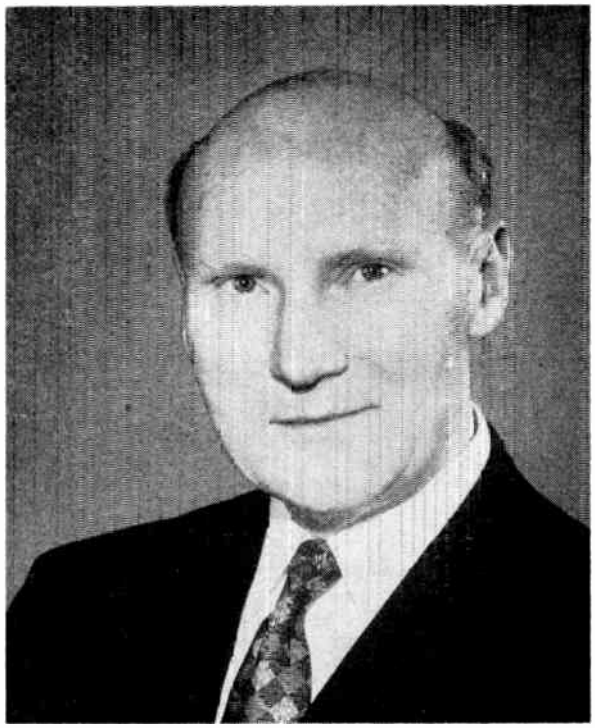

Ernst Weber

President, 1959

Dr. Ernst Weber (M'41–SM'43–F'51) was born in Vienna, Austria, on September 6, 1901. He received the Ph.D. degree in 1926 from the University of Vienna, having studied philosophy, physics, and mathematics, and the D.Sc. degree in 1927 from the Technical University of Vienna, having studied engineering, particularly field theory as applied to machinery.

After working as research engineer for the Austrian Siemens-Schuckert Company, in 1929 he was transferred to the Company's Berlin office, and was also appointed lecturer at the Technical University of Berlin. In the fall of 1930 he accepted an invitation as visiting professor at the Polytechnic Institute of Brooklyn, where a year later he was named a permanent research professor of electrical engineering in charge of graduate study. From 1942 to 1945 he was professor of graduate electrical engineering and head of graduate study and research in that field. Under his direction, enrollment in electrical engineering grew from 405 students to 2204.

Early in World War II he organized a microwave research group which developed, among other things, the precision microwave attenuator, sorely needed for the accurate calibration of radar. In recognition of the contributions of the research group, he was awarded the Presidential Certificate of Merit. Out of this wartime research grew the Microwave Research Institute, which expends each year more than $1,000,000 on research projects for the military services, and the Polytechnic Research and Development Company, owned by the Polytechnic Institute of Brooklyn.

In 1945 he was appointed head of the department of electrical engineering, and director of the Microwave Research Institute. When a vice-presidency for research was created at the Polytechnic Institute of Brooklyn in 1957, he was named to that position; following the death of the Institute's president in June, 1957, he became acting president, and then president. He is also president of the Polytechnic Research and Development Company.

A pioneer in high-frequency electronic research, he holds more than 50 American, Canadian, and British patents in the field of microwave techniques. His published works include many scientific papers on electromagnetic fields, linear and nonlinear circuits, and microwave measurements. He has contributed to several books and has published "Mapping of Fields" and "Linear Transient Analysis." Wilbur M. Brucker, Secretary of the Army, recently appointed him a member of the Army Scientific Advisory Panel.

Dr. Weber is a Fellow of the American Institute of Electrical Engineers and the American Physical Society.

Scanning the Issue

Photoelectronic Circuit Applications (Ghandhi, p. 4)—One of the newest fields in electronics concerns the application of materials which are actuated by or emit light. Photoconductors and electroluminescent cells are receiving a good deal of attention today in connection with the development of light and X-ray amplifiers and panel display devices (see next item). This paper delves into another potentially important application in which these two elements are combined to form a computer circuit element. When an electroluminescent cell is coupled to a photoconductor in such a way that its light output energizes the photoconductor, the voltage-current characteristics of the resulting photoelectronic device have a shape not unlike the *B-H* square loop of a magnetic material. Like certain magnetic devices, the photoelectronic circuit element can be used to perform various switching and logic functions and shows promise of becoming an important addition to the growing family of electronic components.

A Feedback Light-Amplifier Panel for Picture Storage (Kazan, p. 12)—By adding optical feedback to a conventional light amplifier panel, an improved display device has been developed which can store and display an image indefinitely. In addition, the image can be erased much more rapidly by means of a polarity reversal scheme. This development adds substantially to the versatility of a device that is rapidly nearing a point of widespread use.

Development of High-Power Pulsed Klystrons for Practical Applications (Chodorow, *et al.*, p. 20)—Five years ago PROCEEDINGS reported on a 30-megawatt klystron which was developed for a billion-volt linear electron accelerator. The fruits of this work have now been applied to the development of a class of tubes operating at one to two megawatts for use in *S*, *L*, and *X*-band radar transmitters. This paper is noteworthy in several respects. First, it describes an important development program carried out over several years which resulted in unique contributions to the high-power microwave tube field. In so doing, it shows how the design principles reported earlier have been successfully applied to the development of extremely useful electronic devices. Last, but not least, the paper will serve to bring the general reader up to date on what it is possible to do with klystrons.

The Design of Two-Section Symmetrical Zobel Filters for Tchebycheff Insertion Loss (Tuttle, p. 29)—Today's network designer faces a frustrating choice. He has available to him powerful modern methods which would give him the best possible filter design but which involve extremely difficult and laborious calculations. On the other hand, the old cut-and-try methods, while easy to use, provide him with only a limited range of designs and give him no assurance that the final design he arrives at is the most economical or the one requiring the fewest coils. In this paper the author compares a filter designed by old image-parameter methods with the same filter designed by modern insertion-loss techniques, and evolves a design method that combines the advantages of both, *i.e.*, ease of computation plus economy of design. The computational simplicity is achieved by restricting the method to a filter having exactly two sections and by limiting the choice of filter characteristics. However, even with these restrictions the author shows that the method yields good, practical designs within the range of interest of many applications. This paper has something in it for everyone. It is both an original contribution and an excellent tutorial discussion. As such, it will appeal not only to practical designers and network theorists, but to the readership at large.

Minimum Insertion Loss Filters (Fubini and Guillemin, p. 37)—The voluminous literature on filter design theory has for the most part concerned itself with details concerning the shape of the filter output wave. The question of losses was considered secondary and, in fact, was never even considered at all until recently. In microwave systems, however, where low-noise-figure amplification often becomes a primary objective, the problem of losses is all-important. This paper re-examines Butterworth and Tchebycheff filters from the microwave designer's viewpoint of obtaining a minimum loss in the midband. The authors develop some very useful design curves and come to some highly significant and surprising conclusions as to the factors that do and don't determine the amount of loss and the types of filters that are and aren't suited to applications where loss is an important consideration. The results are applicable to narrow-band filters well below the microwave region, too.

The Reactatron—A Low-Noise Semiconductor Diode Microwave Amplifier (Brand, *et al.*, p. 42)—Great strides have been made in the past couple of years in achieving very-low-noise amplification through the development of atomic (maser) and variable reactance (parametric) devices. Of the several varieties of parametric amplifiers, one of the principal types makes use of the nonlinear capacitance of a diode to achieve amplification at UHF and microwave frequencies. Noise figures of the order of 6 db have been obtained by this method, and a noise figure of less than 4.8 db was reported in a PROCEEDINGS letter last June. This brief paper describes a microwave amplifier employing two silicon junction diodes in a balanced hybrid system which achieves 2.7 db, a spectacularly low noise figure for a nonatomic device.

A Semiconductor Current Limiter (Warner, *et al.*, p. 44)—Although constant voltage devices have been available for years, the development of current limiters has lagged far behind. The new device reported here represents an important step forward in this area. It consists, in effect, of a self-biased field effect transistor used as a nonamplifying constant current device. Its importance to the engineering fraternity can be judged from the following imposing list of applications: ac switch, current regulator, ac vs dc discriminator, sawtooth and step function generator, and digital-to-analog converter.

IRE Technical Committee Report on Methods for Testing Radiotelegraph Transmitters (p. 57)—The need for information on methods of testing radiotelegraph transmitters is sufficiently great that the IRE Standards Committee has taken the unusual step of arranging for publication of this material, even though an IRE Standard on the subject has not yet been adopted. The material in this report was developed over a period of many years, and will form the basis of an eventual Standard.

A High-Speed Logic System Using Magnetic Elements and a Connecting Wire Only (Crane, p. 63)—This paper presents a novel system for utilizing multiaperture magnetic devices to achieve digital logic. By appropriate variations in the geometry of the elements, the author achieves a means of performing all the fundamental logic operations. An important property of this system is that unidirectional information flow can be achieved without the necessity of inserting diodes in the circuits. In fact, it now becomes possible to build an entire logic system (aside from driving sources) without any diodes, transistors, tubes, resistors, inductors, or capacitors—only magnetic elements and interconnecting wires—at a substantial reduction in circuit complexity and assembly cost. This development makes an important contribution to a problem that a number of laboratories were wrestling with, and will have far reaching implications in the data processing field.

Scanning the Transactions **appears on page 108.**

Photoelectronic Circuit Applications*

SORAB K. GHANDHI†, SENIOR MEMBER, IRE

Summary—**A photoelectronic circuit consists of a combination of electroluminescent cells and photoconductors, interconnected by electrical as well as optical paths. A study is made of the properties of electroluminescent cells and photoconductors, and of the applications of these elements to the design of switching circuits. The asymmetrical bistable stage is taken up in detail, and analyzed with a view to determining its advantages and disadvantages. It is shown that this stage suffers from the inherent disadvantage that any improvement in the speed of turn-on results in a deterioration of the recovery characteristic. Furthermore, the switching requirements for turn-on and turn-off are dissimilar. A symmetrical version of this circuit is also presented; this circuit eliminates many of the disadvantages of the asymmetrical version, and also considerably speeds up the recovery characteristic without increasing the turn-on time.**

Circuits are developed for performing the logical operations of transmission, negation, conjunction and disjunction, and their principles of operation are described. In conclusion, techniques are developed for the synthesis of over-all computing operations, such as those of a half-adder, even parity checker, and a shift register.

Introduction

A PHOTO-ELECTRONIC circuit consists of a combination of electroluminescent cells (abbreviated to *EL*) and photoconductors (abbreviated to *PC*), interconnected by electrical as well as optical paths. These circuits may be considered as electric circuits where the input and output take the form of electric signals, and light is used as an intermediate actuating source; or else, as optical circuits where the input and output are optical signals, and electricity is used as an intermediate coupling device. At an early phase of the work, it was felt that these devices showed most promise in switching applications; accordingly, this paper is restricted to a study of switching circuits.

The Elements of a Photoelectronic Device

Electroluminescence and Electroluminescent Cells

The term "electroluminescence" may be applied to any phenomenon resulting in a light output from a phosphor when subjected to an electric field. The phenomenon of "intrinsic electroluminescence," concerning light emission from a phosphor embedded in an insulator and subjected to an alternating electric field, was reported [1] in 1936. Phosphors utilizing this effect have undergone considerable development, and are at present the only ones that are most commonly available.

The construction of an electroluminescent (*EL*) cell is as follows: A plate of glass (a section of a microscope slide in the present units) is used as a foundation for the cell. A transparent electrode is formed on this plate by treating its surface, when heated, with a solution of tin chloride. A layer of copper-activated zinc sulphide phosphor is deposited on this electrode. Finally an opaque layer of aquadag is painted on the phosphor, which serves as the second electrode of the *EL* cell. The phosphor is laid in suspension in a dielectric base. It may be shown [2] that this base must have a high dielectric constant in order to obtain a high field strength in the phosphor crystals. The thickness of the phosphor determines the operating voltage of the *EL* cell. In practice, a one to five mil layer of phosphor is used, resulting in a cell whose operating voltage ranges from 100 to 600 volts. The cells used by the author were designed for operation up to 300 volts.

The electrical properties of the cell may be defined in terms of its equivalent shunt capacitance and resistance. This simple equivalent circuit is complicated by the fact that both the capacitance and the resistance are functions of the voltage and frequency of the signal across the cell. Fig. 1 shows a plot of the effective capacitance of an *EL* cell (with an area of one square inch) as a function of the voltage for frequencies of 100 cycles and 1000 cycles. Fig. 2 shows the shunt resistance of the *EL* cell as a function of the voltage across it, also at frequencies of 100 to 1000 cycles. Fig. 3 shows the effective capacitance and the shunt resistance of the *EL* cell as a function of frequency for an impressed signal of 100 volts.

From these curves we note that:

1) The effective capacitance increases and the loss resistance decreases with the magnitude of the impressed voltage.

2) Both the effective capacitance and the loss resistance decrease as the frequency of the impressed signal is increased.

Photoconductivity and Photoconductor Cells

The term photoconductivity [3] may be applied to any process where the conductivity of a material is increased by exposure to radiation. While this phenomenon is exhibited by all insulators and semiconductors and has been the subject of investigation over the past fifty years, it is only in the last twenty years that this phenomenon has been linked with modern solid-state physics.

The experiments outlined in this paper are confined to the use of cadmium sulfide and cadmium selenide photoconductor materials. The photoconductor (*PC*) cells using CdS were of the single crystal type, with a sensitive area of about 0.02 square inches. These units were constructed by fixing the crystal to a mount, which serves as one terminal, and attaching the second lead to the surface of the crystal by silver paint.

* Original manuscript received by the IRE, June 27, 1958; revised manuscript received, November 3, 1958.

† Electronics Lab., General Electric Co., Syracuse, N. Y.

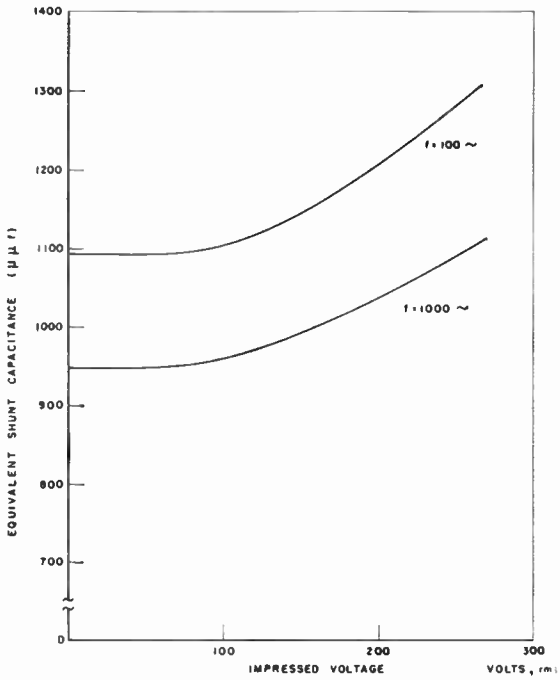

Fig. 1—Capacitance of an *EL* cell vs voltage.

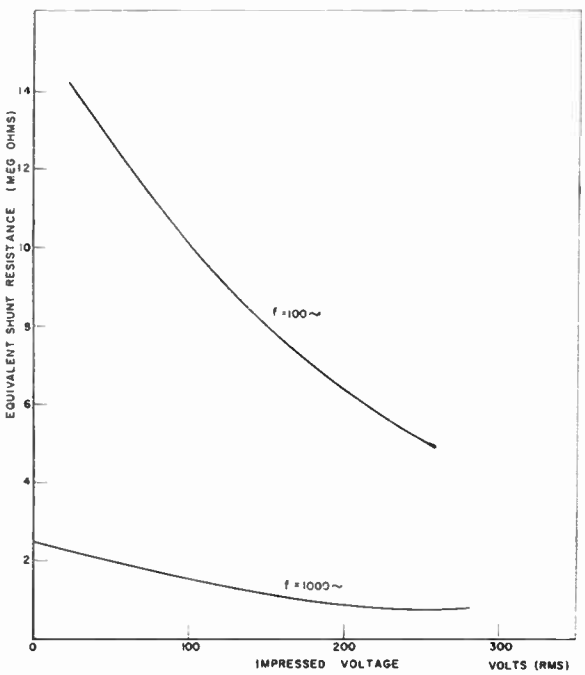

Fig. 2—Shunt resistance of an *EL* cell vs voltage.

The dark resistance of the cells is in excess of 100 megohms; when illuminated by a lit *EL* cell (from 0.5 to 2.0 foot lamberts) this resistance falls to about 60–200 kilohms. All of the tests were carried out at frequencies at which the *PC* impedance showed negligible reactive component. Accordingly, tests were restricted to below 5000 cycles. (It is to be noted here that the response of the CdS cells to *changes* in light intensity was slower than a few cycles per second. Thus, even though 5000 cycles were applied to the circuit, the response of the *PC* is to the change in light intensity when

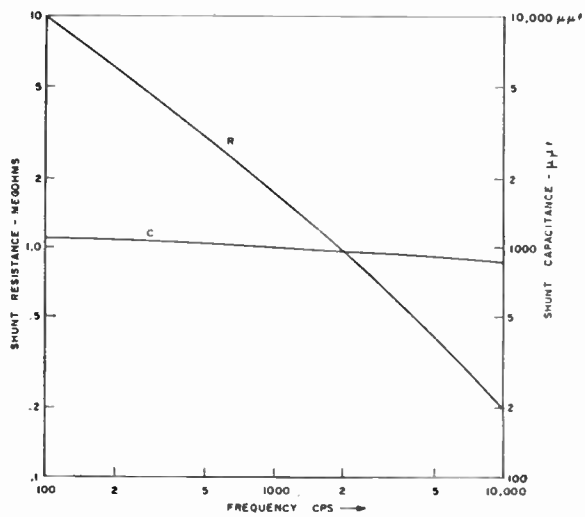

Fig. 3—Performance of an *EL* cell vs frequency.

$$G = 0 \quad V^b \quad \text{FOR} \quad V > V_0$$
$$G = G_0 \simeq 0 \quad \text{FOR} \quad V \leq V_0$$

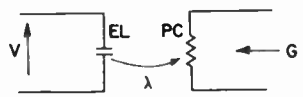

Fig. 4—Basic photoelectronic device.

the supply voltage across the *EL* cell is varied at a few cycles per second.)

The cadmium selenide cells were small area units (about 0.02 square inch) with a layer of CdSe between silver electrodes. The dark resistance of these units is comparable to that for the CdS cells, but the illuminated resistance is about one decade higher. While this corresponded to a reduced dark-to-illuminated resistance ratio, this ratio was still sufficient to operate many of the circuits to be discussed.

The Photoelectronic Device

Fig. 4 shows a two-port, four-terminal network, consisting of an *EL* and a *PC*, coupled by an optical path. Since the *EL* cell is predominantly capacitive it is conveniently indicated by the capacitor symbol. In like manner, the *PC* is indicated by the resistor symbol. The arrow with the λ serves to indicate the optical path.

In this two-port device, the input takes the form of an electrical signal across the *EL* cell. The response takes the form of a fall of resistance of the *PC* unit. While it is possible to study the light output [4] of the *EL* cell as a function of the impressed voltage, and also the conductance [5] of the *PC* as a function of the brightness [6] of the light impressed on it, it is desirable from the circuit standpoint to study the over-all dependence of the conductance of the *PC* on the voltage across the *EL*. For any fixed frequency this may be given empirically by

$$G = aV^b \quad \text{for} \quad V > V_0$$
$$G = G_0 \simeq 0 \quad \text{for} \quad V \leq V_0$$

where G is the conductance of the PC unit, V is the voltage across the EL cell, and V_0 is a threshold voltage[1] at which the conductance of the PC begins to change appreciably.

In practice, this curve is seen to fit the devices reasonably well, except at high intensities, where a saturation occurs in the conductance (see Fig. 5). If G is in mhos and V is in RMS volts, typical values for the devices tested were as follows:

	a	b
Single Crystal CdS	6.38×10^{-14}	3.88
Layer CdSe	1.4×10^{-13}	3.1

Since the same EL cells were used in each of these cases, the variation b is due to the variation in the performance of the PC units. a is indicative of the relative impedance levels of the photoconductors.

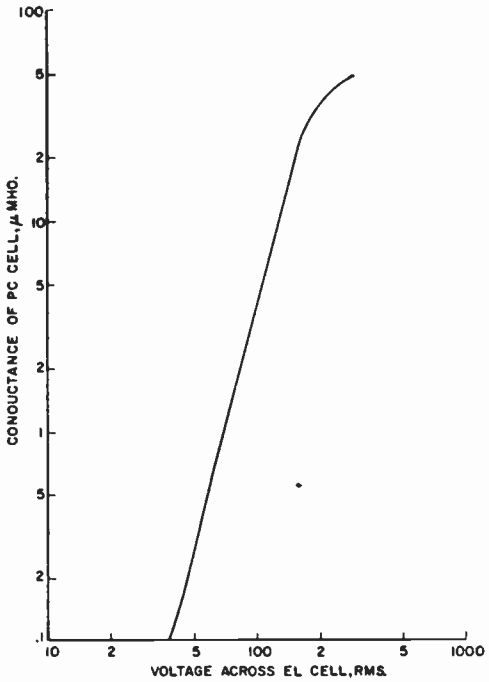

Fig. 5—Transfer characteristic of an EL-PC unit.

The Bistable Stage

The Asymmetrical Bistable Stage

Fig. 6(a) shows a bistable stage [6], [7], consisting of the series combination of an EL and a PC unit, with optical feedback from the EL cell to the PC. This circuit is fed from an ac source whose amplitude may be varied, and behaves as shown in Fig. 6(b). In this circuit it was necessary to shunt the PC with a large resistance so as to lower the initial turn-on voltage. The behavior of the circuit may be explained as follows. Over the region OA the EL cell is dark, and the curve is the V-I characteristic for the dark PC. At A, the EL cell begins to light, the resistance of the PC falls, and thus a larger proportion of the signal voltage is impressed across the EL cell. This positive feedback process results in the transition $A\rightarrow B$, and the EL cell is lit. Any further increase in the voltage results in a corresponding increase in current. Over this region, the resistance of the PC is low compared to that of the EL cell, and the V-I characteristic is that of the EL cell. On reducing the voltage, a point D is reached where the EL cell turns off, and the circuit switches to the dark state, along $D\rightarrow E$.

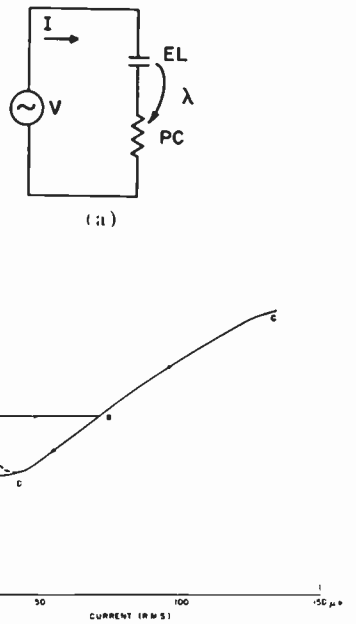

Fig. 6—Asymmetrical bistable stage.

The performance of this circuit may be studied with reference to Fig. 7. Three sets of V-I characteristics are shown here, corresponding to three different values of dark resistance for the photoconductor. It is seen from the Appendix that the turn-on current for the stage is relatively independent of the value of the dark resistance, as is also the turn-off current. Since the EL cell maintains a reasonably constant impedance over its range of operation, this corresponds to a critical turn-on and a critical turn-off voltage for the EL cell. We may, therefore, say that the critical turn-on and turn-off voltages for the EL cell in this circuit are relatively independent of the value of the dark resistance of the PC. The push buttons A and B provide a simple switching arrangement. In practice, the push buttons may be replaced by PC units that are lit by EL cells.

Let the supply voltage be V_1, and let the circuit be in its *off* condition (point 1). The circuit may be turned *on* by momentarily depressing button B, thereby lighting the EL cell. On its release, the stage will stay in the *on* condition at point 2, and the PC will have a low value of resistance. The stage may be re-set by depressing button A. This extinguishes the EL, and the resistance of the PC begins to return to its dark value. In order that the circuit return to the original point 1

[1] It should be emphasized that this is an empirical relationship which gives a simple broken line approximation to the performance of an EL-PC unit. In actuality, the physical reasons for the existence of a threshold voltage are questionable.

when A is released, it is necessary that the resistance of the PC recover to a value such that the voltage ordinate intersects the V-I characteristic in the dark region. Thus, if A were released when the PC recovered to the value R_3, the stage would turn on. However, if the PC recovered to the value R_2 or greater, the stage would stay off. This imposes a restriction on the minimum length of time that is necessary to turn off the stage, and therefore, the "wait" period between one operation and the next. (The speed of *turn-on* is relatively fast, of the order of milliseconds, and is a function of the magnitude of the turn-on pulse.)

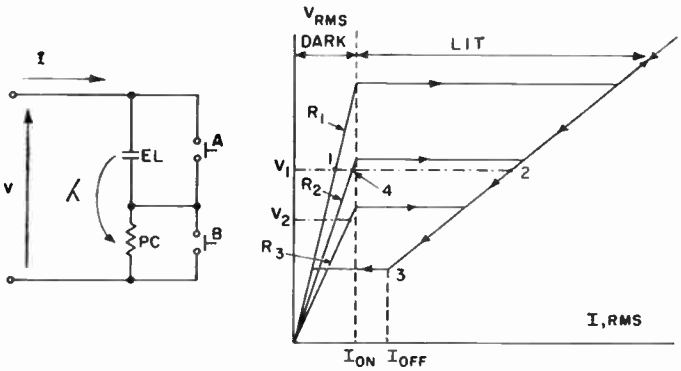

Fig. 7—Idealized characteristics for an asymmetrical bistable stage.

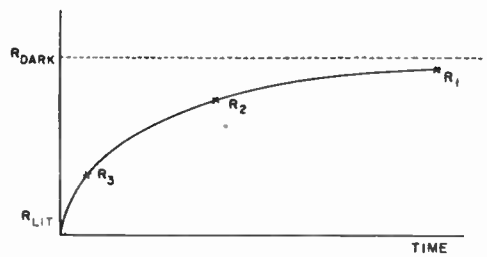

Fig. 8—Recovery characteristic of a PC.

The recovery characteristics for a PC may now be studied. Fig. 8 shows the resistance of a PC as a function of time, after the abrupt removal of the light source. The recovery curve can be shown to consist of a number of exponentially decaying terms, resulting in

1) a relative fast initial increase of resistance followed by
2) a much slower change, and eventually by
3) a change over a period of hours or days returning to its final dark value.

In an operative circuit, the last of these changes is too slow to be of any value. In order to reduce the time between operations, it is necessary to reduce the supply voltage to V_2 (see Fig. 7), resulting in a short recovery time. If this is done, however, the turn-on voltage across the EL cell will be lessened, and the turn-on time will become very long. Using such a stage with the CdS photo-cells, turn-off times of the order of one second were encountered. A fixed dc bias may be placed on the PC to hasten its recovery by sweeping out the trapped carriers in the crystal imperfections. An improvement by a factor of 2 to 3 may be obtained by this technique.

The Symmetrical Bistable Stage

The symmetrical bistable stage [8] consists of two EL and two PC units in the cross-coupled connection shown in Fig. 9. The optical feedback paths are indicated in the figure. It may be shown that the circuit has two stable states corresponding to the lit condition of either one or the other EL cell. Its behavior will now be studied.

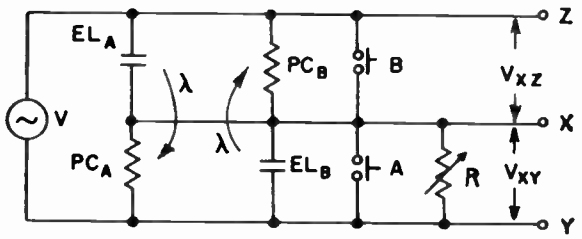

Fig. 9—Symmetrical bistable stage.

Consider the case where EL_B is lit. Then PC_B is a low resistance. Since PC_B shunts EL_A, this EL cell is off, and PC_A is a high resistance. This high resistance is in shunt with EL_B, and so EL_B stays on. The voltage across XY is about 90–95 per cent of the supply voltage.

Now consider the effect of a variable resistance R, across XY. As R is reduced, V_{XY} falls and V_{XZ} rises.

1) If V_{XY} falls to below V_{OFF} for the EL_B, this EL-PC combination will turn off.
2) If V_{XZ} rises above V_{ON} for the EL_A, this EL-PC combination will turn on.
3) If 1) occurs, PC_B will increase in resistance, causing V_{XZ} to rise further, and resulting in the occurrence of 2).
4) If 2) occurs, PC_A will fall in resistance, causing V_{XY} to fall further, and resulting in the occurrence of 1).

Thus, we see that effects 1) and 2) are available in the symmetrical stage, but the cross-connection results in a regenerative feedback action from 1)→2) and from 2)→1). Since the turn-on voltage for an EL-PC pair occurs when the critical voltage V_{ON} is empressed across the EL cell, this turn-on voltage is materially unchanged by the cross-connection; therefore, we may consider the circuit (to a first-order approximation) as two asymmetric stages, except that we now specifically deal with the turn-on times of the stages. Thus, the operation time between pulses is limited largely by the trigger impulse magnitude, and hence by the supply voltage. Using this circuit, with the same photoconductors as before (CsS), the time between operations has been reduced by two orders of magnitude. With CdSe photoconductors, this time has been reduced to about 1–2 milliseconds.

Logic-Performing Elements

It is possible to use *EL-PC* combinations to perform logical functions [9] in computers. Some of the more basic circuits will be discussed in terms of the mathematical functions that are performed.

Transmission Element

The first of these to be considered is one in which a light input is transferred from one point to another. Fig. 10(a) shows a simple scheme to effect this. In this scheme there is only one optical path, between EL_A and PC_A. Each time a light pulse is fed in (by EL_A), a light pulse is emitted by EL_B. The circuit thus has the property of transferring a light pulse from one point to another.

The turn-off time is a function of the time taken for PC_A to recover to its high resistance value after EL_A is turned off. This time interval will determine the minimum time between pulses.

The results are shown in Fig. 10(b). As before, the turn-on time is very small compared to that required for turn-off. In a typical unit with the same *PC* units as were used in the bistable stage, turn-off times of about one second were required.

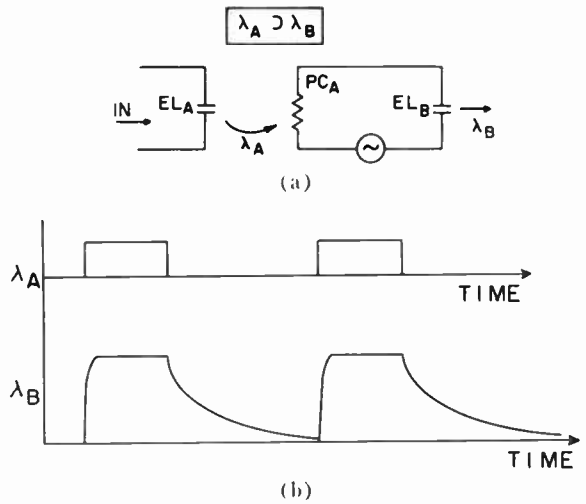

Fig. 10—Transmission element and its performance.

The operation of such a stage may be considerably improved by the connection of Fig. 11(a). In this connection, an asymmetrical bistable stage is cross-connected with the original circuit. With zero input at EL_A, the EL_C-PC_C combination is always on, and EL_B is off. With a signal in at EL_A, PC_A is lowered in resistance, EL_C is turned off, EL_B is turned on, and PC_C has a high resistance. On removal of the signal at EL_A, PC_A increases till EL_C turns on. As EL_C turns on, PC_C falls rapidly, due to the optical feedback, and EL_B is extinguished. Such a stage was found to be not quite as fast as the symmetrical bistable stage, and required from 10 to 25 milliseconds between operations when CdS cells were used. It will be noted that this circuit is similar to that of the symmetrical bistable stage with the important difference that there is *no* optical path between PC_A and EL_B, and also that there is provision for feeding in information at EL_A.

The circuit of Fig. 11(b) may also be used as a negation (INHIBIT) element by using the light output λ_C of EL_C.

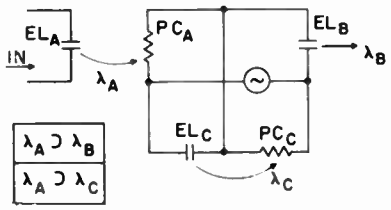

Fig. 11—Transmission element (regenerative connection).

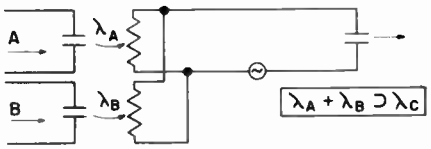

Fig. 12—Disjunction element.

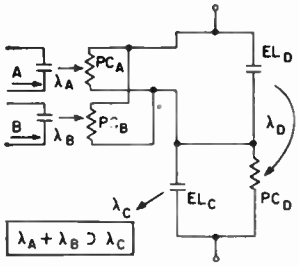

Fig. 13—Disjunction element (regenerative connection).

Disjunction (OR) Element

Fig. 12 shows an OR stage corresponding to the asymmetric type of circuitry. This circuit has the same disadvantage as that of the other asymmetric stages; that is, the time interval between successive operations is large. As before, this time interval can be reduced by the use of cross-connected regenerative circuitry, as in Fig. 13. If necessary, more than two inputs may be used, by paralleling the *PC* units.

Conjunction (AND) Element

Fig. 14 shows an AND stage of the asymmetric type. As before, the operating time was improved by about two orders of magnitude by the addition of cross-connected regenerative circuitry. This is shown in Fig. 15. More inputs are obtained by connecting more *PC* units in series.

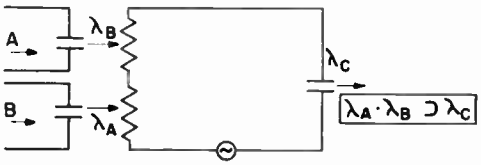

Fig. 14—Conjunction element.

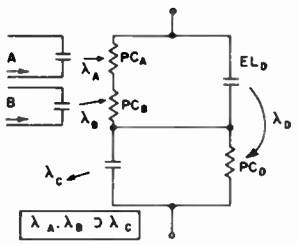

Fig. 15—Conjunction element (regenerative connection).

Switching Circuits

In this section, we shall attempt to show how several switching circuits may be synthesized, using the elements already discussed. These circuits will be preliminary in so far as they will most probably lead to a maximum number of elements used. At present, no consistent minimization technique has been worked out; each problem must be minimized by inspection.

In the various circuits that have been developed, we note that the cross-coupled regenerative circuitry serves to reduce the time taken for *EL* cells to be extinguished. It is important to remember that the time taken by the *PC* to recover is unchanged, and therefore the circuits must be so arranged as to only utilize the *PC* recovery characteristic in conjunction with turning *on* another regenerative circuit. Examples of this technique are now shown.

Half-Adder

A preliminary design for a half-adder may be done in two sections, the Carry section and the Sum section. For the Carry section we wish to have an output C when we have an input at both A and B, *i.e.*, $A \cdot B \supset C$. Fig. 16 shows the Carry section together with input and output storage registers. These storage registers are symmetrical bistable stages, and provision is made to clear them by external clearing pulses.

For the Sum section, we wish to have $A \cdot \overline{B} + \overline{A} \cdot B \supset S$. ($A$-and-not-$B$ or B-and-not-A implies S.)

Fig. 17 shows the Sum section, with storage registers.

Even Parity Checker

An even parity checker is one which gives an output as long as an even number of inputs are energized. For a three-input even parity checker, we have

$$(AB\overline{C}) + (A\overline{B}C) + (\overline{A}BC) + (\overline{A}\,\overline{B}\,\overline{C}) \supset D.$$

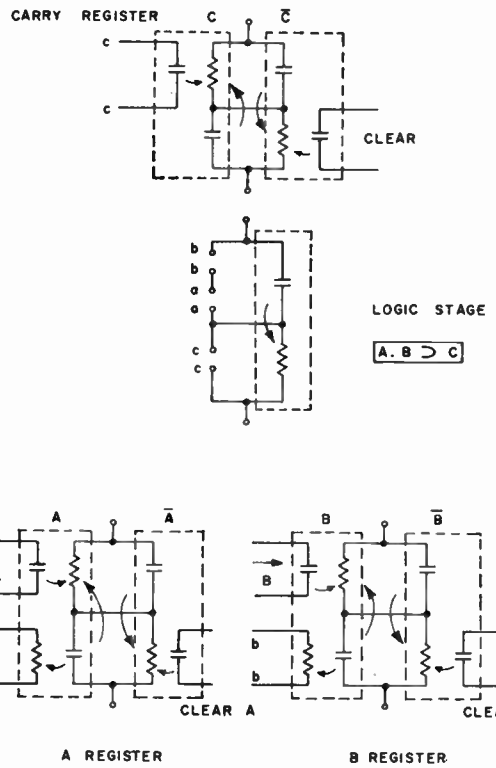

Fig. 16—Half-adder—Carry section.

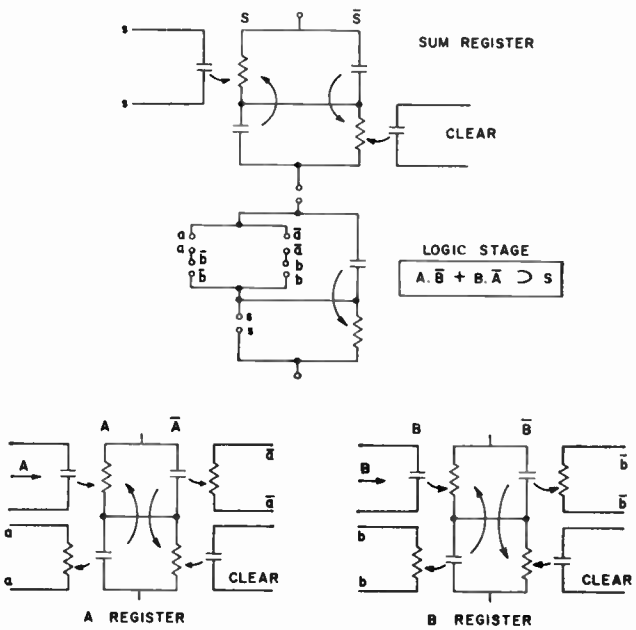

Fig. 17—Half-adder—Sum section.

Thus, the output D is energized when either no input or two inputs are energized.

The relay diagram to synthesize the above function is shown in Fig. 18. Using this diagram, it is seen that the preliminary diagram for the photoelectronic circuit will need two photoconductors, C, and two photoconductors, $\overline{C}$. This means that two storage registers must be used for C. The preliminary circuit is shown in Fig. 19. One

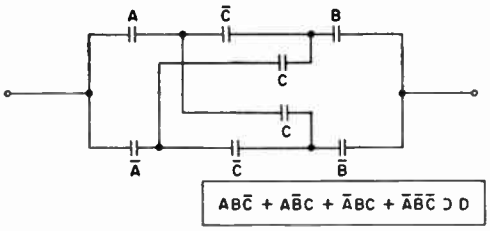

Fig. 18—Relay diagram for an even parity checker.

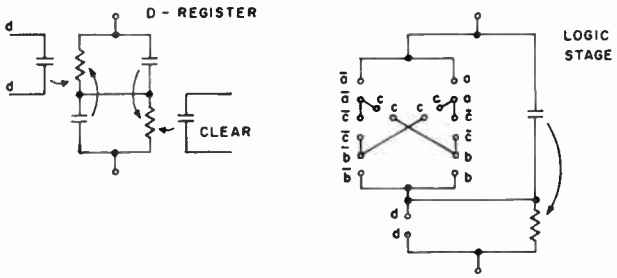

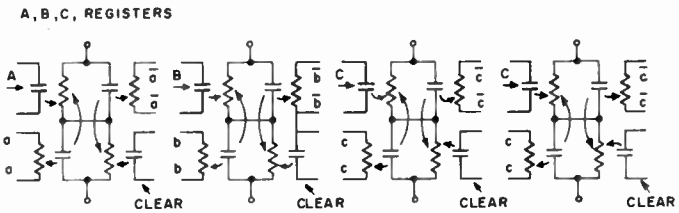

Fig. 19—Even parity checker.

method by which the number of elements may be reduced is by using a duplicate set of *PC*'s to sense the state of register *C*.

Shift Register

Using the techniques outlined, it is possible to develop the preliminary diagram for a shift register. In order to avoid over-complication a shorthand form of drawing is used in Fig. 20. Here we use a master rank and a slave rank. The information is fed in at the master rank, and shifted to the next stage by way of the slave rank. The sequence of operations is performed by the series of gating pulses as follows:

1) Clear Slave rank.
2) Transfer from Master rank to Slave rank.
3) Clear Master rank.
4) Transfer from Slave rank to Master rank and insert next pulse simultaneously.

Outlook for the Future

It is possible, at this point, to assess the advantages and disadvantages of photoelectronic circuits, and to discuss their future in computer applications.

Perhaps their greatest single disadvantage is their present speed of operation. While this is capable of considerable improvement, it does not appear likely that these devices will find use in general purpose "scientific"

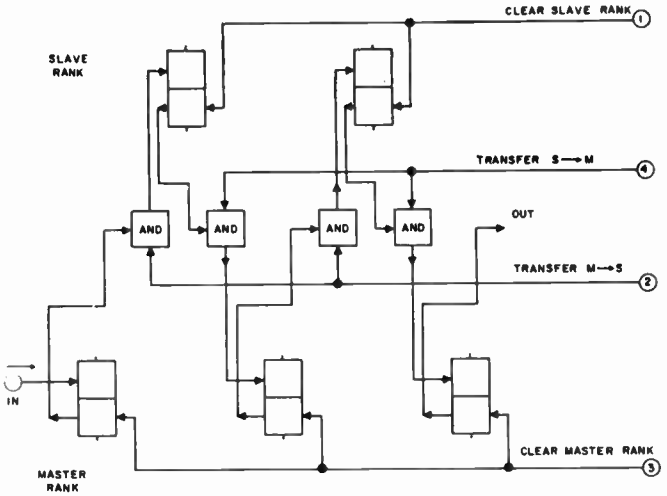

Fig. 20—Shift register.

computers where speed of operation is of paramount importance.

The prime advantage of photoelectronic devices is an economic one—they are extremely easy and inexpensive to make, and it should be possible to lay entire circuits, devices as well as connections, by printed circuit techniques. This, coupled with their small size and freedom from internal feedback, makes them ideal for the many special purpose computing applications where the complexity is in the switching configuration, and not in the number of operations.

Appendix

Analysis of the Asymmetrical Bistable Stage

Fig. 21 shows the circuit for this stage, with a resistance R placed in shunt with the PC unit. The over-all VI characteristic of the device may now be synthesized as follows:

Let I be the current in the circuit. For this current, let V_{EL} be the voltage drop across the EL cell, V_R be the voltage drop across R if the PC is removed from the circuit, and V_{PC} be the voltage drop across the PC if R is removed from the circuit. Assume that the PC is entirely resistive, and the EL is entirely reactive at the supply frequency. Then,

$$V = \left| \frac{1}{\frac{1}{V_R} + \frac{1}{V_{PC}}} - jV_{EL} \right|.$$

This is shown in Fig. 22 for a typical example. The points of interest are the turn-on current and the turn-off current. Now

$$G_{PC} = a \left| V_{EL} \right|^b, \quad V_{EL} > V_0$$
$$G_{PC} = G_0 \simeq 0, \quad V_{EL} < V_0.$$

Since the voltage across the EL cell is a function of the current through it, we may use the current I_{ON} to define the threshold for this combination. This threshold value for the current is, for all practical purposes, the turn-on current for the bistable stage, since the peak value of

$$\left| \frac{1}{\frac{1}{V_R} + \frac{1}{V_{PC}}} \right|$$

occurs at about this value of current. With smaller values of R, the turn-on current will increase, but this increase is negligible in typical circuits. The turn-off current is the current at which $|V|$ is a minimum. In this region, the PC is lit, the effect of R on the turn-off current may be ignored. Then

$$|V| = |V_{PC} - jV_{EL}| .$$

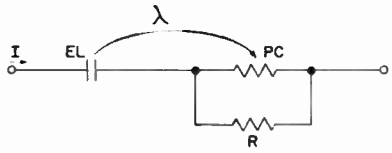

Fig. 21—Asymmetrical stage.

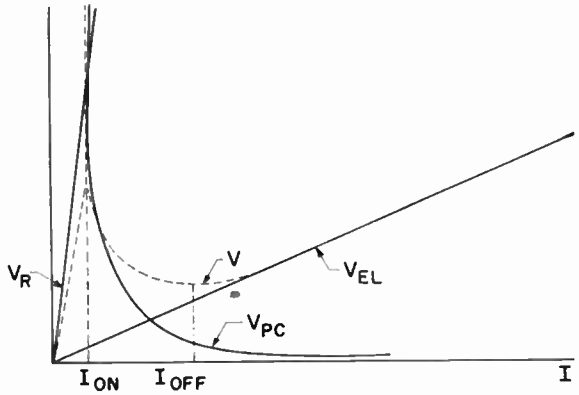

Fig. 22—V-I characteristic for an asymmetrical stage.

Using the assumptions mentioned earlier, and writing X_{EL} as the reactance of the EL cell, we have

$$G_{PC} = a|V_{EL}|^b$$
$$V_{EL} = -jX_{EL}I$$

whence

$$V = [X_{EL}^2 I^2 + a^{-2} X_{EL}^{-2b} I^{-2(b-1)}]^{1/2}$$

solving, the minimum value of I is given by

$$I_{OFF} = (b-1)^{1/2b}\left[\frac{1}{aX_c^{b+1}}\right].$$

For values of b ranging from 3 to 6, *i.e.*, for all practical values of b, we have

$$(b-1)^{1/2b} \simeq 1.14$$

whence

$$I_{OFF} \simeq 1.14\left[\frac{1}{aX_c^{b+1}}\right]^{1/b},$$
$$\simeq 1.14\, I_0'$$

where I_0' is the current at which the reactive impedance of the EL and the PC are of the same magnitude.

Acknowledgment

The author wishes to acknowledge the valuable suggestions of many colleagues during the course of this work. He is grateful especially for the assistance and encouragement given him by Dr. E. Fischer-Colbrie, Dr. J. Elliot and Dr. C. Spitzer, of the Electronics Laboratory.

Bibliography

[1] G. Destriau, "Experimental studies of the action of an electric field on phosphorescent sulfides," *J. Chem. Phys.*, vol. 33, p. 620; 1936.
[2] S. Roberts, "Field strength and temperature studies of electroluminescent powders in dielectric media," *J. Opt. Soc. Am.*, vol. 42, p. 850; 1952.
[3] A. Rose, "Performance of photoconductors," Proc. IRE, vol. 43, pp. 1850–1869; December, 1955. (Contains a bibliography of 54 references.)
[4] G. Destriau and H. Ivey, "Electroluminescence and related topics," Proc. IRE, vol. 43, pp. 1911–1940; December, 1955. (Contains a bibliography of 162 references.)
[5] R. H. Bube, "Photoconductivity of the sulfide, selenide, and telluride of zinc or cadmium," Proc. IRE, vol. 43, pp. 1836–1850; December, 1955. (Contains a bibliography of 118 references.)
[6] B. O. Marshall *et al*, Quart. Rep., No. 3, First Series Computer Components Fellowship No. 347, Mellon Inst., Pittsburgh, Pa., p. VI-9; 1951.
[7] E. E. Loebner, "Opto-electronic devices and networks," Proc. IRE, vol. 43, pp. 1897–1906; December, 1955.
[8] T. B. Tomlinson, "Principles of the light-amplifier and allied devices," *J. Brit. IRE*, vol. 17, pp. 141–154; 1957.
[9] E. A. Sack, "An electroluminescent digital indicator with elpak translation logic," *Comm. and Elec.*, vol. 35, pp. 113–116; 1958.
[10] I. M. Copi, "Symbolic Logic," The Macmillan Company, New York, N. Y.; 1953.

A Feedback Light-Amplifier Panel for Picture Storage*

B. KAZAN†, SENIOR MEMBER, IRE

Summary—**With a new type of light-amplifier panel, incorporating optical feedback, a transient input image can be stored for an indefinite time as a black-and-white or on-off picture. Using 420-cycle operation, an exposure of about 1 foot-candle-second is required for triggering an image on, with the excited elements having a brightness of 0.5 foot-lamberts. When desired, the stored image can be rapidly erased by electrical means without the delay normally required by the decay of the photoconductor. A panel construction of 40 elements per linear inch is used, with each element optically and electrically isolated from its neighbors. By means of separate phosphor layers for viewing and feedback, ambient light on the viewing side is prevented from exciting the panel. Calculated and measured curves are shown, indicating the effects of varying the feedback factor in general light amplifier operation. A relation is also derived, taking into account the build-up and decay properties of the amplifier, which specifies the conditions for bistable operation.**

Introduction

THE conventional light-amplifier panel was designed to eliminate optical feedback entirely by the use of an opaque layer between the photoconductive and electroluminescent layers.[1] Amplifiers of such construction could be evaluated and studied apart from the complexities of operation introduced by feedback.

The use of feedback, however, provides additional possibilities of amplifier operation. With small amounts of feedback, half-tone operation can be retained and the gain and gamma are increased. With increasing feedback, bistability results,[1-4] allowing the indefinite storage of black-and-white or on-off images.

The actual incorporation of small amounts of feedback in the conventional light amplifier is relatively simple. However, where increased feedback is desired for bistable operation, new design problems result.[5] These include obtaining sufficient feedback while retaining sensitivity to input light and the optical isolation of individual elements to prevent image spreading. Although, with low-gain amplifier elements, spreading can be prevented by simple techniques which give partial isolation, with high-gain elements a panel design which gives relatively complete isolation is required.

* Original manuscript received by the IRE, July 16, 1958; revised manuscript received, October 15, 1958. This work was done at the RCA Labs., Princeton, N. J.

† Hughes Research Labs., Culver City, Calif.

[1] B. Kazan and F. H. Nicoll, "An electroluminescent light-amplifying picture panel," PROC. IRE, vol. 43, pp. 1888–1897; December, 1955.

[2] G. Diemer, H. A. Klasens, and J. G. van Santen, "Solid-state image intensifiers," *Philips Res. Rep.*, vol. 10, pp. 401–424; December, 1955.

[3] E. E. Loebner, "Opto-electronic devices and networks," PROC. IRE, vol. 43, pp. 1897–1906; December, 1955.

[4] J. E. Rosenthal, "Theory and experiments on a basic element of a storage light amplifier," PROC. IRE, vol. 43, pp. 1882–1888; December, 1955.

[5] B. Kazan and F. H. Nicoll, "Solid-state light amplifiers," *J. Opt. Soc. Amer.*, vol. 47, pp. 887–894; October, 1957.

As in the case of non-feedback amplifiers, the input-output characteristics of feedback amplifiers are intimately associated with the build-up processes of the photoconductor. When bistable operation is desired and the panel is to be excited with a transient image, it is also necessary to consider the decay processes of the photoconductor in determining the conditions for bistability.

Analytical Model of Feedback Action

In amplifiers without feedback, the output is a function of the input light and also the time of excitation. A typical set of build-up curves of light output as a function of time for such an amplifier is shown in Fig. 1 for various input light levels using 420 cps biased ac operation.[6] (The electrical connections for this type of operation are shown in Fig. 8 together with the amplifier cross

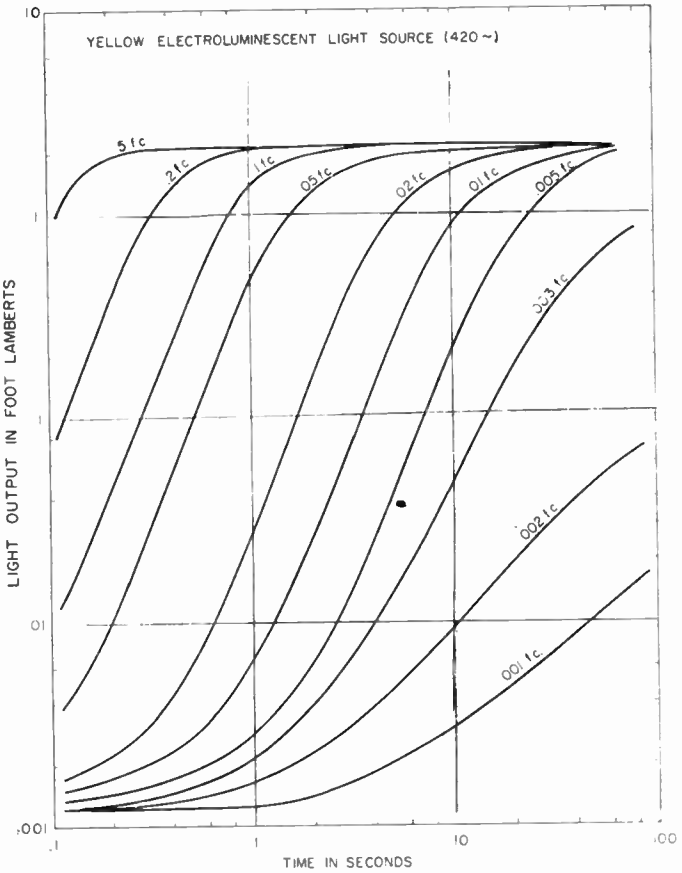

Fig. 1—Light output vs time for various light input levels. Biased ac operation (420~).

[6] B. Kazan, "An improved high-gain panel light amplifier," PROC. IRE, vol. 45, pp. 1358–1364; October, 1957.

section.) As a rough approximation, over a large range of amplifier operation, the output light, L_o, can be expressed as:

$$L_o = A[L_i \cdot t]^3, \tag{1}$$

where L_i is a particular level of input light, t is the time of excitation, and A is a constant. (For large values of $L_i \cdot t$, the output light, L_o, saturates and (1) is not valid.)

Since the output is a function of $L_i \cdot t$ for constant values of L_i, it is assumed that in the more general case, where L_i varies with time:

$$L_o = A\left[\int_0^t L_i \cdot dt\right]^3. \tag{2}$$

If feedback is added, (2) becomes:

$$L_o = A\left[\int_0^t (L_i + \beta L_o) \cdot dt\right]^3, \tag{3}$$

where β is the feedback factor.

Assuming amplifier operation corresponding to (3), computed values of L_o as a function of t are plotted in Fig. 2 for an input light level of 0.01 foot-candles and feedback factors, β, of 0, 0.005, 0.01, and 0.05. (The value of the constant, A, was taken as 1000 using the data of Fig. 1.) These curves show that for output lights below 1 foot-lambert, feedback factors below 0.01 have little effect on the build-up. With a higher feedback factor such as 0.05, the build-up is noticeably more rapid than with no feedback.

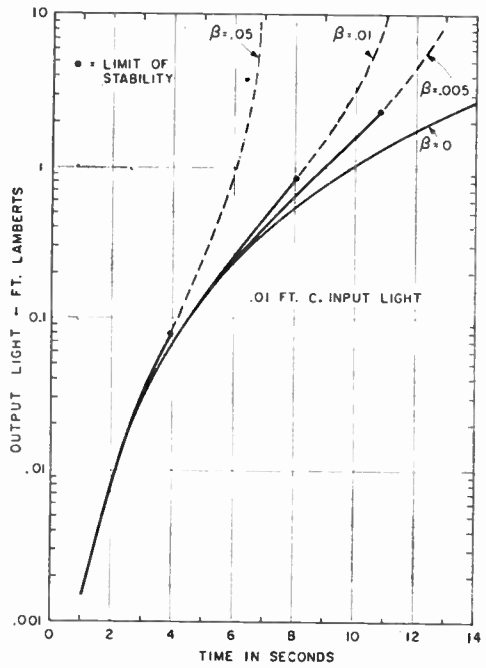

Fig. 2—Effect of feedback on build-up (calculated curves).

Fig. 3 shows curves of output light, L_o, as a function of input light, L_i, for a one-second and a ten-second excitation time using computed values obtained from (3). Two feedback factors, 0 and 0.05, were assumed. In the case of one-second excitation, the effect of feedback is small below 1 foot-lambert output, while in the case of ten-second excitation, the feedback produces a distinct rise in output at the higher levels.

For stable half-tone operation, it is necessary for the output to decay after cutting off the input light, irrespective of the output light level. Otherwise, sufficiently excited points of the amplifier automatically will build up to and remain at a saturation level. Since (3) is valid only for the build-up of light output, it cannot be used for describing the output after the input light, L_i, is cut off. A more general expression for the output requires a modification of (3) to include the decay properties of the amplifier.

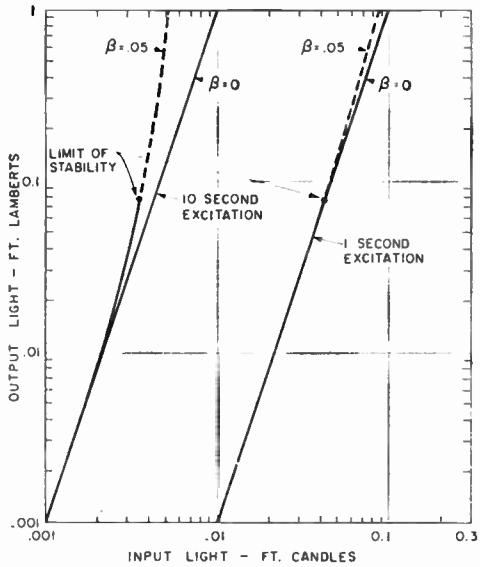

Fig. 3—Effect of feedback on input-output characteristic (calculated curves).

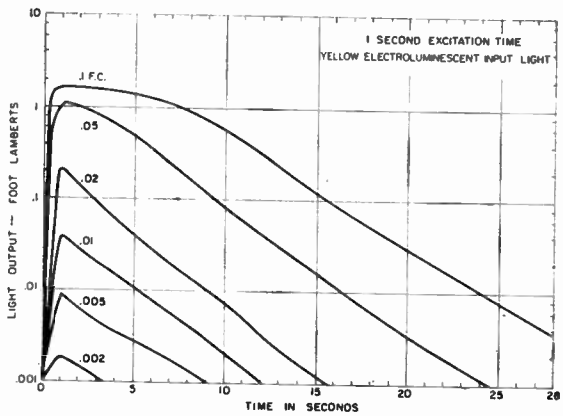

Fig. 4—Decay curves for biased ac operation.

In Fig. 4 is shown a typical set of amplifier decay curves after a one-second excitation using biased ac. The decay here is approximately exponential, so that the output during the decay period can be expressed as:

$$L_o = L_p e^{-t/\tau_1}, \tag{4}$$

where L_p is the output light at the moment the decay begins, and τ_1 is a constant. In analyzing the feedback action, the assumption is made that an exponential decay process with a fixed time constant is continuously acting in the photoconductor during the build-up period as well. Using (3) for the build-up and modifying it to include an exponential decay, the expression for the amplifier operation with feedback can then be written:

$$L_o = A\left[\int_0^t (L_i + \beta L_o)e^{-(t-t_0)/\tau}\cdot dt_0\right]^3, \tag{5}$$

where $t_0 < t$.

This equation expresses L_o as a function of the time, t. It is assumed here that the effect of the total input light $(L_i+\beta L_o)$ at any moment t_0 (where $t_0<t$), is reduced at time t by the exponential factor, $e^{-(t-t_0)/\tau}$, where τ is a constant.

Eq. (5) may be interpreted as a model of the amplifier action where the integral inside the brackets is proportional to the photocurrent at time t. The cubing of the integral represents the fact that the photocurrent flows through the electroluminescent phosphor whose output light is given approximately by the cube of the current. Although the usual CdS powder photoconductor employed in the light amplifier is not always describable by an exponential decay with a fixed time constant as assumed in (5), this is a useful approximation. (For the photoconductor used, the current varies approximately as the fourth power of the voltage.[6] It is assumed for the above model, however, that the degenerative effect of the voltage reduction across the photoconductor as the voltage across the phosphor builds up can be neglected since the phosphor voltage does not exceed a small fraction of the supply voltage.)

In operation it is assumed that at a time $t_1(t_1<t)$ the input light L_i is cut off, having been at a constant level from 0 to time t_1. After t_1 the amplifier is assumed to decay or build up under the influence of the feedback alone. To determine whether the amplifier will decay or build up after t_1, the derivative dL_o/dt is used. It is assumed that if dL_o/dt is positive immediately after t_1 then the amplifier output will continue to build up indefinitely and if the derivative is negative the output will decay to zero. Differentiating (5) with respect to t gives at t_1^+:

$$\frac{dL_o}{dt} = 3A\left(\frac{L_o}{A}\right)^{2/3}\left[\beta L_o - \frac{1}{\tau}\int_0^t (L_i + \beta L_o)e^{-(t-t_0)/\tau}\cdot dt_0\right] \tag{6a}$$

$$= 3A\left(\frac{L_o}{A}\right)^{2/3}\left[\beta L_o - \frac{1}{\tau}\left(\frac{L_o}{A}\right)^{1/3}\right] \tag{6b}$$

for

$$\frac{dL_o}{dt} = 0, \qquad \beta L_o' = \frac{1}{\tau}\left(\frac{L_o}{A}\right)^{1/3} \tag{6c}$$

or

$$L_o' = \frac{1}{A^{1/2}(\beta\tau)^{3/2}}. \tag{6d}$$

where L_o' is the output light at the limit of stability. For values of L_o greater than L_o' of (6d) the amplifier will build up, while for values less than this it will decay.

If after t_1 both the feedback factor, β, and the input light, L_i, are assumed zero, we get, using (5):

$$L_o = A\left[\int_0^t (L_i + \beta L_o)e^{-(t-t_0)/\tau}\cdot dt_0\right]^3$$

where $(t > t_1)$ (7a)

$$= A\left[e^{-(t-t_1)/\tau/3}\int_0^{t_1} (L_i + \beta L_o)e^{-(t_1-t_0)/\tau}\cdot dt_0\right]^3 \tag{7b}$$

$$= L_o(t_1)\cdot e^{-(t-t_1)/\tau/3}. \tag{7c}$$

This last expression corresponds to (4) with $L_o(t_1)$ corresponding to L_p and $\tau/3$ corresponding to τ_1.

For the case of no feedback, and the input light L_i maintained at a constant level, (5) can be written:

$$L_o = A\left[\int_0^t L_i e^{-(t-t_0)/\tau}\cdot dt_0\right]^3 \tag{8a}$$

$$= A\left[\left|\tau L_i e^{-(t-t_0)/\tau}\right|_0^t\right]^3 \tag{8b}$$

$$= A\left[\tau L_i(1 - e^{-(t/\tau)})\right]^3. \tag{8c}$$

For $t/\tau \ll 1$, (8c) reduces to $L_o = A\left[L_i\cdot t\right]^3$ which is the expression of (1) where the effects of decay were neglected.

Inspection of the build-up curves of Fig. 1 shows that for excitation times greater than about 10 seconds, the reciprocity between input light, L_i, and time is no longer valid, as would be expected from (8c). Using data from the experimental build-up curves of Fig. 1 and substituting into (8c), it is possible to calculate an approximate value of τ. Assuming an output light level of 0.03 foot-lamberts, this is reached in 28 seconds with an input of 0.002 foot-candles, or in 1 second with an input of 0.02 foot-candles. Inserting these conditions in (8c) and solving by trial and error results in a value of 10.2 seconds for τ. This gives for $\tau_1(=\tau/3)$ a value of 3.4 seconds.

From the experimentally obtained decay curves of Fig. 4, the actual decay constant, τ_1, of the amplifier is found to be about 4 seconds, in fairly good agreement with the calculated value above. Using the experimental value of τ_1 (corresponding to $\tau = 12$ seconds), (6d) can be used to determine the output light, L_o', at the limit of stability as a function of the feedback factor, β. Assuming a value of the constant, A, as 1000 from the build-up curves of Fig. 1, the values of L_o' are shown on the calculated curves of Fig. 2 and Fig. 3 by the heavy dots. The unstable portions of the curves are shown by the dashed lines.

From the values of L_o' shown, the input exposure required to trigger the amplifier on can be determined from the curves of Fig. 2. For $\beta = 0.005$, 0.01, and 0.05, the input exposures are respectively 0.11, 0.08, and 0.04 foot-candle-seconds, respectively. Although the curves of Fig. 2 and Fig. 3 were obtained using (3) which neglects the decay effects included in (5), these curves are useful approximations in cases where the time of excitation is less than the time constant τ ($=12$).

Experimental Results on Elemental Amplifier

To observe experimentally the effects of different amounts of feedback a single-element amplifier was constructed as shown in the cross section of Fig. 5. Measurements were made on such a unit instead of a feedback panel since the feedback factor could be more accurately determined and varied at will without causing other changes in the amplifier. In Fig. 5 the lower glass plate with its electroluminescent phosphor layer serves as the light source for the feedback unit above. The photoconductive cell of the feedback unit consists, as shown, of a glass plate about 1 inch $\times$ 1 inch with interdigital transparent conducting strips (forming an extended 20-mil gap) covered with a thin layer of CdS powder which can be excited from either side. In series with the photoconductive cell is an electroluminescent layer of about equal area. This emits light through the transparent backing electrode of evaporated aluminum for viewing and measurement by the photomultiplier above, and also through the conducting coating on the glass for feedback to the photoconductor. For varying the feedback factor, β, neutral filters of varying density were inserted between the phosphor layer and the photoconductor.

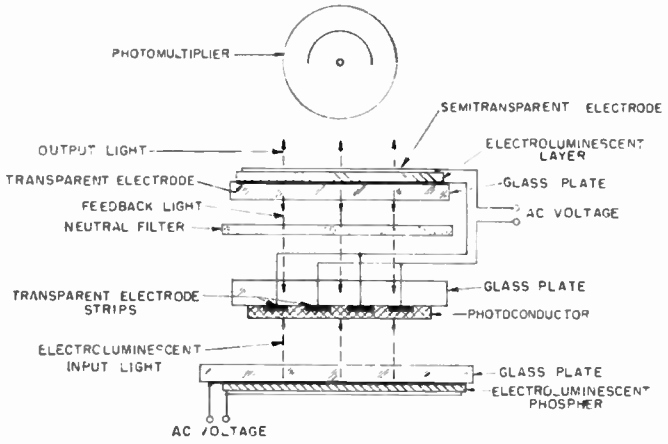

Fig. 5—Test setup for feedback measurements.

Using the experimental arrangement, tests were made with connections for ac operation as indicated and also with biased ac.[6] For the biased ac the interdigital photocell was divided into two equal parts and dc voltage sources inserted in series with each half. Since the effects of the feedback were similar for both types of operation, only the results for the biased ac operation are shown below. For the measurements a 300-volt rms ac supply of 420 cps was used with dc voltages equal to the peak ac voltage.

Fig. 6 shows build-up and decay curves obtained by exciting the amplifier with a fixed light level of about 0.005 foot-candles. For each level of feedback the amplifier was excited 10 seconds and allowed to decay. These build-up curves, as in the case of the similar-shaped calculated curves of Fig. 2, show that at low light outputs the effects of adding feedback are small. (The displacement of the $\beta = 0$ curve from the $\beta = 0.0025$ curve is believed due to experimental error.) At the higher light outputs the effects of the feedback are more noticeable with the curves rising more steeply as the feedback is increased. For a feedback factor of 0.01 an input exposure of 0.05 foot-candle-seconds causes instability. Allowing for differences in photoconductors used, this compares well with the calculated exposure of 0.08 foot-candle-seconds for instability obtained from Fig. 2 for the same feedback factor. In both cases the limit of stability occurs at about 1 foot-lambert.

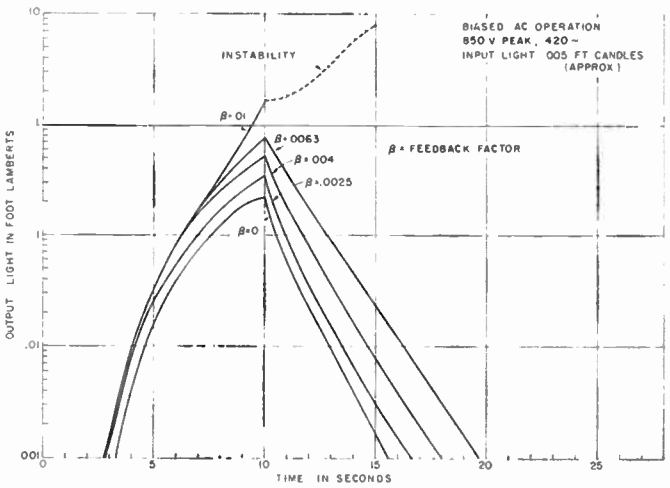

Fig. 6—Build-up and decay as a function of feedback factor (experimental curves).

The curves of Fig. 6 indicate that the rate of decay is only slightly decreased by increasing the feedback factor up to a value of 0.0063. Although between β equal to 0.0063 and 0.01 longer decay times are expected, such operation is relatively critical because of the possibility of instability.

Fig. 7 shows experimentally determined input-output characteristics for the biased ac operation, assuming a 10-second excitation. These curves, as in the case of the calculated curves of Fig. 3 for 10-second excitation, show that the addition of feedback has only a small effect at the low output levels, but increases the gamma at the high levels. However, any marked increase in gamma is accompanied by a serious reduction in the latitude of input light which can be used for half-tone operation.

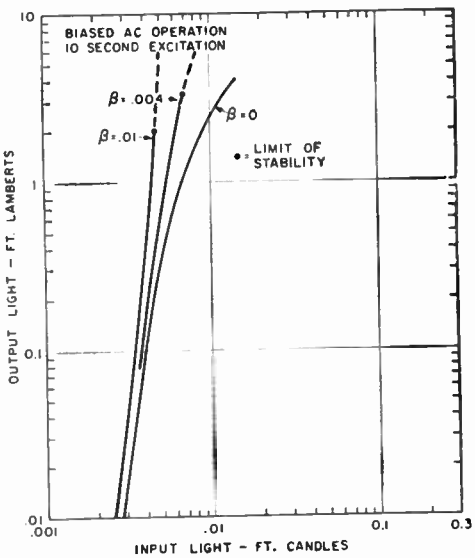

Fig. 7—Effect of feedback on input-output characteristic (experimental curves.)

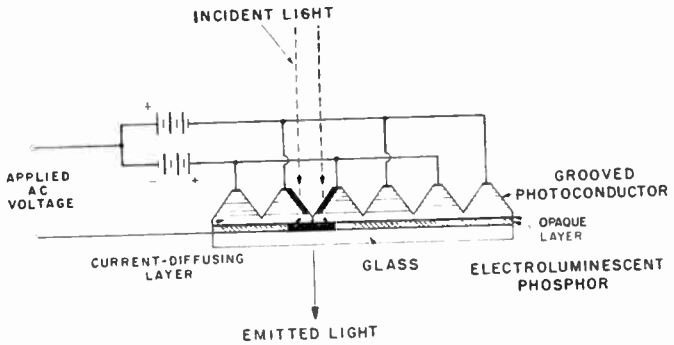

Fig. 8—Cross section of conventional amplifier.

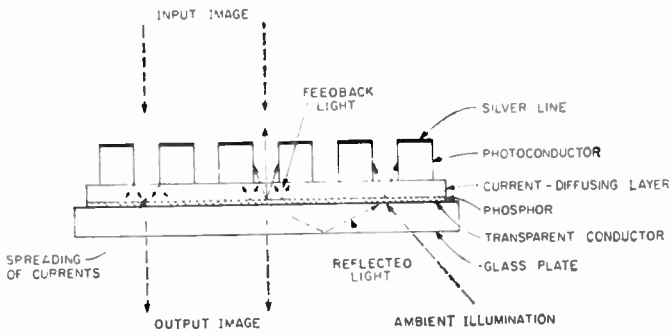

Fig. 9—Modification of light amplifier to produce feedback.

Design of Feedback Panels

Although the conventional light amplifier[6] has no optical feedback, its structure permits convenient modification to obtain feedback operation. Before discussing these modifications the construction of the conventional amplifier is briefly described below. Fig. 8 shows a cross section of the amplifier with the layers greatly exaggerated in thickness. Because of the low light transmission of the CdS powder photoconductor, the photoconductive layer is grooved. This exposes the deep portions to incident light and allows photocurrents to flow down the illuminated surfaces of the ridges. Since at the bottom of the ridges the photocurrents are concentrated into narrow lines, direct contact of the photoconductive layer with the electroluminescent layer would excite the phosphor only in limited areas adjacent to the bottom of the grooves. To avoid this, the current-diffusing layer of conducting CdS is added whose conductivity allows the photocurrents to spread about one groove width in passing through it, resulting in more efficient use of the phosphor area. To completely prevent output light from feeding back through the current-diffusing layer to the photoconductive layer, a thin, opaque, insulating layer is provided between the electroluminescent and current-diffusing layers. For increasing the gain of the amplifier compared to the ac operation used with earlier amplifiers, biased ac is used as shown in Fig. 8. For this purpose alternate conducting lines at the top of the photoconductive ridges are connected to oppositely polarized dc supplies which are in series with the ac supply. The portions of the photoconductor and phosphor area corresponding to a single picture element of the amplifier are shown by the heavy lines.

The simplest manner of obtaining small feedback factors is to eliminate the opaque insulating layer. Feedback light can now reach the photoconductor through the current-diffusing layer, although further attenuated in passing through the photoconductor itself. When this is done in high-gain panels, the operating characteristics are similar to those expected from the calculated and measured curves, *i.e.*, at low input levels, the addition of the feedback produces little effect on the operation. If the amplifier is excited to high levels, the half-tones are lost, and some of the elements become bistable. In addition to reducing the input latitude, the addition of feedback in half-tone amplifiers also accentuates existing nonuniformities in the output image.

In the case of bistable operation with high feedback levels nonuniformities in the amplification properties of the amplifier are of much less concern. However, the initial problem is that of obtaining a panel design with a high feedback factor. One method of obtaining sufficient feedback for good bistable action is shown in the cross section of Fig. 9. Here the opaque layer is eliminated and the photoconductive grooves, instead of being "V"-shaped, are rectangular. This allows feedback light emerging from the current-diffusing layer to strike the walls of the photoconductor without attenuation through the photoconductive material, and also permits incident illumination from outside to excite the surfaces of the photoconductor.

Fig. 10 shows photographs of the stored output of such a 3 inch amplifier. The outputs immediately after triggering, after two minutes, and after five minutes are shown, respectively, in Figs. 10(a), 10(b), 10(c), indicating the gradual spreading of the bright areas. For operation, biased ac was used with relatively low voltages (130-volts rms at 420-cycles ac, and 235-volts dc). At voltages above this the image spreading is more rapid, while at lower voltages the rate of spreading is reduced. In this amplifier the current-diffusing layer was made

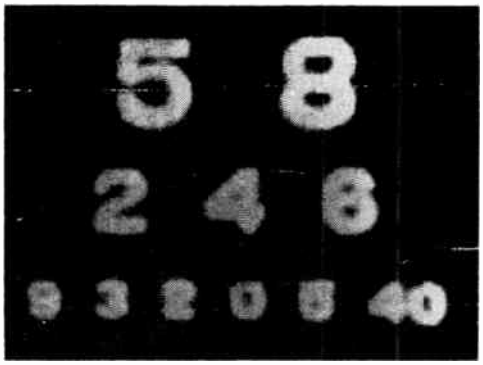

(a)

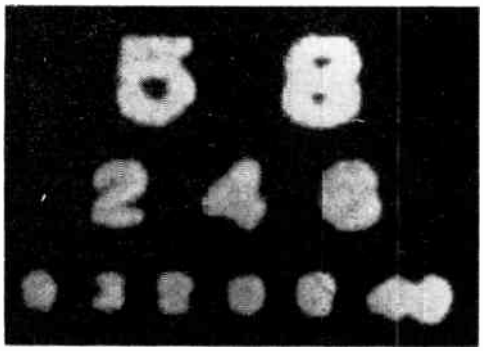

(b)

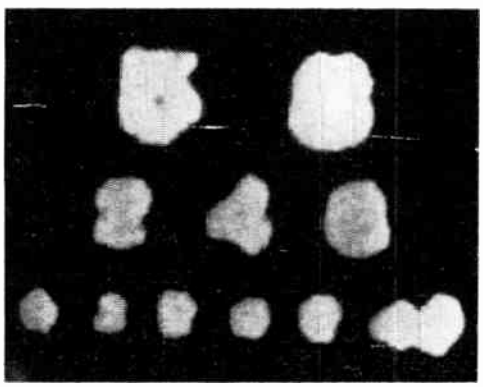

(c)

Fig. 10—Photographs of 3-inch modified feedback light amplifier showing image spreading: (a) immediately after triggering, (b) 2 minutes after triggering, (c) 5 minutes after triggering.

about 4-mils thick, the photoconductor about 10-mils thick, and the rectangular grooves about 10-mils wide on 25-mil centers.

The image spreading of Fig. 10 is caused by several factors as shown in Fig. 9. Because of the conductivity of the current-diffusing layer, photocurrents can spread slightly as they flow through it, expanding the phosphor area which is excited and triggering on new elements. Since the current-diffusing layer is optically diffusing as well, feedback light from an excited phosphor area can also trigger on neighboring elements. In addition, some of the feedback light emerging from the current-diffusing layer can travel along the grooves, exciting other elements. Because of the light transmission of the phosphor layer, ambient light on the viewing side of the panel (assuming the back side shielded) can pass through the phosphor and excite the amplifier. Similarly, a portion of the light from an excited phosphor

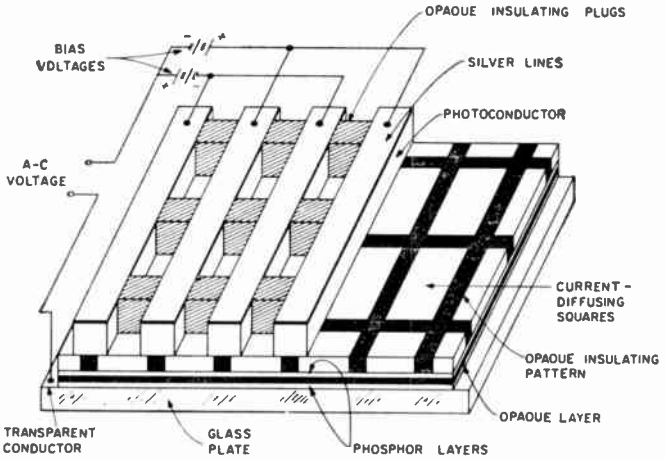

Fig. 11—Design of optical feedback panel.

element, reflected from the outer glass surface back to other areas of the phosphor, can excite new elements.

All of these problems are overcome with the panel design shown (exaggerated in thickness) in Fig. 11. To prevent the effects caused by reflected and ambient light, the single phosphor layer of Fig. 9 is replaced by two thin phosphor layers with an insulating opaque layer between them. The outer phosphor layer provides light for viewing while the inner phosphor layer provides the feedback light. Because of the opaque layer, ambient and reflected light is blocked from reaching the feedback phosphor. The separation of the two phosphor layers also allows the use of different color phosphors. For example, the feedback phosphor light may be matched to the photoconductor and the output phosphor light chosen for optimum viewing conditions. To limit the diffusion or spreading of photocurrents in the current-diffusing layer it is divided into square or rectangular pedestals with insulating strips between them. To prevent the diffusion of light from one current-diffusing square to its neighbor, the insulating strips are made opaque. If necessary, to prevent feedback light from traveling along the grooves and exciting adjacent photoconductive elements, opaque insulating plugs are inserted at regular intervals along the grooves in registry with the opaque strips.

Fig. 12 shows the stored output image produced on a panel of the type shown in Fig. 11. (Since the feedback light traveling along the grooves was not sufficient in this case to cause spreading, opaque insulating plugs were not inserted in the photoconductor grooves.) The image after one minute of storage is shown in Fig. 12(a). For comparison, the images after 5 and 30 minutes are also shown in Figs. 12(b) and 12(c), respectively. For exciting the panel, a one foot-candle projected image of tungsten light (approximately 2800° K) was used for one second. However, because of the reciprocity between input light level and time of exposure of the photoconductor, the panel can be triggered on with much shorter excitation times, for example, 0.01 second or less provided a total exposure of about 1 foot-candle-second is used.

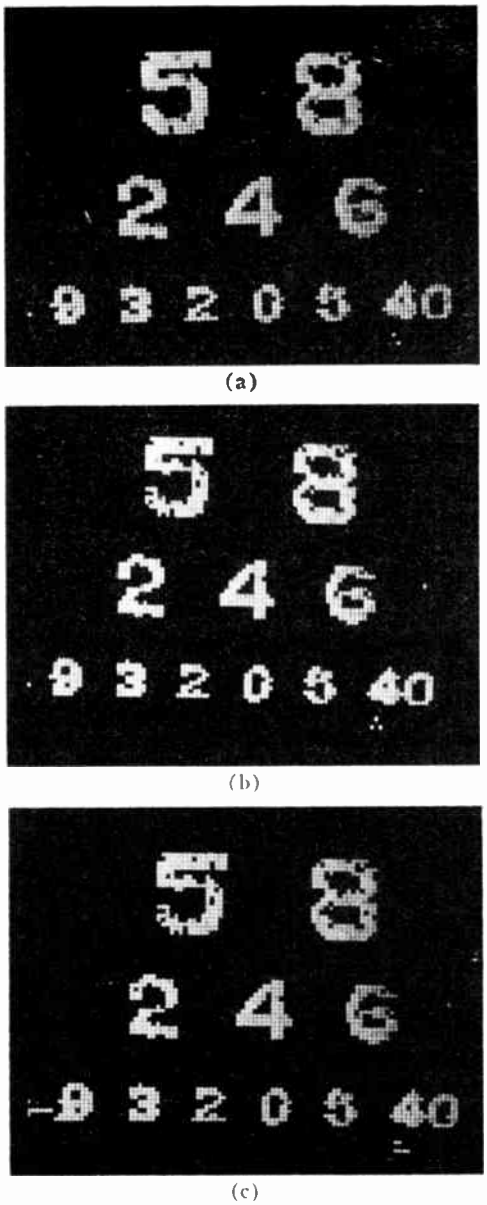

Fig. 12—Stored image on feedback panel: (a) after 1 minute, (b) after 5 minutes, (c) after 30 minutes.

In the photographs the individual elements, whose brightness was about 0.5 foot-lamberts, can be seen separated by dark boundaries. Except for a few additional elements near the numerals 4 and 9 of the lower line, which were excited by leakage or stray room light during the 30-minute period, the small numerals of this line show no deterioration. Due to nonuniformities in the panel several elements in the larger numerals dropped out during the first 5 minutes of storage. However, between 5 and 30 minutes of storage all of the remaining elements stayed on, indicating an indefinite storage time.

When an image such as shown in Fig. 12 is held in storage by the panel, it can also be observed by means of the feedback light emitted from the back side. Fig. 13 shows a photograph of an image seen from the rear of the panel after excitation with the same pattern as in Fig. 12. As in the case of Fig. 12 this image also clearly shows the isolated feedback elements. Since the feedback image viewed from the rear is of relatively low intensity, it was photographed with a time exposure of several minutes.

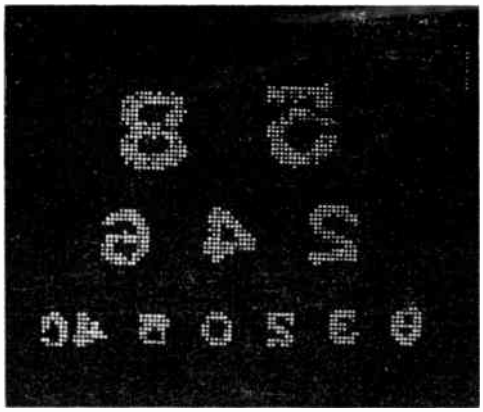

Fig. 13—Stored image viewed from rear of feedback panel.

For the above images, the panel was operated with biased ac as shown in Fig. 11 (300-volts rms, 420 cps; 420-volts dc). As in the case of the conventional light amplifier, rectified ac operation[6] is also possible by substituting rectifying elements for the dc supplies. If ac operation is desired, although at the expense of reduced gain, the silver lines of the photoconductor can all be connected to a common electrode.

With the CdS powder photoconductor used, a stored image can be erased by cutting off the supply voltage for about 10 seconds. During this time the panel cannot be used for storing a new image. However, much more rapid erasure is possible by making use of one of the characteristics of the photoconductive powder whereby the normal decay current following illumination may be cut off at an arbitrary moment by reversing the polarity of the applied voltage if this voltage is unidirectional[7] (as in the case of biased ac and rectified ac operation). This reversal causes an instantaneous drop in the decay current to a level which, for example, may be several orders of magnitude below the level preceding the voltage reversal. Using this effect, the slowly-decaying image of a nonfeedback amplifier panel, such as shown in Fig. 8, can be erased at an arbitrary moment by reversal of the bias voltages (or rectifier polarities).

In the case of the feedback panel, the constant output stored image may similarly be erased instantly by a reversal of the bias voltages (or rectifier polarities). This action extinguishes the stored image and leaves the panel in a condition to be immediately excited with a new image. The erasing action can be repeated with several new images at intervals of a few seconds. However, if the cycle is continuously repeated, a duration of the order of 10 seconds is required between successive erasures, otherwise the voltage reversal will not cause sufficient drop in the photocurrent for good erasing action.[8]

The stored images of Fig. 12 and Fig. 13 were produced on a panel constructed with 40 elements to the

[7] B. Kazan, "A solid-state amplifying fluoroscope screen," *RCA Rev.*, vol. 19, pp. 19–34; March, 1958.

[8] B. Kazan, "Description and properties of the panel X-ray amplifier," *Nondestructive Testing*, vol. 16, pp. 438–447; September–October, 1958.

linear inch. The current-diffusing squares were made about 4-mils thick and the photoconductor about 10-mils thick. Both phosphor layers were a yellow-emitting Zn(S:Se) with a spectral distribution as shown by the dashed line of Fig. 14. For isolating the current-diffusing squares the spaces were filled with an opaque insulating material such as lampblack in Araldite. The photoconductor grooves in registry with the current-diffusing squares were 10-mils wide.

In order to estimate the feedback factor in such amplifiers, separate measurements were made on the current-diffusing layer. In Fig. 14 is shown a spectral transmission curve for the conducting CdS in Araldite binder, using a layer about 2 mils thick. As indicated, for wavelengths of 550 millimicrons and greater, the light transmission is relatively constant, dropping rapidly at wavelengths below 550 millimicrons. As indicated, for the 2-mil layer of CdS, about 10 per cent of the total electroluminescent light is transmitted through the current-diffusing layer.

In practical feedback panels it is desirable, for ease in fabrication, to use thicker current-diffusing layers. To study the effect of varying the thickness of the layer, a number of layers were made with different thickness and the corresponding light transmissions measured. These results are plotted in Fig. 15. In these measurements, the yellow electroluminescent light was used for the input. For the output, a CdS interdigital photoconductive cell was used so that the measurement included only the light components effective in exciting the photoconductor whose spectral response[1] was the same as in the feedback panel. To avoid nonlinearity in the response of the photoconductive cell, for each different thickness of the current-diffusing layer, the input electroluminescent light was varied to produce the same current reading on the photoconductor.

Because of the rectangular grooves of the photoconductor, some of the feedback light emerging from the current-diffusing layer escapes without striking the surfaces of the photoconductor. To estimate the fraction absorbed, the geometric arrangement of a feedback element was simulated experimentally. For this purpose a uniform area source of light was produced by illuminating the under side of a diffusing glass plate. On the top surface a four-walled square enclosure (about 1 inch in each dimension) was set whose inner surfaces consisted of black paper and whose top was open. This enclosure simulated the enclosure at each element of the panel formed by two adjacent photoconductive ridges and two adjacent opaque plugs. The light level was first measured at the surface of the diffusing glass with a photomultiplier. This was then compared to the average light level measured at the top of the enclosure. (Both of these measurements were made with a second piece of diffusing glass attached to the photomultiplier input.) The difference indicated the amount of light absorbed on the four walls of the enclosure.

Since in a feedback element of the actual panel, only two of the walls are photoconductive, half of the absorbed light is useful for feedback. It is assumed in the above, that the photoconductor and the opaque plugs are entirely nonreflecting and also that the darkened walls of the simulated enclosure are entirely nonreflecting. Based on these assumptions it is estimated that about 20 per cent of the light leaving the current-diffusing layer is captured by the photoconductor. With practical current-diffusing layers 3–5-mils thick, this results in feedback factors of 0.02–0.04 in the completed panel. Such feedback factors are adequate for good bistable operation since amplifier gains greater than 100 times[6] are possible with yellow electroluminescent input light.

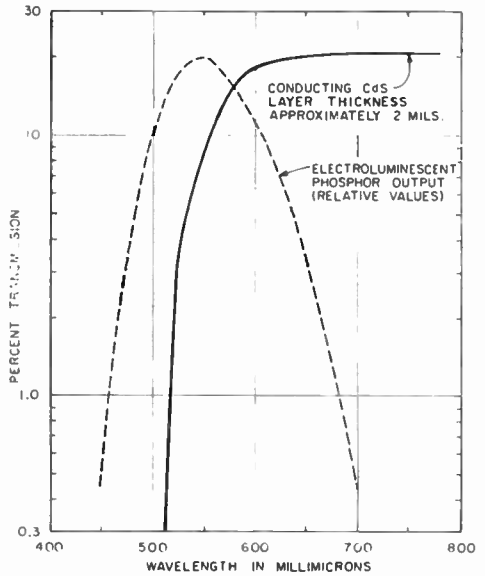

Fig. 14—Spectral transmission of conducting CdS.

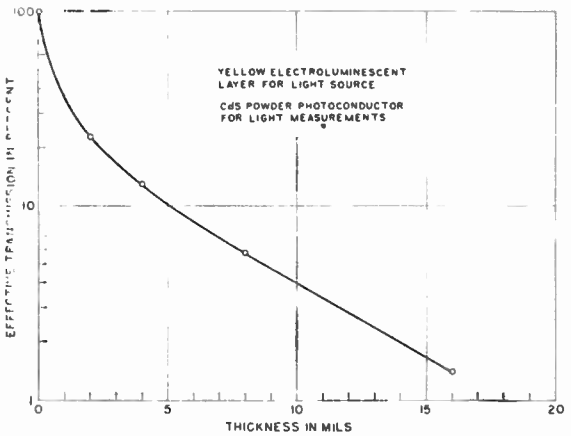

Fig. 15—Effective light transmission of conducting CdS powder as a function of thickness.

Acknowledgment

The assistance of E. G. Ramberg is appreciated in the analytical portions of the paper as well as discussions with A. Rose. The author also wishes to acknowledge the many valuable contributions of J. Bernath in the fabrication techniques.

Additional assistance was provided by J. E. Berkeyheiser in the electrical measurements, and by W. F. Davidson, Jr., in the optical measurements.

Development of High-Power Pulsed Klystrons for Practical Applications*

M. CHODOROW†, FELLOW, IRE, E. L. GINZTON†, FELLOW, IRE, J. JASBERG†, MEMBER, IRE, J. V. LEBACQZ†, SENIOR MEMBER, IRE, AND H. J. SHAW†, MEMBER, IRE

Summary—**This paper describes the development of three practical, sealed-off, tunable klystrons intended for operation in the region of 1 to 2 megw at the *S*, *L*, and *X* radar frequency bands. These tubes are an outgrowth of the previous development at Stanford of a 30-megw *S*-band klystron in conjunction with the billion-volt linear electron accelerator program. Similar design principles apply to all of these tubes, but the three smaller klystrons described make use of cavity tuning methods appropriate to the three frequency bands.**

Introduction

THE PROGRAM of klystron research and development which was started in 1947 at the Microwave Laboratory, Stanford University, had two principal objectives. The first of these was a basic interest in exploring further klystron possibilities, and the second was a specific attempt to develop a high-power klystron which could be used as a radio frequency power source for a large linear electron accelerator which was then under consideration. There existed the possibility that, should a more adequate understanding of the basic principles of pulsed, high-power generation by klystrons be obtained, a class of tubes might evolve which would be suitable for use as radar transmitting sources. These would be power amplifiers, rather than oscillators, since it had become apparent that the satisfactory operation of certain classes of radars would depend upon a stable output frequency which could be controlled by accurate low-frequency elements such as crystals.

The previous development program, which had resulted in a 30-megw klystron, is described in an earlier paper [1]. A summary of the operating characteristics of the 30-megw tube is given in Table I. This tube, when operated at a beam voltage near 400 kv, is capable of 30 megw peak power output at an efficiency approaching 43 per cent. At the present time, this accelerator klystron is continuously pumped, although several experimental tubes have been sealed off, with inconsistent results. In operation during the past five years, these tubes have had an average life of approximately 1500 hours. Fig. 1 shows a simplified assembly drawing of this tube; the reader is referred to the reference cited above for additional details.

TABLE I

OPERATING CHARACTERISTICS OF THE STANFORD 30-MEGW KLYSTRON

Operating frequency	2857 mc
Tuning range	100 mc
Heater power	650 watts
Typical beam voltage	325 kv
Typical beam current	185 amperes
Power gain	35 db
Efficiency	33 per cent
Power output	20 megw

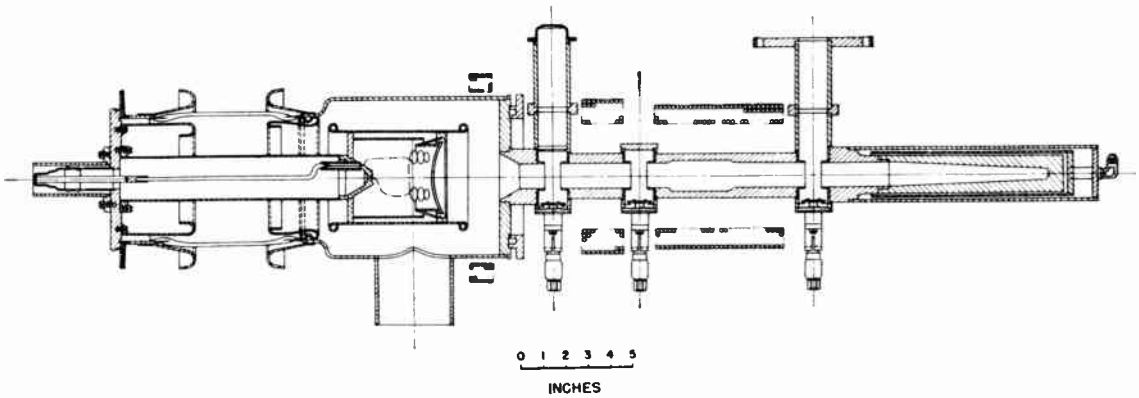

Fig. 1—Simplified assembly drawing of 30-megw accelerator klystron.

Prior to completion of the accelerator klystron program, an interest developed in scaling the 30-megw tube to lower power in order to provide an amplifier suitable for testing in radar systems. A project was initiated at the same frequency, *S*-band, with tentative specifications calling for a sealed-off tube having a peak output power of approximately 1.5 megw, maximum beam voltage of 90 kv, and an electron gun of microperveance 2. Several such *S*-band tubes were built and tested, with results which adequately met design specifi-

* Original manuscript received by the IRE, July 14, 1958; revised manuscript received, October 27, 1958. The research reported in this document was supported jointly by the U. S. Army Signal Corps, the U. S. Air Force, and the U. S. Navy (Office of Naval Research and the Bureau of Ships).

† Microwave Lab., W. W. Hansen Labs. of Phys., Stanford University, Stanford, Calif.

cations. This satisfactory tube stimulated interest in developing power amplifier klystrons for other wavelengths, and several projects were established for this purpose, and also to investigate the related subjects of wider tuning range, increased efficiency, and other aspects of tube design associated with radar system requirements.

Although the three tubes described here are quite similar in over-all design and performance, certain central problems were peculiar to the development of each. At the start of the 1 megw *S*-band program in 1949, there had been previous work on only two other klystrons in the megawatt range (both continuously pumped): the 30-mw *S*-band tube described above, started early in 1947; and a 2- to 4-megw tube at Sperry Gyroscope Company, the SAL 36, which was started somewhat later, and which was also successful. However, there were not in existence any megawatt klystrons of a nonexperimental variety which could be conveniently operated outside of the laboratory in experimental systems to evaluate whether sealed-off klystrons of this kind would have satisfactory characteristics. The only sealed-off klystron of this kind available prior to this was a 30-kw tube developed during the war. The *S*-band tube demonstrated that the problems associated with sealing off a high-power klystron (window life, gas evolution, brazing techniques, etc.) could be adequately resolved. Since the *S*-band tube had a limited tuning range, the emphasis in the *L*-band program shifted to cavity-tuning methods which would permit a tuning range of approximately 10 per cent, and would be operable in vacuum, in the presence of high circulating power. In scaling up in frequency to *X* band, and consequently scaling down in physical size, the primary goal has been to achieve 1 megw peak power and approximately 1 kw average power, since pulsed amplifier tubes supplying powers of this sort are not otherwise available at this frequency.

An important problem common to the development of each of these tubes has been that of output windows. Although satisfactory windows have been devised, and techniques for extending window life have been developed, much of the window design was empirical, and the fundamental causes of window failure remain imperfectly understood to the present time.

Here then, we describe the development of these three practical, sealed-off, tunable klystrons intended for operation in the 1- to 2-megw region as transmitting sources at the *S*, *L*, and *X* radar frequency bands. These three development programs occurred chronologically in the order noted above, overlapping each other through a period of several years. We now propose, however, to consider the tubes jointly, listing together tube performance characteristics and also related development problems for both convenience and comparison. Photographs of the tubes are shown in Figs. 2 through 4.

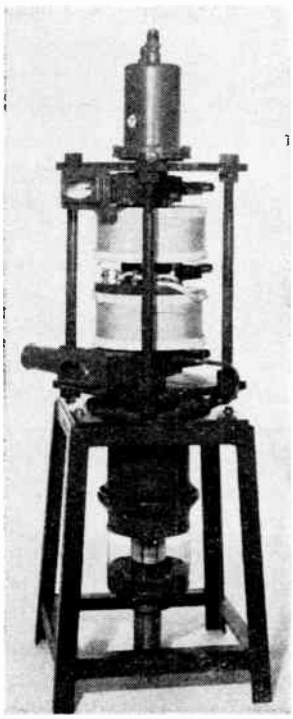

Fig. 2— *S*-band klystron.

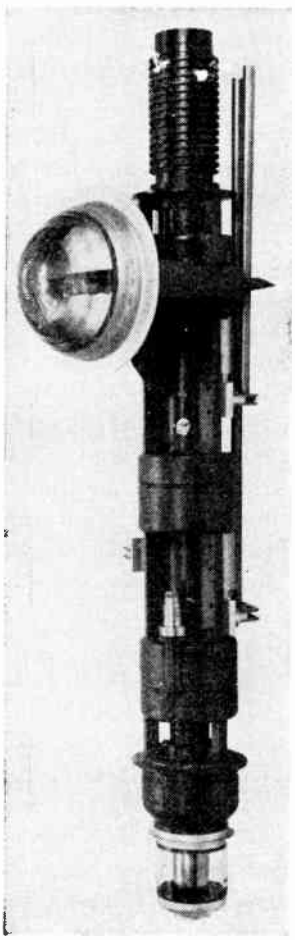

Fig. 3— *L*-band klystron.

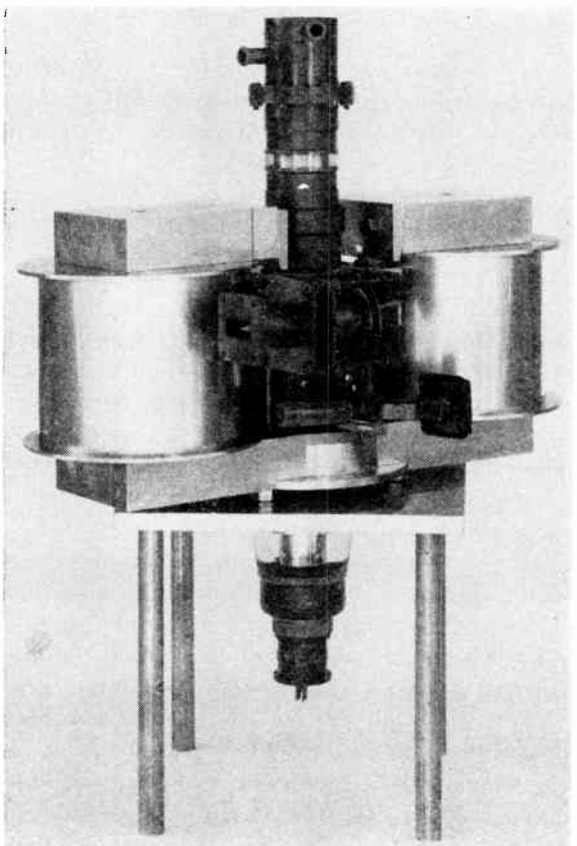

Fig. 4—*X*-band klystron.

TABLE II
DESIGN CRITERIA FOR THE *S*, *L*, AND *X*-BAND KLYSTRONS

	S	*L*	*X*
Peak power (megw)	1.5	2	1
Average power (kw)	1.5	8	1
Frequency (kmc)	2.84–2.88	1.25–1.35	8.5–9.65
Gain (db)	30	30	30
Pulse length (μsec)	2	8	0.4
pps	500	360	2500

TABLE III
KLYSTRON DESIGN PARAMETERS*

	S	*L*	*X*
Center frequency, mc	2856	1300	9000
Center wavelength, cm	10.5	23	3.3
Beam voltage, kv	100	110	120
Beam current, amp	63	73	38
Microperveance	2	2	0.93
Cathode emission density amps/cm^2	2.35	2.7	7.5
Cathode diameter, inches	2.36	2.36	1
Beam diameter, 2a, inches	0.438	0.625	0.180
Drift tube diameter, 2b, inches	0.781	1.125	0.250
Gap spacing, d, inches	0.375	0.75	0.180
Drift lengths between adjacent cavities, l, inches	4.75	9.0	1.44
Normalized drift-tube radius $(\omega/\mu_0)b$	1.08	0.69	0.94
Normalized gap spacing, $(\omega/\mu_0)d$	1.04	0.91	1.37
Normalized drift lengths, $\beta_q l$	72°	76°	40°
External Q, output cavity	35	50	100

* ω = radian frequency, μ_0 = beam velocity, and β_q = reduced plasma wave number [3].

DESIGN PROCEDURES

Objectives

The original design goals for the three tubes are listed in Table II. An efficiency of 25 per cent or higher was also a part of the tentative design specifications for each of the tubes.

Electron Beam

The original 30-megw klystron made use of a cathode with a microperveance of unity. At the start of the present program, higher perveance was desired because it appeared to have the advantage of allowing lower voltage operation, although perhaps with a slight sacrifice in efficiency. The resulting higher cathode current densities, and increased difficulties of design of a gun system with good focusing properties, were disadvantages which had to be accepted.

It was felt, however, that a microperveance of two would represent a reasonable compromise among these factors. (These remarks do not apply to the *X*-band tube, where a perveance of two would require cathode current densities which were considered excessive. A cathode with microperveance slightly less than one was designed for this tube.) The selection of the perveance, together with the required dc power input in each case, determine the operating beam voltage, values of which are shown in Table III.

Previous experience with the 30-megw klystron had shown that operation of ordinary oxide-coated cathodes at the current densities shown in Table III for the *S*-band and *L*-band klystrons, and at the peak voltages required, would be quite practical. Referring to the layout drawings in Figs. 5 and 6, the cathode consists of a "spherical" button, which, together with suitable electrostatic focusing electrodes, produces a beam which starts with the full diameter of the cathode and converges to a parallel beam with diameter shown in Table III upon entrance into the drift-tube region. The beam diameter in the drift-tube is limited by considerations of RF behavior, as will be discussed later. The purpose of the large convergence ratio between cathode area and beam area is to allow the current densities at the emitting surfaces to have the relatively low values indicated in Table III, which contribute to long cathode life.

Stipulation of the perveance and cathode area convergence ratio allowed the gun design to be completed. Electrolytic tank techniques were used, based on the design methods described by Pierce [4].

The *L*-band tube required approximately the same beam voltage and current as did the *S*-band tube; thus, the same electron gun was used. In scaling a klystron to a lower frequency, no corresponding scaling of the electron gun or beam parameters is necessary unless one wishes to also increase the operating power level. In scaling to *X*-band, the RF factors require that the beam diameter be reduced in proportion to wavelength, if the beam voltage is not changed during the scaling. In the present case, an attempt to scale the *S*-band gun directly would result in an increase in cathode emission current density by about one order of magnitude. To avoid this, a gun having lower perveance and higher beam convergence was designed, with specifications as shown in Table III. In spite of these measures, the resulting cathode emission current density was more than three times that of the lower frequency tubes. In all of the cathodes, longer operating life at the high peak emission densities was obtained by means of a roughened emitting surface produced by a nickel wire mesh spot-welded to the surface of the cathode button, or by means of nickel powder sintered on the surface. During normal operation of the tube the emission is completely space-charge limited and accurately follows the proper three-halves power law. The cathodes are heated by noninductive heaters, to reduce beam modulation resulting from magnetic field at the emission surface produced by heater current.

All the tubes use Brillouin-type focusing [4] with the cathode shielded from the magnetic focusing field by means of an iron pole-piece placed near the anode. In the *S*-band tube, focusing field is produced by two coils which are wound directly around the drift-tube sections between the cavities, so that they form an integral part of the tube. Glass-insulated wire is used to withstand the high temperatures of the bakeout cycle during processing of the tube. This system has the advantage

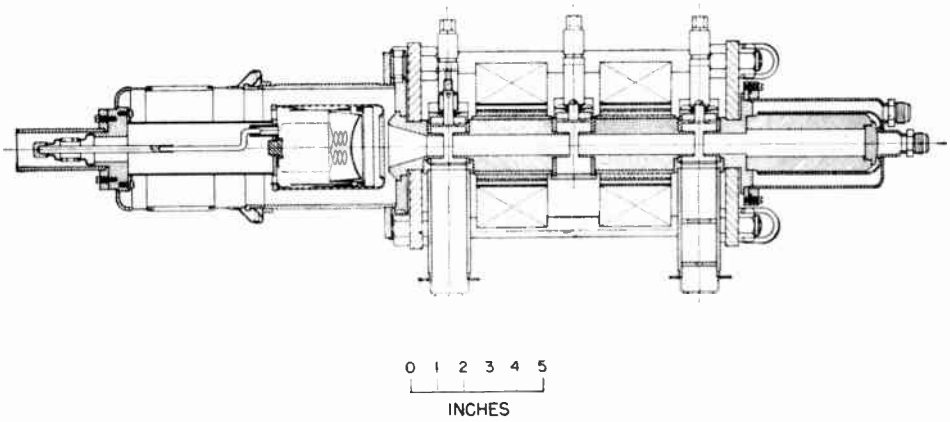

Fig. 5—Layout drawing of *S*-band klystron.

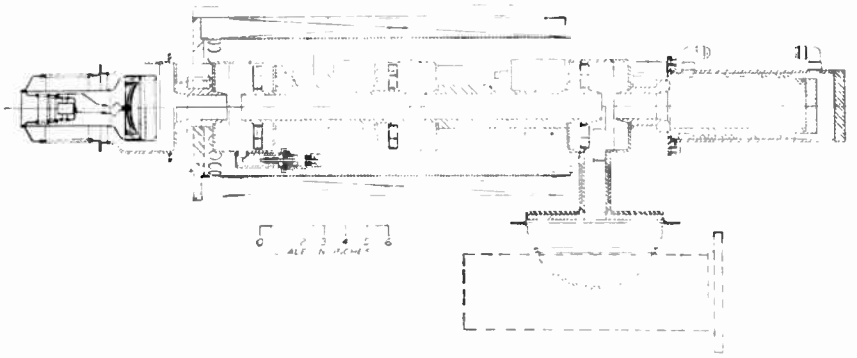

Fig. 6—Layout drawing of *L*-band klystron.

of providing minimum size and weight for the focusing system. The *L*-band tube also uses focusing coils which surround the tube axis, but which have an inside diameter large enough to allow them to be removed from the tube. This allows the focusing structure to be mounted in a system application as an integral part of the system, with replacement tubes being "plugged" into the focusing structure. Tubes may then be shipped and handled without the heavy focusing magnet attached.

The *X*-band tubes use a yoke focusing system, with the magnet coils mounted off to the side on iron cores, and with radial iron yokes to carry the magnetic flux into the beam region. This arrangement was specified for a particular system application, since it permits the tube to be inserted and removed from the side of the magnet system, rather than from the top, by separating the two halves of the yoke system at the vertical center line. The yoke focusing scheme also allows more space for the attachment of tuners and waveguide couplers to the tube cavities. It has the disadvantages of being heavier than the solenoid types, and of requiring higher focusing power in the magnet coils because of core saturation caused by leakage flux.

Radiofrequency Structure

Each of the three tubes is a three-cavity design. The use of a third cavity increases the gain attainable over that of a two-cavity tube by approximately 20 db. It is possible, alternatively, to detune the center cavity of a three-cavity tube so that the efficiency is increased, but at the expense of some of the additional gain. All cavities are of the re-entrant type with gridless gaps.

In determining the dimensions of both gap spacing and gap diameter, there are conflicting requirements. For good interaction of the electron beam with the RF field in the cavity, it is necessary that the gap diameter and the gap spacing be small compared to the distance an electron travels, per cycle. Both gap spacing and gap radius must be of the order of $\frac{1}{6}$ to $\frac{1}{3}$ of this scale factor. On the other hand, a small gap diameter complicates the electron gun design, since it restricts the diameter of the electron beam. This may be important if current density is a limiting factor. In the case of the *S*-band and *X*-band tubes, the size of the beam and the drift tubes was determined, then, by the fact that the gap diameters had some maximum permitted dimension as described above. For the *L*-band tube, however, since an existing beam made possible the use of a gap diameter smaller than the maximum permissible, this smaller diameter was used, presumably with some improvement in the RF interaction. Gun designs for the *S*-band and *X*-band tubes were such that the beam diameter was approximately 0.75 of the drift-tube diameter, to allow for some spreading of the beam under RF conditions. For the gap spacing, the RF interaction would also re-

quire as small a distance as possible. In this case, the conflicting factor is not the problem of electron optics, but merely the fact that small gap spacing increases gap capacity and results in a reduced gain-bandwidth product [5]. The choice, then, was made in terms of the intended application of the tube. In some cases, it might be necessary to sacrifice good interaction, by making a larger gap, in order to improve capacity. This was not true in the present case.

The choice of drift distances between gaps in adjacent cavities is determined by space-charge and large-signal effects. For the first drift-tube, where the signals are small, the optimum length is determined by space charge. The velocity modulation process tends to make the electrons crowd together into regions of high density, and space-charge forces tend to prevent this. There is a natural time constant involved, which is determined by the so-called "plasma" frequency. This determines how long the electrons can drift before the space-charge forces stop the bunching. This time, together with the velocity of the electrons, determines an optimum length. This is usually stated in terms of plasma wavelength, and the optimum length is one-quarter of a plasma wavelength. In the output drift tube, there are large-signal effects present which involve the crossing of electron trajectories, and these indicate that the optimum length should be somewhat shorter. In some of these tubes, the first drift distance was actually shorter than the optimum because of physical limitations; either to reduce the over-all physical length; or, as in the case of the *X*-band tube, to reduce the length over which the magnetic focusing field must be maintained. This decrease in length for the first drift tube resulted in a slight reduction in gain, which did not affect the over-all performance appreciably. Values for the present tubes are shown in Table III.

Cavity Design

As has been stated previously, the basic RF design for these tubes was similar to that used in the accelerator klystron. However, for the *L*- and *X*-band tubes there were requirements of rather wide tuning range. This involved the problem of building a tuner which could operate in a vacuum, without spurious resonances, and with relatively high circulating power in the cavity. Some of the details of these tuners are interesting. We consider first the *S*-band tube, and then the more sophisticated tuners used in the *L*- and *X*-band tubes.

The cavities of the *S*-band klystron are similar to those of the earlier 30-megw klystron, with the various dimensions reduced for lower voltage operation. This tube was designed for essentially fixed-frequency operation. The cavities are provided with a limited tuning range of approximately 30 mc, which is used for trimming. One end wall of each cavity is fitted with a flexible diaphragm, just as in the earlier tube, which allows the effective position of the wall to be moved by a small amount.

The *L*-band cavities utilize a ring tuner [6], which consists of a metal toroid surrounding the drift tube within the cavity, and which can be moved axially. The toroid is of hollow cross section to reduce its weight. The general features may be seen in the layout drawing of Fig. 6. It is mounted at one side on a circular metal rod, which extends out through a hole in one of the cavity end plates, and an external metal bellows is used to obtain a vacuum-tight seal. The support rod slides on tungsten wire springs located just outside the cavity wall, which maintain electrical contact between the rod and the cavity wall and prevent electromagnetic coupling between the main cavity and the cavity formed by the bellows section.

The ring tuner is basically an *LC* tuner; as the ring is moved axially from a position close to the bottom plate of the cavity to a position close to the interaction gap, both the inductance and capacitance of the cavity are increased, resulting in a lowering of the resonant frequency.

The ring tuner has favorable symmetry with regard to the gap field geometry. Also, by suitable adjustment of the inductance and capacitance tuning rates, it is possible to obtain a linear curve of cavity tuning vs ring position. In the design of such tuners, care must be taken to avoid resonances of the tuner ring within the tuning range of the tube, the lowest of such resonances occurring at a frequency for which the ring circumference is approximately one-half wavelength. Also, when operating the klystron at its full average-power level, precautions are necessary to avoid overheating of the rings in the center and output cavities, which may detune the cavities due to thermal expansion of the ring structure.

The *X*-band klystron [7] employs a circular plunger which moves in a hollow cylinder entering the cavity radially from one side, as may be seen in the insert drawing of Fig. 7. The diameter of the cylinder is such that it constitutes a waveguide operating below its cut-off frequency, and the plunger acts on the cavity *H* fields which fringe into the cylinder. The face of the plunger is fitted with projections which extend into the interior of the cavity, and which increase the tuning range by displacing magnetic field within the interior of the cavity. A cylindrical choke joint is included just behind the plunger face, followed by a sliding contacting mechanism. The latter is composed of tungsten wire helices, located in a circumferential slot in the body of the plunger, and compressed into the space between the plunger and the surrounding cylinder. This is based on a design developed at Litton Industries, San Carlos, Calif. It provides a self-centering mechanical bearing which guides the plunger concentrically within the cylinder, and also provides a sliding electrical contact which prevents the coupling of RF fields into external regions beyond the plunger assembly. The choke joint reduces the magnitude of RF current which must be carried by the tungsten spring contacts. An external

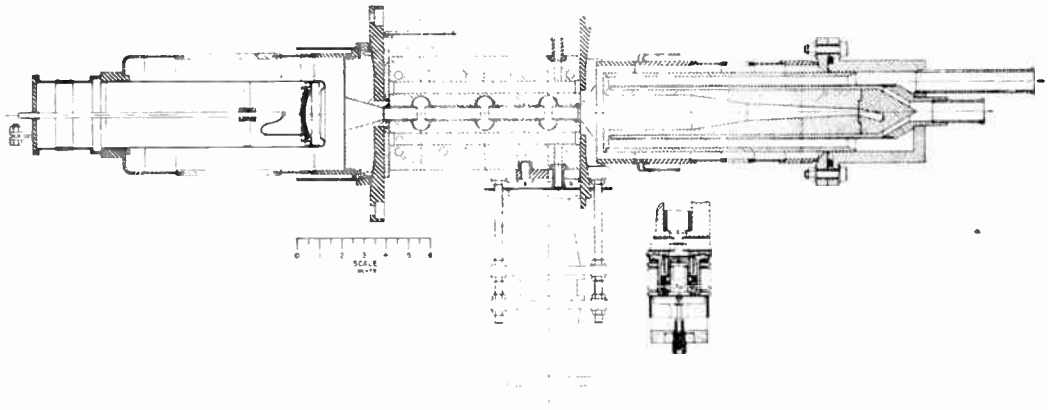

Fig. 7—Layout drawing of X-band klystron.

vacuum-tight bellows section surrounds the entire mechanism. The tuning curves for the tuner as shown have curvature, but curves which are linear over a frequency range of 15 per cent have been obtained by reshaping the projections which extend from the plunger face. In the design of plunger tuners, care must be taken to avoid the introduction of circumferential asymmetries in the gap field when the plunger is at its innermost position.

An advantage of the present tuner is the effective way in which it can be cooled: the plunger has large cross-sectional area, even when designed for the X-band wavelength, with adequate space to circulate water through the interior to cool the inside plunger face directly. This is of considerable importance in view of the high density of average RF power in the X-band klystron. The difficulty arising from heating in tuning mechanisms is not that of destruction due to excessive temperatures, but rather detuning of the cavity as a result of thermal expansions due to small temperature increases. The present tubes have been operated at average RF power output up to 2 kw and no evidence of frequency drift has been observed.

All tubes have waveguide outputs, with the output cavities being coupled to the waveguide by means of an aperture. In some cases, there are additional elements beyond the aperture in the waveguide, which perform impedance-transforming functions. The combination of these, and the aperture, determines the coupling between the waveguide and the cavity, and, for any given impedance in the waveguide, also determines the impedance presented to the beam at the output gap. The coupling, then, must be adjusted so that, with a matched load in the waveguide, the optimum impedance for best efficiency is presented at the interaction gap. For optimum conditions, the RF current driving the output cavity is approximately equal in magnitude to the dc beam current. Consideration of the interaction will then indicate that the RF impedance required at the output gap to extract maximum power from the beam is one which will produce an RF voltage at this gap equal to the dc beam voltage. Under these conditions, most of the electrons in going through the gap will be brought almost to rest and deliver a major portion of their energy to the RF fields. A higher impedance will result in a higher voltage, and some of the electrons will be turned back with a consequent loss of efficiency. A lower impedance will result in a lower RF voltage across the gap so that many of the electrons get through without having delivered their maximum energy to the field. The requirements can be stated in terms of the optimum value of loaded Q, which is equivalent to stating an optimum impedance, since the ratio of the impedance to the Q is a geometric factor. It turns out that the major determining factor in the loaded Q is the external load impedance.

This corresponds to the fact that a very small fraction of the power delivered by the beam is dissipated in cavity losses. The rest is useful power delivered to the load. It is true of all such pulsed klystrons that their circuit efficiency is very large, of the order of 90–95 per cent. It is possible to specify the coupling by giving the value of Q_{ext}, which can be defined as the contribution to the loaded Q of the cavity due to a matched load in the waveguide. Under the circumstances described above, Q_{ext} will be almost the same as Q_L, the loaded Q. Table III shows values of this external Q in the present tubes.

Vacuum Windows

The design of suitable dielectric windows to transmit the power into the output line turns out to be one of the major problems in the design of high power microwave tubes. In the present series of tubes, the vacuum windows were one of the items requiring considerable design effort. No straightforward design procedures were available for windows which would have long life under high-power conditions, and various approaches were tried. Generally speaking, some approaches are more appropriate to one wavelength range than to another, so that the various configurations which were tried, and the final designs which were adopted, are somewhat different in design and characteristics among the three tubes being described here.

The *S*-band klystron uses windows which have been employed on high-power magnetrons, and which were obtained from Litton Industries. In the original experiments with this window, it was found that serious window sparking occurred at peak power levels exceeding 1 megw. There was evidence that this was a result of bombardment of the window by electrons whose source was not definitely known, but which were probably originating at the electron beam in the output gap region. This difficulty was eventually overcome by inserting two metallic irises between the output gap and the window, which together provided complete geometrical shadowing between the window and the interior of the klystron. With this modification, the serious sparking no longer occurred, and the tube could be operated at higher power levels. A version of this geometrical shadowing has been used in the Stanford accelerator klystrons, and has since become, to some extent, standard practice.

The *L*-band and *X*-band tubes require broad-band windows to accommodate the tuning bandwidth of the tubes. This presents little difficulty with regard to input windows, where the power levels are low. The *L*-band tube uses a coaxial ceramic input window, while the *X*-band tube employs a commercial assembly [8] consisting of a thin sheet of mica sealed by means of a glass bead to a standard waveguide flange.

The output window used on the *L*-band tube consists of a glass dome approximately 6 inches in diameter. This configuration is able to withstand the force due to air pressure over the large window area necessitated by the long operating wavelength. The waveguide and coupler geometry provide geometrical shadowing between the window glass and the interior of the tube. As with the *S*-band tube, this arrangement allowed an increase in peak power output, as influenced by window sparking, by a factor of about 2. The glass dome is designed to project directly into standard *L*-band rectangular waveguide in the external circuit, through a hole in the broad side of the waveguide. A shorting plane in the external waveguide, a short distance to one side of the window, completes the transition from tube to standard waveguide.

A ceramic cone output window is used on the *X*-band tube. The first use of cone windows on klystrons appears to be due to the Sperry Gyroscope Company [2]. With windows of this type, a wide-band impedance match is obtained by designing the cone as a tapered section whose length, compared to the guide wavelength, is appreciable. This approach becomes attractive at the shorter wavelengths, such as employed in this tube, since a taper which is relatively gradual in terms of guide wavelength can be obtained with a structure of reasonable dimensions. In the present tube, the window is offset from a direct line into the tube by a 90° bend in the output waveguide, which provides geometrical shielding between the window and the output gap of the tube. The short operating wavelength restricts the dimensions of the window (diameter approximately one inch), so that high peak power density and average power density become problems. The present window has proved quite capable of handling these power densities. The dimensions of the present window system are such that high-Q resonances can exist in the window assembly, which can result in sparking at one or two discrete points in the operating pass bands. These resonances are excited only through accidental asymmetries in the window assembly, which makes careful alignment desirable.

Miscellaneous

All tubes are operated with the cathode high-voltage seal under oil, to assist in standing off the high (approximately 100 kv) cathode-anode potential. Lead shielding is used around the beam collector and other portions of the tube to reduce to safe limits the *X* radiation caused by the high-voltage electrons. Water cooling is used on the collectors of all tubes, the water being circulated at high velocity close to the active beam-collecting surfaces. Water cooling is also used on the magnetic focusing coils. In the *X*-band tube, water is also circulated through passages milled in the RF block to cool the cavities and drift-tube regions, and is also circulated through the cavity tuning plungers on the second and third cavities.

Tube Performance

The RF performance obtained with the three types of tubes, at nominal operating beam voltages, is summarized in Table IV. Reference to the original design goals will indicate that the actual performance has in all cases equaled or exceeded the goals.

TABLE IV

Klystron Performance Compared with Original Design Goals

	S Band		*L* Band		*X* Band	
	Goal	Performance	Goal	Performance	Goal	Performance
Beam voltage (kv)	100	100	110	110	120	120
Beam current (amp)	60	60	70	70	40	38
Peak power output (mw)	1.5	2	2	3.2	1	1.2
Average power output (kw)	1.5	2	8	8	1	2
Gain (db)	30	38	30	37	30	37
Efficiency (per cent)	25	35	25	35	25	30 [9]

Various detailed characteristics of the performance of the tubes are illustrated in Figs. 8 through 14. Fig. 8 shows the power output, efficiency, and power gain as a function of beam voltage for the *S*-band and *L*-band tubes. These two tubes have the same nominal cathode perveance, so that the dc power input for a given beam voltage is the same in both cases. It is clear that these tubes have nearly identical RF behavior, since the curves are substantially continuous in going from the

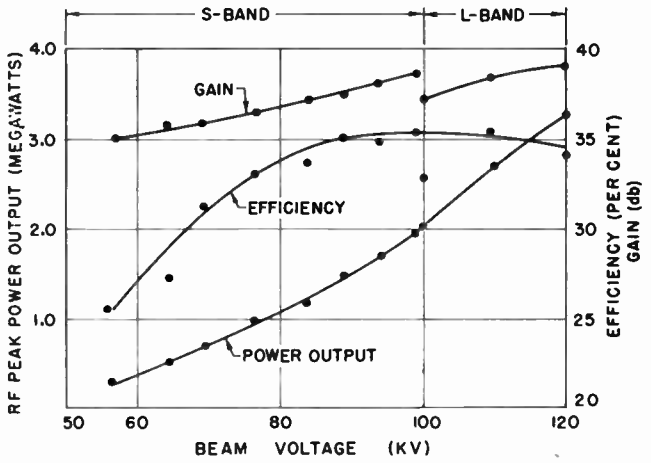

Fig. 8—Power output, efficiency, and power gain as a function of beam voltage for *S*- and *L*-band tubes.

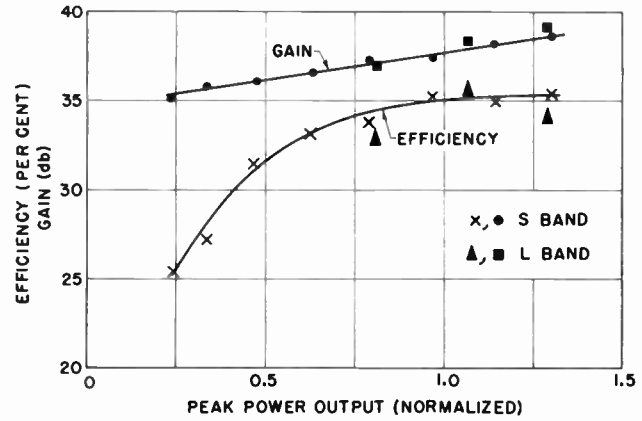

Fig. 9—Efficiency and power gain replotted as functions of RF power output for *S*- and *L*-band tubes.

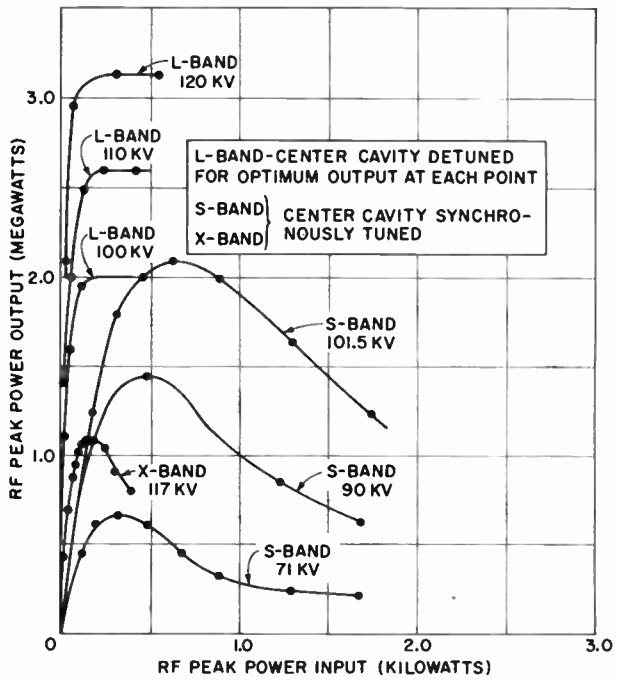

Fig. 10—Saturation curves for the three tubes.

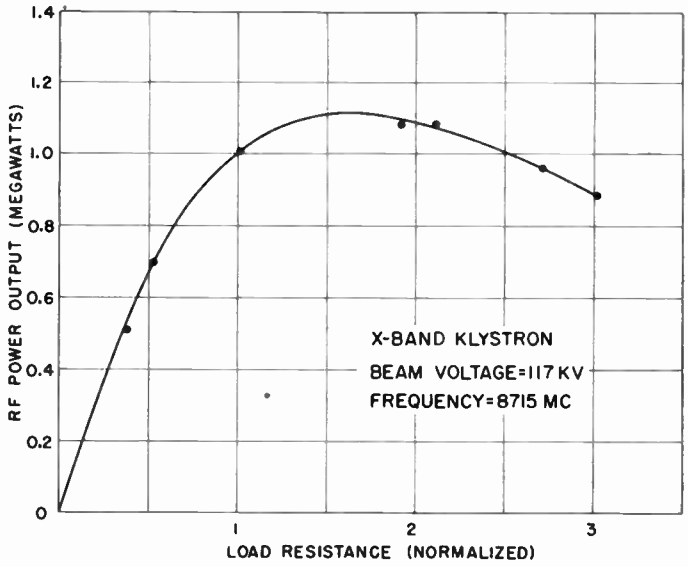

Fig. 11—Dependence of power output upon load resistance, *X*-band tube.

operating voltage region of the *S*-band tube into the operating voltage region of the *L*-band tube. The break in the gain curve is trivial, since, as will be seen below, a 20 per cent change in drive power produces virtually no change in power output. The curves indicate that the power output rises rapidly as the voltage is increased, as one would expect, and that the efficiency goes through a broad maximum near the operating voltage. In Fig. 9, the efficiency and power gain are replotted as functions of RF power output. In this case, power output has been normalized to the design value, which is 1.5 megw for the *S*-band tube, and 2 megw for the *L*-band tube. Again, the points for the two tubes are seen to fall, quite closely, on the same curves.

Fig. 10 gives saturation curves for the three tubes, showing RF power output as a function of RF drive power. The curves for the *S* and *X*-band tubes were taken with all cavities synchronously tuned to the frequency of the input signal. In these cases, the power output is seen to rise to a maximum value and then gradually decrease as the input power is increased. For the *L*-band curves, the center cavity was retuned for maximum power output at each value of RF drive power, and in this case the power output rises to a maximum value and thereafter remains at that value as the drive power is increased.

All of the klystrons are designed to deliver optimum power output when operating into a load impedance which is matched to the characteristic impedance of the output waveguide. A mismatched load, resulting in a standing wave on the output waveguide, will result in decreased power output. The dependence of output on load impedance is, however, a slow one, as is illustrated by the typical curve of Fig. 11. This curve illustrates the dependence of power output upon load resistance for the *X*-band klystron. It is seen that a two-to-one change in load resistance, centered on the optimum

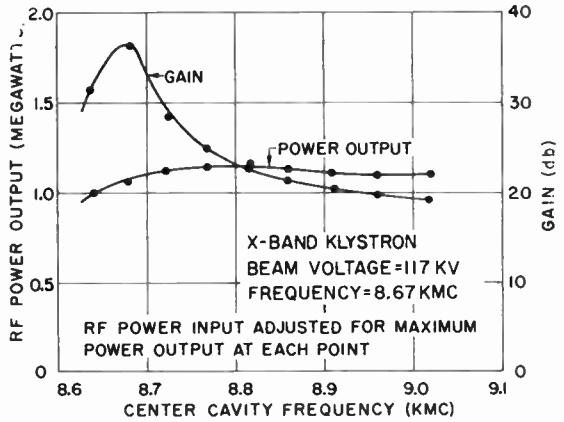

Fig. 12—Power gain and power output as a function of center cavity tuning, *X*-band tube.

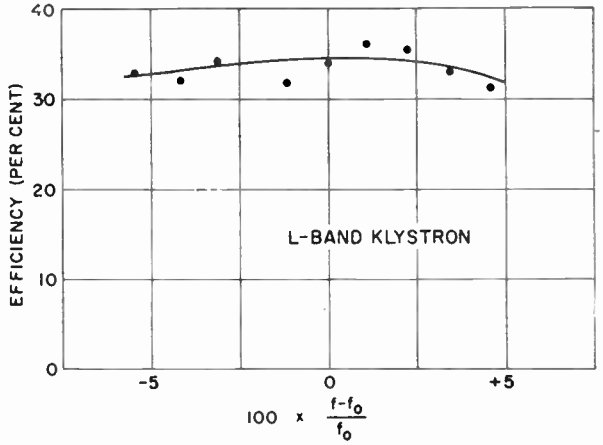

Fig. 13—Efficiency as a function of frequency (normalized), *L*-band tube.

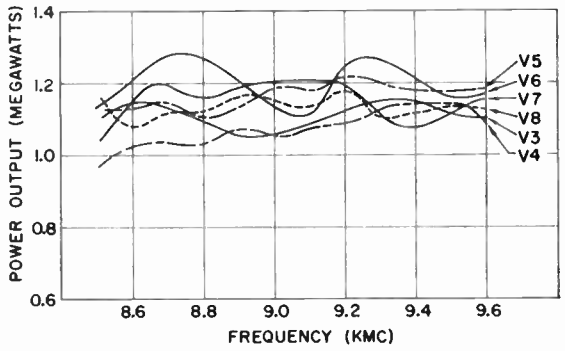

Fig. 14—Power output vs frequency for six models of the *X*-band klystron.

value, will produce a power output change of the order of only 10 per cent. This insensitivity to load variations is characteristic of klystrons and is very important in some applications. It also allows latitude in tube design. For example, the output cavity may be designed for a low value of loaded Q to obtain bandwidth without seriously affecting power output and efficiency.

In three-cavity klystrons of the type being considered the maximum power gain results from tuning all cavities to resonance at the frequency of the input signal. However, enhancement of the power output and efficiency, at the expense of power gain, may be achieved by detuning the center cavity on the high-frequency side of resonance. This is illustrated by the curves of Fig. 12, which show power gain and power output as a function of the resonant frequency of the center cavity for the *X*-band tube operating at a fixed frequency within its tuning range. In this case, with the center cavity detuned about 1.5 per cent above synchronous frequency, an increase in power output of about 15 per cent is obtained, with a simultaneous reduction of about 12 db in power gain.

The *L* and *X*-band tubes, which are tunable over frequency ranges in excess of 10 per cent, are designed to have substantially constant power output over the tuning band. In practice, the output is constant within less than 1 db. This is illustrated for the *L*-band tube in Fig. 13, where efficiency, which is proportional to power output since the dc power input is constant, is shown as a function of normalized frequency across the tuning band. Fig. 14 presents curves of power output vs normalized frequency across the tuning band for six models of the *X*-band tube, indicating both constancy of power output vs frequency and also the tube-to-tube variations of power output experienced on a series of models of the same design.

Conclusions

This paper has described the Stanford experience in the development of a series of tunable klystrons for the megawatt power range. The performance of these tubes represents nearly the optimum which can be achieved with three-cavity design, except in the matter of efficiency. With regard to efficiency, these tubes would be rated as good according to the present state of the art, although high-power klystrons with higher efficiencies exist. For example, Eimac klystrons operating in the *L*-band region have shown efficiencies in excess of 50 per cent. The power gain, while adequate for many purposes, is nevertheless limited to the values shown only by reason of the choice of three-cavity design. For example, Varian Associates' V-87 2-megw klystron, which stemmed from the *S*-band klystron described in this paper, uses four cavities to obtain 60 db power gain. Still higher power gains, through the use of a larger number of cavities, are possible.

Acknowledgment

The authors wish to express their appreciation for the important contributions of the following people to the development of the three tubes reported here: in the *S*-band work, E. J. Nalos and R. H. Winkler, who supervised much of the design and construction of the *S*-band tube. In the *L*-band work, B. G. Ryland, E. Goldfarb, and V. Varenhorst. In the *X*-band work, J. A. Snyder, who supervised the mechanical design and fabrication of the *X*-band tube; S. Sonkin, D. K. Winslow, B. G. Ryland, V. W. Dryden, J. Fitch, and E. Goldfarb.

BIBLIOGRAPHY

[1] M. Chodorow, E. L. Ginzton, I. R. Neilsen, and S. Sonkin, "Design and performance of a high-power pulsed klystron," PROC. IRE, vol. 41, pp. 1584–1602; November, 1953.
[2] J. E. Shepherd, "Harnessing the electron," *Sperry Eng. Rev.*, vol. 10, pp. 2–18; March/April, 1957.
[3] L. T. Zitelli, "Space-Charge Effects in Gridless Klystrons," Microwave Lab., Stanford University, Stanford, Calif., Rep. No. 149; October, 1951. The symbol δ' is used for the reduced plasma wave number in this reference, rather than the more usual β_q.
[4] J. R. Pierce, "Theory and Design of Electron Beams," D. Van Nostrand Co., Inc., New York, N. Y., 2nd ed., pp. 152–159; 1954.
[5] Small gap spacing may also lead to multipactoring (heavy secondary electron loading, which dissipates energy).
[6] Litton Industries, San Carlos, Calif., participated jointly with Stanford in the development of the *L*-band tube. In particular, much of the work which led to a successful tuner for this tube was done by P. Crapuchettes of Litton Industries.
[7] Varian Associates, Palo Alto, Calif., participated in early work on the *X*-band klystron. A successful fixed-tuned megawatt *X*-band klystron was developed by L. T. Zitelli. The general cavity configurations and focusing system of the present *X*-band tube are adaptations of Varian designs.
[8] Obtained from Varian Associates, Palo Alto, Calif.
[9] With detuned center cavity, corresponding to power gain of 25 db. For synchronous tuning (power gain 37 db), efficiency = 26 per cent.

The Design of Two-Section Symmetrical Zobel Filters for Tchebycheff Insertion Loss*

W. N. TUTTLE†

Summary—**It is shown that the complete Tchebycheff insertion-loss function giving equal valley heights in the stop band and equal ripple heights in the pass band can be realized with two Zobel *m*-derived sections by suitable choice of the *m* values and the terminating resistance. The limitation in comparison with more general synthesis techniques is that for each width of the cutoff region only one Tchebycheff-Zobel filter is possible, having a fixed value of pass-band ripple. The ripple levels obtained, however, are in the range of interest and the filters are of practical value. Data are given in chart and tabular form so that the design procedure is very simple. The results show that prototype sections do not appear in the optimum designs, and that terminating half sections need not be used to obtain flat pass-band transmission.**

INTRODUCTION

A SERIOUS limitation of the Zobel image-parameter method of designing filters has been the lack of any straightforward procedure for arriving at the best choice of parameters. Not only is much cut-and-try involved in meeting a given set of specifications, but the designer has doubts, after the specifications have been met, whether he has achieved the most economical design or the one having the fewest coils. But, by using the image-parameter method, it is very easy to determine the element values after the design parameters have been selected. A few minutes with a slide rule is all that is required.

In contrast, insertion-loss methods of design provide elegant solutions to the approximation problem but involve laborious computation in the determination of the element values.

A start has now been made in simplifying insertion-loss design by the publication of tables,[1] step-by-step design procedures[2] and sets of design curves;[3] but the subject is still one for the specialist, and insertion-loss design is seldom attempted unless a full-fledged computing service is available.

Image-parameter methods seem to be in disrepute among the network theorists, partly because of the cut-and-try that is involved and partly because of restricted freedom of design. Saraga[4] has shown that in the case of a two-section filter the same critical frequencies can be achieved by image-parameter methods as by the general insertion-parameter synthesis, but that the multiplying factor in the expression for the loss can no longer be chosen freely. This restricts the range of designs available to meet given specifications. The practical significance of this limitation, however, does not seem to have been adequately explored. Also, very little seems to have been done in applying the results of modern theory to improve the image-parameter design procedure. It would be very useful to know how good a Zobel filter of a given configuration can be made and how an optimum Zobel design compares with a similar design obtained by modern methods. If the Zobel filters can hold their own, there is need for new rules to arrive at the best designs to meet given specifications. If the Zobel design procedure can be brought up

* Original manuscript received by the IRE, August 14, 1958; revised manuscript received, November 17, 1958. Reprinted from 1958 WESCON CONVENTION RECORD, pt. 2, pp. 23–32.
† Gen. Radio Co., West Concord, Mass.

[1] S. D. Bedrosian, E. L. Luke, and H. N. Putschi, "On the tabulation of insertion loss low-pass chain matrix coefficients and network element values," *Proc. Natl. Electronics Conf.*, vol. 11, pp. 697–717; 1955.
[2] A. J. Grossman, "Synthesis of Tchebycheff parameter symmetrical filters," PROC. IRE, vol. 45, pp. 454–473; April, 1957.
[3] J. K. Skwirzynski and J. Zdunek, "Design data for symmetrical Darlington filters," *Proc. IEE*, vol. 104, pt. C, pp. 366–380; September, 1957.
[4] W. Saraga, "Insertion parameter filters," *TMC Tech. J.*, vol. 2, pp. 25–36; March, 1951.

to date, it might provide economical filters easy to design and adequate for most of the common applications.

As a start on this problem the present paper will compare a two-section symmetrical Zobel filter with a Darlington elliptic-function filter of order 5. Both filters employ two inductors and five capacitors in the same configuration, shown in Fig. 1. One object will be to compare the best Zobel design with the Darlington design in terms of insertion loss. Another object will be to show how the Cauer parameters used in the Darlington design can be applied to the Zobel filter to obtain Tchebycheff insertion loss without cut-and-try design methods.

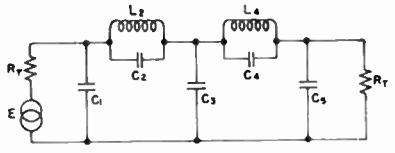

Fig. 1—Two-section filter configuration used in both Zobel and Darlington designs.

Insertion Loss of Zobel Filter

In image-parameter theory the insertion loss is usually computed as the sum of the image attenuation, the reflection loss and the interaction loss. This method is useful for computing the loss of a filter whose constants have been determined, but it is not convenient for showing how the insertion loss varies with the choice of parameters. It is possible, however, to obtain complete insertion loss formulas for multisection image-parameter filters in analytic form suitable for study. Saraga[5] has computed the equivalent lattice-arm reactances for various multisection Zobel filters for use in insertion-loss computations by means of charts or a special slide rule. Complete insertion loss formulas can also be computed from Saraga's expressions.

For the case of two m-derived sections in the circuit of Fig. 1, Saraga gives the following formulas:

$$u = X_x/R_t = -r\,\frac{m_1 + m_2}{1 + m_1m_2}\,\frac{x}{x^2 - \dfrac{1}{1 + m_1m_2}} \tag{1}$$

$$v = X_y/R_t = -r\,\frac{1 + m_1m_2}{m_1 + m_2}\,\frac{x^2 - \dfrac{1}{1 + m_1m_2}}{x(x^2 - 1)} \tag{2}$$

where

X_x is the series-arm lattice reactance
X_y is the diagonal-arm lattice reactance
R_t is the resistance of generator and load
R is the design resistance of the filter sections
m_1 and m_2 are the m values of the two Zobel sections
f_c is the image-parameter cutoff frequency
$r = R/R_t$
$x = f/f_c$.

The insertion loss in terms of the lattice reactances is given by the formula

$$L = 10\log_{10}\left[1 + \left(\frac{1 + uv}{u - v}\right)^2\right] = 10\log_{10}\left[1 + E^2\right]. \tag{3}$$

The quantity E can be computed directly from (1) and (2):

$$E = \frac{-(m_1 + m_2)(1 + m_1m_2)}{r(1 - m_1^2)(1 - m_2^2)}\,\frac{x[x^2 - (1 - r^2)]\left(x^2 - \dfrac{1}{1 + m_1m_2}\right)}{\left(x^2 - \dfrac{1}{1 - m_1^2}\right)\left(x^2 - \dfrac{1}{1 - m_2^2}\right)}. \tag{4}$$

This expression, also obtained by Saraga,[4] not only makes it possible to compute readily the complete insertion-loss characteristic of the filter, but it also gives the location of the poles and zeros. The two peaks of infinite stop-band loss appear in familiar form as the two factors in the denominator. It will be noted that for $r<1$, there are two finite zeros in the pass band, one determined by the product of the m values and the other determined solely by r, the ratio of the design resistance to the terminating resistance. For unity ratio, which is frequently employed, this second pass-band zero moves back to zero frequency. The equation is valid if one or both of the sections is of the constant-k type, corresponding to $m=1$. The expression for E shows, as it must, that if either m is given the value unity, then the corresponding stop-band loss peak moves to infinite frequency. For two constant-k sections both m's are equal to unity and the pass-band zero determined by the m's occurs at 0.707 times the cutoff frequency.

The most interesting possibility indicated by (4) is that of controlling the pass-band ripple by proper choice of the design resistance relative to the terminations. The zero determined by r can be located freely, without regard to the other design constants, at the point in the pass band which gives the minimum ripple. This is the point which makes the two ripple peaks of equal amplitude.

This is illustrated in Fig. 2, where the solid curve shows the single pass-band zero and single ripple occurring when the design resistance is made equal to the terminating resistance. The dashed curve shows what happens when the terminating resistances are increased twenty per cent, corresponding to $r=0.833$ for the particular design illustrated. A second pass-band zero is brought in at $\sqrt{1-r^2}$, or at 0.553 times the cutoff frequency. This reduces the ripple amplitude more than

[5] W. Saraga, "Insertion loss and insertion phase shift of multisection Zobel filters with equal image impedances," *P.O. Elec. Eng. J.*, vol. 39, pp. 167–172; January, 1947.

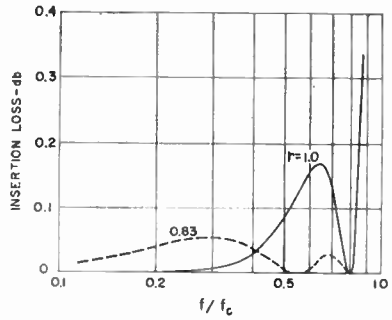

Fig. 2—Pass-band insertion loss of two-section Zobel filter showing the reduction of ripple from changing r, the design resistance ratio.

three to one, and the termination is not yet optimum. If the terminating resistance is made about 17 per cent greater than the design resistance, rather than 20 per cent, the two ripples can be made equal and the amplitude reduction is then more than four to one.

It is evident, then, that the pass-band ripple can be controlled by selecting the terminating resistance in much the same way that the stop-band peaks and valleys can be controlled by choice of the m values. If the filter specification is in terms of maximum pass-band ripple and minimum stop-band loss, the optimum design for a given width of the transition region is evidently the one for which the two m values are selected to give equal stop-band valley heights and the design resistance is selected to give equal pass-band ripples. When this is done the characteristic will appear as in Fig. 3. Here α_p is the pass-band ripple amplitude and α_a is the stop-band valley height. The end of the pass band is indicated as f_1 and the beginning of the stop band as f_2. It will be shown that the Cauer parameters used in the Darlington elliptic-function design can also be used to determine the constants of two-section symmetrical Zobel filters to obtain this desirable Tchebycheff type of response.

Characteristics of the Darlington Elliptic-Function Filter

For the present purpose only the results of the approximation part of the Darlington synthesis need be considered. The reader interested in the underlying theory is referred to Darlington's original work[6] or to the tutorial review included in Grossman's paper.[2] For the two-section, symmetrical, low-pass filter, the performance characteristics of the Darlington design can be concisely stated, without bringing in complex-variable theory. The quantity E of the insertion-loss function, (3), is given by:

$$E = \frac{Hy(y^2 - a_2^2)(y^2 - a_4^2)}{a_2^2 a_4^2 \left(y^2 - \frac{1}{a_4^2}\right)\left(y^2 - \frac{1}{a_2^2}\right)} \qquad (5)$$

[6] S. Darlington, "Synthesis of reactance 4-poles which produce prescribed insertion loss characteristics," *J. Math. Phys.*, vol. 18, pp. 257–353; September, 1939.

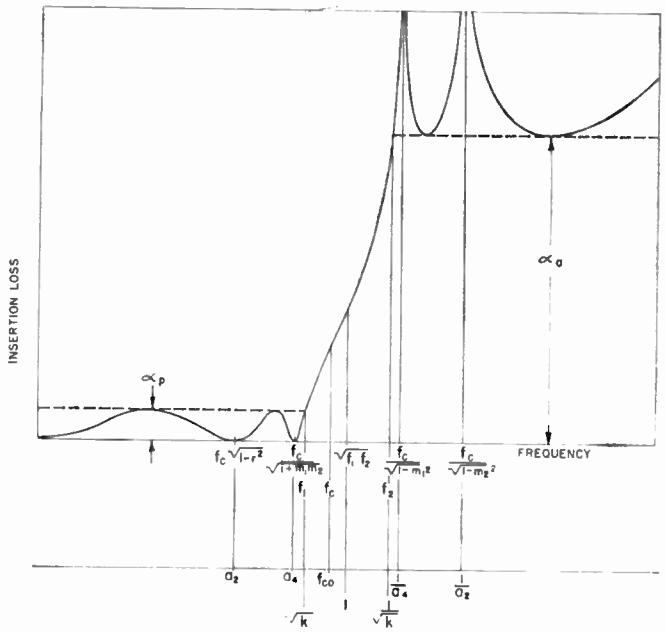

Fig. 3—Filter characteristic showing Zobel design frequencies on the first line, and normalized Darlington design frequencies on the second line.

where $y = f/\sqrt{f_1 f_2}$, the ratio of the frequency to the mid-frequency of the cutoff region. In (4) for the Zobel filter, the variable x is the ratio of the frequency to the image-parameter cutoff frequency. The two reference frequencies are in general different. It will be noted from (5) that the elliptic-function filter gives two finite second-order zeros and two finite second-order poles, just as does the Zobel filter, but in this case the poles are reciprocally related to the zeros about the mid-frequency of the cutoff region. The width of the cutoff region determines the modulus k of the elliptic-function design. For each value of k the parameters a_2 and a_4 in (5) can be determined which will give the complete Tchebycheff insertion-loss function. Because of the reciprocal relationship only two numbers are required.

The quantities a_2 and a_4 are known as Cauer parameters because of their early use by him.[7] This was not in insertion-loss design but in the design of filters with Tchebycheff approximations to constant pass-band image impedance and to constant stop-band image attenuation. These parameters have now been tabulated by Glowatzki,[8] so are conveniently available for filter design without the labor of computation. They are defined in terms of elliptic functions, as follows:

$$a_2 = \sqrt{k}\ \mathrm{sn}\left(\frac{2K}{5},\ k\right) \qquad (6)$$

$$a_4 = \sqrt{k}\ \mathrm{sn}\left(\frac{4K}{5},\ k\right) \qquad (7)$$

[7] W. Cauer, "Siebschaltungen," VDI-Verlag GMBH, Berlin, Ger., pp. 8, 20–21; 1931.

[8] E. Glowatzki, "Sechsstellige Tafel der Cauer-Parameter," Abhandlungen der Bayerischen Akademie der Wissenschaften, Neue Folge, Heft 67; 1955.

where, following the usual terminology, K is the complete elliptic integral of the first kind for the modulus k, and sn is the elliptic sine function.

The Darlington procedure permits great flexibility of design. By increasing the pass-band ripple to the maximum permitted by the application, the greatest stop-band insertion loss is obtained for a given width of the cutoff region. More rejection can be obtained at the price of increased pass-band ripple. The range of characteristics possible is shown in Fig. 4. If the pass-band ripple is held constant, the stop-band loss can be increased, as for all types of filters, by widening the transition region.

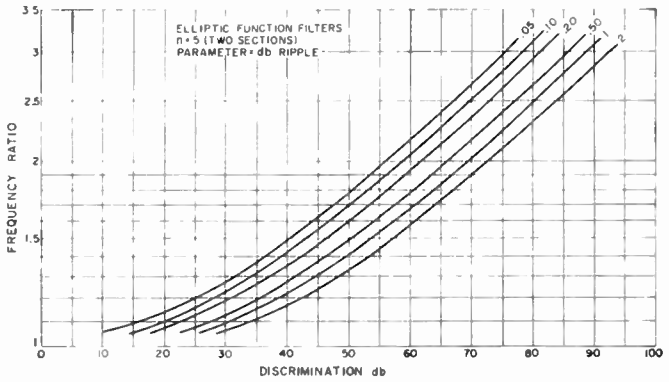

Fig. 4—Range of characteristics possible with Darlington two-section filter. The designs with higher pass-band ripple have greater stop-band insertion loss.

Design of the Zobel Filter for Tchebycheff Insertion Loss

The complete Tchebycheff insertion-loss function can be realized by the Zobel filter if the pole and zero locations of (4) can be matched to those of the elliptic function filter as given by (5). The problem is illustrated by Fig. 3 which shows the filter characteristic with the Zobel design frequencies marked on the first line and the normalized points of the elliptic function design marked on the second line. The Zobel frequencies can be brought to the elliptic-function scale by multiplying by f_{co}/f_c where $f_{co}^2 = f_c^2/f_1f_2$. The frequencies of the two designs can then be equated, giving

$$a_2 = f_{co}\sqrt{1 - r^2} \tag{8}$$

$$a_1 = \frac{f_{co}}{\sqrt{1 + m_1m_2}} \tag{9}$$

$$\frac{1}{a_1} = \frac{f_{co}}{\sqrt{1 - m_1^2}} \tag{10}$$

$$\frac{1}{a_2} = \frac{f_{co}}{\sqrt{1 - m_2^2}}. \tag{11}$$

From (9), (10) and (11) the m's can be eliminated and the image-parameter cutoff frequency can be obtained on the normalized elliptic function scale in terms of the Cauer parameters as

$$f_{co}^2 = \frac{2a_1^2 - a_1^4(a_2^2 + a_1^2)}{1 - a_2^2a_1^6}. \tag{12}$$

The m values can then be obtained from (10) and (11) in the form

$$m_1^2 = 1 - a_1^2f_{co}^2 \qquad m_2^2 = 1 - a_2^2f_{co}^2 \tag{13}$$

and the design resistance ratio from (8) rewritten as

$$r^2 = 1 - a_2^2/f_{co}^2. \tag{14}$$

It will be noted from Fig. 3 that the image-parameter cutoff frequency can be located precisely with respect to the end of the pass band by the relation,

$$f_c/f_1 = f_{co}/\sqrt{k} \qquad f_c = f_1f_{co}/\sqrt{k} \tag{15}$$

Eqs. (12) to (15) give all the parameters of the Tchebycheff-Zobel design in terms of $k = f_1/f_2$ and the two Cauer parameters a_2 and a_1, which are given as functions of k, either by (6) and (7) or in Glowatzki's tables. The design constants can be inserted in (3) and (4) and the insertion loss computed, but this is not necessary, as the additional information can be obtained directly from a third Cauer parameter, the deviation constant Δ, which is also tabulated by Glowatzki. This quantity is defined as

$$\Delta = k^{5/2}\,\mathrm{sn}^2\left(\frac{K}{5},\ k\right)\mathrm{sn}^2\left(\frac{3K}{5},\ k\right). \tag{16}$$

The additional quantities desired are α_a, the minimum stop-band loss, and α_p, the maximum pass-band ripple. These quantities in decibels are given by the following expressions:

$$\alpha_a = 10\log_{10}(1 + H^2/\Delta^2) \tag{17}$$

$$\alpha_p = 10\log_{10}(1 + H^2\Delta^2). \tag{18}$$

In the generalized insertion-loss design, the constant H can be freely chosen according to (18) to correspond to the maximum acceptable pass-band ripple. This value of H inserted in (17) then gives the minimum stop-band loss that will be obtained for the selected value of ripple. In the Zobel design, however, H can have only one value for a given value of k. This value can be determined by bringing (4) to the frequency scale of (5) by substituting $x = y/f_{co}$, giving

$$E = \frac{-(m_1 + m_2)(1 + m_1m_2)}{rf_{co}^5} \cdot \frac{y(y^2 - a_2^2)(y^2 - a_4^2)}{a_2^2a_4^2\left(y^2 - \frac{1}{a_4^2}\right)\left(y^2 - \frac{1}{a_2^2}\right)} \tag{19}$$

where the alternative expressions for the critical frequencies have been taken from (8) to (11). H can then be evaluated by comparing (19) with (5), giving,

$$H = \frac{(m_1 + m_2)(1 + m_1m_2)}{rf_{co}^5}. \tag{20}$$

TABLE I

DESIGN DATA COMPUTED FOR VARIOUS VALUES OF $\theta = \sin^{-1} f_1/f_2$

θ	$k=f_1/f_2$	f_{co}	r	m_1	m_2	α_p	α_a	f_∞/f_1
5	0.087156	0.396292	0.898770	0.993788	0.997627	0.0175	130.118	1.34235
10	0.173648	0.556122	0.896698	0.975373	0.990585	0.0182	100.107	1.33455
15	0.258819	0.672515	0.893189	0.945396	0.979100	0.0195	82.647	1.32192
20	0.342020	0.763182	0.888148	0.904856	0.963511	0.0214	70.354	1.30498
25	0.422618	0.834970	0.881441	0.855025	0.944235	0.0240	60.908	1.28439
30	0.500000	0.891591	0.872882	0.797349	0.921713	0.0276	53.270	1.26090
35	0.573576	0.935536	0.862221	0.733350	0.896358	0.0324	46.880	1.23528
40	0.642788	0.968726	0.849127	0.664548	0.868511	0.0389	41.399	1.20828
45	0.707107	0.992778	0.833163	0.592402	0.838391	0.0476	36.604	1.18062
50	0.766044	1.00911	0.813747	0.518271	0.806044	0.0596	32.337	1.15295
55	0.819152	1.01899	0.790094	0.443404	0.771287	0.0761	28.482	1.12587
60	0.866025	1.02358	0.761110	0.368944	0.733611	0.0994	24.944	1.09991
65	0.906308	1.02395	0.725221	0.295952	0.692014	0.1332	21.647	1.07557
70	0.939693	1.02110	0.680023	0.225463	0.644667	0.1843	18.518	1.05336
75	0.965926	1.01605	0.621509	0.158555	0.588141	0.2659	15.476	1.03382
80	0.984808	1.00984	0.541926	0.096544	0.515232	0.4084	12.413	1.01760
85	0.996195	1.00375	0.421188	0.041475	0.406175	0.6722	8.875	1.00567

This expression makes it possible to calculate the maximum pass-band ripple and minimum stop-band valley height from (17) and (18) in terms of the image-parameter design constants and the deviation constant Δ taken from Glowatzki's tables or computed from (16). This completes the set of equations for determining the design constants and the performance data for Tchebycheff-Zobel filters.

The computations have been carried through at 5° intervals of the modular angle $\theta = \sin^{-1} k$, providing complete design data for 17 widths of the cutoff region. These data are given in Table I and are also plotted as functions of the minimum stop-band loss in Fig. 5.

These filters are optimum Zobel designs for the particular configuration of Fig. 1 where the specifications, as for the elliptic-function design, are in the usual terms of maximum pass-band ripple and minimum stop-band loss. Referring to Fig. 5, it is seen that 30 db of rejection can be obtained in a frequency ratio of 1.25 to 1 with a pass-band ripple of 0.07 db, or 50 db can be obtained in a ratio of 1.86 to 1 with a ripple of 0.03 db. These filters will satisfy almost any practical requirements on flat transmission, except for special applications, discussed below, where extreme flatness is required to obtain a low reflection coefficient. The fact that this performance can be obtained with the supposedly undesirable but economical constant-k impedance characteristics shows that balancing the ripple caused by reflection and interaction is very effective in securing flat transmission.

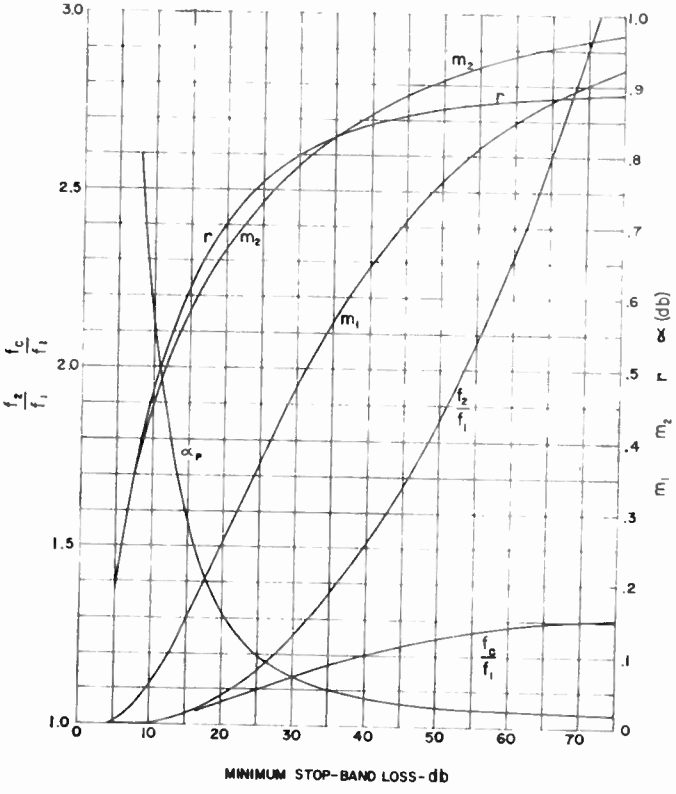

Fig. 5—Design data for two-section Tchebycheff-Zobel filters plotted against minimum stop-band insertion loss.

COMPARISON OF PERFORMANCE

It has been shown that the essential limitation of the Tchebycheff-Zobel filter in comparison with the Darlington elliptic-function design is that for the former the constant in the insertion-loss equation cannot be freely chosen. In practical terms this means that only one Tchebycheff-Zobel design is possible, having a particular level of pass-band ripple, for each width of the cutoff region. In the more general Darlington synthesis procedure, as has been shown, a range of designs is possible in which greater stop-band loss can be obtained at the price of greater pass-band ripple. If the Darlington filter is designed to have the same ripple as the Tchebycheff-Zobel filter, it will be identical with it. The Darlington design is superior only to the extent that other ripple levels than those provided by the Zobel designs are preferable. For example, if a Darlington design for 0.2 db ripple is compared with the second Zobel example given above which had 0.03 db ripple, the Darlington design will be found from Fig. 4 to give 58 db rejection instead of 50 db in the same transition interval of 1.86 to 1. In the usual practical cases, then, the virtue of the Darlington design is not that it will give flatter trans-

mission but that it can capitalize on the cases where a relatively large pass-band ripple is permissible and give greater discrimination. Putting it the other way, the fault of the Zobel design is usually not that it cannot give sufficiently flat transmission, but that the transmission is too flat and some discrimination is lost in consequence.

The situation is different when the filter must be designed for low reflection. The reflection coefficient is directly related to the insertion loss and to obtain a low reflection coefficient it is usually necessary to design the filter for flatter transmission than would otherwise be necessary. The Tchebycheff-Zobel filters with a minimum stop-band insertion loss of 40 db or more have reflection coefficients of less than 10 per cent, so they can be used in many applications where low reflection is a consideration. However they will not meet extremely severe requirements, which sometimes call for reflection factors of 5 per cent or lower.

It is concluded that the Tchebycheff-Zobel filters have intermediate values of pass-band ripple and reflection coefficient suitable for general application. The more general Darlington elliptic-function design is preferable either when maximum stop-band loss must be obtained at the expense of higher pass-band ripple, or where very flat transmission is needed to secure low reflection. Except for these extreme cases, the Tchebycheff-Zobel filters should be satisfactory, and the simplicity of the design procedure is a great advantage.

Practical Design Information

An important advantage of the image-parameter design method is that the constants usually do not have to be determined with high accuracy. If the m values vary slightly from the optimum values, there is no internal mismatch and no unexpected deviation from the desired insertion loss. This is because the sections are designed for the same image impedance, regardless of the m values. In many cases the data can be read with sufficient accuracy from the curves of Fig. 5. More accurate values, when required, can be obtained by plotting the data of Table I to a larger scale, or a design from Table I can be used directly. In the middle of the range the tabulated designs differ by about 5 db in minimum stop-band loss, so one of these designs will usually be suitable. Even where an intermediate design must be accurately computed, this can be done with only moderate labor using Glowatzki's tables and the formulas given.

Details of the design procedure will be discussed for low-pass, high-pass, and band-pass filters. It must be emphasized that the performance figures are for ideal filters with no dissipation in the elements.

Low-Pass Filters

The equations given and the data in Table I and Fig. 5 apply directly to this case. Assume the specifications to be a filter to work between 500-ohm resistances, pass frequencies up to 1000 cps, and provide at least 35 db insertion loss at 1500 cps and beyond.

Fig. 5 shows that 35 db can be provided in a frequency ratio of 1.375, so the requirements are within the capabilities of the two-section Zobel filter. Since the stop-band loss increases with the width of the transition interval, the excess performance can be used to obtain greater stop-band loss, using the entire available transition interval. Another possibility is to narrow the transition interval until the required loss is just obtained and a frequency margin provided at the end of the pass band.

The latter choice is frequently desirable because dissipation effects are most pronounced at the end of the pass band. A tabulated design giving a satisfactory compromise can usually be found where the performance of the filter exceeds the minimum requirements.

The design in Table I for $\theta = 45°$ gives 36.6 db in a frequency ratio 1.414. If the end of the pass band is taken at 1040 cps, then the design insertion loss of 36.6 db will be reached at 1471 cps and a margin will be provided at each end of the cutoff interval. The table shows that this filter will have a pass-band ripple of 0.048 db, neglecting the effects of dissipation. To achieve this performance, the m values should be 0.592402 and 0.838391, the design resistance, $R = rR_t$, should be 416.6 ohms, and the cutoff frequency should be $1040 \times 1.18062 = 1228$ cps.

The two sections can be designed from the above data and the usual Zobel formulas and the elements then combined to form the complete filter. Since the configuration is always the same, it is more convenient to use expressions for the elements of the complete filter, incorporating in them the resistance ratio r. The actual design resistance R need not then be considered, since the designer uses the formulas with the actual terminating resistance R_t.

Referring to Fig. 1, element values for the complete Zobel low-pass filter, normalized for terminating resistances of 1 ohm and for a cutoff frequency of 1 radian per second, are as follows,

$$C_1 = m_1/r = 0.71103 \text{ f}$$
$$L_2 = 2m_1r = 0.98714 \text{ h}$$
$$C_2 = (1 - m_1^2)/2m_1r = 0.65752 \text{ f}$$
$$C_3 = (m_1 + m_2)/r = 1.71730 \text{ f}$$
$$L_4 = 2m_2r = 1.39703 \text{ h}$$
$$C_4 = (1 - m_2^2)/2m_2r = 0.21266 \text{ f}$$
$$C_5 = m_2/r = 1.00628 \text{ f}.$$

These expressions differ from those for the usual Zobel filter only in the inclusion of the design resistance ratio r, which appears in the numerator for the inductances and in the denominator for the capacitances. The design is thus normalized with respect to the actual terminating resistances, rather than the design resistance of the sections.

The actual element values for terminating resistances of 500 ohms and an image-parameter cutoff frequency of 1228 cps are obtained by multiplying the capacitances by $1/R_t 2\pi f_c = 0.25921 \times 10^{-6}$ and the inductances by $R_t/2\pi f_c = 0.064803$, giving for the final design,

$$C_1 = 0.1843\ \mu f$$
$$L_2 = 0.06397\ h$$
$$C_2 = 0.1704\ \mu f$$
$$C_3 = 0.4451\ \mu f$$
$$L_4 = 0.09054\ h$$
$$C_4 = 0.05512\ \mu f$$
$$C_5 = 0.2608\ \mu f.$$

High-Pass Filters

In applying the formulas and data to this case, f_2 is taken as the end of the stop band and f_1 as the beginning of the pass band, just as in the low-pass case, and f_2 becomes the lower frequency. Then f_2/f_1 must be substituted for f_1/f_2 and f_1/f_c for f_c/f_1 in using the data of Table I and Fig. 5. Also, to use the minimum number of coils, the filter should be mid-series terminated instead of mid-shunt terminated, giving the structure shown in Fig. 6. This type of termination, however, requires that the design resistance R should be greater than the terminating resistances, rather than less. Hence r must be taken as R_t/R instead of R/R_t.

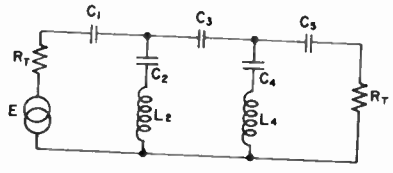

Fig. 6—Equivalent high-pass filter using two inductors and five capacitors.

A high-pass filter with characteristics similar to those of the low-pass filter just considered, but to pass 500 cps and beyond, would have the design constants

$$f_1 = 500/1.04 = 480.8\ \text{cps}$$
$$f_c = 500/1.04 \times 1.18062 = 407.2\ \text{cps}$$
$$f_2 = 340.0\ \text{cps}.$$

For this case the normalized element values of the complete filter become

$$C_1 = r/m_1 = 1.40641\ f$$
$$L_2 = 1/2m_1 r = 1.01303\ h$$
$$C_2 = 2m_1 r/(1 - m_1^2) = 1.52087\ f$$
$$C_3 = r/(m_1 + m_2) = 0.58231\ f$$
$$L_4 = 1/2m_2 r = 0.71580\ h$$
$$C_4 = 2m_2 r/(1 - m_2^2) = 4.70225\ f$$
$$C_5 = r/m_2 = 0.99376\ f.$$

It is useful to note that each element of the normalized high-pass design is the reciprocal of the like-numbered element of the low-pass design. As before, the element values for terminating resistances of 500 ohms and a cutoff frequency of 407.2 cps are obtained by multiplying the capacitances by $1/R_t 2\pi f_c = 0.78170 \times 10^{-6}$ and the inductances by $R_t/2\pi f_c = 0.19543$, giving

$$C_1 = 1.0994\ \mu f$$
$$L_2 = 0.1980\ h$$
$$C_2 = 1.1889\ \mu f$$
$$C_3 = 0.4552\ \mu f$$
$$L_4 = 0.1399\ h$$
$$C_4 = 3.6758\ \mu f$$
$$C_5 = 0.7768\ \mu f.$$

Band-Pass Filters

The low-pass designs can be transformed into band-pass designs by means of the usual frequency transformation. Details can be found in the Grossman[2] and Skwirzynski and Zdunek[3] references. The resulting filter requires 7 inductors and 7 capacitors, and more economical designs of other types can frequently be found to meet practical requirements. Another limiting factor is that dissipation becomes more important in narrow band-pass filters, and a dissipation-compensated design may be required to realize sufficiently flat transmission.

It is believed that the present Tchebycheff-Zobel designs will be found very useful where the pass band is relatively wide, of the order of 2 to 1 or more. In this case the band-pass characteristic can be realized as a high-pass, low-pass combination. This requires 4 inductors and 10 capacitors, so is economical to construct. Although the pass-band response is not strictly Tchebycheff, there is very little interaction between the halves and the performance is very good. The regular band-pass design always gives greater discrimination than the high-pass, low-pass combination, the more so the narrower the band, but where the latter gives sufficient stop-band loss it may prove preferable both for economy and for the simplicity of the design procedure.

The high-pass and low-pass designs given above can be used in tandem to pass the octave from 500 to 1000 cps. It is interesting to note that with this combination the terminating resistances are 500 ohms, the design resistance of the high-pass half is 600.1 ohms, and that of the low-pass half 416.6 ohms.

The high-pass, low-pass combination has an additional advantage in that different characteristics can be employed at the two ends of the band without complicating the design.

Discussion

Use of Prototype Sections

It will be noted that the Tchebycheff-Zobel filters, which are optimum Zobel designs for a constant-loss

specification, never include a prototype, or constant-k, section. The idea dies hard that one or more prototype sections should always be used in a composite filter, but seems to have no foundation in fact. It probably originated because (in the low-pass case) an m-derived section has a finite value of image attenuation at infinite frequency, and allowance was not made for the fact that the reflection losses become infinite. The reflection losses provide sufficient insertion loss at the very high frequencies so that a prototype section is not needed.

Use of Terminating Half Sections

The image impedance of a filter may be made more nearly constant in the pass band by using m-derived terminating half sections with an m value of about 0.6. This gives flatter transmission and correspondingly reduced reflection. Although this arrangement was proposed originally to reduce reflection on long telephone lines, the idea is widely held that terminating half sections are needed to obtain flat transmission, even when reflection is not a problem. This is clearly not the case with the Zobel filters described, for which the termination ratio is chosen to give Tchebycheff insertion loss. The data given show that these filters have very low pass-band ripple and will satisfy the most critical requirements for flat transmission. Even for the usual design, however, the ripple is not large. The filter of Fig. 2, for example, gives only a 0.17 db ripple of the pass-band insertion loss with unity termination ratio. It is apparent that in many cases m-derived terminating half sections have been used only because no computation was made of the ripple for the simple and economical constant-k termination.

Even where reflection is the controlling factor, the filter designs with Tchebycheff or equal-ripple response are generally better than those of the same order using terminating half sections, which are restricted in regard to the location of the poles and zeros. Since in the case of a nondissipative network the reflection coefficient is determined by the insertion loss, a filter with equal ripples of insertion loss will also have equal ripples of reflection factor and will be an optimum design with respect to either characteristic. The limitations of the design with terminating half sections can be shown from the complete insertion loss formula for the two-section case, which can be derived in the manner described above for the constant-k type of termination. For this case the quantity E in the insertion-loss formula (3) is given by

$$E = \frac{(m_1 + m_2)(1 + m_1 m_2)x^3\left[x^2 - \dfrac{2}{1 - m_1^2} + \dfrac{1}{(1 - m_1^2)^2}\right]\left(x^2 - \dfrac{1}{1 + m_1 m_2}\right)}{(1 - m_2^2)\left(x^2 - \dfrac{1}{1 - m_1^2}\right)^2\left(x^2 - \dfrac{1}{1 - m_2^2}\right)} \tag{21}$$

where the termination ratio r is unity and m_1 refers to the terminating half sections. Computation of the insertion loss from this expression shows that for the case $m_1 = 0.6$, $m_2 = 0.84$ the maximum pass-band ripple is 0.0055 db, corresponding to a reflection factor of 3.6 per cent.

Although this design achieves very low reflection, it does so by a wasteful distribution of the poles and zeros. From the insertion-loss standpoint, the order of the filter has been raised from 5 to 7, which means that the sum of the orders of the pass-band zeros is 7, as is the sum of the stop-band poles. In the pass band the order of the zero at zero frequency has been raised from 1 to 3, and in the stop band the order of the first pole, that contributed by the terminating half sections, has been raised from 2 to 4. The two finite zeros are almost coincident, so there is no resemblance to Tchebycheff pass-band loss.

In the stop band the design is restricted by assigning the value 0.6 to m_1, and the fact that the corresponding pole is of the fourth order further limits the performance. The design uses the same number of coils as a three-section filter and is far inferior to it.

It must be concluded that terminating half sections should not be used unless reflection is the controlling factor. Even in this case an elliptic-function design, if available in a structure of the same order, will give superior performance.

ACKNOWLEDGMENT

The writer is indebted to W. Saraga and to A. J. Grossman for helpful comments on the preliminary version of the paper.

Minimum Insertion Loss Filters*

E. G. FUBINI† AND E. A. GUILLEMIN‡

Summary—**A generalized criterion is given for the design of minimum loss Butterworth and Tchebycheff filters of arbitrary bandwidth and component quality. This criterion is chosen to minimize the insertion loss in the center of the band and is particularly useful for microwave filters, where insertion loss must be minimized. Two general curves are given for this design, together with information as to the method followed in obtaining them. It is shown that, if insertion losses are to be minimized, the use of Tchebycheff filters with ripples greater than very small fractions of one decibel must be discouraged.**

Introduction

In microwave applications, it is important to minimize the midband insertion loss of filters. This requirement represents one of the most important differences between the design of low-frequency filters and microwave filters and is due to the fact that low-noise-figure amplification is a problem at microwave frequencies.

Since microwave filters have been in existence for a short time, the problem of losses played a secondary role in the theory of filter synthesis; only recently has the problem even been considered.

This paper has four objectives:

1) to assign the minimum midband loss realizable in a band-pass (or low-pass) filter of the Butterworth or Tchebycheff type,
2) to show that two universal curves give satisfactory approximations for all bandwidths, quality of components, number of sections, and acceptable ripple in the pass band,
3) to show that a filter with minimum loss can actually be designed,
4) to prove that Tchebycheff filters are very undesirable from the point of view of losses.

Use of Design Curves

This paper refers to the case of band-pass filters, including the low-pass prototypes, whose bandwidth is sufficiently narrow for the coupling between sections to be considered independent of frequency. In this case, Dishal has shown that exact Butterworth and Tchebycheff shapes can be obtained, provided that the loss in each section (considered isolated and unloaded) does not exceed a specific amount. It is convenient to use the unloaded $Q = Q_{unl}$ of each section as a measure of this loss. Dishal has given the values that the unloaded Q must exceed for a given set of specifications to be realizable

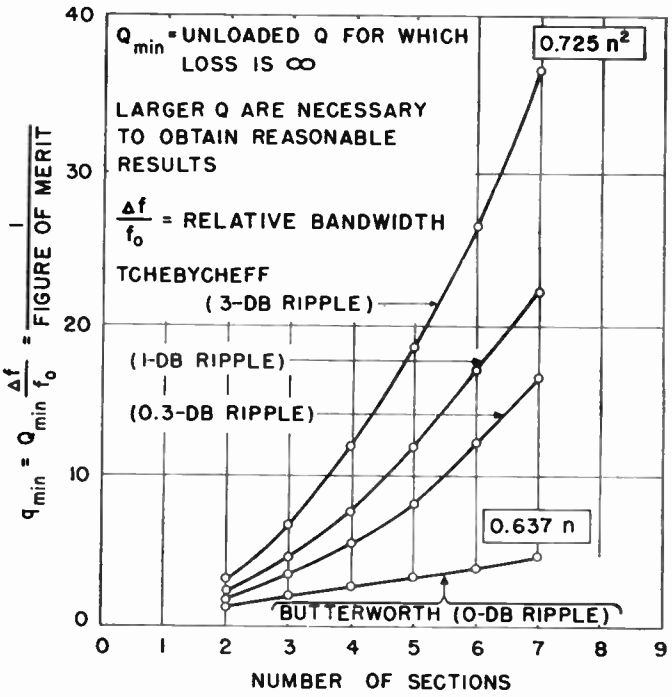

Fig. 1—Relative minimum unloaded Q for Butterworth and Tchebycheff filters.

Fig. 1 gives the minimum unloaded $Q = Q_{min}$. Note that the ordinates are normalized to unity bandwidth—that is, instead of plotting Q_{min}, a more general set of curves has been obtained by plotting

$$q_{min} = Q_{min}\frac{\Delta f}{f_0} = \frac{1}{\text{figure of merit}}$$

where $\Delta f/f_0$ is the relative bandwidth of the complete filter connected to the proper load and generator. In Fig. 1, note how for a given bandwidth the requirements in component quality (higher q_{min}) increase sharply from the no-ripple (Butterworth) case to the cases where ripples of a few decibels are specified. It must also be remembered that, if one were trying to use components whose unloaded Q (Q_{unl}) is barely equal to the required minimum,

$$Q_{min} = \frac{f_0}{\Delta f}\,q_{min}$$

the desired filter shape could indeed be achieved *but with an infinite midband loss.*

The question then arises: *if the unloaded Q of each filter section is $Q_{unl} > Q_{min}$ what is the minimum midband loss L?* Up to this point, all we have stated is that using the minimum acceptable Q produces infinite losses; however, one question remains unanswered: what quality can we expect in a filter as a function of the losses in

* Original manuscript received by the IRE, August 6, 1958; revised manuscript received, November 13, 1958. Reprinted from 1958 IRE National Convention Record, pt. 2, pp. 11–17.

† Airborne Instruments Lab., Div. of Cutler-Hammer, Inc., Mineola, N. Y.
‡ Mass. Inst. Tech., Cambridge, Mass.

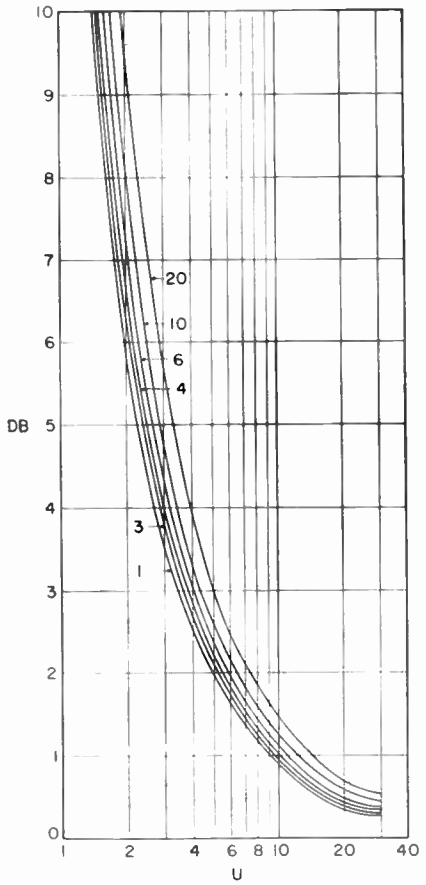

Fig. 2—Minimum insertion loss at midband in Butterworth filters of 1, 2, 3, 4, 6, 10, and 20 sections. The abscissa is the ratio u between the unloaded Q of each section and the minimum Q defined by Fig. 1.

the individual sections? The answer for the case of three sections was given by Taub and Bogner[1] in graphical form and by Fubini[1] in analytical form. The solution for the case of four sections was calculated by Aylward[2] using a digital computer. Here, we want to show the surprising fact that the answer does not primarily depend upon the number of sections and is almost exclusively controlled by the value of the ratio

$$u = \frac{Q_{unl}}{Q_{min}}$$

between the unloaded Q of the components used and the minimum acceptable value of such Q. In other words, *once the minimum value of Q_{unl} is obtained from Fig. 1 and the quality of available components is determined by their unloaded Q, the loss L is almost completely defined and varies very little with the number of sections, the shape of the filter, the bandwidth, etc.* It must be remembered that this statement is not exactly true, and it is definitely incorrect if shapes other than Butterworth or Tchebycheff are considered.

Fig. 2 shows a set of curves that give the minimum insertion loss L (db) of Butterworth filters plotted as a function of the ratio u previously defined. The curves are labeled with a number, which indicates the number of sections. It is clear that at least for moderate losses the curves are very close to each other. The curves for one and two sections are exactly the same and given by

$$L = 20 \log_{10} \frac{u}{u-1}.$$

Although the curves for Tchebycheff filters are not shown, they fall in close proximity to the corresponding Butterworth curves as shown below (Fig. 4).

Figs. 3 and 4 show a group of curves of loss (db) plotted vs the relative value of unloaded Q:

$$Q_{unl} \frac{\Delta f}{f_0} = m.$$

The surprising relation between such curves, already shown in Fig. 1, is shown again in Fig. 4. It would be desirable if a single curve could be substituted for the family of curves shown in Figs. 2 and 4. This could be accomplished with fair approximation using the two curves shown in Figs. 5 and 6. The first curve (Fig. 5) is the same as the curve plotted in Fig. 2 for one and two sections [see (1)]. Fig. 6 introduces a correction in Fig. 5 by introducing a multiplying factor that depends upon the number of sections. Although the data shown in Fig. 6 are not exact, they greatly improve the accuracy of the data shown in Fig. 5; however, this is only approximately true. These two curves (Figs. 5 and 6) are completely sufficient for all practical purposes. For example, let a filter be required with a Butterworth response and six sections. (Let it be required that the filter have a minimum midband loss and a relative bandwidth of 1 per cent.) Assume that the unloaded Q of each section is 2000. From Fig. 1 we find that, for a Butterworth type of six-section filter

$$q_{min} = Q_{min} \frac{\Delta f}{f} = \frac{1}{100} Q_{min} = 3.86.$$

The value of u can now be computed as follows:

$$u = \frac{Q_{unl}}{Q_{min}} = \frac{2000}{386} = 5.18.$$

Entering Fig. 5 with this value of u, one finds $L = 1.91$ db, which is the minimum insertion loss for one and two sections. In our case, since the required number of sections is six, we find (from Fig. 6) that the loss is higher by a correction factor of 1.23. We conclude that the filter will have a minimum midband loss of

$$L = 1.91 \times 1.23 = 2.35 \text{ db}$$

[1] J. J. Taub and B. F. Bogner, "Design of three-resonator dissipative band-pass filters having minimum insertion loss," PROC. IRE, vol. 45, pp. 681–687; May, 1957.
[2] W. R. Aylward, unpublished thesis, Polytechnic Institute of Brooklyn, Brooklyn, N. Y.; 1956.

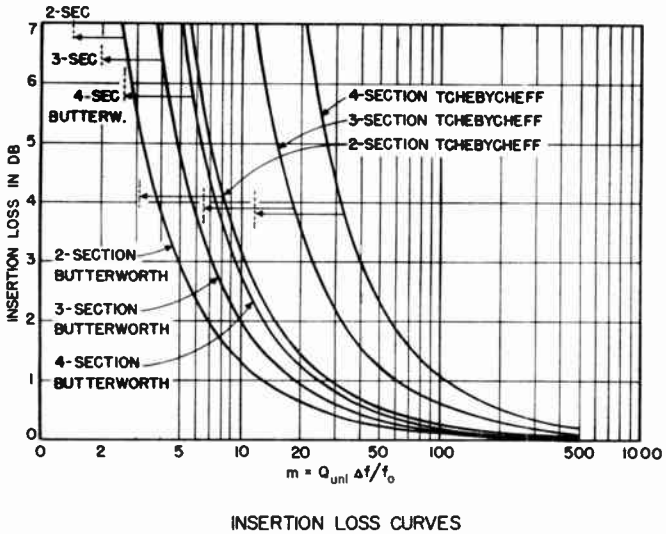

Fig. 3—Minimum midband insertion loss for a number of filters plotted as a function of the product m between the unloaded Q of each section times the relative bandwidth of the filter.

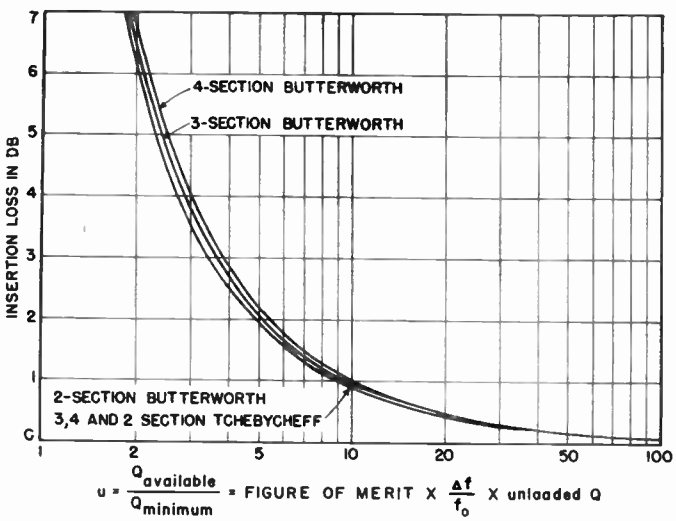

Fig. 4—The curves of Fig. 3 when normalized to the variable u = available unloaded Q/minimum unloaded Q.

which differs only by 5 per cent[3] or 0.1 db from the value $L = 2.25$ db given by accurate computations and noted in Fig. 2.

Optimum Filters

Fig. 5 shows that for a given quality of components, filters with the lowest q_{min} have the minimum midband loss. Fig. 6 shows that for filters with six sections or less the correction due to the number of sections does not exceed 25 per cent. For these reasons, $1/q_{min}$ can be considered as a figure of merit; it is interesting to compare

[3] This is a typical error. The use of Fig. 6 does not introduce errors greater than 7 per cent in db for a filter with less than 20 sections.

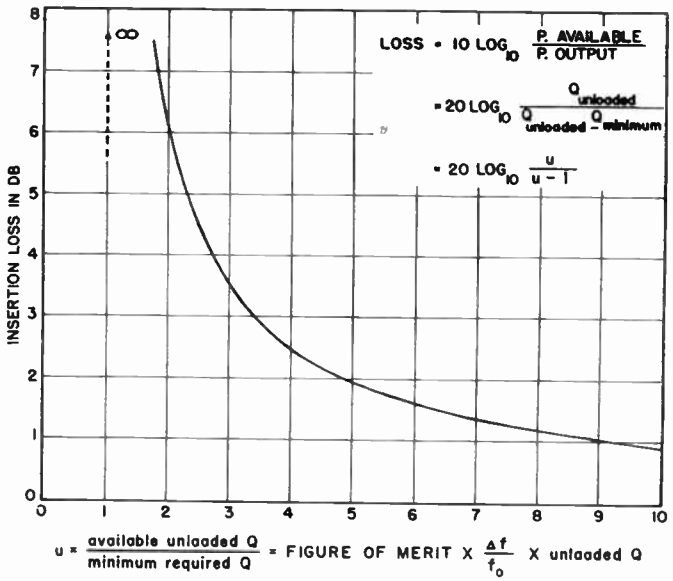

Fig. 5—General curve for minimum insertion loss. Minimum required Q can be found using Fig. 1.

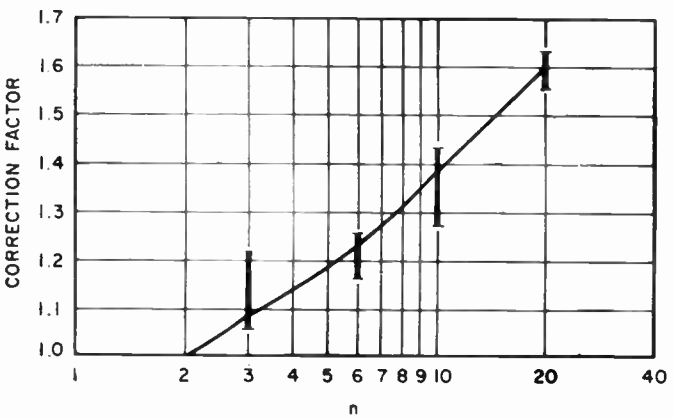

Fig. 6—Multiplying factor to be applied to the ordinates (db loss) of Fig. 5 to obtain a corrected value of loss if the number of sections is greater than two.

several filters to determine those that are best from the point of view of minimum loss.

This has been accomplished in Fig. 7, where the figure of merit of a group of filters has been plotted as a function of the skirt selectivity. Each curve corresponds to a given number of sections, and each point of the curves corresponds to Tchebycheff filters of variable ripple. The upper points of every curve correspond to Butterworth filters. It is clear that for a given skirt selectivity the figure of merit is higher and therefore the losses lower if selectivity is obtained by increasing the number of sections and not increasing the ripples. In this respect Tchebycheff filters are much worse than Butterworth filters. A curve can be imagined that joins all the upper points in the curves shown in Fig. 7. The curve obtained by means of this procedure supplies information as to the best possible figure of merit for this type of filter for a given skirt selectivity.

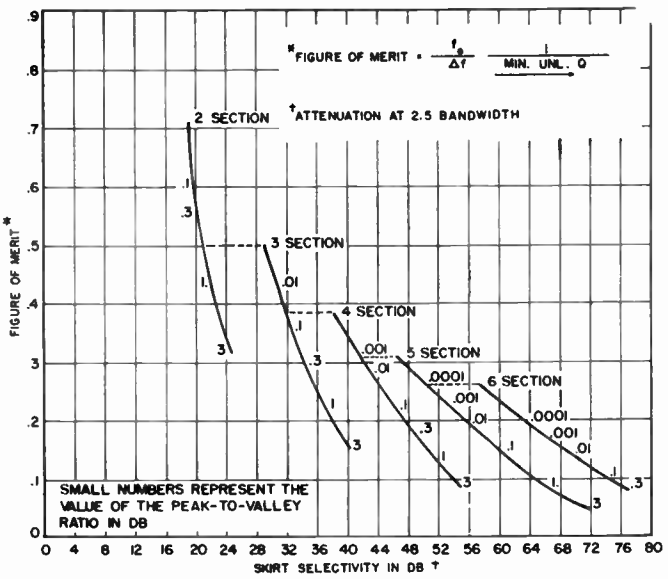

Fig. 7—The approximate quality of Tchebycheff and Butterworth filters as a function of skirt selectivity.

Theoretical Considerations

It is well known that the effect of losses can be eliminated from the synthesis process in the case of identical sections: a Butterworth filter, for example, can be obtained by requiring that the poles lie on a circle whose center is not on the frequency axis but whose distance from this axis is equal to the unloaded decrement of the elements of the filter. As shown in Fig. 8, if the filter were lossless, l would be the frequency axis and the response would be of the Butterworth type. Because of the losses, the poles had to be predistorted; this operation is equivalent to that of taking f as the frequency axis. Obviously, the response along f will be peaked, and the maximum value of this peak cannot exceed unity. This is equivalent to the statement that, in the response

$$I(s) = \frac{K}{(s - s_1)(s - s_2) \cdots (s - s_n)}$$

K must be smaller than the maximum value K_0 of $\Pi(s-s_i)$. Therefore, this maximum value K_0 represents the maximum filter efficiency and $1/K_0$ represents the minimum loss.

Let the Butterworth polynomial be

$$P(s) = (s - s_1)(s - s_2) \cdots (s - s_n) \tag{1}$$

with

$$s_v = je^{j(2v-1)\pi/2n} \tag{2}$$

where $v = 1, 2, \cdots, n$.

Write

$$P^*(s) = (s - s_2)(s - s_3) \cdots (s - s_n) \tag{3}$$

so that

$$P(s) = (s - s_1)P^*(s) \tag{4}$$

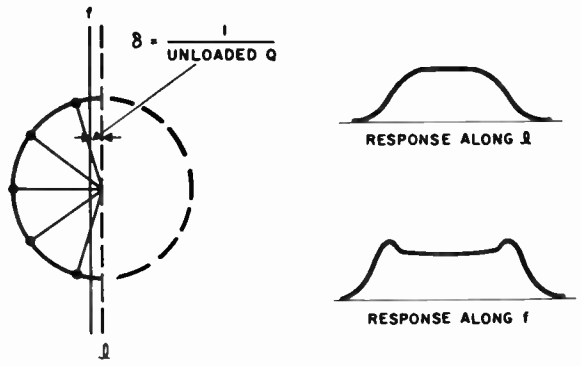

Fig. 8—The effect of finite losses in a Butterworth filter corresponds to shifting the circle of the poles toward the frequency axis by an amount δ equal to the reciprocal of the unloaded Q of each section.

The horizontal distance from s_1 to the j axis is

$$a = \sin \pi/2n. \tag{5}$$

At the point (s_1+a) on the j axis, we assume that the magnitude of $P(s)$ is very nearly unity, because this point is still in the pass band. Eq. (4) therefore gives

$$|P(s_1 + a)| \approx 1 \approx a|P^*(s_1 + a)|$$

or

$$|P^*(s_1 + a)| \approx 1/a$$
$$= 1/(\sin \pi/2n) \approx 2n/\pi \text{ for large } n. \tag{6}$$

If we assume that $P^*(s)$ does not vary appreciably in the interval between $s=s_1$ and $s=s_1+a$ (to be justified later), then in (4) we can replace $|P^*(s)|$ by the constant value [given in (6)] and have

$$\frac{1}{|P(s)|} = \frac{a}{|s - s_1|} \tag{7}$$

which yields unity (as it should) at $s=s_1+a$. If we write $s=s_1+a-\delta$, where δ is the shift of the pole pattern, then within the interval $s=s_1$ to $s=s_1+a$ we have (for the Butterworth function) an approximate representation that reads

$$\frac{1}{|P(s)|} = \frac{a}{a - \delta} = \frac{1}{1 - (\delta/a)}. \tag{8}$$

This is of course equal to the reciprocal of the maximum value K_0 of $\Pi(s-s_i)$.

Observe that this relation gives the correct value (unity) for $\delta=0$ regardless of the order n, and approximately correct values for $0<\delta<a$ to the extent that $P^*(s)$ in (3) is constant within this interval. To investigate the latter, let us compute the ratio

$$P^*(s_1)/P^*(s_1+a),$$

or, since $s_1+a \approx j$ for large n, the ratio $P^*(s_1)/P^*(j)$.

From (3) we find, in a straightforward manner,

$$\left(\frac{dP^*}{ds}\right)_{s=j} = P^*(j)\sum_{r=2}^{n}\frac{1}{j-s_r} = \frac{2n}{\pi}\sum_{r=2}^{n}\frac{1}{j-s_r} \tag{9}$$

where (6) is used in the last step. If we use the relation

$$P^*(s_1) = P^*(j) - a\left(\frac{dP^*}{ds}\right)_{s=j} \tag{10}$$

and substitute for a the value $\pi/2n$, we have

$$\frac{P^*(s_1)}{P^*(j)} = 1 - \left(\frac{\pi}{2n}\right)^2\left(\frac{dP^*}{ds}\right)_{s=j} = 1 - \frac{\pi}{2n}\sum_{r=2}^{n}\frac{1}{j-s_r}. \tag{11}$$

Substituting the value of s_r in (2),

$$x = (2r-1)\frac{\pi}{2n}, \tag{12}$$

and noting that

$$\frac{1}{j(1-e^{jx})} = \frac{1}{2j}\left(1 + j\cot\frac{x}{2}\right) = \frac{1}{2}\left(\cot\frac{x}{2} - j\right), \tag{13}$$

(11) becomes

$$\frac{P^*(s_1)}{P^*(j)} = 1 - \frac{\pi}{4n}\sum_{r=2}^{n}\left(\cot\frac{x}{2} - j\right) = 1 + j\frac{(n-1)\pi}{4n} - \frac{1}{2}\sum_{x/2=3\pi/4n}^{x/2=\pi/2-\pi/4n}\left(\cot\frac{x}{2}\right)\frac{\Delta x}{2} \tag{14}$$

where $\Delta x = \pi/n$. From a graphical sketch of the cotangent function and its step approximation in (14) we see that a very close value for this sum may be obtained from the integral:

$$\frac{1}{2}\int_{\pi/2n}^{\pi/2}\cot x\,dx = \frac{1}{2}\ln(\sin x)\Big]_{\pi/2n}^{\pi/2} \cong \frac{1}{2}\ln\frac{2n}{\pi} \tag{15}$$

where x has been substituted for $x/2$. And so we finally obtain

$$\frac{P^*(s_1)}{P^*(j)} = \left(1 - \frac{1}{2}\ln\frac{2n}{\pi}\right) + j\frac{(n-1)\pi}{4n}. \tag{16}$$

The magnitude of this ratio for various values of n is tabulated below.

n =	3	6	10	15
ratio =	0.855	0.733	0.708	0.744
n =	20	30	40	50
ratio =	0.793	0.898	0.984	1.06

These results show that the assumption made in the derivation of the approximate result given in (8) is entirely reasonable for any values of n to be encountered in a practical problem. One should observe also that the result [given in (8)] is exact for $\delta = 0$ and has its greatest degree of approximation near $\delta = a$, where the Butterworth function blows up. Such values for the shift δ will hardly be used in a practical problem.

The design of the filter can be now described as follows.

Starting from the normal unshifted Butterworth transfer function $t(s) = 1/P(s)$, where $P(s)$ is the usual Butterworth polynomial, we form the shifted and K-multiplied function $Kt(s-\delta)$, where K is determined so that the absolute value of this function for $s = j$ never exceeds unity. This is the condition that fixes the largest possible value of K (least midband loss) that can yield a positive real $Z_1(s)$ function. Our approximate formula (8) determines this largest K value; and the necessary positive-real character of $Z_1(s)$ is the reason that the resulting midband loss is minimum. $Z_1(s)$ is determined from the relation

$$Z_1(s) = \frac{1-\rho(s)}{1+\rho(s)}$$

where $\rho(s)$ is obtained from

$$|\rho(j\omega)|^2 = 1 - K|t(j\omega - \delta)|^2.$$

The $Z_1(s)$ function thus obtained is the desired preshifted impedance function. It is realized in the normal manner by a lossless network terminated in resistance. The incidental loss that is present in the actual network then shifts the pole pattern of $Kt(s)$ back to the original Butterworth position.

The Reactatron[1]—A Low-Noise, Semiconductor Diode, Microwave Amplifier*

F. A. BRAND†, MEMBER, IRE, W. G. MATTHEI†, MEMBER, IRE, AND T. SAAD‡, SENIOR MEMBER, IRE

Summary—**A low-noise, microwave amplifier has been constructed using two non-linear capacitor microwave *p-n* junction diodes in a balanced hybrid system. Power gains in excess of 30 db with effective input noise temperatures less than 290°K have been observed at a frequency of 2900 mc.**

Introduction

IT has been known for some time that radio frequency power could be converted and amplified by the proper use of special nonlinear capacitor diodes[2–9] or other nonlinear devices.[10,11] Uhlir and others at the Bell Telephone Laboratories, under Signal Corps sponsorship, have developed diffused-junction silicon diodes capable of very efficient operation as nonlinear capacitors at microwave frequencies.[12] A number of variable capacitance diode amplifiers have been built recently which have served to demonstrate the feasibility of easily generating, converting, and amplifying microwave energy efficiently, economically, and reliably by devices of this type.[13–20]

Discussion

In the order to investigate the amplification properties of this class of semiconductor devices, a balanced waveguide dual-hybrid system was designed and constructed. The present discussion concerns this system, shown in block diagram in Fig. 1. A hybrid system was used to provide separation between input and output signals without recourse to a microwave circulator. The present hybrid provided adequate bilateral isolation for our purposes (Fig. 2 is a photograph of the system).

The low-level signal input, of the order of microwatts or less, was arbitrarily set at 2900 mc. This signal was introduced into the balanced hybrid mixer[21] where it was mixed with *C*-band energy from a local oscillator or pump, as it is frequently called in amplifiers of this type. The frequency of the pump was set at approximately twice the signal frequency or 5800 mc. Pump power, of the order of 50–100 milliwatts, was fed into the two amplifying diodes by means of a second hybrid at *C*-band. The only purpose in using a hybrid in this case was to provide a simple means for feeding the pump power equally to the two diodes. The amplified *S*-band signal and the *S*-band lower sideband were then fed into the superheterodyne receiving system. The signal and lower sideband were both down-converted by a second

[1] It is recognized that this is a controversial area; however, the terms "parametric amplifier," "dielectric amplifier," "MAVAR," and "reactance amplifier" all could and sometimes do refer to the same phenomenon or amplifier. To the best of our knowledge, no term has been proposed which refers specifically to a microwave amplifier which uses a semiconductor diode (only) for its nonlinear reactance. We are, therefore, proposing the word "reactatron" which would signify a semiconductor diode microwave amplifier.

* Original manuscript received by the IRE, August 13, 1958.

† U. S. Army Signal Research and Development Lab., Fort Monmouth, N. J.

‡ Sage Labs., Inc., Wellesley, Mass.

[2] A. Van der Ziel, "On the mixing properties of non-linear condensers," *J. Appl. Phys.*, vol. 19, pp. 999–1006; November, 1948.

[3] H. C. Torrey and C. A. Whitmer, "Crystal Rectifiers," McGraw-Hill Book Co., Inc., New York, N. Y.; 1948.

[4] J. Von Neumann, "Non-linear capacitance or inductance switching, amplifying, and memory organs," U. S. Patent No. 2,815,488; filed April 28, 1954.

[5] "Crystal Rectifiers," Second Interim Tech. Rep., Signal Corps Contract DA 36-039 sc-5589 (Task 8); October 1, 1954–December 31, 1954. In addition, there is much information relating to this subject in the rest of the reports on this contract and the succeeding contract, DA 36-039 sc-73224.

[6] L. J. Giacoletto and J. O'Connell, "A variable capacitance germanium junction diode for UHF," *RCA Rev.*, vol. 17, p. 68; March, 1956.

[7] "Semiconductor diodes yield converter gain," *BTL Record*, vol. 35, p. 412; October, 1957.

[8] J. P. Wittke, "New approaches to the amplification of microwaves," *RCA Rev.*, vol. 18, pp. 441–457; December, 1957.

[9] A. Uhlir, "Two terminal *P-N* junction devices for frequency conversion and computation," PROC. IRE, vol. 44, pp. 1183–1191; September, 1956.

[10] J. M. Manley and H. E. Rowe, "Some general properties of nonlinear elements—Part I, general energy relations," PROC. IRE, vol. 44, pp. 904–913; July, 1956. This excellent paper contains a good historical background and a copious bibliography of early work in this area.

[11] H. E. Rowe, "Some general properties of non-linear elements—Part II, small signal theory," PROC. IRE, vol. 46, pp. 859–860; May, 1958. See footnotes for additional references.

[12] These silicon diffused diodes were developed by BTL under Signal Corps Contract DA 36-039 sc-5589 (Task 8), "Crystal Rectifiers," and Contract DA 36-039 sc-73224, "Improved Crystal Rectifiers," now titled "Microwave Solid State Devices."

[13] M. E. Hines, "Amplification in Non-Linear Reactance Modulators," presented at the 15th Annual Conference on Electron Tube Research, Berkeley, Calif.; June, 1957.

[14] H. Heffner and K. Kotzebue, "Experimental characteristics of a microwave parametric amplifier using a semiconductor diode," PROC. IRE, vol. 46, p. 1301; June, 1958.

[15] B. Salzberg and E. W. Sard, "A low-noise wide-band reactance amplifier," PROC. IRE, vol. 46, p. 1303; June, 1958.

[16] G. F. Hermann, M. Uenohara, and A. Uhlir, Jr., "Noise figure measurements on two types of variable reactance amplifiers using semiconductor diodes," PROC. IRE, vol. 46, pp. 1301–1303; June, 1958.

[17] A. Uhlir, Jr., "The potential of semiconductor diodes in high-frequency communications," PROC. IRE, vol. 46, pp. 1099–1115; June, 1958.

[18] R. S. Engelbrecht, "A Low-Noise Non-Linear Reactance Traveling Wave Amplifier," presented at the AIEE-IRE Solid-State Device Research Conference, Ohio State University, Columbus, Ohio; June, 1958.

[19] S. Bloom and K. K. N. Chang, "Parametric amplifiers using low-frequency pumping," *J. Appl. Phys.*, vol. 29, p. 594; March, 1958.

[20] K. K. N. Chang and S. Bloom, "A parametric amplifier using lower-frequency pumping," PROC. IRE, vol. 46, pp. 1383–1386; July, 1958.

[21] The mixer was designed and developed at Sage Labs. by Theodore Saad under Signal Corps Contract DA 36-039 sc-71149.

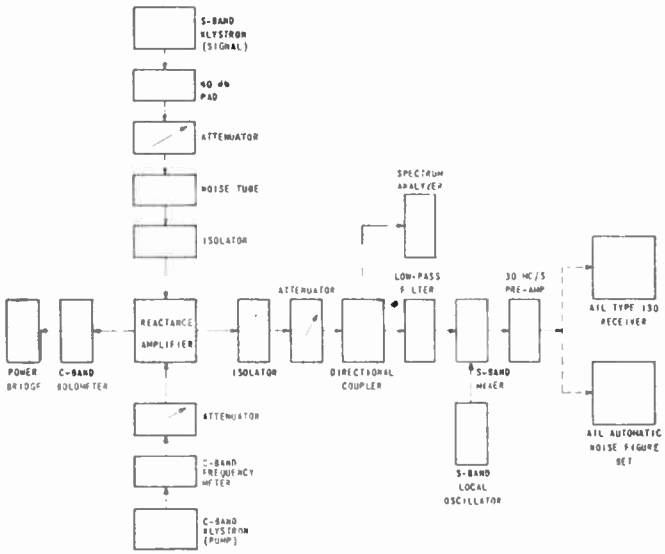

Fig. 1—Block diagram of the equipment used to measure the semiconductor diode microwave amplifier.

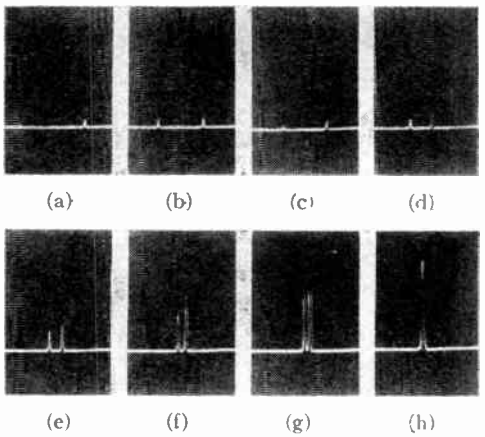

Fig. 3—Photographs of spectrum analyzer traces of semiconductor diode microwave amplifier showing the signal (on the left) and the lower sideband (on the right) of semiconductor diode microwave amplifier. The signal frequency was changed until it overlapped with the lower sideband. The frequency between the signal and the lower sideband is: (a) 3.35 mc; (b) 2.30 mc; (c) 2.2 mc; (d) 1.1 mc; (e) 0.7 mc; (f) 0.45 mc; (g) 0.1 mc; (h) width of base line of signal 0.2 mc.

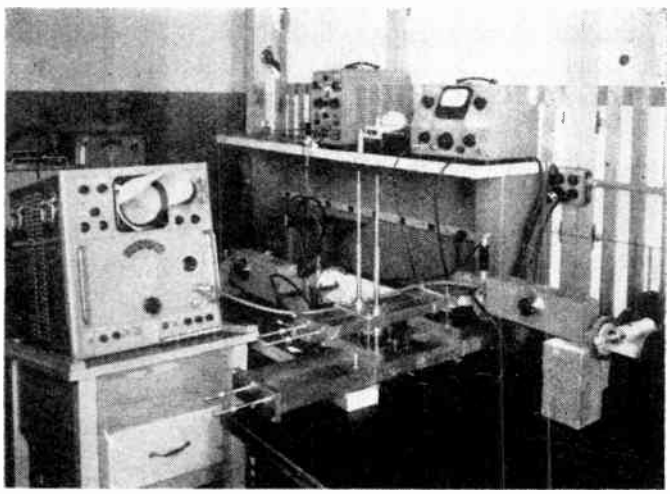

Fig. 2—Photograph of semiconductor diode microwave amplifier and associated measuring equipment.

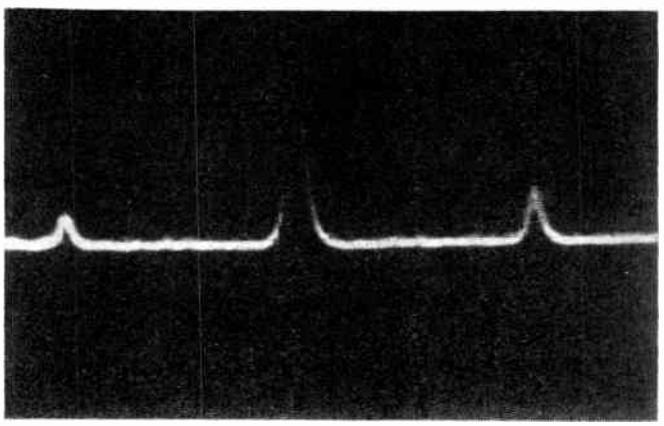

Fig. 4—Photograph of spectrum analyzer trace showing a condition of oscillation at one-half the pump frequency; the signal frequency being the one on the left and the lower sideband frequency that on the right.

S-band local oscillator to an intermediate frequency of 30 mc in a fairly conventional crystal mixer arrangement. In order to be certain that the measurements were being made while the amplifier was in a stable condition, a directional coupler was used in the output, and a portion of the signal was fed into a spectrum analyzer to monitor constantly the signal and the lower sideband. The amplifier was isolated from the signal or the load by a ferrite isolator. In addition, a low-pass filter with a frequency cutoff of 4000 mc was inserted between the amplifier and the *S*-band receiver in order to avoid the possibility of *C*-band power leaking directly into the receiver and generating harmonics on the crystal mixer.

Gain and noise figure measurements were made by two methods. The 30 mc IF output from the mixer was fed into an AIL-type 13130 preamplifier, and then into either an AIL-type 130 receiver or an AIL-type 72 automatic noise figure set. An argon gas lamp was utilized as the noise source for the following measurements. Noise figure was measured automatically using the type 72 set, and by the *Y* factor technique using the AIL receiver. Power gain was measured by comparing the signal output as indicated by the receiver with the amplifier, and without the amplifier. Power gain was also determined by inserting a known amount of attenuation between the amplifier and the receiver, and noting the change in over-all noise figure.[22]

It should be noted that lower sideband conversion is potentially unstable, and that the lower sideband gain, being a negative resistance phenomenon, can be made arbitrarily large by operating close to the point of instability.[23] By use of the spectrum analyzer, it was pos-

[22] This method was suggested by P. Lombardo of AIL in a private communication.

[23] Manley and Rowe, *op. cit.*

sible to observe simultaneously not only gain at the lower sideband, but also gain at the signal frequency when the frequency separation between the signal and lower sideband was sufficiently small, or when the two were brought into coincidence. By "sufficiently small" we mean a few hundred kilocycles. Gain at both signal and lower sidebands is expected for a difference frequency amplifier such as this.[24,25]

Fig. 3 is a composite photograph of spectrum analyzer traces showing the signal on the left, and the lower sideband on the right. When the frequency separation of the signal and lower sideband is decreased, the amplitude of both signal and sideband are increased until, when they coincide, a condition of high gain exists at a single frequency. Fig. 4 depicts a condition of oscillation at one-half the pump frequency. This condition of oscillation was most easily attained by increasing the pump power.

The tuning arrangement, however, was also very critical in this respect, and the system could be made to oscillate by certain adjustments of the sliding shorts in the *S*-band hybrid.

Stable gain and noise figure measurements were made for many different tuning configurations. The highest stable gain observed in these preliminary measurements was 33 db. For one particular adjustment, a stable gain of 19.2 db was obtained with a noise figure of 2.7 db (an effective noise temperature of 250°K) with a 3-db bandwidth of 0.5 mc. It should be noted that the low-noise figure quoted refers to the amplifier, and not to the over-all system. The *S*-band receiver plus associated attenuators, filters, isolators, and IF amplifier had a measured over-all noise figure of 20 db.

The two diodes were of the silicon diffused "mesa" type with "spreading resistances" (R_s) of 2.61 ohms and 4.04 ohms; zero bias capacity [at 100 kc (C_0)] of 3.05 $\mu\mu$f and 2.11 $\mu\mu$f; and a frequency cutoff (f_c) of 45.0 kmc and 45.6 kmc, respectively. Further data relating the parameters of the semiconductor diodes to the properties of the amplifier will be discussed in a later paper.

[24] *Ibid.*
[25] B. Salzberg, "Masers and reactance amplifiers—basic power relations," PROC. IRE, vol. 45, p. 1544; October, 1957.

ACKNOWLEDGMENT

Acknowledgment is given to George Gregory Associates, Inc. for the loan of the Airborne Instrument Laboratory IF preamplifier, superheterodyne receiver, and automatic noise figure indicator; to R. Tenenholtz of Ewen-Knight for the use of the argon gas tube noise source; to H. Ellowitz of Microwave Associates for the loan of the isolator and attenuator; and to R. Ryder and A. Uhlir of Bell Telephone Laboratories for their helpful discussions in this area.

A Semiconductor Current Limiter*

R. M. WARNER, JR.†, W. H. JACKSON†, E. I. DOUCETTE†, AND H. A. STONE, JR.†

Summary—**The two-terminal constant-current device described herein employs the principles of the field effect transistor. Current flows parallel to a junction through a thin sheet of semiconductor. The reverse bias on the junction controls the effective thickness of the sheet and thereby controls its conductance. An extension of Shockley's step-junction-device theory is presented, as well as a formulation for the graded-junction case. Several structures are discussed and compared, and fabrication procedure for the presently used structure is outlined. The current limiter has been employed advantageously as an ac switch, a current regulator, for discrimination between ac and dc, and in simple circuits for sawtooth and step function generation and for digital-to-analog conversion.**

INTRODUCTION

THE phenomenon of field effect, or modulation of the conductance of a thin region of semiconductor by transverse electric fields, has been applied to the development of a current limiter (field effect varistor) with useful circuit properties.[1] This device is in essence a self-biased field effect transistor, the basic principles of which were originally developed by Shockley.[2]

Constant voltage devices have been available for years in the form of gas tubes and avalanche breakdown diodes, and their field of application is now well understood. Until now there has been no comparable progress in the development of constant current devices. The usefulness of a circuit element in which the current is independent of the voltage is potentially high, but heretofore the only components exhibiting anything approaching constant current behavior have been thermal devices, and these have inherent drawbacks which have severely limited their application. To be sure, some reverse biased semiconductor junctions have constant

* Original manuscript received by the IRE, September 15, 1958.
† Bell Telephone Labs., Inc., Murray Hill, N. J.

[1] R. M. Warner, Jr., "A new passive semiconductor component," 1958 IRE NATIONAL CONVENTION RECORD, vol. 6, pt. 3, pp. 43–48; 1958.
[2] W. Shockley, "A unipolar 'field-effect' transistor," PROC. IRE, vol. 40, pp. 1365–1376; November, 1952.

current characteristics, but the currents at which they regulate are far too small to be useful. The field effect limiter described herein can be designed for current levels in ranges appropriate for practical transistor circuitry.

Field effect and the field effect transistor have been of interest to investigators for at least a decade. Shockley's work on the field effect transistor was published in 1952,[2] but even as early as 1948, work had been done on modulation of conductance by transverse fields.[3] In 1953 experimental field effect transistors, both of silicon[4] and germanium,[5] were announced, and in 1955 Dacey and Ross extended the theory and applied it to the problem of high frequency gain.[6]

As an amplifier, the field effect transistor has never become competitive with minority-carrier devices; this has been due, at least in part, to the difficulty of realizing some of the critical dimensions in a practical structure. However it is not unreasonable to suppose that as new techniques are developed this outlook will change.

There do not seem to be any previous developments aimed specifically at nongain device applications of field effect. Yet for the two-terminal current limiter described here, the problems in structure are far less formidable and approaches are practical which could not have been used where high frequency gain was the objective. Field effect current limiters are now being made in the laboratory in sufficient numbers to support systems development, and large scale manufacture is planned.

Conductance Modulation in a Self-Biased Channel

Consider a semiconductor junction connected as shown in Fig. 1(a). Since the *n* region, or channel, is carrying current from right to left and since the entire *p* region is at ground potential, the reverse voltage across the junction varies from zero at the left end to the full applied voltage V at the right end. The depletion layer, or space charge region, whose thickness at any point depends on the voltage across the junction at that point, will take on a contour consistent with this voltage distribution.

For simplicity we will assume that the *p* region is highly doped so that depletion layer penetration into it is negligible. The effect of the depletion layer in the *n* region is to constrict its current-carrying cross section, and thus to raise its resistance.

If the applied voltage is increased, the depletion layer will penetrate deeper into the *n* channel, further increasing its resistance. The resulting current-voltage characteristic is illustrated as region 1 in Fig. 2. In-

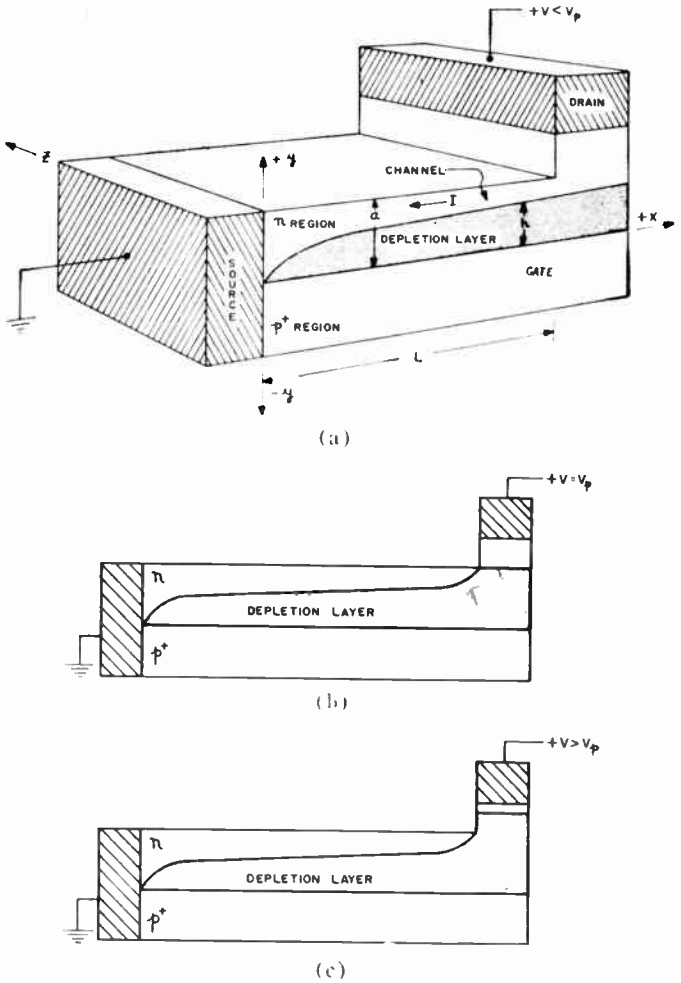

Fig. 1—Depletion layer penetration in self-biased channel. (a) $V<V_p$. (b) $V=V_p$. (c) $V>V_p$.

creases in voltage give rise to something less than proportionate increases in current.

If the voltage is raised to a critical value called the "pinch-off" voltage (V_p) the depletion layer will extend completely across the channel, as illustrated in Fig. 1(b). Further increases in voltage have very little effect on the depletion layer boundary within the channel. Voltage in excess of V_p is absorbed in a thickening of the depletion layer beyond the channel, as shown in Fig. 1(c). The charge carriers, reaching the end of the channel, are now swept across this intervening portion of the depletion layer. Since the voltage drop through the channel remains at the value V_p, the resistance of the channel is unchanged and the resulting current becomes essentially a constant for voltages higher than V_p. This is shown as region 2 in Fig. 2.

The constant current condition obtains until the applied voltage becomes high enough to give rise to avalanche breakdown. From then on the device behaves like any other diode in the breakdown condition. Region 3 of Fig. 2 illustrates this condition.

Actually, it is not necessary to provide a physical connection to the *p* region. If it is left floating, it will adopt practically the same potential as the less positive

[3] W. Shockley and G. L. Pearson, "Modulation of conductance of thin films of semiconductors by surface charges," *Phys. Rev.*, vol. 74, pp. 232–233; July 15, 1948.
[4] G. L. Pearson, "High impedance field effect silicon transistors," *Phys. Rev.*, vol. 90, p. 336; April 15, 1953.
[5] G. C. Dacey and I. M. Ross, "Unipolar field-effect transistor," Proc. IRE, vol. 41, pp. 970–979; August, 1953.
[6] G. C. Dacey and I. M. Ross, "The field-effect transistor," *Bell Sys. Tech. J.*, vol. 34, pp. 1149–1189; November, 1955.

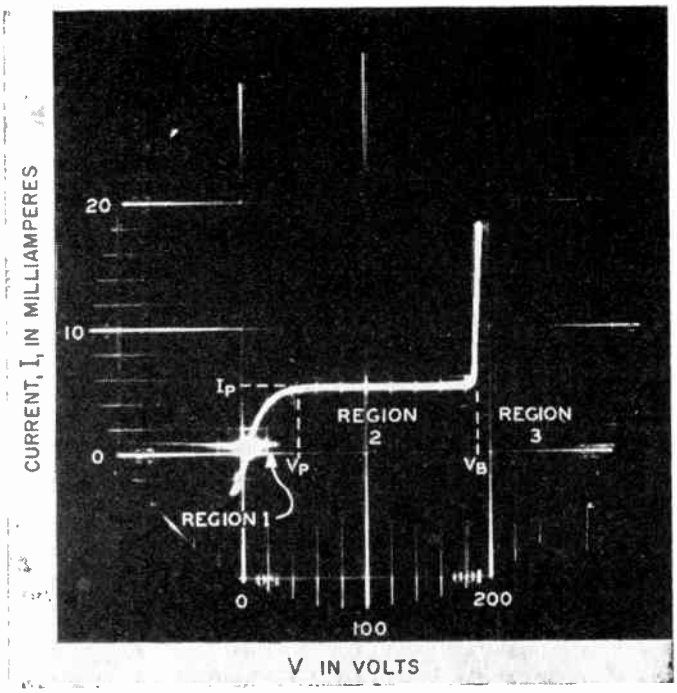

Fig. 2—Current-voltage characteristic of field effect limiter displaying three distinct regions.

end of the *n* channel. The device then becomes nonpolar, with the same voltage-current characteristic for either direction of applied voltage. In practice, however, there has been little circuit interest in nonpolar units and there are certain practical advantages in making the connections as shown.

The choice of the *n* region as the conducting channel has not been entirely arbitrary. Although similar arguments could have been used for a *p* channel, the fact is that in practice it is desirable to use *n* channels and take advantage of the higher electron mobility.

Typical Characteristics

In order for the constricting effect of the depletion layer to be significant, that is, to achieve a reasonably low pinch-off voltage, it is necessary that the channel be thin—of the order of a few microns—and that it be composed of reasonably high resistivity material. Both of these conditions tend to restrict the current to low values. While some of the geometric parameters which will be discussed allow a considerable flexibility in design, the limiter is essentially a high resistance device. Initial resistances in the order of 200 ohms are about as low as are now practicable.

The pinch-off resistance, or ratio of pinch-off voltage V_p to pinch-off current I_p is inherently 2.5 or 3 times initial resistance depending on whether graded or step junctions are used. A typical unit might have 1000 ohms initial resistance, pinch off at 10 volts and regulate at 4 ma.

The pinch-off voltage V_p is a function not only of the channel thickness, the carrier density and distribution, but also of the dielectric constant of the semiconductor. For this reason, low pinch-off voltages are more easily achieved with germanium than with silicon. On the other hand, silicon has the advantage of high breakdown voltage, and for this reason all of the units now being made for systems application are of silicon. They are designed to have pinch-off voltages from 5 to 15 volts and pinch-off currents in the range from 1 to 20 ma.

While the I-V curve actually has a slope in the pinch-off region, this can be made remarkably small. It is convenient to refer to this slope in terms of the incremental (or small signal) resistance; in these terms slopes of 20 megohms have been achieved.

The voltage range for constant current is limited at the low end by the pinch-off voltage and at the upper end by avalanche breakdown. With good silicon junctions, breakdown may be above 200 volts. Thus it is possible to maintain constant current with a tenfold to twentyfold change in voltage.

One characteristic which cannot be overlooked in practical applications is internal heating. A 5 ma unit working at 100 volts dissipates half a watt and must be designed for it. The limiters that have been made so far are suitable for several hundred milliwatts continuous dissipation and there is little doubt that considerable improvement can be realized in this aspect of design.

Another characteristic of practical importance is the effect of temperature on the pinch-off current. This depends primarily on the carrier mobility and thus, in the room temperature range, it is negative and at most about 0.5%/°C.

Finally, the effect of environment on the aging and drift characteristics must be considered. A structure will be described in which the exposed periphery of the junction has no potential across it and therefore needs no protection. Unfortunately, such a structure cannot be realized without exposing one side of the channel, and this is at least as sensitive to environment as the junction itself. It follows that encapsulation is essential to insure stability. When properly carried out, it will reduce drift to an acceptably low magnitude.

Areas of Application

The most obvious applications of the current limiter make direct use of its constant current characteristic, illustrated as region 2 in Fig. 2. As a simple current regulator between a power supply and its load, it will maintain constant current in spite of wide variations either in supply voltage or load impedance and it will suppress transient disturbances.

Because of its high ratio of ac to dc resistance, the device bears a certain analogy to a choke and can be used in place of a choke for isolation of circuits fed by the same source. In broad-band applications, it has the advantage that the discrimination between dc and ac is independent of frequency over a wide range. The ac response is independent of minority carrier transit times since the significant conduction is all by majority carrier. The operating frequency is limited, however, by the junction capacitance, the effects of which will be considered in some detail later on.

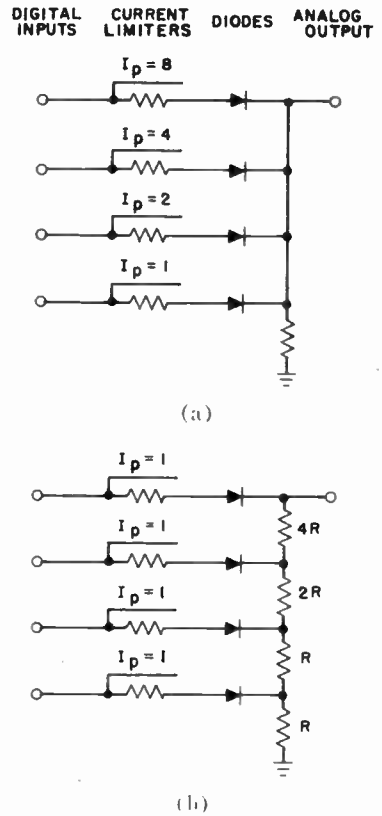

Fig. 3—Digital-analog encoder using current limiters. (a) Weighted pinch-off currents. (b) Matched pinch-off currents.

The device can be used for circuit protection against overload, although in this application it is limited by its own breakdown voltage. It has implications for wave shaping, *e.g.*, as a saw tooth generator, because the voltage of a capacitor charged at constant current will rise linearly.

Fig. 3 suggests two forms of a digital-analog encoder. In each case the encoder input consists of a current limiter and diode for each digit. In Fig. 3(a), the pinch-off currents of the limiters are appropriately weighted so that the voltage developed across the output is the analog of the digital input. In Fig. 3(b), all the limiters have the same pinch-off current and the weighting is accomplished in the output resistor. The advantages offered by either version of the encoder are that the analog input voltage need only exceed a certain critical value, and this value can be relatively small.

Other applications take advantage of the contrast in characteristics between two, or among all three of the regions. Use of the limiter as an ac switch depends on the fact that the ac resistance can be varied from a relatively low value (region 1) to an extremely high value (region 2) as a function of bias.

Step functions can be generated by using several limiters in series with successively higher pinch-off currents. So long as the voltage is low enough so that none of the units are pinched off, it divides in proportion to their resistances. But as soon as one unit pinches off, the current will stabilize and the pinched off unit will absorb all further increase in voltage. This obtains until the first unit reaches avalanche breakdown. The current then again increases with the applied voltage until another unit pinches off. The process thus repeats for each unit and a step function is generated. An example of a three step characteristic is shown in Fig. 4. Other wave shaping applications will suggest themselves in the areas of clipping, modulation, signal compression, etc.

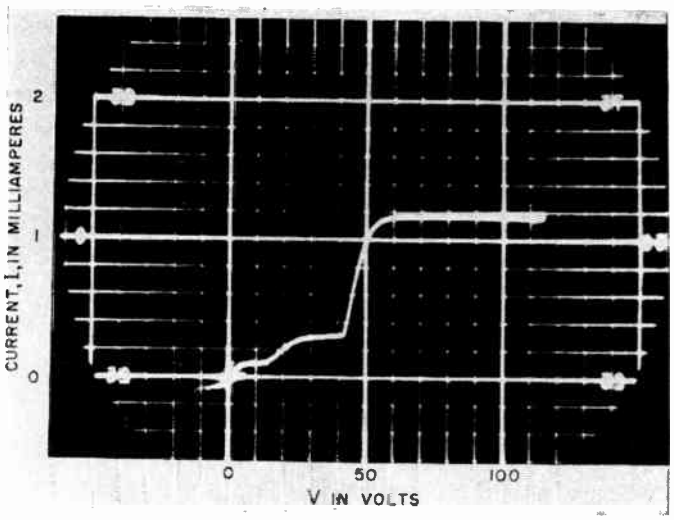

Fig. 4—Step characteristic using current limiters.

Idealized Step-Junction Model

In this section we shall consider an idealized model of the current limiter which contains one step junction. With this model the essential features of the device may be demonstrated without the complicating factors of impurity gradients and complex geometries. Some of these extensions will be considered in subsequent sections.

The geometrical configuration of the model to be discussed is illustrated in Fig. 1. This model contains a simple planar n-p^+ junction positioned at $y=0$. Two ohmic contacts are indicated, one short-circuiting the junction[7] at $x=0$ and another connected only to the n region at $x=L$. These are called the source and drain, respectively, to be consistent with the original nomenclature of Shockley.[2]

To simplify the calculations, the built-in junction voltage and saturation current will be neglected and the entire p^+ region will be assumed to be at the source potential. This is reasonable because of their small magnitudes when compared to realistic device parameters. Because the p^+ region is very heavily doped, we shall also assume that the depletion layer does not penetrate this region to any significant extent.

If the source terminal is kept at ground potential and a positive voltage is applied to the drain contact at $x=L$, electrons will flow in the n region from the source to the drain. As a result of this current, the n-p^+ junction will become reverse biased at any point in the chan-

[7] The device will operate approximately the same without the external short circuit. The saturation current of the entire area of the junction will cause the junction at $x=0$ to be driven into forward bias resulting in a low resistance shunt.

nel to an extent determined by the amount of current and the resistivity of the material. The amount of the reverse bias along x, on the other hand, uniquely determines the extent to which the depletion layer moves into the channel and increases the resistance. If the length of the channel, L, is very large with respect to the thickness a then the x component of the field in the depletion layer and the y component of the field in the channel are quite small and may be neglected. Shockley[2] has called this the gradual approximation. As a consequence, the potential in the channel may be written

$$v(x) = \frac{qN_n h^2}{2\kappa\epsilon_0}, \tag{1}$$

where $v(x)$ is the potential in the channel, q is the electronic charge, N_n is the excess impurity density in the n region, h is the depletion layer thickness (a function of x), κ is the dielectric constant of the base material and ϵ_0 is the permittivity of free space. Since the depletion layer thickness increases along the x axis and the total current in the steady state is independent of x, the current density in the channel must increase with increasing x.

As the potential applied to the drain is increased, the depletion layer in the channel continues to expand. This process will continue with increasing bias until the depletion layer extends completely across the channel. The voltage at which this occurs is called the pinch-off voltage, and is given by

$$V_p = \frac{qN_n a^2}{2\kappa\epsilon_0}, \tag{2}$$

where V_p is the voltage applied to the drain terminal at $x = L$, and a is the channel thickness.

From Ohm's law, the current density in the channel is

$$\vec{J}(x) = \sigma\vec{E}(x), \tag{3}$$

where the current density and field are both functions of x and the channel conductivity, σ, is a constant. From the geometrical considerations given above, the field in the channel is assumed to be parallel to the plane of the junction. The total current in the channel is independent of x, and the current density may be expressed in terms of the depletion layer thickness,

$$\vec{J}(x) = \frac{\vec{I}}{Z(a - h)}, \tag{4}$$

where Z is the third dimension of the device. Inserting this relationship into (3) results in

$$\frac{dv}{dx} = \frac{I}{\sigma Z(a - h)}, \tag{5}$$

where I is the magnitude of the current. Inserting (1) and (2) into (5) results in

$$\left[1 - \left(\frac{v}{V_p}\right)^{1/2}\right]\frac{dv}{dx} = \frac{I}{\sigma aZ}, \tag{6}$$

which may be integrated directly to

$$v\left[1 - \frac{2}{3}\left(\frac{v}{V_p}\right)^{1/2}\right] = \frac{Ix}{\sigma aZ}. \tag{7}$$

This equation defines the potential at any point in the channel as a function of known or defined parameters. From (7) the current in the channel as a function of the applied voltage at the drain is given by

$$I = \frac{\sigma aZV}{L}\left[1 - \frac{2}{3}\left(\frac{V}{V_p}\right)^{1/2}\right], \tag{8}$$

where V is the potential applied to the drain. Eq. (8) reduces to

$$I_p = \frac{\sigma aZV_p}{3L} \tag{9}$$

at the pinch-off voltage, where I_p is defined as the pinch-off current. Inserting (9) into (8) results in

$$\frac{I}{I_p} = 3\frac{V}{V_p}\left[1 - \frac{2}{3}\left(\frac{V}{V_p}\right)^{1/2}\right], \tag{10}$$

which is a dimensionless equation defining the device characteristics below pinch-off. This characteristic is demonstrated graphically in Fig. 5. An examination of this curve will show that the current in the device increases with increasing applied voltage in an essentially linear manner for V/V_p less than about 0.3. Further increases in potential result in successively smaller increments of current. As V approaches V_p, the current approaches the limiting value of I_p.

Eqs. (2) and (9) give magnitudes for the pinch-off voltage and current, and (10) describes the V-I characteristic below pinch-off for a simple rectangular geometry. Actually, in practice, it is desirable to use a geometry in which the channel is a closed figure, either a circle or a complex pattern such as that described below. The advantage of the closed figure is that there need be no potential across the exposed periphery of the junction. So long as the perimeter of the channel is large compared to the length L, the above equations are still valid. Z, in this case, will stand for the perimeter.

When the pinch-off potential is approached, the gradual approximation fails in the region of the channel near $x = L$, where the depletion layer extends essentially all the way across the channel. The field distribution in this region at voltages near and beyond pinch-off is not easily analyzed. The most favored assumption has been that voltages in excess of pinch-off are absorbed in an extension of the depletion layer beyond the channel, as illustrated in Fig. 1(c). Since the voltage at the end of the channel remains at V_p, the depletion layer contour within the channel is unaffected by the excess voltage.

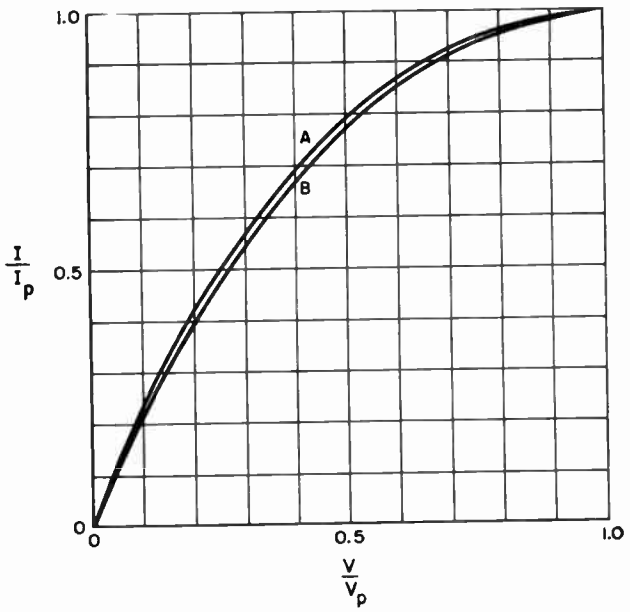

Fig. 5—I-V characteristic below pinch-off. (a) Step junction. (b) Graded junction.

One of the important features of the characteristic curve shown in Fig. 5 is the change in slope with increasing applied potential. The slope of the curve may be interpreted as the small signal ac conductance of the device. Thus, the small signal ac resistance characteristic below pinch-off may be obtained from (10) by differentiation, resulting in

$$R_{ac} = \frac{1}{3\left(\frac{I_p}{V_p}\right)\left[1 - \left(\frac{V}{V_p}\right)^{1/2}\right]}. \tag{11}$$

This relationship for the small signal ac resistance is plotted in Fig. 6 and indicates that the ac resistance approaches infinity as a limit as the applied bias approaches the pinch-off voltage. It is found that the small signal ac resistance does, in fact, reach very high values as the applied potential approaches and exceeds the pinch-off voltage.

The dc resistance of the device may be obtained by dividing the applied potential by the device current (10):

$$R_{dc} = \frac{1}{3\left(\frac{I_p}{V_p}\right)\left[1 - \frac{2}{3}\left(\frac{V}{V_p}\right)^{1/2}\right]}. \tag{12}$$

This relationship is also plotted in Fig. 6. In this case the dc resistance approaches a finite limit at $V = V_p$. If R_0 denotes the initial resistance of the device at zero applied potential, and R_p the dc resistance at pinch-off, then the pinch-off resistance is given by the simple expression,

$$R_p = 3R_0. \tag{13}$$

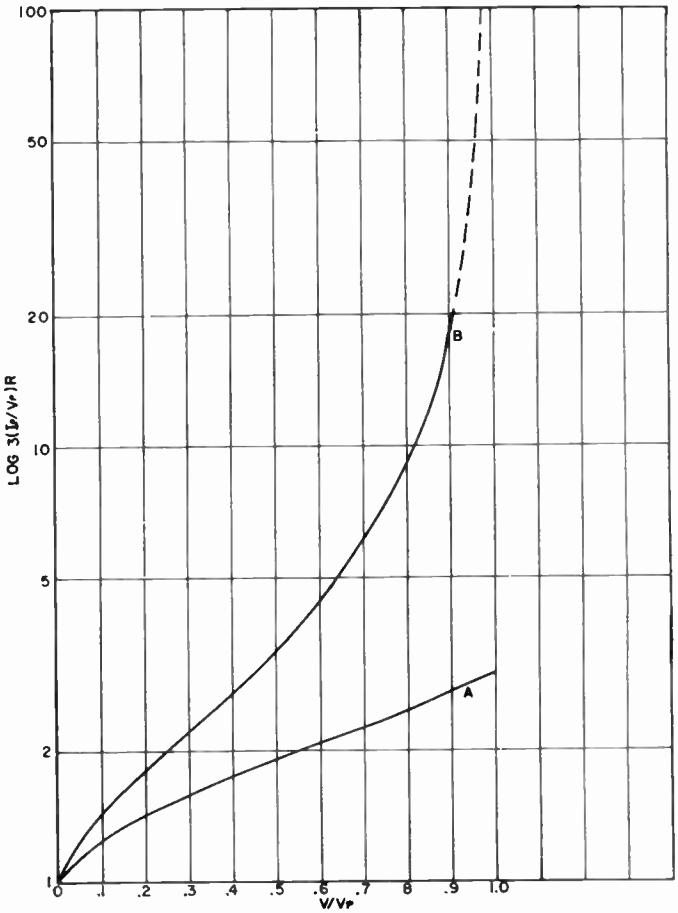

Fig. 6—Resistance characteristics below pinch-off. (a) DC resistance for step junction. (b) Small signal ac resistance for step junction.

One of the useful characteristics of the field effect limiter is this nonlinear behavior of the resistances, and the ratio of the ac to dc resistance is an important parameter. In the ideal case under consideration, this ratio increases from one to infinity as the applied bias is raised from zero to V_p.

Graded Junction Model

So far, the analysis has assumed a step junction between regions of uniform carrier density. However, most of the approaches now used or contemplated for actual device fabrication involve diffusion and, of course, graded junctions. The behavior of graded junction limiters is the same as that of step junctions, but the magnitudes are different. And at least for one parameter —the channel thickness—the behavior becomes far more critical.

In a diffused junction, the gradient is in general a function of y, the dimension normal to the plane of the junction (Fig. 1). But the channel thickness is a small fraction of the diffusion depth, and in this thin region we assume a constant gradient, A. The conductivity will be

$$\sigma(y) = q\mu A y. \tag{14}$$

Once more using the gradual approximation, the current density which is now a function of both x and y becomes

$$J(x, y) = E\sigma = q\mu AEy. \tag{15}$$

The current, at any point, x, is

$$I = Z\int_h^a J dy = q\mu AZE\int_h^a y dy$$
$$= \tfrac{1}{2}q\mu AZ(a^2 - h^2)E. \tag{16}$$

In a linearly-graded reverse-biased junction the depletion layer thickness in the channel is given by

$$v(x) = \frac{2qAh^3}{3\kappa\epsilon_0}, \tag{17}$$

where v is the potential difference across the junction. Since, in the device under study, the gate region is at zero potential, at any point along the axis, the potential across the junction is identically the potential in the channel. The applied voltage at which pinch-off will occur is

$$V_p = \frac{2qAa^3}{3\kappa\epsilon_0}. \tag{18}$$

Eliminating h in (16) and (17),

$$I = \frac{1}{2}q\mu Aa^2Z\left[1 - \left(\frac{v}{V_p}\right)^{2/3}\right]E. \tag{19}$$

Or, since

$$E = -\frac{dv}{dx},$$

$$Idx = -\frac{1}{2}q\mu Aa^2Z\left[1 - \left(\frac{v}{V_p}\right)^{2/3}\right]dv. \tag{20}$$

Integrating

$$I\int_0^L dx = -\frac{1}{2}q\mu Aa^2Z\int_0^V\left[1 - \left(\frac{v}{V_p}\right)^{2/3}\right]dv, \tag{21}$$

$$I = \frac{q\mu Aa^2Z}{2L}V\left[1 - \frac{3}{5}\left(\frac{V}{V_p}\right)^{2/3}\right] \tag{22}$$

where I is the magnitude of the current. In view of (18) this may be written

$$I = \frac{q^2\mu A^2a^5Z}{3\kappa\epsilon_0 L}\frac{V}{V_p}\left[1 - \frac{3}{5}\left(\frac{V}{V_p}\right)^{2/3}\right]. \tag{23}$$

The pinch-off current is

$$I_p = \frac{2q^2\mu A^2a^5Z}{15\kappa\epsilon_0 L}. \tag{24}$$

Eq. (23) may be written

$$\frac{I}{I_p} = \frac{5}{2}\frac{V}{V_p}\left[1 - \frac{3}{5}\left(\frac{V}{V_p}\right)^{2/3}\right]. \tag{25}$$

Eqs. (18), (24), and (25) correspond, for a linearly graded junction, to (2), (9) and (10). They give the magnitudes of the pinch-off voltage and current, and the V-I characteristic below pinch-off. It is seen that in a step junction the pinch-off current varies as the cube of the channel thickness, whereas in the graded junction it varies as the fifth power (Fig. 5). In the linearly graded junction the initial resistance depends on the mean carrier density, $Aa/2$, and is

$$R_0 = \frac{L}{q\mu\frac{Aa}{2}aZ} = \frac{2L}{q\mu Aa^2Z}. \tag{26}$$

At pinch-off, from (18) and (14)

$$R_p = \frac{5L}{q\mu Aa^2Z} = \frac{5}{2}R_0. \tag{27}$$

Device Design

The graded-junction structure analyzed above approximates to a reasonable degree the structure of the limiter now being made in model shop quantities. Structural features of this device are shown in Fig. 7. The most important factors in designing such a limiter are considered below.

In a frequently encountered design problem one is given a current level (*i.e.*, a pinch-off current) and is asked for the lowest pinch-off voltage which can accompany it. A current regulator, for example, should start its regulating action at a low voltage. Eqs. (18) and (24) give the pinch-off voltage and current, respectively, for the idealized case. Inspection of these equations shows that large values for μ and Z/L will permit small values for A and a, thus achieving the stated aim. (The dielectric constant κ may be ignored here because it enters both equations in the same way.)

Because the factor μ enters as it does, a lower pinch-off voltage can be achieved in germanium than in silicon at a given current level. This consideration suggests the use of certain intermetallic compounds in field effect limiters. At least one of these, gallium arsenide, is reported to possess an electron mobility greater than that of germanium, and an energy gap greater than that of silicon.[8]

A large value of Z/L means that the trench shown in Fig. 7 should have a length large compared to its width. Achieving this in a limited junction area leads naturally to a convoluted or "comb" structure of the sort shown in the plan view at the top of column 1, Fig. 8.

An upper limit on Z/L is imposed by considerations of size, thermal dissipation, or fabricational difficulty. It therefore becomes profitable to look more closely at the way a and A enter the pinch-off relations. With I_p, μ, and Z/L all specified, and with a fixed current level se-

[8] A. Coblenz, "Semiconductor compounds," *Electronics*, vol. 30, pp. 144–149; November, 1957.

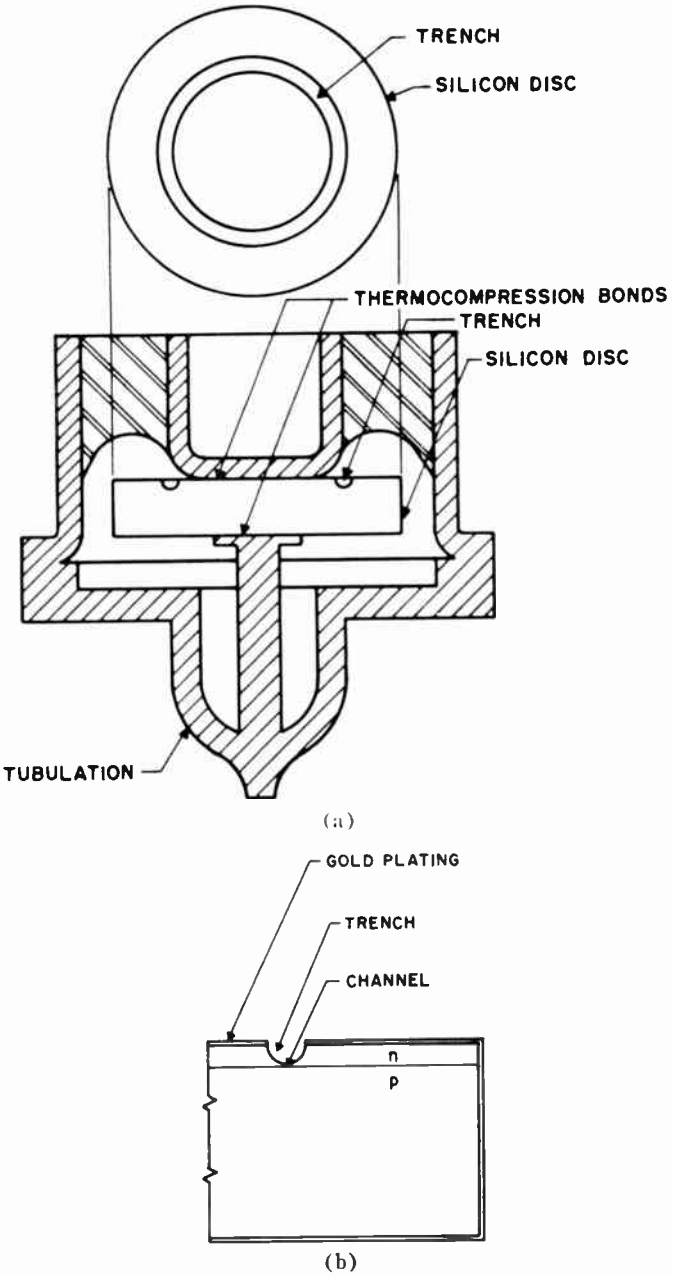

Fig. 7—Structural features of encapsulated device.

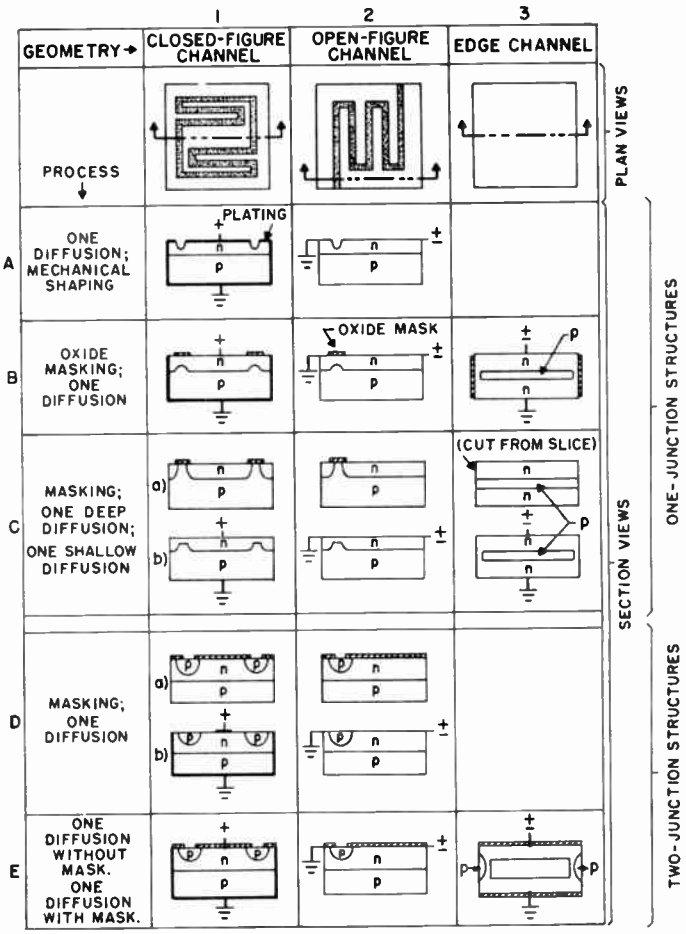

Fig. 8—Several field effect limiter structures.

lected, then in (24) we can let

$$A^2a^5 = K. \tag{28}$$

From (18) it is then possible to state that V_p is proportional to the quantity

$$\left(\frac{K^3}{A}\right)^{1/5} = (Ka)^{1/2}. \tag{29}$$

These expressions make it apparent that low pinch-off voltage is favored by increasing A and decreasing a in a compensating way to achieve the selected current level. (Breakdown voltage requirements, of course, place an upper limit on A.)

Fig. 9 sums up these considerations by showing the relationship of I_p, V_p, a, and Z/L for an n-type channel in silicon having a gradient of 5×10^{18} cm^{-4}. This sample design chart is based on (18) and (24), and, as indicated previously, it is reasonably valid for the device shown in Fig. 7.

Before discussing design features of this specific device, let us outline some of the steps in its fabrication: The starting material is a slice of 10-ohm-cm p-type silicon having a diffused n layer approximately 5×10^{-3} cm thick on one side. Disks are cut from this slice using an ultrasonic tool and are heavily gold plated on all surfaces. With another ultrasonic tool, a circular trench is cut through the gold plating and approximately half way through the n layer. Then the trench is deepened by chemical etching to produce a channel region between its bottom surface and the junction. The thickness of this channel is typically about 3×10^{-4} cm. As indicated in Fig. 7, both contacts are made by thermocompression bonding.[9]

External features of the package were largely dictated by the application for which this limiter was developed. Note in Fig. 7 how conveniently the disc and circular trench lend themselves to use in this package. Another important reason for choosing a circular trench is the

[9] O. L. Anderson, H. Christensen, and P. Andreatch, "Technique for connecting electrical leads to semiconductors," *J. Appl. Phys.*, vol. 28, p. 923; August, 1957.

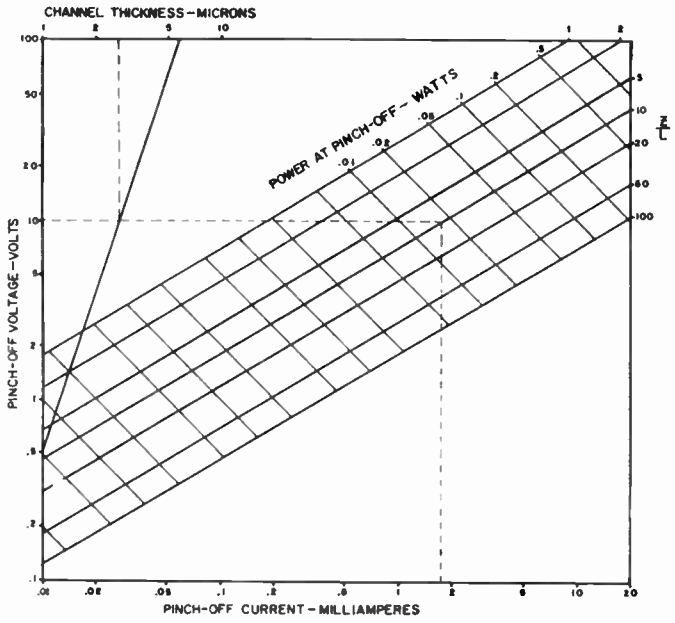

Fig. 9—Typical design chart: n-type silicon with 5×10^{18} cm^{-4} gradient.

ease with which a circular ultrasonic tool can be fabricated.

When these devices are biased above pinch-off, they display a parasitic capacity which to a good approximation is a shunt element. For a unit which pinches off sharply, the capacity is essentially that of the drain region of the junction—*i.e.*, that portion of the junction lying inside the trench circle. Its value is approximately 30 $\mu\mu$f in the present device. If it were necessary to diminish this capacitance, it could be accomplished by adopting a comb-type trench (or, indeed, any closed figure other than a circle). The object of this change of course would be to increase the ratio of drain region perimeter to area. It should be noted too that a low value for A favors a low parasitic capacity.

Another practical factor makes low A desirable: Since the channel is formed by mechanical shaping, it is difficult to achieve uniform channel thickness. If we use a low value of A, and hence a thick channel, then a given absolute variation in channel thickness is proportionately less significant. It is clear that sizeable percentage variations in a will cut down the effective Z of the device. That is, the thin regions will pinch off at low voltages and leave the thicker regions in parallel with them to determine I_p and V_p. Hence, there probably exists an optimum A from the point of view of achieving a low pinch-off resistance for a given degree of nonuniformity in channel thickness. The compromise involved here has not been thoroughly assayed, even empirically, but interesting and useful devices are being made at present with gradients in the range from 10^{18} to 10^{19} cm^{-4}. In this connection it is interesting to note in Fig. 9 that for $I_p=1$ ma, $V_p=10$ volts, and $A=5\times10^{18}$ cm^{-4}, which are currently typical values, then $Z/L\approx5$. The apparent value of Z/L is much larger; channel nonuniformity may contribute to this result.

The electrical properties of the present device are sensitive to the condition of the free surface of the channel. Buck[10] has shown the relation between various surface treatments and surface resistivity. The units constructed in the model laboratory are treated to provide a slightly inverted layer which both improves the shape of the V-I characteristic and reduces the sensitivity of the surface to moisture. This treatment increases the small signal resistance and decreases the pinch-off current and the pinch-off voltage. The current and voltage reductions are much the same as if the effective channel thickness had been reduced by the formation of a gate region at the surface.

Moisture as present in air of 30 per cent relative humidity reverses the benefits of the surface inverting treatment. Finished units are therefore vacuum baked and sealed. Stability of these units has proven entirely adequate for the exploratory circuit studies in which they are being used.

Present-day diffusion techniques—notably, oxide masking[11]—suggest many field effect limiter structures in addition to the one which we have been considering. Some of these are outlined in Fig. 8. These structures are grouped in various ways. First, it will be noted that each of the three columns represents a basic plan-view geometry. The device of Fig. 7 falls, of course, into column 1 (specifically it is 1A) because its channel forms a closed figure.

In the column-1 structures it is customary to make the drain contact to the region inside this closed figure, or to make it positive in the case of an n-type channel. This makes the entire periphery of the n region a source terminal. Hence, it is possible and even desirable to plate over the exposed junction edge in any of these structures, for this leads to a coaxial terminal arrangement. The metal-clad junction edge makes these structures rather novel among semiconductor junction devices. The device in this form has an unsymmetrical V-I characteristic. For the polarity indicated in Fig. 8 it is a current limiter, while for the opposite polarity it is effectively a forward biased diode shunted by the low-voltage conductance of the channel.

The structures of column 2 are symmetrical both physically and electrically. Metal plating over the junction is omitted and hence the source and drain are interchangeable. Note that the gates are "floating" as a consequence, and therefore take on the source potential by the mechanism sketched earlier. If handling or other considerations so dictate, the active region of any of the column 2 structures can be formed as a "mesa" on a bulkier gate region.

Column 3 depicts structures which are basically simpler than any of the others. Here the gate is com-

[10] T. M. Buck, "Effects of certain surface treatments and ambient atmospheres on surface properties of silicon," Meeting of the Electrochem. Soc., New York, N. Y.; April 17–May 1, 1958.

[11] C. J. Frosch and L. Derick, "Surface protection and selective masking during diffusion in silicon," *J. Electrochem. Soc.*, vol. 104, pp. 547–552; September, 1957.

pletely internal (except for the auxiliary gates in the last example), the terminals are coaxial, and the source and drain are again interchangeable; thus, these structures too are mechanically and electrically symmetrical.

A field effect limiter channel formed directly by diffusion should have more uniform properties than one could ever achieve by a process involving mechanical shaping. This is one of the important reasons for pursuing such structures. Because of the uniformity of the diffused channel, the effective Z/L is the same as the apparent Z/L and the advantage claimed above for a high A can be exploited. Much lower pinch-off resistance can thus be achieved.

The primary difficulty encountered in making all-diffused structures is that of achieving reproducibly the high sheet resistance required in the channel, which is of the order of several thousand ohms per square.

Another advantage of some of the all-diffused devices, 1C for example, is that the breakdown and channel pinch-off characteristic are to some degree decoupled. That is, the breakdown is mainly a property of the deeply-diffused, low-gradient junction, while the pinch-off resistance is determined by the shallow, high-gradient junction.

It will also be noted that the structures represented in Fig. 8 are divided into two broad groups, depending on whether their channels are bounded by one or two junctions. (We note in passing that the original field effect transistors were two-junction structures.)[4,5] A double-junction field effect device has the advantage that its reliability problems are essentially those of conventional junction transistors and diodes. That is, its sensitive region is the exposed edge of a reverse-biased junction.

Fig. 8 also indicates the major process steps in fabricating the various structures. About half of them have been realized in practice, and the remainder are logical variations and extensions of these. All of the structures of Fig. 8 are essentially rectangular. Because some interest attaches to circular structures, three of these are considered briefly in Appendix I.

A significant departure in fabrication procedure is now being explored. This involves the substitution of a thermal oxidation process for the second diffusion in the C structure of Fig. 8. A process recently described[12] induces an n-type channel on p-type silicon, and this channel can be produced with a sheet resistance appropriate for a field effect channel.

At the same time the process grows a silicon oxide layer which covers and protects the channel surface. These devices differ in several respects from those with channel junctions produced by conventional methods. One consequence of these differences is a more nearly linear initial region and a sharper "knee" in the V-I characteristic.

[12] M. M. Atalla, "Stabilization of silicon surfaces by thermal oxidation," Meeting of the Electrochem. Soc., New York, N. Y.; April 27–May 1, 1958.

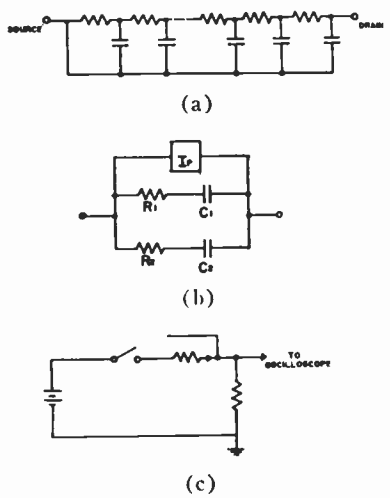

Fig. 10—Equivalent circuits and measuring circuits. (a) The equivalent circuit. (b) Approximate equivalent circuit. (c) Test circuit.

Equivalent Circuits

Measurements have been made on units produced in the laboratory to determine their response to small signal and step voltages. The device suggests circuit models which are appropriate to given operating conditions and to which the measured data can be applied.

The equivalent circuit of the current limiter, Fig. 10(a), is an RC transmission line in which the value of each element is a function of the voltage at that element. The capacitor at the drain end is the drain region depletion layer capacitance. For the step-junction gradual approximation, Appendix II provides an expression for depletion layer thickness from which R and C may be computed. Appendix III provides a means of computing the resistance between two points in the channel. This resistance may be used in calculations of the second phase of the step response described below.

No solution has been obtained for the exact circuit but, for an impressed step voltage that exceeds V_p, a reasonable constant-element circuit, Fig. 10(b), can be deduced from Fig. 10(a). Assume a step voltage between the source and the drain. At the first instant, current flows into the drain and charges the drain capacitance and the part of the channel capacitance which is adjacent to the drain. This capacitance decreases rapidly with voltage but the current still has an exponential-like decay. This phase of the transient response may be described by R_1 and C_1 of Fig. 10(b). Fig. 11(a) is a photograph of the initial transient of a unit connected as in Fig. 10(c). R_1 may be calculated from the peak value of the current and C_1 may be calculated from the exponent of a fitted exponential curve. The box in the figure labeled I_p may be considered an ideal current limiter and is provided so that the transient currents may decay to zero as they must with RC elements.

The second phase of the transient response is that of the current that charges the remainder of the channel capacitance, C_2. If one remembers that the charging of

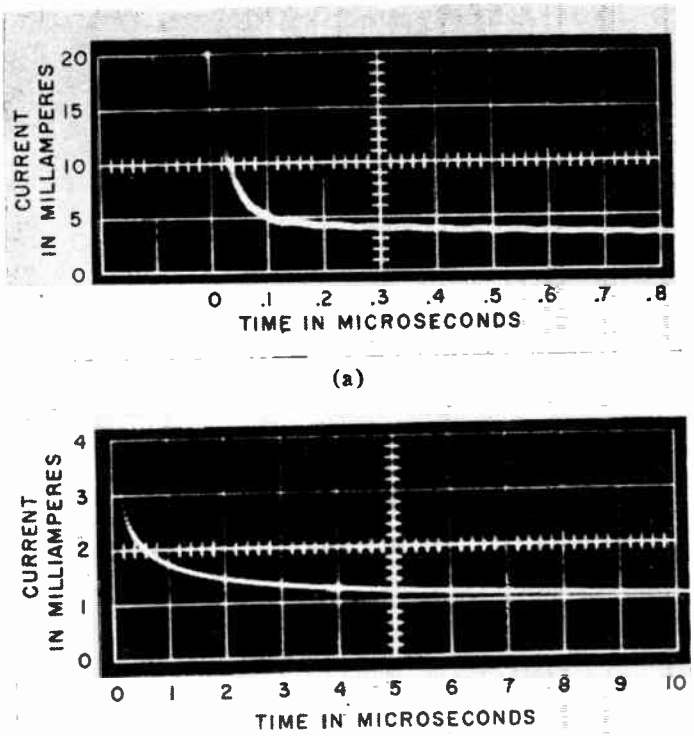

Fig. 11—Current response to applied step voltage. (a) First time constant. (b) Second time constant.

the capacitance near the drain implies that the conductance of the drain end of the channel has been greatly reduced, it is apparent that R_2 is considerably larger than R_1. Furthermore, since the voltages in the channel are always less than V_p, capacitance per unit area is considerably greater in the channel than in the drain and C_2 may be surprisingly large. Fig. 11(b) is a photograph of the long time current decay. R_2 and C_2 are determined from a zero time intercept and the exponent of a fitted exponential curve. Fitting the channel current decay with an exponential is somewhat crude because the transmission line current does not decay exponentially. However, some value of current and time may be chosen as an intersection which assures that the decay calculated from the equivalent circuit will meet the needs of a given application.

Fig. 10(b) may be given a second interpretation which makes it a suitable model for a small ac signal superimposed on a dc voltage that is greater than V_p. Again, R_1 and C_1 are associated with the drain region. R_1 is of the order of a few ohms and represents contact and body resistance. C_1, the drain capacitance, has an average value of 15 to 30 $\mu\mu$f depending on the bias voltage and is approximately one half of the value determined from the step voltage data.

R_2 and C_2 represent the pinched-off channel. The values of R_2 and C_2 derived from the step voltage data are averages over the period of the transient, while in the small signal equivalent circuit they are averages near the end of the transient and are larger and smaller, respectively. Since these elements are averages, their dependence on frequency is not surprising. Measurements of the unit, in the range of 1 to 200 kc, show a capacitance decreasing with frequency in the low-frequency region and a constant capacitance in the high-frequency region. The crossover is near 40 kc. R_2 behaves similarly. C_1, the drain capacitance, is taken to be the high-frequency constant capacitance because the reactance of C_2 is so small at these frequencies that it has a negligible effect on the measured value. The additional capacitance at low frequencies is assigned to C_2. R_2 and C_2 vary with frequency in such a way that the magnitude of the impedance of the limiter increases gently with decreasing frequency in the low-frequency region.

The measurements cited in this section were obtained from current limiters of a single design. Clearly, the values of the equivalent circuit elements can be substantially altered by appropriate design.

Appendix I

In addition to the geometries considered above, there are other configurations which warrant attention. In situations where high impedance is not objectionable some of these might find favor because of other attributes, such as ease of fabrication in the case of the first example. Expressions for pinch-off voltage and current are given.

I. Step-Junction, Circular, Filamentary Channel

Consider a device whose channel has the form of a circular filament of radius r_0 and length L, defined by a cylindrical, step, gate junction. Here

$$V_p = \frac{qN_a r_0^2}{4\kappa\epsilon_0} \tag{30}$$

and

$$I_p = \frac{\pi q^2 \mu N_a r_0^4}{16\kappa\epsilon_0 L}. \tag{31}$$

II. Step-Junction, Annular Channel

This is simply the circular case mentioned in the section on the idealized step-junction model, but with a substantial difference in the annular radii. If we call the outer radius r_s and the inner radius r_d (for source and drain, respectively) then

$$I_p = \frac{\pi q^2 N_a^2 \mu a^3}{3\kappa\epsilon_0 \ln \dfrac{r_s}{r_d}}. \tag{32}$$

So long as $r_s/r_d < e$, the error incurred in using the corresponding expression for the step-junction case is less than 10 per cent, if one lets $r_s - r_d = L$ and $\pi(r_s + r_d) = Z$. The expression for V_p is the same as for the rectangular case.

III. Graded-Junction, Annular Channel

Here

$$I_p = \frac{4\pi q^2 u_n A^2 a^5}{15\kappa\epsilon_0 \ln \frac{r_s}{r_d}}, \tag{33}$$

and once again V_p is given by the same expression as in the corresponding rectangular case.

Appendix II

An expression is developed herein for depletion layer thickness along the channel as a function of applied voltage.

Substitute (1), (2), and (9) in (7):

$$h^3 - \frac{3}{2}ah^2 + \frac{a^3 Ix}{2I_p L} = 0. \tag{34}$$

This equation may be transformed to the standard cubic form:

$$\lambda^3 + \alpha\lambda + \beta = 0, \tag{35}$$

where

$$\lambda = h - \frac{a}{2}. \tag{36}$$

$$\alpha = -\frac{3}{4}a^2 \tag{37}$$

$$\beta = \frac{a^3 Ix}{2I_p L} - \frac{a^3}{4}. \tag{38}$$

The form of the solutions to (35) may be investigated by examining the quantity

$$\frac{\beta^2}{4} + \frac{\alpha^3}{27} = \frac{a^6 Ix}{16 I_p L}\left[\frac{Ix}{I_p L} - 1\right]. \tag{39}$$

Since Ix/I_pL is always a number less than one, the quantity in the brackets is always negative. As a consequence, (39) will always be negative and one must expect three real and unequal roots to (35). The only solution, however, which satisfies the boundary conditions is the one of the form

$$\lambda = -\frac{1}{2}[A + B] - \frac{\sqrt{-3}}{2}[A - B] \tag{40}$$

where

$$A = \left[-\frac{\beta}{2} + \left(\frac{\beta^2}{4} + \frac{\alpha^3}{27}\right)^{1/2}\right]^{1/3} \tag{41}$$

and

$$B = \left[-\frac{\beta}{2} - \left(\frac{\beta^2}{4} + \frac{\alpha^3}{27}\right)^{1/2}\right]^{1/3}. \tag{42}$$

The boundary conditions to be satisfied are $h=0$ at $x=0$, $0<h<a$ at $0<x<L$, and $h=a$ at $x=L$, when $I=I_p$. Then (41) and (42) may be written in the form

$$A = \frac{a}{2}[\delta + j\epsilon]^{1/3}$$
$$B = \frac{a}{2}[\delta - j\epsilon]^{1/3} \tag{43}$$

where

$$\delta = \left(1 - \frac{2Ix}{I_p L}\right)$$
$$\epsilon = 2\left[\frac{Ix}{I_p L} - \left(\frac{Ix}{I_p L}\right)^2\right]^{1/2}$$

and $j=\sqrt{-1}$. Combining (40) and (43) results in the desired relation

$$\lambda = -\frac{a(\delta^2+\epsilon^2)^{1/6}}{4}\left[e^{j(\theta/3)} + e^{-j(\theta/3)}\right] + j\sqrt{3}\left[e^{j(\theta/3)} - e^{-j(\theta/3)}\right] \tag{44}$$

where $(\delta^2+\epsilon^2)=1$ and $\theta=\arctan \epsilon/\delta$. Converting (44) to the trigonometric form

$$\lambda = \frac{\sqrt{3}}{2}a \operatorname{Sin}\frac{\theta}{3} - \frac{a}{2}\operatorname{Cos}\frac{\theta}{3} \tag{45}$$

results in the depletion layer width, from (36)

$$h = \frac{a}{2}\left[1 + \sqrt{3}\operatorname{Sin}\frac{\theta}{3} - \operatorname{Cos}\frac{\theta}{3}\right] \tag{46}$$

where

$$\theta = \operatorname{Arc Cos}\left(1 - \frac{2Ix}{I_p L}\right) \tag{47}$$

or

$$\theta = \operatorname{Arc Cos}\left[1 - \frac{6x}{L}\left(\frac{V}{V_p}\right) + \frac{4x}{L}\left(\frac{V}{V_p}\right)^{3/2}\right] \tag{48}$$

Eq. (46) is the desired expression relating the thickness of the depletion layer at a point x in the channel as a function of the device current or applied voltage. Eq. (46) is demonstrated graphically in Fig. 12 for various values of current up to I_p.

It is interesting to note that (46) may be very closely approximated by the relation

$$h = \frac{a\theta}{\pi} \tag{49}$$

where θ (in radians) is given by (47) or (48). This relationship and its agreement with the calculated points from (46) is shown in Fig. 13.

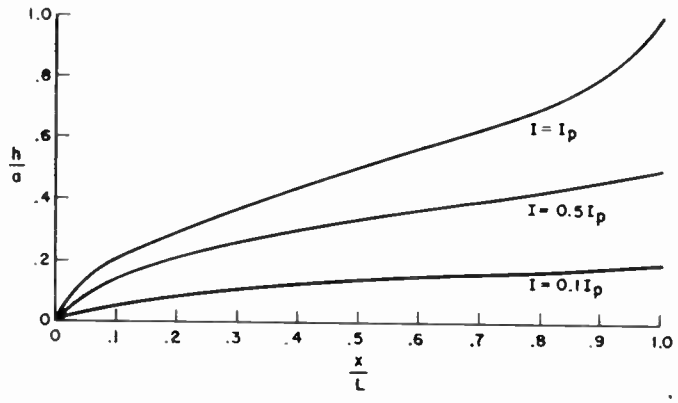

Fig. 12—Shape of depletion layer boundary.

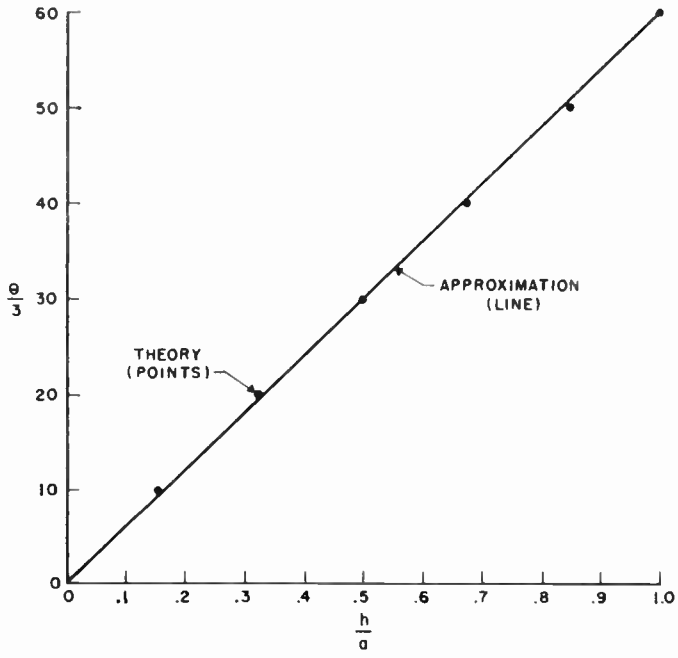

Fig. 13—Comparison of approximate and exact solutions for the depletion layer boundary.

Appendix III

It is of interest in discussions relating to the transient response of the current limiter to speak of the resistance of the channel between specified points along x. Since the resistance per unit length along the channel may be written

$$R(x) = \frac{1}{\sigma Z(a - h)} \tag{50}$$

inserting the expression for the depletion layer thickness derived in Appendix II results in

$$R(x) = \frac{2}{\sigma a Z\left[1 - \sqrt{3}\,\mathrm{Sin}\,\theta/3 + \mathrm{Cos}\,\theta/3\right]}. \tag{51}$$

The resistance between two points in the channel is therefore the integral of (51) between the two points in question,

$$R(\Delta x) = \frac{2}{\sigma a Z}\int_{x_1}^{x_2} \frac{dx}{1 - \sqrt{3}\,\mathrm{Sin}\,\theta/3 + \mathrm{Cos}\,\theta/3}. \tag{52}$$

This integration may be performed quite readily by letting

$$u = \mathrm{Cos}\,\psi = \mathrm{Cos}\,(\phi + \pi/3) = (\theta/3 + \pi/3). \tag{53}$$

The ϕ form of the integral is

$$R(\Delta x) = \frac{3I_pL}{\sigma a I Z}\int_{x_1}^{x_2} \frac{\mathrm{Sin}\,3\phi d\phi}{1 - \sqrt{3}\,\mathrm{Sin}\,\phi + \mathrm{Cos}\,\phi}, \tag{54}$$

which may be easily converted to the u form by recognizing that

$$2\,\mathrm{Cos}\,\psi = \mathrm{Cos}\,\phi - \sqrt{3}\,\mathrm{Sin}\,\phi. \tag{55}$$

Using the relations of (53) and (55), then (54) converts to the easily integrated form

$$R(\Delta x) = \frac{3I_pL}{\sigma a I Z}\int_{x_1}^{x_2}(2u - 1)du = \frac{3I_pL}{\sigma a I Z}(u^2 - u)\Big|_{x_1}^{x_2}. \tag{56}$$

Returning to the original notation in θ, and inserting the limits of the integration results in

$$R(\Delta x) = \frac{3I_pL}{\sigma a I Z}\left\{\left[\mathrm{Cos}^2(\theta^2/3 + \pi/3) - \mathrm{Cos}^2(\theta_1/3 + \pi/3)\right] - \left[\mathrm{Cos}\,(\theta_2/3 + \pi/3) - \mathrm{Cos}\,(\theta_1/3 + \pi/3)\right]\right\} \tag{57}$$

which is the desired expression giving the resistance between any two points along x in the channel. After insertion of the values for x of $x_1 = 0$ and $x_2 = L$, (57) gives the value of the resistance of the entire channel as a function of the device current in agreement with (12), derived earlier.

Acknowledgment

The writers are indebted to many of their associates at Bell Telephone Laboratories for contributions to this development. Thanks are especially due to V. L. Ronci and his coworkers for development of the encapsulation shown in Fig. 7, to W. J. Grubbs and H. Lawrence for proposals on structure, to E. F. O'Connell for exploratory device fabrication and to L. W. Hussey and his associates for their work in characterization and circuit applications.

IRE Technical Committee Report: Methods for Testing Radiotelegraph Transmitters (Below 50 MC)*

58 IRE 15.TR1

COMMITTEE PERSONNEL

Subcommittee on Radiotelegraph Transmitters up to 50 MC

I. R. Weir, *Chairman* 1958–
B. Sheffield, *Chairman* 1957–58, 1955–56, 1953–54
H. R. Butler, *Chairman* 1956–57, 1948–53
H. E. Goldstine, *Chairman* 1954–55

H. R. Butler 1948–58
J. F. McDonald 1948–57
B. Sheffield 1948–58
F. D. Webster 1948–57
I. R. Weir 1948–57

Committee on Radio Transmitters

A. E. Kerwien, *Chairman* 1958–
H. Goldberg, *Chairman* 1957–58
A. E. Kerwien, *Vice-Chairman* 1957–58
J. B. Singel, *Vice-Chairman* 1958–

J. H. Battison 1957–58
M. R. Briggs 1957–58
A. Brown 1957–58
H. R. Butler 1957–58
T. Clark 1957–58
C. G. Dietsch 1957–58
W. R. Donsbach 1957–58
L. K. Findley 1957–58
H. Goldberg 1958–
H. E. Goldstine 1957–58
F. B. Gunter 1957–58
R. N. Harmon 1957–58–
J. B. Heffelfinger 1957–58
P. J. Herbst 1957–58
L. A. Looney 1957–58
J. F. McDonald 1957–58
S. M. Morrison 1957–58
J. Ruston 1957–58
G. W. Sellers 1957–58
B. Sheffield 1957–58
J. B. Singel 1957–58
B. D. Smith 1957–58–
M. G. Staton 1957–58
V. E. Trouant 1957–58
I. R. Weir 1957–58–
V. Ziemelis 1957–58–

Committee on Standards 1958–59

R. F. Shea, *Chairman*
J. G. Kreer, Jr., *Vice-Chairman*
C. H. Page, *Vice-Chairman*
L. G. Cumming, *Vice-Chairman*

J. Avins
W. F. Bailey
M. W. Baldwin, Jr.
J. T. Bangert
W. R. Bennett
J. G. Brainerd
D. R. Brown
T. J. Carroll
P. S. Carter
A. G. Clavier
G. A. Deschamps
D. S. Dewire
S. Doba, Jr.
P. Elias
G. A. Espersen
D. Frezzolini
E. A. Gerber
A. B. Glenn
V. M. Graham
R. A. Hackbusch
H. C. Hardy
R. T. Haviland
A. G. Jensen
A. E. Kerwien
G. S. Ley
Wayne Mason
D. E. Maxwell
H. R. Mimno
E. Mittelmann
L. H. Montgomery, Jr.
G. A. Morton
R. C. Moyer
J. H. Mulligan, Jr.
W. Palmer
R. L. Pritchard
P. A. Redhead
R. Serrell
W. A. Shipman
H. R. Terhune
E. Weber
R. B. Wilcox
W. T. Wintringham

Measurements Coordinator

J. G. Kreer, Jr.

* Reprints of this report, 58 IRE 15. TR1, may be purchased while available from the Institute of Radio Engineers, 1 East 79 Street, New York 21, N. Y., at $0.60 per copy. A 20 per cent discount will be allowed for 100 or more copies mailed to one address.

Foreword

For many years there has been a strong need in industry for standardization of methods of testing radio telegraph transmitters. The report presented here is the result of activity over a long period by a subcommittee of the Radio Transmitters Committee. The material in its present form is not completely suitable for adoption as an IRE Standard because of the inclusion of material more appropriate for a manufacturing specification, and because the test methods described are not in all cases adequately specified.

Nevertheless, it is the feeling of the Standards Committee that publication of this report in its present form will usefully serve industry until such time as a true standard can be adopted. This report indicates the type of test procedures under consideration and will form the basis for a forthcoming standard. Constructive comments from the membership will be welcomed.—The Standards Committee

1.0 Introduction

Radiotelegraph transmitters, as considered by these notes, are radio transmitters intended for modulation by externally-generated telegraphic signals which may be produced manually, or by machines which convert intelligence into codes, such as Morse or the various teleprinter codes.

Radiotelegraph transmitters are used for point-to-point fixed, and for marine, vehicular and aviation mobile services using radio frequencies up to about 50 mc. These notes cover only radiotelegraph transmitters in which the telegraph signal either keys the carrier on and off or in which the carrier frequency is shifted in accordance with the telegraph signals. The specifications for a radiotelegraph transmitter are stated by a manufacturer or user, and include a number of specific items of technical performance that characterize the capabilities of the equipment.

It is recognized that there may be many satisfactory and correct methods of measuring any particular performance characteristic. In general, the preferred methods described herein are the simplest known and require the simplest measuring equipment for measurements within the accepted tolerances of current good engineering practice.

2.0 Classification of Tests To Be Performed

In testing a complete transmitter, it is assumed that the individual components, such as transformers, reactors, capacitors, contactors, relays, etc., have been tested as components in advance of assembly. Test methods for these items are adequately covered by publications such as those of the National Electrical Manufacturers Association, the Electronic Industries Association, and the Armed Services Electronic Standards Agency (JAN and MIL specifications).

Tests to be performed on complete transmitters fall into three general classes: Production Tests, Type Tests, and Design Model Tests. The purpose and extent of these classes of test are outlined below.

2.1 Production Tests

A production test is an abbreviated test to demonstrate that individual transmitters conform to certain standards of quality and uniformity. The following items are usually included in a production test: a check of vacuum tube voltages and currents under both key up and key down conditions; operation of controls, interlocks, and other personnel protection devices; setting of overload and time delay devices; a check of keyed waveform; a check of RF power output at one or more critical frequencies; and a heat run under specified operating conditions.

2.2 Type Tests

In the case of the manufacture of a group of transmitters whose number is sufficiently great, it is customary to type test a certain percentage of all production units (for instance, one out of every five of a small run of large transmitters, or possibly one out of fifty for a large run of comparatively small and simple transmitters). The type test is much more complete than the production test and is designed to reveal trends which indicate departure from the basic design. Units to be type-tested are usually selected at random from complete production-tested units. Additional items, such as the following, are usually tested during a type test: currents and voltages of all components; operation of the equipment at the extreme limits of rated power, frequency, and voltage; operation of control circuits under normal conditions and overload conditions; measurement of the per cent ripple from each power supply; oscillographic check of inrush currents to filaments of the larger tubes; oscillographic check of keyed waveform; voltage regulation and peak currents of power supplies; frequency stability, coverage and overlap; and heat run.

The heat run of a type test is more comprehensive than that of a production test. Its exact nature is normally covered by specifications prepared by either manufacturer or customer.

If humidity specifications are involved, type tests should also include observation of operation with variations of humidity within the required range.

The type test should also include sequence operation tests on automatic operation and check of the facilities for personnel protection. In the case of mobile equipment, type tests should include certain mechanical tests, such as resistance to shock and vibration.

2.3 Design Model Tests

Design model tests are for the purpose of verifying all aspects of the basic design for conformance with specification requirements, good engineering practice, and the needs of the customer in the field. Such tests are normally made on a preproduction type of model (engineering model, service test model, etc.) in advance of embarking on quantity manufacturing. In addition to all the tests listed in 2.1 and 2.2, design model tests include such items as shock and vibration tests (when required), tests for spurious output (both radiated and conducted), and tests under significant abnormal operating and ambient conditions.

3.0 Specific Methods of Transmitter Testing

3.1 Power Output

3.1.1 Power Rating: The power rating of a radiotelegraph transmitter is the RF power which it must deliver at its output terminals when connected to the normal specified load circuit or its equivalent. This rating may be different for different types of service, such as: 1) ON-OFF KEYING; 2) FREQUENCY SHIFT KEYING (FSK); 3) MODULATED CONTINUOUS WAVE (MCW) KEYING, etc. Transmitters are usually rated in terms of sea level operation and may be de-rated for operation at high altitudes.

The method of test should take into consideration the duty cycle for which the transmitter is designed. Transmitters which are intended for ON-OFF KEYING only, may be incapable of locked key operation at full power. In such cases, a duty cycle should be specified. This means that during tests the transmitter should be keyed, or operated at reduced output, so that the specified duty cycle (or its equivalent) is not exceeded.[1] Most telegraph transmitters, however, are designed to withstand locked key operation at rated power.

3.1.1.1 The power rating for ON-OFF KEYING is based on the power available in the ON (MARKING) condition with the stipulation that the marking time may not average more than a specified percentage of the total time.[2]

3.1.1.2 The power rating for FSK is the RF power available continuously and must be the same for both the marking and the spacing condition.

3.1.1.3 The power rating for MCW is that of the modulated carrier in the ON (MARKING) condition. The percentage modulation required must be stated. It is recommended that the maximum allowable per cent marking time also be stated.[2]

3.1.2 Methods of Power Measurement

3.1.2.1 General. A load which is designed for RF power measurement is connected to the transmitter output terminals. The impedance of the load (including any instrument) should be within the range of impedances into which the transmitter is designed to operate. The transmitter shall be operated at rated service conditions.

There are several methods of measuring the power delivered by a transmitter, of which typical methods are given below. The Calorimetric method is basic and is the preferred method; all others are considered alternate methods.[3] The actual choice of method is usually dictated by convenience as well as by practicality. For instance, low-frequency (kilocycles) low-power (tens of watts) transmitters can efficiently and accurately use the "Current-Resistance" method, whereas similar transmitters rated up to about one kilowatt, but operating at high frequency (megacycles), could efficiently, but not quite as accurately, use the "Photometric" method. The reason is that reactance-free resistors capable of dissipating medium power at high frequency are not easy to obtain.

3.1.2.2 Methods

3.1.2.2.1 Calorimetric Method. The calorimetric method employs the observation of the temperature rise of a coolant of known specific gravity, specific heat and rate of flow in which coolant the power output of the transmitter is being dissipated. The heat developed in the load shall be transferred to the liquid coolant of known specific heat. The construction of the load shall be such that the loss of heat due to conduction and radiation from the apparatus is negligible.

The load shall be equipped with means for accurately measuring the volume rate of flow of the coolant and with precision thermometers for measuring the temperature of the liquid entering and leaving the device. After the RF power has been applied, the rate of flow of the coolant shall be adjusted until an adequate difference between the input and output thermometer readings is obtained. Sufficient time shall be allowed to elapse to insure no further changes in the thermometer readings. When steady conditions have been obtained, both thermometer readings and the rate of flow of the coolant shall be noted. The average power dissipated in the load is calculated from the rise in temperature, rate of flow, specific gravity, and specific heat of the coolant. It is given by:

[1] F. E. Terman, "Notes on the effective heating of code transmitters," Proc. IRE, vol. 16, pp. 802–804; June, 1928.

[2] A typical specification might stipulate that the marking time must not exceed 60 per cent of the total time in any five-minute period.

[3] Theoretical background and extensive bibliography on this subject will be found in "Radio Frequency Power Measurements," NBS Circular 536, March 16, 1953; obtainable from the Superintendent of Documents, U. S. Government Printing Office, Washington 25, D. C.

$W_p = 264\ QGS\ (T_2 - T_1)$ where

W_p = Average power dissipated in watts

Q = Coolant flow in U. S. Gallons per minute

G = Specific gravity of coolant (equal to 1 for water)

S = Specific heat of coolant (equal to 1 for water)

T_2 = Outlet temperature of coolant in degrees centigrade

T_1 = Inlet temperature of coolant in degrees centigrade.

3.1.2.2.2 Alternate Calorimetric Method. In the calorimetric method, the power may also be measured by dissipating dc or low-frequency ac power in the same load and noting the amount of power measured in a conventional manner that is necessary to produce the same temperature rise in the coolant at the same flow rate.

3.1.2.2.3 Current-Resistance Method. This method consists of measuring the rms RF current through the load and calculating the average power as the current squared times the equivalent series resistance of the load. The load may be a dissipative line.

3.1.2.2.4 Photometric Method. In this method the load consists of one or more incandescent lamps. The light output of the lamps when acting as the transmitter load is measured by use of a photometer. The power absorbed by the lamps is then calibrated at the same light output level by replacing the transmitter with an ac or dc power source.

3.1.2.2.5 Directional Wattmeter Method. This method uses a device which is usually designed for specified impedance and frequency ranges, and is calibrated to measure the incident and reflected power in the transmission line. The difference is the power absorbed by the load.

3.2 Spurious Transmitter Output

3.2.1 Definition (Proposed Standard): Any part of the radio frequency output which is not a component of the theoretical output as determined by the type of modulation and specified bandwidth limitations.

3.2.2 General: Spurious transmitter output may appear: 1) across the output terminals of the transmitter; 2) from output terminals to ground (if output is balanced to ground); 3) on power supply, control, or other wiring emerging from the transmitter; 4) by direct radiation from transmitter circuits due to imperfect shielding.

Sources of spurious output are: 1) harmonics of the oscillator frequency; 2) cross modulation products within the transmitter; 3) sideband components due to ripple modulation or to improper shaping of the applied keying wave; 4) parasitic oscillations; 5) components producing steep wave front electrical discharges (gaseous rectifiers, brush-type motors, ball-bearings, etc.).

3.2.2.1 Harmonics of Oscillator Frequency. Harmonics of the oscillator frequency (including the first or fundamental) are inherently present in any transmitter.

Those harmonics below the output frequency are generated in the lower power stages of the transmitter and are, therefore, usually of much less magnitude than those above the output frequency, but can emerge from any of the sources listed above. These components may, of course, be amplified in the final or output stage of the transmitter, and, in an ON-OFF KEYED transmitter, can become objectionable under key-up conditions unless suitable care is taken with shielding of unkeyed stages and with blocking of keyed stages.

Since it is customary to operate the output or power stage of a telegraph transmitter as a Class C amplifier, harmonics of the output frequency of considerable magnitude appear in the output stage plate circuit. The amplitude of these harmonics must be maintained within the specified limits by suitable shielding and selectivity in the output circuits.[4]

3.2.2.2 Sideband Components. Adjacent channel interference, produced by telegraph transmitters using FREQUENCY SHIFT or ON-OFF KEYING, is due in part to the strong side frequencies generated by keying characters which are essentially square or rectangular in shape. Measurable side frequencies may extend to the vicinity of the 50th harmonic of the dot rate.[5] The side frequency spectrum occupied by a telegraph transmitter may be reduced considerably by controlling the shape of the keying characters.

3.2.2.3 Parasitic Oscillations. The causes and cures of such oscillations are very numerous and frequently quite complicated. Considerable information on this subject is available in published technical literature.[6]

3.2.2.4 Noise. The term "radiated or conducted noise" is usually applied to spurious outputs in the radio frequency range which result from various types of steep wave front discharges, such as those from corona, gaseous rectifier tubes, and sparking contacts. These outputs have the characteristics of damped waves, are frequently aperiodic, and are, therefore, made up of a multitude of component frequencies. These produce a signal in a radio-detecting device which is characterized as noise (hash). Considerable investigation is being done by commercial and government agencies in determining the various causes and cures of spurious outputs of this type, but little useful information has as yet appeared in technical periodicals.

3.2.3 Methods of Spurious Output Measurement

3.2.3.1 Actual Radiation. Measurement of actual radiation (sometimes called cabinet radiation) from a transmitter is made with some form of field strength meter. In order to obtain reliable measurements, the transmitter must be located in an area which is free from

[4] J. W. Labus and H. Roder, "The suppression of radio frequency harmonics in transmitters," PROC. IRE, vol. 19, pp. 949–962; June, 1931.

[5] G. S. Wickizer, "Relative amplitude of side frequencies in on-off and frequency shift telegraph keying," *RCA Rev.*, vol. 8, pp. 158–168; March, 1947.

[6] G. W. Fyler, "Parasites and instability in radio transmitters," PROC. IRE, vol. 23, pp. 985–1012; September, 1935.

ambient radio frequency fields, or alternately, in a suitable shielded room with all conductors entering the shielded area properly filtered to prevent radio frequency disturbances from being conducted into the room. Measurements are made with the transmitter delivering rated output into a dummy load representing its normal specified load. The transmitter output leads and the load itself must be carefully shielded to prevent setting up fields within the shielded room which would interfere with the measurements.

Improvements in measuring equipment and techniques for measuring direct radiation from transmitters are being carried on continuously. Techniques in making measurements are quite involved and attempts to establish standard methods whereby reproducible results can be obtained have not yet been very successful due to wide variations in ground conditions, screened room conditions, etc. In general, measurements made in the open, with the transmitter located on a conducting ground plane are considered standard, but the suitable environmental conditions are very difficult to achieve in practice. When measuring in a screened room, effects of standing waves have to be averaged out by exploratory movement of the pickup (loop, rod, or dipole antenna) before taking a reading. Readings are usually taken with the pickup about three feet from the equipment under observation and with the pickup oriented by exploration to record the maximum radiation at each frequency or frequency band involved.

3.2.3.2 Conducted Spurious Outputs. Measurement of conducted spurious outputs may, in general, be made with the same measuring equipment as used for radiation measurements, except that the pickup antenna is removed and the measuring equipment used as a frequency selective RF voltmeter to measure each frequency component appearing between any of the external connections to the transmitter (RF output terminal(s), power leads, control leads, etc.) and ground. In measuring spurious outputs from the normal RF output terminal(s) of a transmitter under key-down conditions, a voltage divider is generally required to avoid overloading the measuring gear. The ratio of the divider must either be flat over the frequency range of measurements being made, or its frequency characteristics must be known. In many cases it will be necessary to insert a carrier frequency rejector circuit in the input of the measuring device when measuring components other than the carrier frequency in order to avoid erroneous readings due to generation of harmonics and cross-modulation products in the input circuits of the measuring device.

3.2.3.2.1 Sideband Components. In practice the sideband components are measured indirectly and approximately by observation and analysis of the keying pulse. A sample of the output of the transmitter under test may be applied to the vertical plates of a cathode ray oscilloscope which has an accurate adjustable delay control of the horizontal sweep. The time base for the sweep on the oscilloscope is then synchronized with the keying rate in order to produce a stable trace of one or more keying pulses on the screen. The build-up and decay time of the keying pulse can then be accurately measured and the approximate value of sideband components calculated. Alternately, the pulse may be traced or photographed and analyzed graphically. For FSK transmitters, the shape of keyed pulse can be derived by applying a portion of the transmitter RF output to a suitable frequency discriminator and analyzing the output. Alternately, the applied keying pulse (after shaping) can be observed at the point at which control of the carrier frequency is obtained. This latter procedure is valid only if the control of output frequency is substantially linear with variation of applied voltage, and no appreciable amplitude transients are introduced in the keying process.

3.3 Frequency Stability

3.3.1 Definition (1948 IRE Standard): The carrier frequency stability of a transmitter is a measure of the ability of the transmitter to maintain an assigned average frequency.

3.3.2 Determination of Frequency Stability: The frequency stability is usually expressed as a percentage departure from the nominal operating frequency. Frequency stability is determined by making a series of discrete frequency measurements over a suitable range of controlled conditions that cause frequency variations, such as temperature, humidity, power supply variations, elapsed time, keying duty cycle, etc.

3.3.3 Methods of Frequency Measurement

3.3.3.1 General. Considerable material has been published regarding the techniques of frequency measurement and the apparatus involved.[7-9] The method of frequency measurement to be used is governed by factors of desired accuracy, speed of measurement, nature of observed signals, interference conditions, and simplicity of measuring equipment.

3.3.3.2 Preferred Method. Frequency is measured by using an instrument which counts events (carrier cycles) per unit time (seconds). Such an instrument usually reads directly in cycles per second. It must be noted that the precision of the instrument in determining unit time must be at least an order of magnitude better than the desired precision of measurement.

3.3.3.3 Alternate Method. Wide usage has been made of a method which employs a primary frequency standard consisting of a 100 kc quartz crystal oscillator and

[7] G. E. Sterling, "The Radio Manual," D. Van Nostrand Company, Inc., New York, N. Y.; 1943. Chapter on "Radio . . . Frequency Measurements and Frequency Monitors" contains a complete description of frequency measuring apparatus and techniques.

[8] F. E. Terman, "Radio Engineers' Handbook," McGraw-Hill Book Co., Inc., New York, N. Y.; 1950 Material on "Measurements" consists of a concise summary of some frequency measuring apparatus.

[9] H. O. Peterson and J. B. Atwood, "Frequency Measuring System," U. S. Patent No. 2,321,315, describes a frequency measuring set

associated multivibrators to give frequencies distributed over the entire spectrum at 10 kc intervals. A calibrated receiver is used to identify the particular 10 kc harmonic which is nearest to that of the signal to be measured, and the difference frequency between that harmonic and the unknown signal is measured by means of a calibrated audio oscillator. The long time frequency stability of the reference standard is checked by operating a clock from the multivibrator and checking the clock against standard time. The short time frequency stability is checked by comparison with standard frequencies as transmitted by standard frequency stations. Schedules and data concerning such transmissions can be obtained by applying to the Superintendent, U. S. Naval Observatory, Washington, D. C. The schedules are published in various technical magazines from time to time.

When transmitter and frequency measuring apparatus are in close proximity, false measurement may result from spurious receiver response. This effect can be minimized by effective receiver shielding and orientation, and also by adequate attenuation of signal applied to the receiver input terminals. In any event, it is necessary to determine that the receiver response is to the desired signal frequency and not a spurious response.

3.4 Carrier Hum

3.4.1 General: Carrier hum caused by commutator ripple, and other power supply causes may occur both as amplitude modulation and frequency modulation of the emission of a transmitter. Amplitude modulated hum is of importance in both amplitude keyed and frequency shift keyed transmitters and is ususally expressed as a percentage of the carrier amplitude. The frequency modulation hum is of importance only in frequency shift keyed transmitters and is usually expressed as a percentage of the rated frequency deviation of the transmitter. In measuring carrier hum, the transmitter should be operated normally, at rated power output, into a dummy load of specified impedance characteristics.

3.4.2 Methods of Measuring Amplitude Modulation Hum: The preferred method for measuring AM hum is as follows. Use a suitable AM demodulator to derive both the AM hum and the carrier amplitude of a portion of the transmitter output. Measure the carrier amplitude and the rms value of the hum over the desired frequency band. The carrier hum is (rms hum/carrier amplitude $\times 0.707$), expressed as per cent.

3.4.3 Method of Measuring Frequency Modulation Hum: The preferred method for measuring FM Carrier hum on an FSK transmitter is as follows. Detect a portion of the transmitter output with a suitable angular modulation demodulator, which is accurately calibrated in frequency deviation versus output voltage. With the transmitter on mark, measure the deviation of each hum frequency component using a wave analyzer. The hum is then expressed as a per cent of modulation at each significant hum frequency.

If a phase modulation detector is used, 100 per cent modulation is equivalent to 1 radian of phase modulation. Using a FM demodulator, the per cent modulation is 100 times the ratio of the frequency deviation due to the hum component divided by the frequency of the particular hum component.

3.5 Keying Characteristics

3.5.1 General: To test a transmitter to determine its keying characteristics, the transmitter is connected to the equivalent of the load called for by its specifications and operated at rated power. When a selective load is a specified condition, the test should be made with the most selective load specified and the lowest radio frequency. This condition is relevant only in the case of radio-telegraph transmitters of low and very low frequencies where the load selectivity may be of significance.

A source of keying signals is connected to the transmitter keying input. This source must be suitable for signals with any and all the characteristics with which the transmitter is required to operate. This must include reversals at all speeds from zero up to the highest speed specified, widely-spaced minimum length marking characters, and widely-spaced minimum length spacing characters.

3.5.2 Telegraph Keying Distortion

3.5.2.1 General. Telegraph keying distortion in ON-OFF and FREQUENCY SHIFT KEYING is the departure of the waveshape of the demodulated carrier from a desired waveshape. The desired waveshape is a compromise between the square wave for maximum intelligibility and wave forms which produce minimum adjacent-channel interference. The interference-producing potentialities of various keying waveshapes are described in the literature[5,10] to aid in determining the desired waveshape. Change of the relative time lengths for mark and space between the input and output of the transmitter is also a form of distortion, generally undesirable in a transmitter.

3.5.2.2 Qualitative Methods of Measurement.[11,12] With the telegraph transmitter operating under rated conditions, with rated keying signal voltage applied to the keying-input terminals, the RF output of the transmitter should be demodulated by an essentially distortionless AM or frequency shift detector (for ON-OFF KEYING and FREQUENCY SHIFT KEYING, respectively) and the detector output should be applied to a cathode-ray oscilloscope, having provisions for a time base to determine keying speed. The departure of the waveshape presentation on the oscilloscope from the

[10] A. D. Watt, V. J. Zurick, and R. M. Loon, "Reduction of adjacent channel interference from on-off keyed carrier," IRE TRANS. ON COMMUNICATION SYSTEMS, vol. CS-4, pp. 41–58; October, 1956.

[11] R. B. Shanck, F. A. Cowan, and S. I. Cory, "Recent developments in the measurement of telegraph transmission," *Bell Sys. Tech. J.*, vol. 18, pp. 143–189; January, 1939.

[12] A. B. Shone and R. T. Fatehchand, "The measurement of telegraph distortion," *Electronic Eng.*, vol. 20, pp. 181–185; June, 1948.

"desired waveshape" is a qualitative measure of telegraph keying distortion. Photographs of oscilloscope traces are useful for comparative analysis. The two most important characteristics to observe are the per cent bias,[13] marking or spacing, and the general wave formation. The latter includes rise and decay slopes, transients, and extraneous modulations of the wave.

3.5.2.3 Quantitative Methods of Measurement. An oscilloscopic presentation of the pulses will yield this information with sufficient accuracy. It is possible to measure marking or spacing bias to within 5 per cent by using the mark/space overlay method which consists of adjusting the oscilloscope sweep so that a mark lies on top of the space pulse, such as when the scope sweep rate is adjusted to 1.5 times the keying speed. By this method, keying bias may be measured without very special equipment. With trapezoidal keying pulses, this results in an x pattern so called after the pattern formed by the successive superimposed pulses.

3.5.3 Telegraph Keying Speed Capability

3.5.3.1 General. A dot-cycle is one cycle of a periodic alternation between two signaling conditions, each condition having unit duration. Thus, in two condition signaling, it consists of a dot, or marking element, followed by spacing element.

Dot-Cycle per Second defines keying speed and is equal to the reciprocal of the duration of the Dot-Cycle in seconds.

Telegraph Keying Speed Capability is the capability of the transmitter to perform satisfactorily at rated keying speed.

3.5.3.2 Method of Measurement. With the transmitter set up as in paragraph 3.5.2, and with continuous Dot-Cycle keying signal of rated voltage applied to the keying input terminal, raise the applied keying speed (Dot-Cycle per Second) to the maximum required by the performance specifications, and by oscillographic observation assure that the transmitter keying circuits follow with no chatter, misses, or waveshape distortion in excess of that permitted by the specifications.

[13] Published IRE Definition of Bias Telegraph Distortion: "Distortion in which all mark pulses are lengthened (positive bias) or shortened (negative bias). It may be measured with a steady stream of "unbiased reversals," square waves having equal-length mark and space pulses. The average lengthening or shortening gives true bias distortion only if other types of distortion are negligible."

A High-Speed Logic System Using Magnetic Elements and Connecting Wire Only*

HEWITT D. CRANE†, SENIOR MEMBER, IRE

Summary—**By introducing geometric variation in the basic magnetic core toroidal structure, new logic design freedom is achieved and effective decoupling is obtained between different windings linking the same element. By proper interconnection such elements may be used to provide unilateral information-flow properties without the use of explicit unilateral devices such as diodes. A practical system to accomplish this is outlined in this paper. The resulting circuits are relatively fast and inexpensive. Magnetic elements and connecting wires only are required. In particular, single-turn windings may be used in the coupling loops. Furthermore, inherent nondestructive read properties allow a great deal of logic facility. Simple shift register structures and logic elements and circuits are described.**

Introduction

SIMPLE, toroidal magnetic cores exhibit properties that make them well suited for digital storage applications. For logic operations, however, they are inherently less well suited. Because of bilateral properties, coupling or transfer loops connecting two such cores usually contain extra elements (usually diodes) to yield unidirectional data flow properties [1]. It has been found that by making use of geometrical variations of the basic toroidal core shape, multiaperture or multipath logic devices can be designed which may be connected together simply with wire. Thus entire logic systems may be constructed using only magnetic elements and connecting wires, aside from driving sources. Such a system is described in this paper. The system yields relatively high speeds of operation (*e.g.*, one-quarter mc information rates) and results in relatively low assembly costs because of the simplicity of the windings.

In this paper the basic system is described, and the significant properties of the system are delineated. Main emphasis is on the basic shift register structure. Papers currently being prepared for publication cover the theory of operation, a number of useful circuit variations and means for obtaining more complicated logic functions.

The development of the basic transfer loop and clock cycle leads directly into a simple shift register. The

* Original manuscript received by the IRE, June 13, 1958; revised manuscript received, October 15, 1958. The work reported here was carried on at Stanford Res. Inst., Menlo Park, Calif., under the sponsorship of Burroughs Corp. Res. Center, Paoli, Pa.

† Stanford Res. Inst., Menlo Park, Calif.

operational transfer loop properties are described in terms of an intuitive development, which nonetheless singles out the significant properties. The properties of elements with many apertures are discussed, and applications indicated, including the logic of multidimensional shifting arrays. Device geometry is discussed from two different aspects: 1) detailed shape requirements of any element in order to obtain good operational properties; and 2) specific geometrical shapes for achieving certain logic functions, such as NEGATION. The final section covers some aspects of wired logic, *i.e.*, logic functions obtained by appropriate interconnection of elements.

General Properties of MAD's

A MAD (Multiaperture Device) may be symbolically indicated as in Fig. 1(a). The element has a number of inputs n and outputs m. Also, a CLEAR winding links each element. Any input may be used to read information into the element, without crosstalk to the other information windings. Subsequently, this information may be read from any output winding, also without crosstalk to other windings. Furthermore, the information may be read out successively from some or all of the outputs, since the basic read-out process is nondestructive in the sense that binary information read from one output does not affect the information state at any other output. Only when an element is cleared is its information state destroyed.

In particular, one of the output apertures may be used as a connection point for an indicator to display the binary state of the element.

Logic functions may be formed directly within the elements so that given inputs x, y the output (s) may yield: x, y, $x+y$ (POSITIVE, POSITIVE OR); $x \cdot y$ (AND); $x \oplus y$ (EXCLUSIVE OR); $\bar{x}$, $\bar{y}$, $\overline{x+y}$ (NEGATION, NEGATIVE OR); etc. Examples of elements to perform these various logic functions are shown in Fig. 1(b). The EXCLUSIVE OR and AND elements are double input, single output, *i.e.*, form $x \oplus y$, $x \cdot y$. The negation element, which is single input, single output, is discussed further in connection with Fig. 15.

These elements may also be simply interconnected to perform logical functions (Fig. 16), *e.g.*, one output may control several inputs. Several outputs may be interconnected so as to transfer logical combinations of the variables; *e.g.*, given variable x stored in one element and y in another, then $x+y$, or $x \cdot y$ may be transferred to a third element. Further, the elements may be independently cleared.

Basic Transfer Loop

Properties of Input, Output Apertures

The first step in the development of the basic coupling loop is to discuss some of the properties of apertures as input and output access points. For now, consider the basic element structure to be a toroidal core (*e.g.*, of ferrite), in which small apertures are cut in the wall [3],

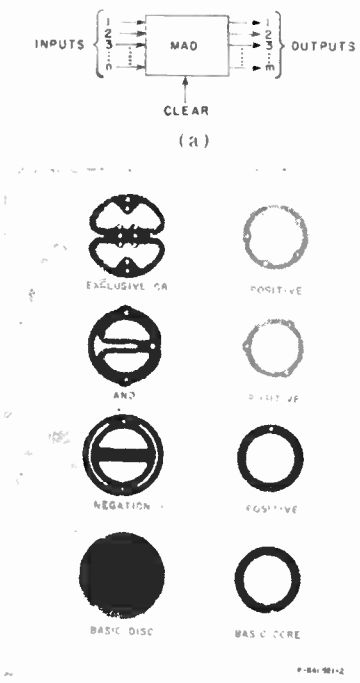

Fig. 1—(a) General characterization of MAD device. (b) Various MAD elements.

[4]. Input and output apertures may be identical, the distinction being made in the way that the windings linking these apertures are connected into the system. Consider first an aperture for output use, termed an output aperture (Fig. 2).

A winding of N_T turns links the aperture as indicated in Fig. 2(a). The main output property to consider is the family of ϕ_T vs F_T curves shown idealized in Fig. 2(d), where F_T is the mmf $N_T I_T$ and ϕ_T represents the switched flux per turn as a result of a current I_T. (The subscript T denotes that this winding will represent the transmitter end of a coupling loop.) As I_T (and hence the mmf $F_T = N_T I_T$) is increased from zero, an amount of magnetic flux ϕ_T ($= \int e dt / N_T$) is switched, the magnitude of which depends on the initial state of flux about the output aperture before the current I_T is applied. In Fig. 2(a), the element is shown in its CLEAR state, obtained by passing a sufficiently large current through the CLEAR winding. The mmf F_T tends to switch the flux in Leg ℓ_4 in a counterclockwise sense. With the element in its CLEAR state, the flux in Leg ℓ_3 is already completely saturated in the counterclockwise state with respect to the output aperture, so no flux may be switched locally (between Legs ℓ_2 and ℓ_4) as a result of F_T. In order to switch flux in Leg ℓ_4, F_T must be large enough to switch flux completely about the central aperture, as indicated by the dashed path in Fig. 2(a). Thus, before switching may occur, F_T must increase beyond a threshold F_2 which is related to the length of the switching path. As F_T increases beyond F_2, flux switches until Leg ℓ_4 is completely switched. The resulting ϕ_T vs F_T curve for this case is illustrated as curve (a) in Fig. 2(d).

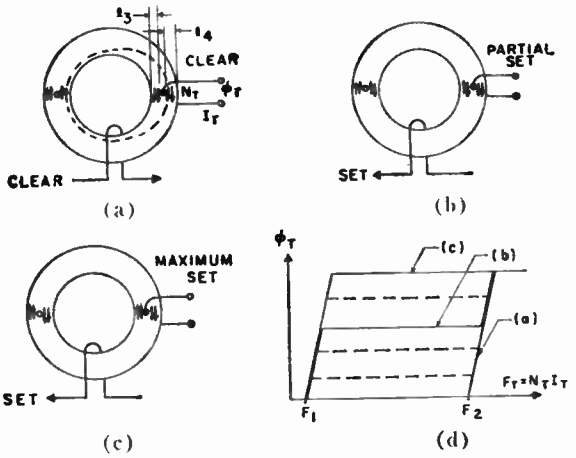

Fig. 2—Output-aperture properties.

The element may be in some flux state other than the CLEAR state before F_T is applied. For example, with the device initially in the CLEAR state, the element may be set by a current on the SET winding. Setting implies that flux is switched about the main central aperture. The magnitude of SET flux increases with the magnitude of SET current. With a particular value of current, the element may be maximally SET, in which case just half of the flux about the central aperture is switched. Under these circumstances, the flux in Legs ℓ_3 and ℓ_4 are both in the clockwise sense with respect to the output aperture. Thus, in this case, an output mmf F_T will be able to switch flux locally about the output aperture with only small values of F_T, the threshold, in this case, F_1, being related to the relatively short path length about the output aperture. As F_T increases beyond F_1, flux switches in Legs ℓ_3 and ℓ_4 until both legs are completely saturated in the counterclockwise direction, assuming Legs ℓ_3 and ℓ_4 have equal cross sectional areas. The resulting ϕ_T vs F_T curve for this case is labeled (c) in Fig. 2(d).

By controlling the magnitude of SET current, any value of SET flux may be obtained [3], [4]. For example, in Fig. 2(b), the element is shown partially SET. In this case, F_T may switch locally about the output aperture an amount of flux equal to the amount of SET flux. F_T must then increase in value beyond F_2 to switch the remainder of the flux switchable in Leg ℓ_4 about the central aperture. The resulting curve is labeled (b) in Fig. 2(d). Clearly, there exists a family of ϕ_T vs F_T curves, with the magnitude of SET flux as the parameter, as indicated in Fig. 2(d) in highly idealized form.

An element in the CLEAR state is defined as being in the binary *zero* state. An element in the SET (maximally SET) state is defined as being in the binary *one* state. In order to switch an element from its *zero* to *one* state, it is important to have a reliable means of maximally setting an element, without having to accurately control the magnitude of SET current. This property is obtained by using another aperture, an input aperture, for setting [Fig. 3(a)] [3], [4].

The input aperture is linked with a winding of N_R turns. (The subscript $_R$ denotes that this winding will represent the receiver end of a transmission loop.) The ϕ_R vs F_R curve for the element initially in its CLEAR state is illustrated in Fig. 3(b). It is identical to the ϕ_T vs F_T curve for a CLEAR element, since the threshold in this case is related to the same path length as in the case of the output aperture. As F_R increases beyond F_2, ϕ_R increases until all of the flux in Leg ℓ_1 (and Leg ℓ_3) is switched. This is the maximally SET case, Fig. 3(c), and regardless of the magnitude of I_R, no additional flux may be switched about the central aperture. Because of the unequal path lengths, the SET flux tends to switch in Leg ℓ_3 rather than in Leg ℓ_4. Some flux tends to switch in Leg ℓ_4, but actually it is an insignificant amount in the system to be described. There is no family of ϕ_R vs F_R curves to be considered here since the receiver element will be in the reference (or CLEAR) state before the input is applied.

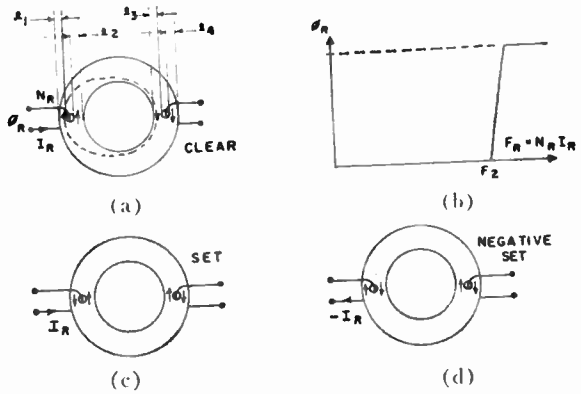

Fig. 3—Input-aperture properties.

The input aperture provides another extremely important property other than the setting feature just described. In an ordinary magnetic core, a negative mmf following a positive mmf tends to reverse, symmetrically, any flux switched by the positive signal. This is not true here, however, in the case where an input aperture is used. Fig. 3(c) indicates a maximally SET element, as a result of an input current flow I_R. Fig. 3(d) illustrates the effect of a subsequent negative input current, $-I_R$. Notice that the negative current merely reverses the flux *locally* about the input aperture *without* affecting the flux state at the output aperture. This decoupling feature is very important in the logic of the basic transfer loop.

Transfer Loop

A transfer loop may be constructed by connecting in parallel a transmitter winding of N_T turns and receiver winding of N_R turns. The transfer loop is then connected in series with an ADVANCE pulse source [Fig. 4(a)]. As indicated below, successful shift register operation may be obtained with $N_T \gtrless N_R$. In particular, the case $N_T = N_R$ is interesting since the transfer loop is

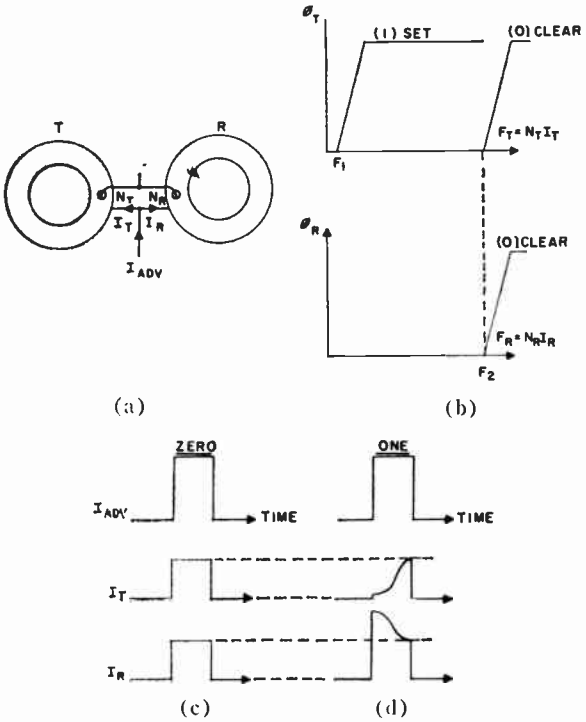

Fig. 4—Basic coupling loop.

symmetrical with inherent bidirectional shifting properties. For simplicity, this case is considered here; the extension to the general N_T, N_R case is straightforward.

The transmission problem is to ensure that as a result of an ADVANCE pulse, I_{ADV}, the receiver element ends up in the same state as the transmitter.

The transmitter is assumed to be in either the *zero* (CLEAR) or *one* (maximally SET) state. The receiver is initially in the *zero* (CLEAR) state, implying thereby that *zero* transmission occurs by "default." To insure that there will be no flux switching during *zero* transmission, the ADVANCE current must be limited in magnitude so that in this case the branch currents ($I_T = I_R = I_{ADV}/2$), are just large enough to bring their respective elements to the region of threshold F_2, but without causing any flux to switch [Fig. 4(c)]. With the transmitter in the *one* state, however, this same magnitude of ADVANCE current "swamps" the transmitter branch which now operates along the *one* (SET) curve with low threshold F_1. Thus the transmitter switches flux *locally* about its output aperture with low values of I_T, and by voltage or impedance "steering," the majority of ADVANCE current flows through the receiver, causing it to go over its setting threshold (F_2) and be SET. Typical current waveforms for this case are indicated in Fig. 4(d). In time, as the flux switching is completed, both currents return to their nominally equal values.

The transmitter readout is nondestructive in the sense that flux is switched only locally about the output aperture without disturbing the flux state elsewhere in the transmitter core.

Clock Cycle

Before the basic clock cycle is developed, it will be well to consider some related properties of basic core-diode shift registers [1]. A classical two-core-per-bit register is indicated in Fig. 5. The cores are considered in two groups arbitrarily labeled *O* (odd) and *E* (even), and an ADVANCE line links each core of a group in series. The transmission problem is to shift the stored information from one group of cores to the other at each ADVANCE pulse. In this case, with the conventional definition of *zero* and *one*, transmission of a zero is by default since the ADVANCE pulse causes no flux switching in a *zero* transmitter core. However, the ADVANCE pulse will switch a transmitter core storing a *one*, which results in a transfer loop current that switches the receiver core. Consider *one* transmission from the *O* to *E* core in the figure. Ideally, no effects of this transmission should be felt in any other elements. To so isolate the transmission effects, a series diode is generally used to prevent current from flowing in the following $E \rightarrow O$ loop as a result of the *E* (receiver) core switching, and a shunt diode is used to prevent backward transmission from the *O* (transmitter) core to the previous *E* core. Thus unilateralization is obtained by the use of unilateral elements.

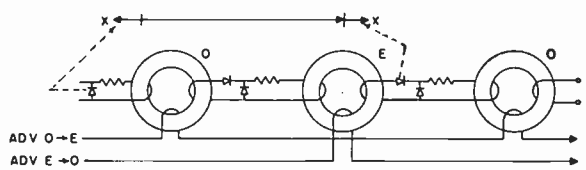

Fig. 5—Magnetic core-diode shift register.

Actually, each ADVANCE pulse has two functions. For example, the ADV $O \rightarrow E$ pulse causes the information stored in the *O* cores to be advanced to the *E* cores, but also, in so doing, leaves the *O* cores in the CLEAR (or reference) state, immediately ready to receive new information. With this orientation the development of the basic clock cycle for a MAD shift register is relatively straightforward.

Because of the nondestructive read-out properties of a multiaperture element, the ADVANCE current cannot satisfy the requirement of simultaneously advancing the information and clearing the transmitters as in a core-diode register. Thus specific CLEAR windings must be used, which results in a basic four clock system, as indicated in Fig. 6. The properties of each coupling loop are as previously described.

To get started in the cycle, assume the data are initially stored in the *O* elements. The ADV $O \rightarrow E$ pulse shifts the information to the *E* elements. The *O* elements are then explicitly cleared by the CL *O* pulse. The ADV $E \rightarrow O$ pulse shifts the information to the *O* elements, and the *E* elements are then cleared by the CL *E*

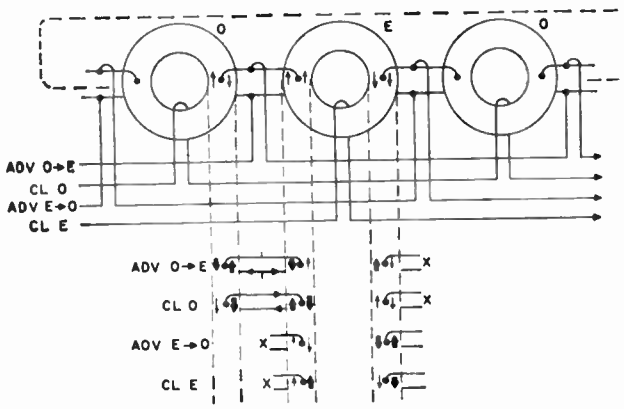

Fig. 6—Basic clock cycle.

signal, etc. Thus the basic cycle is:

$$\cdots, \text{ADV } O \rightarrow E, \text{ CL } O, \text{ ADV } E \rightarrow O, \text{ CL } E, \cdots$$

By tracing the details of the data transmission, one may see how the MAD's and basic clock cycle work together to yield unilateral transmission. As previously indicated, transmission of a *zero* is trivial. Transfer of a *one* is followed in detail in Fig. 6. Statements made with reference to this particular *one* transfer are true as well for every $O \rightarrow E$ loop simultaneously transferring a *one*.

Flux switched in any leg as a result of a particular pulse is indicated by a heavy arrow. The ADV $O \rightarrow E$ pulse switches flux locally about the output aperture of the O element and causes the E element to be SET. The CL O pulse then clears the O element and in so doing switches flux through the output winding. This results in a loop current flow that "negatively sets" the E element (receiver) [Fig. 3(d)] *without* affecting the flux state about the output aperture of the E element. Note that neither the ADV $O \rightarrow E$ nor CL O pulse causes any flux to be switched in the output leg of the E element (indicated by the crosses opposite the output winding), eliminating thereby the need for the conventional series diode. ADVANCE $E \rightarrow O$ shifts the binary *one* to the next O element in the direction of transmission, and CL E then clears the E element. Note again that neither the ADV $E \rightarrow O$ nor CL E pulses cause any flux to be switched in the input winding of the E element, eliminating the need for the shunt diode to prevent backward transmission. Thus unilateral data flow is achieved. Because at no stage is there any "unwanted" flux that must be dissipated slowly in resistance, the transfer rates may be relatively high.

Shift Register

The circuit of Fig. 6 satisfies all requirements of a shift register. It may be open ended or closed (as indicated by the dashed connection) and may be of arbitrary length. Furthermore, a great deal of design flexibility is possible in the choice of elements and turns. As previously suggested, for example, transfer loops may be operated with $N_T = N_R = N$ turns. In particular, however, N may be a single turn, as indicated in the circuit configuration of Fig. 7(a) and 7(b). Actually, the main significance is in connection with the single-turn transfer-loop windings, since these must be wound through the small apertures. The use of indicators will be discussed below.

With a symmetrical transfer loop ($N_T = N_R$), bilateral shifting is an inherent property. The clock cycle for left shifting is

$$\cdots, \text{ADV } A, \text{ CL } E, \text{ ADV } B, \text{ CL } O, \cdots$$

and for right shifting is

$$\cdots, \text{ADV } A, \text{ CL } O, \text{ ADV } B, \text{ CL } E, \cdots$$

where for clarity, the ADVANCE pulses have been arbitrarily renamed ADV A, ADV B [Fig. 7(a)]. Actually, the names ADV $O \rightarrow E$ and $E \rightarrow O$ have meaning only for shifting in a single direction, since ADV A, for example, causes $O \rightarrow E$ shifting in the right shift cycle, but $E \rightarrow O$ shifting in the left shift cycle. The shifting mode may be alternated from cycle to cycle, so that left and right shifts may be arbitrarily sequenced.

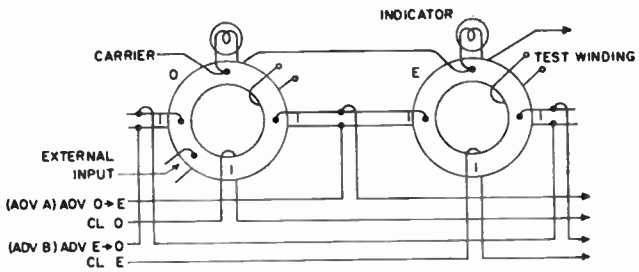

(a)

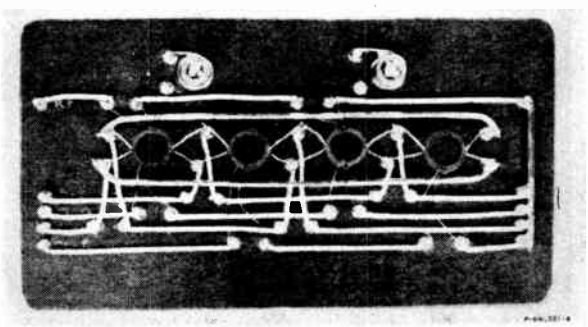

(b)

Fig. 7—Single-turn MAD shift register.

Information may be inserted into these registers by use of a winding on an external-input aperture, as indicated in Fig. 7(a). The use of extra input apertures will be clearer after the discussion of the properties of elements with many apertures (Fig. 10).

Transfer Loop Properties

Flux Gain Requirements

In order to operate stably, a closed-loop shift register must be able to circulate indefinitely an arbitrary stored

pattern of information without any change in the pattern. Thus if we follow a particular bit from stage to stage, the flux level representing it must be essentially identical at corresponding points in successive stages. In particular, it is necessary that $\phi_{TE}=\phi_{TO}$ [Fig. 9(a) and 9(b)] at the nominal *zero* and *one* flux levels, where ϕ_{TE} and ϕ_{TO} are the amounts of flux "transmitted" from adjacent stages (E following O) for a given bit of information moving along the register.

Let ϕ_U (ϕ_{UPPER}) and ϕ_L (ϕ_{LOWER}) be the nominal *one* and *zero* levels of flux respectively. Then for *stable* transfer of *ones*, it is necessary that the curve of flux gain $G=\phi_{TE}/\phi_{TO}$ plotted against ϕ_{TO} cross the unity gain line with negative slope where $\phi_{TO}=\phi_U$, as indicated in Fig. 8(a). (Note that with positive slope, any slight perturbation in transmitted flux level would result in ϕ_T moving away from the unity gain point ϕ_U on successive transfers.) For *stable* transfer of *zeros*, the same remarks hold for the behavior of $G(\phi_{TO})$ in the vicinity of ϕ_L, provided $\phi_L>0$.[1] Hence note the curve segment A in Fig. 8(a). Given the above, it is obvious that any gain curve, in order to be completed, must cross the unity-gain line with positive slope at some point, resulting in an unstable unity-gain point, ϕ_I in Fig. 8(a).

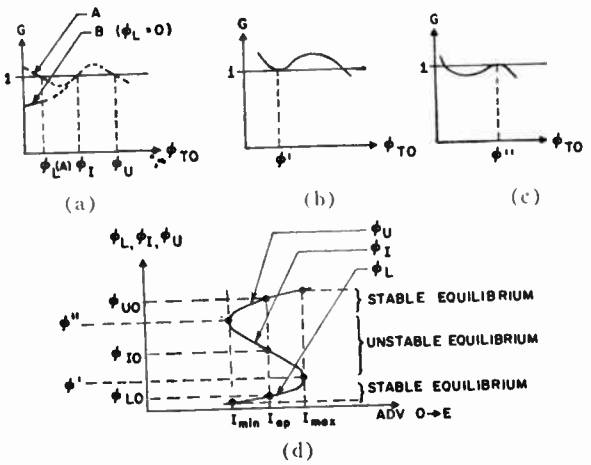

Fig. 8—Coupling loop gain curves.

Assume curve A in Fig. 8(a) to have been drawn for the nominal operating value (I_{op}) of ADVANCE current (ADV $O\rightarrow E$). The particular values of ϕ_L, ϕ_I, and ϕ_U obtained (subscript O) are represented as points on the diagram of Fig. 8(d). Now let the amplitude of ADV $O\rightarrow E$ be increased. There will be a tendency for $G(\phi_{TO})$ to increase for each value of ϕ_{TO}. That is, the gain curve will move "upward" in some fashion. As a result, ϕ_U and ϕ_L will increase in value, but ϕ_I will decrease, as plotted in Fig. 8(d). The register will continue to operate stably until ADV $O\rightarrow E$ is increased to the value I_{max}, the point where $\phi_I=\phi_L=\phi'$ [Fig. 8(b)]. At this point, "zero build-up" begins to occur since the lower stable unity-gain point disappears. On the other hand, if the amplitude of ADV $O\rightarrow E$ is decreased below I_{op}, the gain curve will move downward from its position in Fig. 8(a). Again, the operation is stable until ADV $O\rightarrow E$ is decreased to the value I_{min}, where $\phi_I=\phi_U=\phi''$ [Fig. 8(c)]. For (ADV $O\rightarrow E$) $<I_{min}$, an upper or *one* level of flux cannot be maintained since $G<1$ for any value of ϕ_{TO} greater than ϕ_L.

The "S curve" of Fig. 8(d) is typical of such curves obtained experimentally. The central portion of the curve is plotted by trial-and-error determination (for each value of ADV $O\rightarrow E$) of the minimum value of preestablished ϕ_T resulting in build-up to ϕ_U when the register is operated.

Note that for any value of current between I_{min} and I_{max}, flux discrimination ϕ_U/ϕ_L is just the ratio of points on the upper and lower segments of the "S curve" of Fig. 8(d). Furthermore, the fact that current amplitude is allowed to vary between I_{min} and I_{max} is an indication of the ADVANCE current tolerances or "range." Specifically, percentage range R as referred to in this paper is defined by

$$R = 100\left(\frac{I_{max} - I_{min}}{I_{op}}\right)$$

where

$$I_{op}=\tfrac{1}{2}(I_{max}+I_{min}).$$

Operation with Unity Turns Ratio

The possibility of obtaining the required type of flux gain characteristic with $N_T \gtrless N_R$ will now be considered for the cases of a simple core register on the one hand and a MAD register on the other [Fig. 9(a) and 9(b), respectively]. The "coupling circuit" in the core register is assumed to contain passive elements only.

For the MAD register, one may write (with all linear inductance neglected, for simplicity)

$$N_R\frac{d\phi_{RE}}{dt} = N_T\frac{d\phi_{TO}}{dt} - R_l I_l$$

where R_l is the loop resistance, and where I_l is the loop current superimposed upon the steady-state branch currents that would result if the current ADV $O\rightarrow E$ were left on until

$$\frac{d\phi_{TO}}{dt} = \frac{d\phi_{RE}}{dt} = 0.$$

By integration and rearrangement of the above equation, one obtains

$$\frac{\phi_{RE}}{\phi_{TO}} = \frac{N_T}{N_R} - \frac{\psi_{loss}}{N_R\phi_{TO}}$$

where $\psi_{loss}=R_l\int I_l dt$. The same equation holds for the core register, where, although the term ψ_{loss} may have a more complex form, it will in any case be positive be-

[1] If $\phi_L=0$, $\phi_{TE}=\phi_{TO}=0$ for any finite value of $G(0)$, but $G(\phi_{TO})<1$ near zero for stability. Hence segment B in Fig. 8(a) represents a possible alternate behavior of the gain curve at flux levels near zero. This case is a singular one, more of theoretical than practical interest.

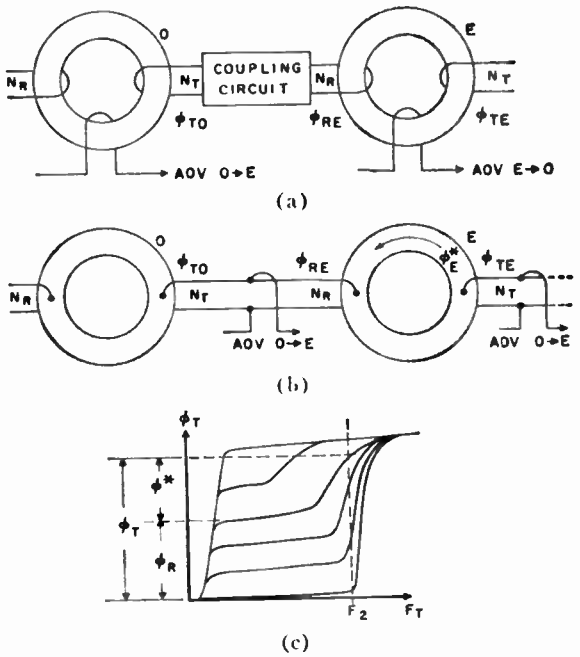

Fig. 9—Core-diode and MAD shift registers; typical family of MAD output curves.

cause of the passive nature of the coupling circuit.

Now for the core register, $\phi_{TE}=\phi_{RE}$, since the flux transmitted from a core is just equal to that previously received. Therefore,

$$G=\frac{\phi_{TE}}{\phi_{TO}}=\frac{N_T}{N_R}-\frac{\psi_{\text{loss}}}{N_R\phi_{TO}}.$$

From this equation it is seen that flux gain greater than unity, and hence stable operation as well, cannot possibly be achieved unless $N_T/N_R>1$.

On the other hand, for the MAD register, ϕ_{TE} may be greater than ϕ_{RE}. Specifically,

$$\phi_{TE}=\phi_{RE}+\phi_E^*$$

where ϕ_E^* represents any flux that may be switched around the *central* aperture of E due to excitation of ADV $E\rightarrow O$. Note that this enhancement of ϕ_{TE} relative to ϕ_{RE} would not be possible were it not true that the mmf driving the transmitter, although reversing flux equal to ϕ_{RE} around the output aperture, pushes in a direction so as to add to the set level ϕ_{RE} around the *central* aperture an amount of flux ϕ^* [Fig. 9(b)]. With $\phi_{RE}=\phi_{TE}-\phi_E^*$ substituted in the equation for ϕ_{RE}/ϕ_{TO}, the gain equation becomes

$$G=\frac{\phi_{TE}}{\phi_{TO}}=\frac{N_T}{N_R}+\frac{\phi_E^*}{\phi_{TO}}-\frac{\psi_{\text{loss}}}{N_R\phi_{TO}}.$$

Hence, in this case, stable operation may conceivably be obtained with N_T equal to or even less than N_R, provided the condition $\phi_E^*/\phi_{TO}>\psi_{\text{loss}}/N_R\phi_{TO}$ can be achieved over a suitable range of values of ϕ_{TO}. This prognosis has been proven with working laboratory shift registers for the case of $N_T<N_R$ as well as for $N_T=N_R$. The former case is of little practical interest, but the latter one is of great importance, as discussed elsewhere in this paper.

In order to obtain an idea of how substantial amounts of flux ϕ^* may be obtained, consider the more realistic [relative to the curves of Fig. 2(d)] family of output curves illustrated in Fig. 9(c). Suppose that an amount of flux ϕ_R has previously been received in an element. Now when flux is transferred out during an ADVANCE pulse, the *net* mmf acting on the element will initially be considerably less than F_2 while flux equal to ϕ_R is being reversed about the output aperture [Fig. 4(d)]. However, as this part of the process dies out, transmitter mmf N_TI_T builds up towards the steady-state value near the threshold value F_2. Therefore, primarily because the thresholds of the intermediate output curves are lower than F_2, a substantial amount of flux ϕ^* may be switched around the central aperture, enhancing or "boosting" the value of ϕ_T relative to ϕ_R.

In the case illustrated, the indicated value of ϕ_T is almost twice as great as the previously received ϕ_R. Note however, that for very low values, the ϕ^* boost is relatively small. Hence it is conceivable that the additive term ϕ_E^*/ϕ_{TO} of the gain eq. can be greater than the subtractive term $\psi_{\text{loss}}/N_R\phi_{TO}$ over a range of high values of flux and less than it over a range of lower values; if so, then with $N_T/N_R=1$, the gain curve will have the required type of behavior.

The above analysis has been highly heuristic. A precise analysis is difficult for several reasons:

1) The switching process in polycrystalline materials is not well understood.
2) A circularly symmetric geometry cannot be assumed, as in the case of toroidal cores. In particular, the flux switching about an output aperture cannot be treated merely as though it were switching in a small toroidal core. The problem is really a highly nonlinear field problem in a complex geometry.
3) The net mmf acting on any element during the transfer of a *one* varies with time and is in the vicinity of the threshold mmf for part of the pulse period. Hence, approximations assuming drive high compared to threshold cannot be used.

In spite of the above limitations, a great deal can be done in the way of understanding and predicting performance by extending the above type of reasoning with heavy reliance on empirical results, such as families of output curves, "peaking delay" curves (Fig. 13), etc. These properties are now being studied in detail.

Positive Elements with Many Apertures

So far the discussion has been mainly in terms of positive elements with a single input and single output aperture. By inserting more apertures, new circuit properties are possible. Because at most only one half of the total switchable flux about the central aperture is ever switched, it is possible to arrange the windings linking

the different apertures so that there is no undesirable crosstalk among them.

An element with n apertures is illustrated in its CLEAR state in Fig. 10(a). Any aperture may be used either as an input or output. The element may be SET from any input aperture. For example, in Fig. 10(b), the element is shown SET from input aperture 2. Note that no signals are induced in any other winding, as a result of the setting, regardless of whether it links an aperture designated as input or output. The key to this isolation is that no more than half of the circumferential flux about the central aperture is ever switched by any input winding. At every aperture then the SET flux switches in the leg not linked by a winding, and in this way effective isolation is achieved.

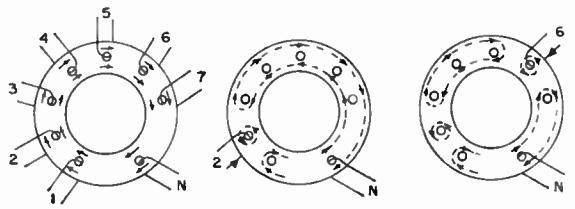

Fig. 10—POSITIVE MAD with many apertures.

The output circuits are likewise independent. Fig. 10(c) illustrates the case of transmission from output aperture 6. As described previously, flux changes occur only locally about the output aperture of a transmitter element. In this sense then, readout is nondestructive, since transmission from one output aperture does not alter the flux state about any other output aperture, which may therefore be subsequently used for data transmission as well.

Thus the many apertures exhibit a great deal of independence from each other. In the next two sections are illustrated examples of devices utilizing three or more apertures per element.

Indicators

With three apertures, an indicator may be added to the basic shift register by connecting a suitable lamp and exciting winding (shown as a carrier) through the third aperture (Fig. 7). The carrier amplitude must be limited in value so that it does not cause any flux to be switched about the central aperture, but merely alternates flux locally about its own aperture. In this way, it senses the state of the element nondestructively. The amount of flux available for local switching depends upon the state of the element. In the *zero* (CLEAR) state there is no flux available for local switching. Therefore, substantially no voltages are induced in the lamp circuit as a result of the carrier current, and the lamp remains dark. In the *one* (SET) state, relatively large amounts of flux are available for local switching and as a result of the voltages induced in the lamp circuit, relatively large currents cause the lamp to glow.

Since the carrier modulates the effective value of the threshold F_2 (Fig. 2), its presence affects the transfer properties of the circuit. In order to minimize its effect on operation, the carrier may be de-energized while the normal circuit operations occur, and reconnected to indicate the state of the register.

Multidimensional Arrays

It has been indicated that unity-turns-ratio shift registers are inherently bidirectional, it is interesting for illustrative purposes. However, to consider how a bidirectional register may be constructed using unilateral transfer loops, *e.g.*, $N_T > N_R$. Such a register is shown schematically in Fig. 11 using elements with three apertures. In this case three ADVANCE chains are required, ADV $E \rightarrow O$, ADV $O \rightarrow E_L$, ADV $O \rightarrow E_R$. For right shifting the basic cycle is

$$\cdots, \text{ADV } E \rightarrow O, \text{ CL } E, \text{ ADV } O \rightarrow E_R, \text{ CL } O, \cdots$$

and for left shifting the basic cycle is

$$\cdots, \text{ADV } E \rightarrow O, \text{ CL } E, \text{ ADV } O \rightarrow E_L, \text{ CL } O, \cdots.$$

Using exactly the same elements as in Fig. 11, the circuit may be rearranged to yield a two-dimensional shift register, as illustrated schematically in Fig. 12 (a).

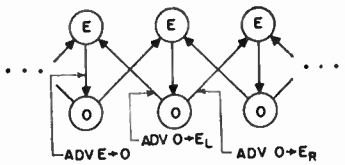

Fig. 11—Bidirectional shift register.

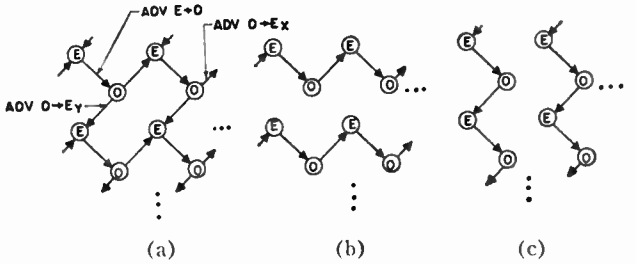

Fig. 12—Bidimensional shift register.

For x-direction shifting the basic cycle is

$$\cdots, \text{ADV } E \rightarrow O, \text{ CL } E, \text{ ADV } O \rightarrow E_x, \text{ CL } O, \cdots$$

as illustrated in Fig. 12(b), and for y-directional shifting the basic cycle is

$$\cdots, \text{ADV } E \rightarrow O, \text{ CL } E, \text{ ADV } O \rightarrow E_y, \text{ CL } O, \cdots$$

as illustrated in Fig. 12(c).

Actually, the circuits of Figs. 11 and 12 each exhibit two shifting modes. In the former case, the two modes are left and right (bidirectional) shifting. In the latter case, the two modes are horizontal and vertical (bidimensional) shifting. By extending this approach, it is

easily seen that for n different shifting modes (or dimensions) that $(n+1)$ apertures are required in each element. In the E elements there are n input and one output apertures. In the O elements, there are one input and n output apertures. Still additional apertures could be used in each element; *e.g.*, an extra aperture could be used for an indicator, another input aperture for entry of external information, or another output aperture for connection to an external circuit.

Moreover, by using symmetrical transfer loops, each of the n modes is inherently bidirectional, resulting, in a sense, in $2n$ modes. For example, a two-dimensional array would have $\pm x$, $\pm y$ shift facility.

One of the more interesting properties of the basic transfer system lies in this independence of the many apertures of an element allowing for the simple interconnection of multidimensional arrays without crosstalk.

Geometric Properties

Operational Aspects

For drafting simplicity, POSITIVE elements have been shown in most of the figures as ordinary toroidal cores with small apertures added. However, such elements do not have the optimum geometry for best operation. The main disadvantages are in the relatively poor ϕ vs F curves and switching properties. The major difficulty is that with apertures cut in the wall, no matter how hard the device is cleared, not all of the material can be left in major-loop saturation. This results in remanent reverse domains and hence minor-loop operation in parts of the core with resulting rounded threshold to the CLEAR state ϕ vs F curve, with considerable slope below threshold.

Switching properties are also poor in the following sense. The family of curves of Fig. 13(a) are curves of the voltage induced in a winding as a result of switching currents of various magnitudes, applied to a well saturated toroidal core of suitable material (see below). For example, a magnitude of current sufficient to switch only a small amount of flux results in a long switching time and large "peaking delay." For larger current pulses, the switching is faster but the tails of the various curves essentially overlap, until the current pulse magnitude is increased to the point that all flux is switched. Beyond that, increasing the current causes faster and faster switching. For example, as indicated in Fig. 13(a), a 3-μsec pulse may be long enough for full switching at high flux level, but very little switching takes place in that time at low levels. This is a very desirable property, since with short pulses there is a significant decrease in zero build-up tendencies without penalty to high level transmission. However, by merely cutting a pair of apertures in the wall of such a core, the family of curves for the multiaperture element (tested simply as a core) may look more like those in Fig. 13(b). As seen in the figure, there is essentially no peaking delay. (It may be noted that different materials intrinsically exhibit differing amounts of peaking delay, and the materials generally best suited to these circuits are those exhibiting maximum peaking delay. At the present state of the art, the slower commercial square-loop materials exhibit this property most markedly.)

The switching properties discussed above are significantly improved in the element design of Fig. 14, which has substantially equal cross sectional area everywhere. This first order improvement in shaping yields an element that can be almost completely saturated in its CLEAR state, with a minimum of remanent reverse domains. The CLEAR state ϕ vs F curve for such an element is significantly squarer than the corresponding curve for an unshaped element. Further, whereas the switching curves for an unshaped MAD element are more like those of Fig. 13(b), the curves for the element of Fig. 14 are more like those of Fig. 13(a).

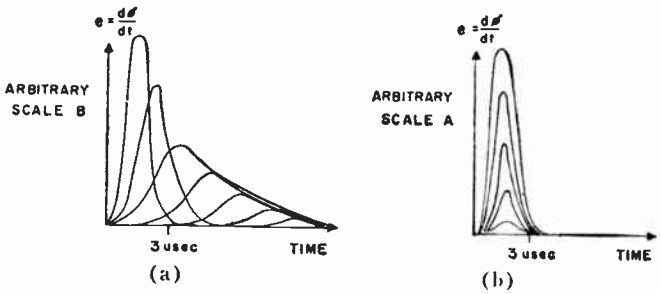

Fig. 13—Comparison of voltage vs time switching curves for (a) shaped and (b) unshaped MAD's.

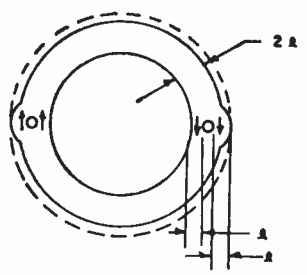

Fig. 14—Shaped POSITIVE MAD element.

It is quite apparent then that once the rotational symmetry of a toroidal core is destroyed, a great deal of attention must be paid to the geometrical design. The shape illustrated here is merely one example of the types of geometrical shaping required to obtain desirable circuit properties.

Logical Aspects

Thus far, all discussion has been in terms of a simple POSITIVE element. However, other logical functions can be obtained. For example, Fig. 15 illustrates a NEGATION device in which an input variable x, is transmitted as $\bar{x}$ (x inverse).

Fig. 15(a) illustrates the basic NEGATION device as some appropriate geometry connecting an input and output aperture. As far as the input aperture is con-

cerned, it is only necessary that in the CLEAR state the flux in the legs adjacent to the input aperture be parallel so that the device is "settable." That is, in this condition any flux switched in the input will switch through the connecting geometry into the output region. If the flux were initially "antiparallel," then any flux switched in the input leg would switch locally about the input aperture without affecting the output region [Fig. 3(d)]. In fact, this CLEAR state flux requirement holds for all input apertures of all devices operable within this system. For a NEGATION device, the CLEAR state output aperture requirement is that the flux in the legs adjacent to the output aperture should be "antiparallel." Under these conditions, with no input a binary *one* will be transmitted. The appropriate geometry indicated in Fig. 15(a) may take many forms, such as in the element of Fig. 15(b). The extra central leg is provided only for flux-closure properties, and it is prevented from having any flux switched in it by a "hold" winding energized either continuously or at the appropriate pulse times.

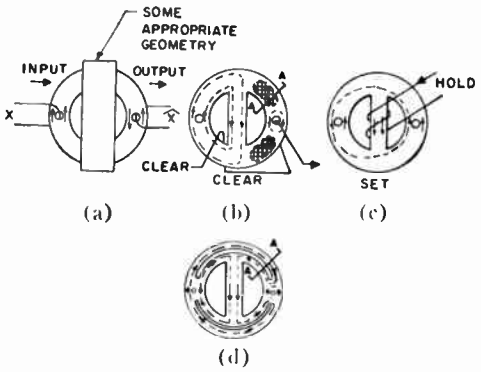

Fig. 15—NEGATION MAD element.

With the NEGATION device in its CLEAR state [Fig. 15(b)], the output ADVANCE current pulse will cause a *one* to be transmitted to the receiver. If previously, however, the NEGATION device were SET (had received a *one*), Fig. 15(c), then the input flux would have blocked the output, thereby resulting in a subsequent transmission of a *zero*.

With respect to detailed geometric shaping, the NEGATION device of Fig. 15(b), although logically correct, is operationally poor. The input ϕ_R vs I_R curves have very poor threshold properties. This is primarily due to the unsaturated regions about the output aperture (shown cross-hatched) in the CLEAR element of Fig. 15(b). By the use of arcuate slots, however, as indicated in Fig. 15(d), these unsaturated regions can be substantially eliminated. In both cases [Fig. 15(b) and 15(d)], the net flux passing cross section A–A is *zero;* however, in Fig. 15(d), the net of *zero* is obtained by the controlled difference of two equal saturation levels, so that in the CLEAR state essentially all material is on a major hysteresis loop. This results in significantly improved threshold properties of the device, and hence greatly improved circuit properties. The element of Fig. 15(d) is indicated in the photograph, Fig. 1.

It is clear from this example that by selecting proper shaping, interesting logic functions can be performed directly within the element. These techniques can be extended to more complicated functions such as AND, or EXCLUSIVE OR (Fig. 1). However, in designing such elements, the geometrical aspects of both the logic functions and operational properties must be kept clearly in mind.

Wired Logic

In the previous section it was shown how logical functions could be formed in the material itself. Alternately, certain logical functions, *e.g.*, OR and AND can be formed simply by proper interwiring. Fig. 16(a) indicates a two input OR arrangement which forms the output $(x+y)$ from inputs x, y. Having a second element in the transmitting branch does not change the basic operation. If both $x=y=0$, then no transmitter current is "steered" to the receiver and it remains *zero*. With only a single input in the *one* state, transmission is normal, *i.e.*, as previously described. With both $x=y=1$ the current steering is even more complete, and the receiver is SET.

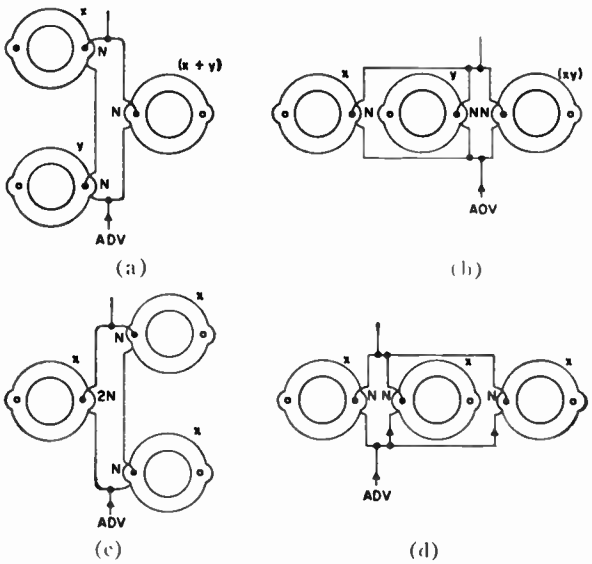

Fig. 16—Wired logic.

Similar arguments show that the arrangement of Fig. 16(b) yields the correct binary product xy from inputs x, y.

In either case, since thresholds are not perfect and extra wire losses are introduced into the branch circuits, there are second order effects of multiple inputs so that the process cannot be carried on indefinitely. However, OR and AND circuits with several inputs are operable.

Fig. 16(c) and 16(d) indicate alternate circuit arrangements for a single transmitter to control two (or more) receivers. The multiple receivers may be connected in series [Fig. 16(c)] or parallel [Fig. 16(d)]. In

the former case, the transmitter must have a nominal $2N$ (in general, nN) turns to control 2 (or n) receivers. With parallel receivers, all windings may nominally have the same number of turns. In either case, however, the current steered to switch a receiver (for *one* transmission) is decreased roughly by a factor of 2 (or n) from the single receiver case. This can be simply seen from Fig. 16(d) where any current steered from the transmitter must divide equally between two receivers switching in parallel. In Fig. 16(c) although the same current flows through both receivers, this current is roughly one half of the value in the single receiver case, since the maximum *zero* state transmitter current can only be half as large, in view of its $2N$ turns in this case. Thus, there is a limit to how many receivers may be simultaneously controlled in this way. Early experiments have shown that three receivers per transmitter are quite feasible with this arrangement. However, because of the nondestructive transmitter read-out properties (see Fig. 10), by the use of extra output apertures and subclocks a large number of receivers may be controlled from a single transmitter. For example, with n receivers controllable simultaneously from a single output aperture, by using m output apertures (and m subclocks) a fan-out ratio of mn may be achieved.

Results

Most efforts to date have been in developing basic circuit arrangements and understanding the fundamental processes. No large scale general logic systems have yet been constructed; however, all circuits and elements described here have been operated in closed loop stable fashion. Until recently all elements were ultrasonically cut from commercially available cores and disks and therefore have been available in only small quantities. Initial samples of experimentally moded 5-aperture POSITIVE elements have operated quite satisfactorily. Availability of these and other types of molded elements should greatly increase the capacity for larger scale testing.

Typical shift register operating characteristics are listed below.

In the circuit of Fig. 7, CLEAR currents have large range since they may have essentially any magnitude above the magnitude necessary to effectively clear their associated elements. ADVANCE currents, however, are necessarily more restricted in range since they operate against threshold regions. Typical value of range for each ADVANCE current is 20 per cent, while the other ADVANCE current is held fixed. However, by simple circuit variation—but with $N_T = N_R = 1$ retained—range may be greatly improved. For example, values well in excess of 50 per cent are obtained.

As discussed in connection with Fig. 13, the slower commercial ferrite materials (*e.g.*, Telemeter Magnetics T-5, and General Ceramics S-5) are most suited to these circuits. With these materials, bit rates of 100 kc and over are easily achieved.

Registers have operated successfully over a temperature range of -50 to $+100$ degrees Centigrade without significant decrease in current ranges. However, the center of the range varies with the ferrite threshold, which is a function of temperature changing about -0.7 per cent/degree Centigrade.

Registers constructed of molded POSITIVE MAD's 0.060 inch high, and 0.375 inch OD dissipate approximately 300 mw per bit at 100 kc bit rate, for the case of all *ones* being circulated. By using smaller elements this value may be reduced by several factors.

The circuit in Fig. 7(b) is constructed on a flat bread board to indicate the simplicity of interconnection. Actually, these circuits lend themselves to high density 3-dimensional packing.

Conclusion

These new devices and techniques present interesting possibilities for general application in the digital processing field. Logic and data manipulative systems can be made with only square-loop magnetic elements and interconnecting wires. No diodes, transistors, tubes, resistors, inductors or capacitors are required for these basic systems. Such devices are required only for the generation of the system clock pulses. Information-bit rates of over one-quarter mc can be obtained with elements fabricated from commercial ferrite materials. The elements are small, inexpensive, light, and rugged, and promise an extremely high degree of reliability. Certain unique functional possibilities are also apparent which give even greater attractiveness to these techniques: for example, simple multidimensional (multimode) shift registers, simple low cost methods of obtaining visual indications of internal binary states, and completely nonvolatile information status of the entire system at the end of any given clock pulse.

Acknowledgment

The author wishes to thank David R. Bennion and Fred C. Heinzmann for their significant contributions and assistance in developing this system. In addition, the laboratory assistance of Vernon Baughman and Jeanette Barnes is gratefully acknowledged. The permission of the Burroughs Corporation for release of the material presented here is also acknowledged.

Bibliography

[1] A. Wang and W. D. Woo, "Static magnetic storage and delay line," *J. Appl. Phys.*, vol. 21, pp. 49–54; January, 1950.
[2] J. A. Rajchman and A. W. Lo, "The transfluxor—a magnetic gate with stored variable setting," *RCA Rev.*, vol. 16, pp. 303–311; June, 1955.
[3] J. A. Rajchman and A. W. Lo, "The Transfluxor," Proc. IRE, vol. 44, pp. 321–332; March, 1956.
[4] L. P. Hunter and E. W. Bauer, "High speed coincident-flux magnetic storage principles," *J. Appl. Phys.*, vol. 27, pp. 1257–61; November, 1956.
[5] J. A. Rajchman and H. D. Crane, "Current steering in magnetic circuits," IRE Trans. on Electronic Computers, vol. EC-6, pp. 21–30; March, 1957.
[6] H. W. Abbott and J. J. Suran, "Multihole ferrite core configurations and applications," Proc. IRE, vol. 45, pp. 1081–93; August, 1957.

Correspondence

WWV Standard Frequency Transmissions*

Since October 9, 1957, the National Bureau of Standards radio stations WWV and WWVH have been maintained as constant as possible with respect to atomic frequency standards maintained and operated by the Boulder Laboratories, National Bureau of Standards. On October 9, 1957, the USA Frequency Standard was 1.4 parts in 10^9 high with respect to the frequency derived from the UT 2 second (provisional value) as determined by the U. S. Naval Observatory. The atomic frequency standards remain constant and are known to be constant to 1 part in 10^9 or better. The broadcast frequency can be further corrected with respect to the USA Frequency Standard as indicated in the table below. This correction is *not* with respect to the current value of frequency based on UT 2. A minus sign indicates that the broadcast frequency was low.

The WWV and WWVH time signals are synchronized; however, they may gradually depart from UT 2 (mean solar time corrected for polar variation and annual fluctuation in the rotation of the earth). Corrections are determined and published by the U. S. Navy Observatory.

WWV and WWVH time signals are maintained in close agreement with UT 2 by making step adjustments in time of precisely plus or minus twenty milliseconds on Wednesdays at 1900 UT when necessary; one retarding adjustment was made at WWV and WWVH on October 22, 1958.

WWV FREQUENCY†

1958 October 1500 UT	Parts in 10^9
1	−2.4
2	−2.4
3	−2.4
4	−2.3
5	−2.3
6	−2.2
7	−2.3
8	−2.2
9	−2.2
10	−2.2
11	−2.1
12	−2.0
13	−1.9
14	−1.9
15	−1.9
16	−1.9
17	−1.8
18	−1.8
18	−1.7
20	−1.6
21	−1.7
22	−1.7
23	−1.7
24	−1.7
25	−1.8
26	−1.8
27	−1.8
28	−1.8
29	−1.9
30	−2.0
31	−2.0

NATIONAL BUREAU OF STANDARDS
Boulder, Colo.

* Received by the IRE, November 14, 1958.
† WWVH frequency is synchronized with that of WWV.

Limitations of Satellite Antennas Using Spherical Arrays*

Current emphasis on application of electronic systems to space vehicles has resulted in several proposals for steerable-beam arrays which can be mounted on the surface of a spherical satellite, with provision for scanning through the total solid angle about the vehicle. The space-age minded system engineer is to be cautioned against the glib assumption that it is possible to scan a beam over 4π steradians in any simple manner. The more obvious configurations cannot be utilized. The following paragraphs discuss limitations of such a scanning system with regard to polarization and array geometry and offer interim solutions to the general problem.

Polarization Limitation

The general philosophy of the two-dimensional steerable-beam circular array is based upon introduction of the proper phase shift into an omnidirectional array to obtain directivity. If this premise is used for the spherical array with a specified polarization in mind, it is seen from Brouwer and Mathis[1,2] that the required isotropic array is impossible.

The proofs of Brouwer and Mathis are for a linearly polarized antenna, the far field pattern of which is represented by a continuous vector field. It is easily seen that if a set of linear radiating elements are arranged to give optimum performance in the equatorial plane, the polarization contours will be as shown in Fig. 1(a), and no radiation can be obtained in the directions of the poles.

One technique for avoiding this problem involves a second array overlaid on the first, with its poles on the original equator, as shown in Fig. 1(b). If the arrays are fed in phase quadrature, it is possible to radiate energy in every direction, although the polarization varies greatly as in the circularly polarized crossed dipole configuration.

The polarization problem is thus solved, if one will accept a variable polarization range from linear to circular. Although this element can radiate in all directions, the polarization characteristics necessitates some consideration for the receiving antenna. The two general techniques of orthogonal and opposite sense polarization can be employed. The second antenna might consist of two radiators with orthogonal polarizations, so that a maximum polarization loss between the antennas would be 3 db. Alternatively the spherical antenna would utilize a hybrid arrangement to give two inputs providing opposite sense polarization. This is not completely satisfactory, in that the plane containing the four poles radiates linear polarization which remains linear in the opposite sense. A linearly-polarized, ground-based antenna might have considerable polarization loss when it lies in the plane containing the four poles.

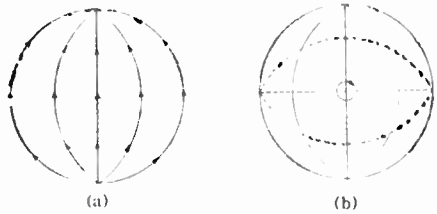

Fig. 1—Polarization contours of single and overlapping spherical arrays.

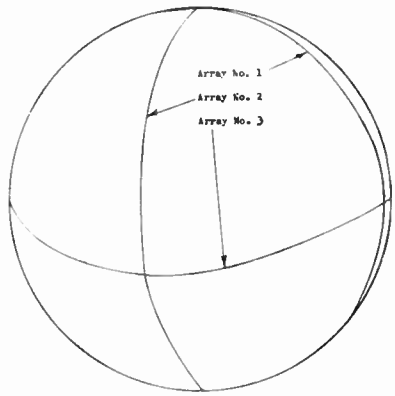

Fig. 2—Configuration of three crossed steerable fan-beam circular arrays.

Geometrical Limitations

Another fundamental problem in the spherical array is the location of identical radiating elements on the surface. The use of spherically symmetric geometry would limit one to the use of regular polyhedrons for array patterns, placing the maximum number of elements at twenty and imposing a severe limitation on the realizable aperture size in wavelengths. The complexity of this problem is considerably reduced by the change from total spherical symmetry, together with the availability of two arrays for forming an aperture, which relaxes the geometrical requirements, and no strict limitation is placed on aperture size.

Alternate System

Thus far, the implication has been that if the polarization and geometry are established, one has only to introduce variable amplitude and phase to obtain his steerable beam. The problem of introducing the required amplitude and phase has not been completely solved for simple circular arrays. The three-dimensional, spherical array represents another order of magnitude in difficulty of development. Significant improvements over existing microwave commutators are required.

Therefore, while the required commutators are being developed, the following sys-

* Received by the IRE, September 15, 1958.
[1] H. F. Mathis, "A short proof that an isotropic radiator is impossible," PROC. IRE, vol. 39, p. 970; August, 1951.
[2] L. E. Brouwer, "Over Continue Vectordistributies op Oppervlakken," *Proc. Koninkl. Ned. Akad. van Wetenschap.*, vol. 11, pp. 850–858; 1909.

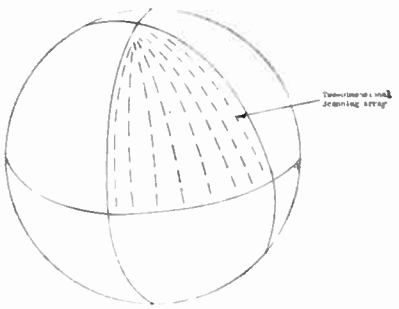

Fig. 3—Polyhedral arrangement of eight scanning two-dimensional arrays.

tems, which are within the state-of-the-art, are proposed. If directivity is required, but no gain, the configuration of Fig. 2 can be used. This is the well-known cross-type array with which two fan beams are formed, and the intersection gives the desired resolution. In the three-dimensional case it is desirable to use three perpendicular circular arrays in order to provide the cross beam capability in all directions. Two commutators and a switching arrangement provide the necessary scanning of two fan beams at a time.

The second interim system is shown in Fig. 3. The sphere is divided into regular polyhedral sectors, and each sector contains a two-dimensional scanning array. Scanning from one sector to another is achieved by switching.

The advantages of this system are a) an effective area almost the size of the vehicle cross section can be realized, b) the vehicle need not be spherical; it can be polyhedral or, if the effective area is much smaller than the vehicle dimensions, almost any shape such as the common doughnut conception, c) the number of sectors can range from four to twenty and d) any polarization may be used.

These alternate proposals can be considered as interim systems until more development work has been done on compact microwave commutators and RF circuitry for application to three-dimensional pencil-beam scanning.

K. S. Kelleher
J. P. Shelton
Aero Geo Astro Corp.
Alexandria, Va.

Determination of the Orbit on an Artificial Satellite*

The Doppler effect of the radio signals from artificial satellites is substantial and easy to detect. It is well known that the effect depends both on the position of the receiving station with respect to the orbit, and on the shape of the orbit.

In order to determine from the Doppler effect some parameters of the orbit, with a single receiving station, it is necessary to introduce some assumptions about the orbit itself. The most commonly adopted assumption is that the orbit is a straight line, at least during the time interval of the reception, and that the velocity of the satellite is a constant.[1] However, it is to be noted that, in this way, an error is introduced which depends on the actual shape of the orbit; as a consequence, the values of the parameters of the orbit turn out to be affected by an error of many per cents, which increases with the distance of the satellite from the earth.

After a critical study of these errors, we developed a method for the determination of the orbit of an artificial satellite, which does not require any assumption about the orbit under investigation.

Our method requires four receiving stations. If the stations are located conveniently far apart from one another, the four curves $f_i(t)$, [where $f_i(t)$ is the frequency received at the ith station] are sufficiently different, or at least displaced in the sense of the time axis. As is well known, $f_i(t)$ is related to the velocity v_{iR} of the source with respect to the observer by the law of the Doppler effect, which may be written for $v \ll c$ (v = velocity of the source)

$$v_{iR}(t) = c\frac{f_i(t) - f_0}{f_i(t)}. \qquad (1)$$

Here f_0 indicates the frequency emitted by the satellite, and must be considered as constant during the time of each reception. The sign convention is to consider v_{iR} positive when the source approaches the observer. By calling $R_i(t)$ the instantaneous distance of the satellite from ith station, we have

$$v_{iR}(t) = -\frac{dR_i(t)}{dt} \qquad (2)$$

or also

$$R_i(t) = R_{0i} - \int_{t_{0i}}^{t} v_{iR}(t)dt \qquad (3)$$

where R_{0i} denotes the distance $R_i(t)$ at an arbitrary time $t = t_{0i}$. If f_0 and R_{0i} were known (this is the case when the stations receive the signals from the instant of launching) three stations would be sufficient in order to follow the satellite. However, in general, f_0 and the R_{0i}'s are unknown. The fourth station used in our method provides a fourth equation like (1), which may be utilized as follows:

The distance $R_4(t)$ between the satellite and the fourth station can be expressed in terms of the coordinates of this station and of $R_1(t)$, $R_2(t)$, $R_3(t)$. In this way, $R_4(t)$ turns out to be a function of the unknown quantities: $R_4(t) = R_4(t; f_0, R_{01}, R_{02}, R_{03})$. On the other hand, (2) and (1) give, for $i = 4$

$$\frac{dR_4(t)}{dt} = -v_{4R}(t) = -c\frac{f_4(t) - f_0}{f_4(t)}.$$

By combining these two equations for $R_4(t)$, and evaluating them for a number of values of t, we obtain as many equations as are required for determining the unknown quantities.

The accuracy of this method depends solely on the instrumental precision with which the Doppler effect curves may be recorded at the four stations.

N. Carrara
P. F. Checcacci
L. Ronchi
Centro Microonde
University of Florence
Florence, Italy

* Received by the IRE, July 8, 1958.

[1] Staff of the Royal Aircraft Establishment, Farnborough, Eng., "Observations on the orbit of the first Russian earth satellite," *Nature, London*, vol. 180, pp. 937–941; November 9, 1957.
Staff of the Mullard Radio Astronomy Observatory, Cambridge, Eng., "Radio observations of the Russian earth satellite," *Nature, London*, vol. 180, pp. 879–883; November 2, 1957.
R. R. Brown, P. E. Green, Jr., B. Howland, R. M. Lerner, R. Manasse, and G. Pettengill, "Radio observations of the Russian earth satellite," Proc. IRE, vol. 45, pp. 1552–1553; November, 1957.
A. M. Peterson, "Radio and radar tracking of the Russian earth satellite," Proc. IRE, pp. 1553–1554; November, 1957.
"Sputnik's Doppler shift measured and recorded with -hp- counter and digital recorder," *Hewlett-Packard J.*, suppl. to vol. 9, pp. 1–2; January–February, 1957.
"How Doppler shift records provide satellite range and height data," *Hewlett-Packard J.*, vol. 9, pp. 5–6; November–December, 1957.
A. Peterson, "On the tracking of satellites," *Gen. Radio Experimenter*, vol. 32, pp. 3–6; December, 1957.
"Artificial satellites of the earth," *Wireless World*, pp. 574–578; December, 1957.
"Russians find orbit with Doppler," *Electronics* (Bus. Ed.), vol. 31, pp. 21–27, May 2, 1958.
M. Bernstein, G. H. Gougoulis, O. P. Layden, W. T. Scott, and H. D. Tanzman, "Satellite Doppler measurements," Proc. IRE, vol. 46, pp. 782–783; April, 1958.
A. Schwartzman and P. D. Stahl, "Doppler equation for earth satellite measurements," Proc. IRE, vol. 46, pp. 915–916; May, 1958.

Doppler Satellite Measurements*

The electronic tracking of U. S. satellites at the United States Army Signal Research and Development Laboratory, as reported by Bernstein, Gougoulis, Layden, Scott, and Tanzman,[1] has continued during the past several months. Data compiled and analyzed on lift-off of Explorer II and Explorer III clearly show all increases in velocity after the initial firing.

The Doppler curve of Explorer II is shown in Fig. 1. The sharp frequency changes shown by this curve indicate a change in Doppler velocity, which can be contributed to a sudden change of direction and/or acceleration due to the firing of one stage. It can be seen quite clearly that two rocket stages fired after the initial lift-off. Thus, only three of the four stages of the rocket fired. Also, the velocity calculated at the time the satellite signal disappeared was less than the required orbiting velocity of approximately five miles per second.

Fig. 2 is the Doppler curve for the time during which the successive stages of the rocket were due to be fired for Explorer III. An analysis similar to that of Fig. 1 would readily show that all four stages fired and that the velocity necessary for orbiting was obtained.

The output frequencies of these two satellites (*i.e.*, 108.0 and 108.03 mc) are

* Received by the IRE, October 10, 1958.

[1] M. Bernstein, G. H. Gougoulis, O. P. Layden, W. T. Scott, and H. D. Tanzman, "Satellite Doppler measurements," Proc. IRE, vol. 46, pp. 782–783; April, 1958.

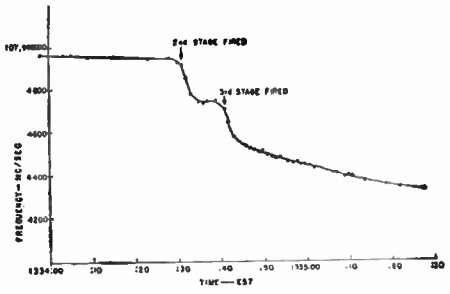

Fig. 1—Detail of frequency-time curve, firing of Explorer II, March 5, 1958.

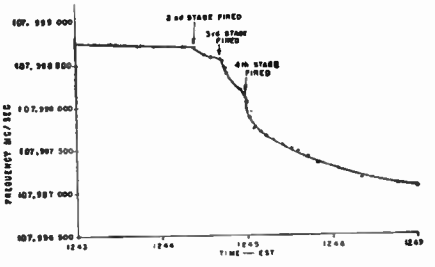

Fig. 2—Detail of frequency-time curve, firing of Explorer III, March 26, 1958.

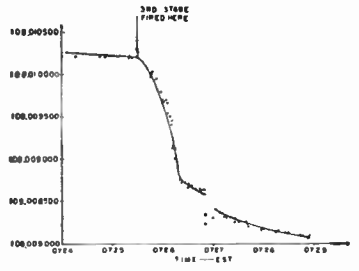

Fig. 3—Detail of frequency-time curve, firing of Vanguard, March 17, 1958.

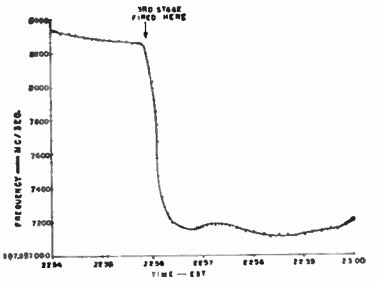

Fig. 4—Detail of frequency-time curve, firing of Vanguard II, May 27, 1958.

derived from two crystal oscillators operating at 54.0 and 54.015 mc. The ruggedized, highly stable quartz crystals used in these oscillators were developed by the United States Army Signal Research and Development Laboratory and designed to have good frequency stability during vibration. Thus, little frequency change is introduced by the crystal oscillator during take-off, and the curves give an accurate picture of the frequency change due to the Doppler effect.

On March 17, 1958, the first successful firing of a satellite-carrying Vanguard rocket was made. The Doppler curve of this launching is shown in Fig. 3. Stage number three burned for 48 seconds after being fired at 0725:30 EST. The flutter in frequency observed for 20 seconds could be caused by the shock of ejection of the satellite from the rocket. After this discontinuity the measurements indicate that orbital velocity was obtained.

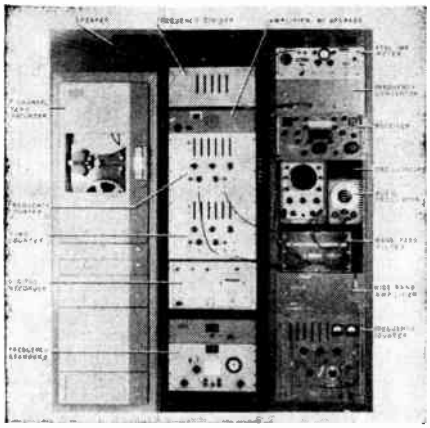

Fig. 5—Over-all front view of experimental Doppler measuring system (laboratory designed and constructed), showing components.

In contrast to the curve of Fig. 3 is the curve of Fig. 4 which is a Doppler curve for the lift-off of a Vanguard rocket on May 27, 1958, with a full-sized satellite aboard. In a normal successful firing the satellite can be tracked from the location for approximately 10 minutes. However, in the case of this lift-off, the high altitude attained allowed the signal to be received for 25 minutes although only six minutes are shown in this figure. The third stage of this rocket burned for 34 seconds after being fired at 2255:47 EST. After the burn-out of the third stage the Doppler frequency started to increase. This was due to the velocity change of the vehicle as it reentered the atmosphere.

Fig. 5 is a photograph of the system now being used at Fort Monmouth. This work will be described later in greater detail.

H. D. Tanzman
G. A. MacLeod
W. T. Scott
U. S. Army Signal Res. and Dev. Lab.
Fort Monmouth, N. J.

Novel Method for Measuring Impedances on Surface Wave Transmission Lines*

Two methods exist in the microwave region for measuring impedances or reflection coefficients on a transmission line:

1) The standing wave method, *i.e.*, the measurement of the standing wave pattern on the line with an antenna probe. The ratio of the maximum and minimum values of field strength and the position of the maxima or minima yield the impedance or the reflection coefficient, respectively.
2) The reflectometer method. Here the amplitudes of the two waves, the one coming from the generator, the other reflected by the impedance, are measured independently by two directional couplers. The ratio of the two amplitudes represents the reflection coefficient.

For hollow waveguides the first method is for several reasons more precise than the reflectometer method and is, therefore, used in nearly all cases. But at shorter wavelengths, that is at millimeter or submillimeter waves, and on surface wave transmission lines (Sommerfeld-wire, Goubau-wire, dielectric rod, dielectric image line) the reflectometer method seems to offer advantages.

While ordinary waveguides have cross sections of the order of λ^2 or smaller, surface wave lines make it possible to deal with a cross-sectional field area many times larger than λ^2, *e.g.*, 100 λ^2. This justifies a more optical point of view. In order to influence the waves one can, therefore, look after devices which have dimensions much larger than the wavelength. The measuring devices described here have these properties. One of them uses the principle of the reflectometer while the other two represent a sort of combination of the reflectometer and the standing wave principle.

The Switch Reflectometer

A simple broad-band highly directive directional coupler for the dielectric image line consists of a thin plane dielectric sheet, standing normally to the image plane and making an angle of 45 degrees with the direction of wave propagation. It works as a partially permeable mirror. Depending on the direction of propagation of a wave a small part of its energy is radiated either to the right or to the left side as a free wave. The quantity of the radiated energy depends on the permittivity ϵ of the dielectric and is proportional to $(d/\lambda)^2$, if $d \ll \lambda$ (d = thickness of the sheet).

The sheet can be turned by 90 degrees around an axis vertical to the image plane. Fig. 1 shows the device working as a reflectometer for measuring reflection coefficients on the image line. The detecting horn on the right picks up the radiated energy, an absorber on the left absorbs without reflection the energy radiated to the left. In position I, the amplitude of the wave coming from the generator is measured; in position II, the amplitude of the wave reflected by the impedance.

The Movable Reflectometer

Similar to the switch reflectometer a thin dielectric sheet is used and oriented in the same manner. There are two horns on both sides of the image line. Both the horns and the dielectric sheet can be moved simultaneously along the line parallel to the direction of propagation. The two signals picked up by the horns are transmitted through waveguides to a symmetrical junction (*e.g.*, Magic Tee) which adds up the amplitudes with correct phase and detects the resulting

* Received by the IRE, July 28, 1958.

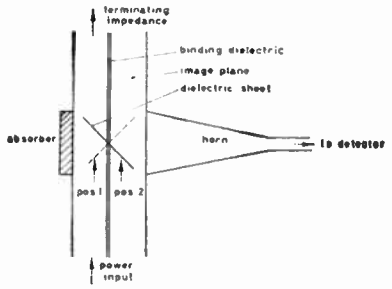

Fig. 1—The switch reflectometer.

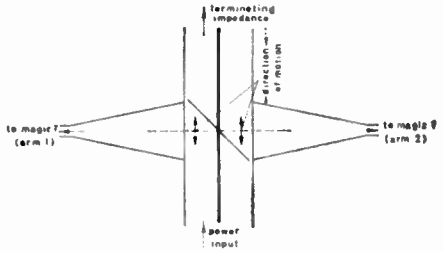

Fig. 2—The movable reflectometer.

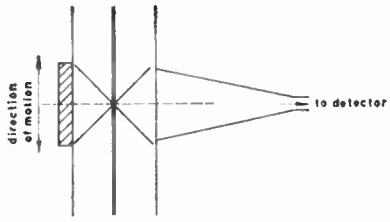

Fig. 3—The movable reflectometer, crossed sheet type.

signal. By moving the system the detector shows maxima and minima corresponding to the standing wave on the line because the two signals are shifted in phase depending on the position of the sheet (Fig. 2).

Instead of one sheet two crossed sheets can be used. Thus only one detecting horn is necessary. The crossed sheets and the horn are moved simultaneously (Fig. 3).

G. Schulten
Philips Research Labs.
Hamburg, West Germany

Microwave Parametric Amplifier by Means of Germanium Diode*

Earlier, one of the authors discovered the phenomenon that microwave oscillation and amplification at about 4000 mc were possible by use of the welded contact germanium diode.[1] This diode was made of *N*-type germanium and platinum-rhodium whisker, having welded contact between them. This phenomenon was, no doubt, due

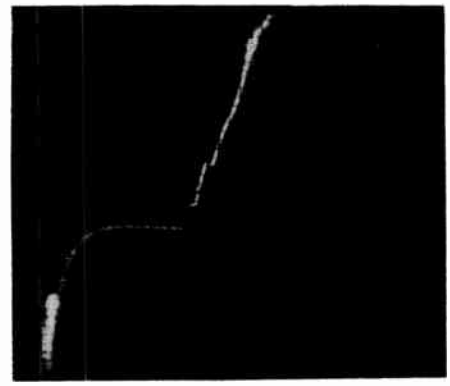

(a)

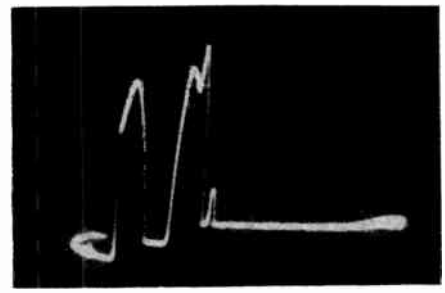

(b)

Fig. 4—(a) V-I characteristics of a diode having negative resistance. (b) Oscillation characteristics: abscissa is bias voltage.

to the negative resistance effect caused by the nonlinearity of the barrier capacity of the diode; however, because the characteristics of the diode were rather poor and a circulator was lacking, we were prevented from getting fairly good results at that time.

Recently, one of the authors discovered in his experiments on the harmonic generator that the gold-bonded germanium diode had a large nonlinear barrier capacity in the region of negative bias.[2] These diodes seemed to be fit for microwave parametric oscillator and amplifier, so we constructed them, the measured data of which are given below.

Two types of germanium diodes were used, one of which was the gold-bonded type made of *N*-type germanium and gold-gallium whisker of 100μ in diameter; the other was silver-bonded type which used silver instead of gold. The silver-bonded type was superior to the gold-bonded type. As the microwave circuit, a cross-type waveguide and a tuning stub were used rather than a cavity with an aim at broad-band characteristics. In this circuit two waveguides with the same height but different widths were joined crosswise, having the diode at the center. Pump power at about 8000 mc was applied to the diode from the smaller guide. In the amplifier the Faraday rotation-type circulator was used to provide isolation between input and output signals so as to prevent oscillation.

After the circuit was adjusted properly, the diode got the negative resistance characteristics when pump power was supplied, and oscillation at about 4,000 mc took place.

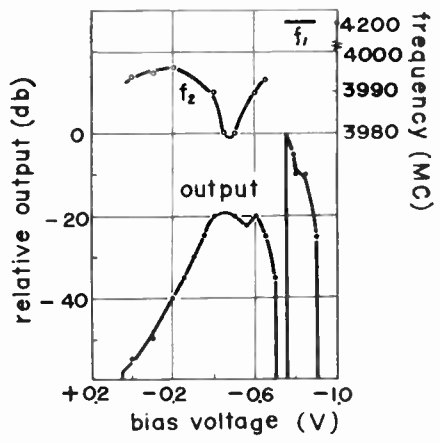

Fig. 2—Oscillation characteristics (f_p =8400 mc).

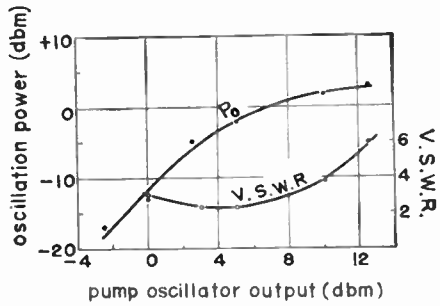

Fig. 3—Oscillation power and pump circuit VSWR characteristics for the first kind (f_p =8400 mc).

These were displayed on CRO's, which were working at 50 cycles for the observation of the diode and oscillation characteristics, as shown in Fig. 1.

There were two different kinds of oscillation. The oscillation frequency of the first kind, represented by f_1, was accurately half of the pump frequency and remained unaffected by the circuit conditions. On the other hand, the frequency of the other, f_2, was independent of the pump frequency, but depended on the circuit conditions. It is noted that, in some cases, two different types of oscillation took place at different values of bias voltage in the same diode, and each oscillation had its own frequency as shown in Fig. 1(b) and Fig. 2. Oscillation power increased as the pump power became large, as shown in Fig. 3. The maximum oscillation power was about $+3\pm1$ dbm, and this value was about 20 per cent of the absorbed pump power, because the input VSWR of the pump circuit was rather high.

With proper adjustments of the circuit conditions, the negative resistance which caused the oscillation could give rise to the amplification of the microwave signal in the same frequency as that of the oscillation. Of course, amplifier characteristics were somewhat different for the two kinds of oscillation. In spite of its powerfulness, the oscillation of the first kind was found inadequate to amplify the signal with bandwidth, because the beat component produced between pump power and the signal had a bad effect in the amplified band. Hence, we have used the oscillation characteristics of the second kind in the amplifier.

* Received by the IRE, July 21, 1958.

[1] S. Kita and T. Fujii, "Microwave Amplification by Use of Crystal Diode," E. C. L. Internal Rep.; February, 1954. Also Annual Convention, Inst. of Elec. Commun. Eng. of Japan; October, 1954.

[2] S. Kita, "A harmonic generator by use of the nonlinear capacitance of germanium diode," Proc. IRE, vol. 46, p. 1307; June, 1953.

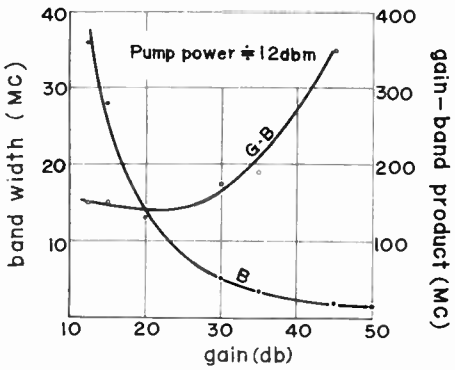

Fig. 4—The relation between gain and bandwidth.

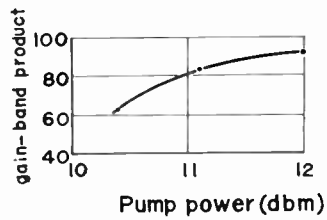

Fig. 5—The relation between pump power and gainband product.

Since this amplifier has a regenerative character, extremely high gain can be obtained, but the stability becomes poor as the gain increases too much. In our experiment, a gain of 15–20 db was obtained with enough stability, where the pump frequency was 8,100 mc and the center frequency of the signal was 4,170 mc. The bandwidth was about 15–25 mc, and the gainband product was rather constant except in the case of very large gain, as shown in Fig. 4. Fig. 5 shows that the gainband product increases a little as the pump power becomes large. The noise figure of the amplifier was about 10 db, but this value will, no doubt, decrease when better diodes are available.

The authors wish to express their gratitude to Y. Nakamura, I. Someya, and Z. Kiyasu for their interest and encouragement in the work. They are also grateful to M. Watanabe for his advice about germanium diode.

B. Oguchi
S. Kita
N. Inage
T. Okajima
Electrical Commun. Lab.
Nippon Telegraph and
Telephone Public Corp.
Tokyo, Japan

Signal Strength Recordings of the Satellite 1958 δ 2 (Sputnik III) at College, Alaska*

Since the launching of the first earth satellite in 1957, a large number of observations have been made by various workers interested in the field of upper atmospheric physics. The Doppler traces of the received frequencies have been used to derive electron density distributions, and the Faraday rotation of the plane of polarization of the signal to derive the total electron content between the satellite and the receiver over unit area. This note presents a summary of the observations of signal strength obtained at College, Alaska, (64°.9 N, 147°.8 W) during recent months from Satellite 1958 δ 2 (Sputnik III).

The 20.005-mc signal is received using a Collins 51-J communications receiver and recorded on a high-speed Sanborn recorder. Matched folded dipoles 0.25λ above ground, one in the North-South and the other in the East-West direction, have been used for the antennas. Since early August the second harmonic from the 20.005-mc transmitter has also been recorded using a Hammarlund SP600 receiver. Single-stage preamplifiers were used in conjunction with both receivers. The signal inputs to the preamplifiers have been in the region of 5–10 microvolts at 20.005 mc and less than 0.5 microvolt at 40.010 mc.

It is known from magneto-ionic theory[1] that the plane of polarization of the satellite signal will be rotated through an angle

$$\theta = 2.97 \times 10^{-2} \frac{H}{f^2} \cos\phi \int N dr$$

where

H = earth's magnetic field in ampere turns per meter;
N = electron density per cubic meter;
θ = angle between the direction of propagation and the earth's magnetic field.

The latitude of College is very nearly equal to the orbital inclination of 1958 δ 2, so that during overhead passes the satellite is traveling in the West-East direction. Under these conditions it can be shown that

$$\cos\phi = \frac{vt \cos\delta \sin\alpha - h_0 \sin\delta}{(h_0^2 + v^2t^2)^{1/2}},$$

and

$$\int N \cdot dr = N_0(h_0^2 + v^2t^2)^{1/2}/h_0,$$

where

h_0 = height of the satellite in meters;
v = velocity in meters per second;
δ = magnetic dip (77°);
α = magnetic declination (30°);
N_0 = total electron content between satellite and ground over a column of 1 square meter base;
t = time after closest approach in seconds.

Hence

$$\frac{d\theta}{dt} = \frac{2.97 \times 10^{-2}}{f^2} H N_0 \cos\delta \sin\alpha \frac{v}{h_0}.$$

The Faraday period T (measured between adjacent minima) therefore becomes

$$T = \frac{\pi}{d\theta/dt} = \frac{\pi f^2}{2.97 \times 10^{-2} H N_0 \cos\delta \sin\alpha v/h_0}.$$

The period T is thus independent of t, and the record should show a series of equally-spaced minima under normal ionospheric conditions. Several records showing this equal spacing near the time of closest approach have been selected, and the period T measured. The height h_0 is obtained from the Doppler trace and in some cases the predicted values from the Smithsonian data have been used. Table I shows the corresponding values of N_0 for several values of the satellite height.

TABLE I

Height (km)	N_0
584	2.35×10^{17}
592	2.48×10^{17}
600	3.24×10^{17}
640	3.24×10^{17}

An interesting sidelight to the observations is the appearance of sudden, persistent and violent fluctuation in the signal strength. When a check was made with the predicted tracks, these break-ups did not appear to tie up with any particular region of geographic or geomagnetic latitude. On many occasions the entire record is either unbroken or completely broken. When the break-ups occur in the course of the passage, they do not indicate any significant trend relative to the time of nearest approach, and it is therefore difficult to attribute them to the ionization produced in front of the satellite as has recently been suggested.[2]

Two other possible mechanisms have been considered; first, that the satellite itself may create irregularities in ionization by shock-wave formation. This must be ruled out in view of the large mean free paths of the gas molecules at these heights (several hundred meters). The second possibility is that the fluctuation is a diffraction phenomenon analogous to radio star scintillation, and caused by the same ionospheric irregularities. The Geophysical Institute is recording radio star scintillation continuously at frequencies of 223 and 456 mc, and rough comparisons of these records with the satellite recordings have been carried out. Since both theoretical and experimental investigations of radio star scintillation show that the scintillation amplitude should increase as the square of the wavelength, it might be expected that even a trace of scintillation at 223 mc would produce violent fluctuations in the 20-mc signal. However, on many occasions the satellite signal has shown less than 5 per cent fluctuation while the 223-mc scintillations have been as high as 30 to 50 per cent. This would imply that either the scintillating region is very sharply bounded in the horizontal plane, or that the satellite is itself moving in or below the irregularities. In view of the great heights of the satellite to which these observations refer (>600 km), this implies a greater height for the scintillating region than seems currently acceptable.

* Received by the IRE, October 20, 1958. This work was supported by the Natl. Sci. Found. under Grant No. Y/32:42/268.

[1] F. B. Daniels, "Scientific Uses of Earth Satellites," J. A. Van Allen, ed., Univ. of Michigan Press, Ann Arbor, Mich.: 1956.

[2] J. D. Kraus and J. S. Albus, "A note on some signal characteristics of Sputnik I," Proc. IRE, vol. 46, pp. 610–611; March, 1958.

The authors are greatly indebted to their colleagues N. Warman, R. P. Basler, and R. N. Dewitt for much assistance in operating the equipment, and to J. Distad for providing his predicted tracks of the satellite.

R. Parthasarathy
G. C. Reid
Geophysical Institute
College, Alaska

A New Method for Pumping a Fast Space-Charge Wave*

Some months ago it was pointed out from theoretical considerations that parametric amplification of a fast wave on an electron beam could well be an attractive means for obtaining low noise amplification.[1-3] Recently this was demonstrated to be true by the results of experiments on a tube in which the pumping was done on the fast cyclotron wave.[4] Louisell and Quate[2] have described ways in which a fast space charge wave might be pumped. This paper presents an alternative method for pumping a fast space-charge wave.

It is possible to visualize the process of parametric amplification of space-charge waves by means of a simple mechanical model and to draw some interesting conclusions. Fig. 1 shows a pendulum whose harmonic motion represents a signal we wish to amplify. Assume that we have means for controlling at will the magnitude of the downward force acting on the pendulum bob. It is apparent that we can cause the pendulum motion to grow by suddenly increasing the force whenever the pendulum reaches either of the two positions of maximum excursion and suddenly decreasing the force whenever the pendulum swings through its equilibrium position. In this fashion the potential energy available for motion is suddenly increased at the top of the swing. This potential energy becomes completely converted to kinetic energy by the time the pendulum reaches the equilibrium position. A sudden decrease in the downward force to its original value at that time has no effect on the kinetic energy. It is entirely converted to potential energy when the pendulum reaches its maximum excursion on the other side. Since this amount of potential energy is greater than that corresponding to the previous maximum excursion and since the force on the pendulum is the same, the excursion itself must be greater. In this way each successive excursion becomes bigger than the preceding one and the pendulum motion is made to grow. Changing the magnitude of the downward force constitutes parametric pumping. In the process described there are two cycles of pumping for each cycle of pendulum motion.

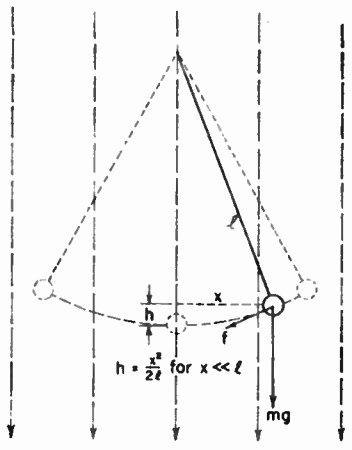

Fig. 1—A pendulum whose motion can be pumped by means of a time varying force field.

A pendulum in which this process could be carried out would not be hard to construct. For example, the variation in the downward force could be accomplished by placing an electric charge on the pendulum bob and providing a vertical electric field as represented by the dashed arrows in Fig. 1. A square wave modulation on the electric field at the appropriate frequency and phase would then produce the desired result. As is shown below, the modulation can be sinusoidal rather than square wave. Net energy still can be made to flow from the pump into the pendulum motion to produce growth.

The relation between the instantaneous restoring force and the instantaneous excursion is

$$f = -\frac{mg}{l}x; \qquad \frac{mg}{l} = -\frac{\partial f}{\partial x}. \tag{1}$$

(In all of the equations which follow, including those pertaining to electron motion, it is assumed that the excursions are small. Thus in essence we make the small signal assumption.) If the pendulum rises from a position x to a new position $x+dx$ during a time interval dt, kinetic energy T is used up. The rate of loss of kinetic energy equals the rate of work expended against restoring force f. That is

$$\frac{dT}{dt} = f\frac{dx}{dt} = -\frac{mg}{l}x\frac{dx}{dt} = -\frac{1}{2}\frac{mg}{l}\frac{d}{dt}(x^2). \tag{2}$$

Because of the geometrical relation

$$h = \frac{1}{2}\frac{x^2}{l},$$

the potential energy V of the pendulum is given by

$$V = mgh = \frac{1}{2}\frac{mg}{l}x^2. \tag{3}$$

Its rate of change is

$$\frac{dV}{dt} = \frac{d}{dt}\left(\frac{1}{2}\frac{mg}{l}x^2\right). \tag{4}$$

As long as g is constant, this is simply

$$\frac{dV(0)}{dt} = \frac{1}{2}\frac{mg}{l}\frac{d}{dt}(x^2) \tag{5}$$

so that the sum of potential and kinetic energy is constant:

$$\frac{d}{dt}(V(0) + T) = 0. \tag{6}$$

Let us now assume a time variation in the downward force and represent it by a variation in g. We then have

$$\frac{dV}{dt} = \frac{dV(0)}{dt} + \frac{1}{2}x^2\frac{d}{dt}\left(\frac{mg}{l}\right). \tag{7}$$

The rate of change of the total energy, which must equal the power pumped into the pendulum by the time-varying field, is

$$p = \frac{d}{dt}(V + T) = \frac{1}{2}x^2\frac{d}{dt}\left(\frac{mg}{l}\right) \tag{8}$$

or, from (1):

$$p = \frac{1}{2}x^2\frac{d}{dt}\left(-\frac{\partial f}{\partial x}\right). \tag{9}$$

Note that $\partial f/\partial x$ is the derivative of the restoring force, or minus the second derivative of the potential energy, with respect to distance.

In order to simplify the calculations of the growth due to the pumping let us assume essentially sinusoidal motion and sinusoidal pumping. Thus we assume

$$x = x_m \sin \omega_q t \tag{10}$$

and

$$-\frac{\partial f}{\partial x} = \frac{mg}{l} = \frac{mg_0}{l} - \frac{mg_m}{l}\sin 2\omega_q t = G_0 - G_m \sin 2\omega_q t. \tag{11}$$

By substituting (10) and (11) into (9) and by taking the time average we have

$$\bar{p} = \frac{\omega_q}{4}x_m^2 G_m. \tag{12}$$

The oscillatory energy in the pendulum motion is

$$\bar{e} = \tfrac{1}{2}x_m^2 G_0. \tag{13}$$

Let us assume that the oscillatory energy grows as $\exp[2\alpha' t]$. Then

$$\alpha' = \frac{\bar{p}}{2\bar{e}} = \frac{\omega_q}{4}\frac{G_m}{G_0}. \tag{14}$$

Note that the exponential growth factor is proportional to G_m, which is a measure of how hard we pump. G_m is also the magnitude of the time variable portion of the derivative of the restoring force with respect to distance.

In an electron beam on which a signal of frequency ω has generated a space charge wave, an observer moving forward with the stream sees the electrons move back and forth at the reduced plasma frequency ω_q. To him the electrons appear like harmonic resonators at that frequency.

Suppose the same observer also saw an electric field moving along with the stream, varying at what appeared to him (in his

* Received by the IRE, September 17, 1958.

[1] R. Adler, "A new principle of signal amplification," presented at Conference on Electron Tube Research, Berkeley, Calif.; June, 1957.

[2] W. H. Louisell and C. F. Quate, "Parametric amplification of space charge waves," Proc. IRE, vol. 46, pp. 707–716; April, 1958.

[3] R. Adler, "Parametric amplification of the fast electron wave," Proc. IRE, vol. 46, pp. 1300–1301; June, 1958.

[4] R. Adler, G. Hrbek, and G. Wade, "A low-noise electron-beam parametric amplifier," Proc. IRE, vol. 46, pp. 1756–1757; October, 1958.

moving frame of reference) to be a frequency $2\omega_q$. Under the proper phase conditions he would expect the electron motion, and hence the signal on the beam, to grow in accordance with the derivative of the field with respect to distance. In other words, parametric amplification should occur in response to a nonhomogeneous longitudinal field varying in time at an appropriate rate.

Let us extend our theory to fit the case of an electron beam with fast space charge wave modulation. A mechanical model for such a beam is a conveyor belt carrying an assembly of uniformly spaced pendulums. The conveyor belt moves forward at a velocity u_0. The electron motion is simulated by the motion of the pendulum bobs. For fast wave modulation the pattern of motion is illustrated in Fig. 2(a). In Fig. 2(b) are shown plots of RF current i, RF velocity v, the electron displacement x, and the negative of the time varying portion of the derivative of the restoring force with respect to distance ΔG. The coordinate z' represents distance along the axis in the moving frame of reference.

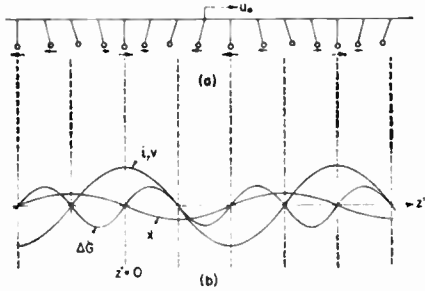

Fig. 2—(a) A time instantaneous picture of the system of pendulums portraying electron motion in a fast wave modulated beam. (b) Plots of i, v, x, and ΔG for the equivalent electron beam.

In order to pump the assembly of pendulums we would have to provide a moving field such that

$$\Delta G = -G_m \sin\left(2\omega_q t - \frac{2\omega_q}{v_f - u_0} z'\right) \quad (15)$$

where v_f = the phase velocity of the wave motion, this

$$\text{can be shown to be } \frac{u_0}{1-\frac{\omega_q}{\omega}}.$$

Consider the motion of only one of the pendulums, the one located at $z'=0$. For that pendulum, the excursion x is identical to z'.

In the beam being simulated, the forces on the electrons are actually provided by space-charge forces and external electric fields. Let us assume that the pumping is done by means of an external electric field E_p. Thus for an electron corresponding to the pendulum at $z'=0$ we can write

$$f = -m\omega_q^2 x - eE_p(x, t) \quad (16)$$

and

$$-\frac{\partial f}{\partial x} = m\omega_q^2 - \left[-e\frac{\partial}{\partial x}E_p(x, t)\right]. \quad (17)$$

The first term in (17) corresponds to G_0 and the second term, to the expression in (15). From this we find that

$$E_p(x, t) = -E_{pm}\cos\left(2\omega_q t - \frac{2\omega_q}{v_f - u_0}x\right) \quad (18)$$

where x and z' are identical. From (12) we see that

$$eE_{pm}\frac{2\omega_q}{v_f - u_0}$$

corresponds to G_m. Hence α' for the electron beam is given by

$$\alpha' = \frac{1}{2}\eta\frac{E_{pm}}{v_f - u_0}. \quad (19)$$

Eq. (18) shows how the pumping field travels relative to the moving frame of reference. We can determine how the field travels relative to the stationary frame of reference by recognizing that

$$z = z' + u_0 t \quad (20)$$

where z is the coordinate for distance in the stationary frame. Using (20) in (18) and using the relationship between v_f and u_0 we obtain

$$E_p(z, t) = -E_{pm}\cos\left[2\omega t - \left(\frac{2\omega}{u_0} - \frac{2\omega_q}{u_0}\right)z\right]. \quad (21)$$

The growth as a function of distance along the beam is a more useful quantity than as a function of time. Let α be the growth factor as a function of distance. Then

$$\alpha = \alpha'\frac{t}{z} = \frac{\alpha'}{u_0}. \quad (22)$$

If the pumping field is carried by a slow wave structure in the vicinity of the beam we can determine the equivalent pumping power P_p from the relationship

$$P_p = \frac{E_{pm}^2}{2\left(\frac{\omega}{v_f}\right)^2 K} \quad (23)$$

where K is Pierce's impedance parameter. From (19), (22) and (23) we obtain

$$\alpha = \frac{1}{2}\frac{\omega}{u_0}\frac{\sqrt{2KP_p}}{V_0}\frac{\omega}{\omega_q}\left(1-\frac{\omega_q}{\omega}\right)^2 \quad (24)$$

where V_0 is the dc beam voltage.

In this device an external pumping field is provided by means of a slow wave structure in the vicinity of the beam. Louisell and Quate[2] have proposed and have derived the theory for a tube in which an intense space-charge wave is applied to an electron beam which already carries the signal. We now see their tube in a new light. The function which the intense space-charge wave performs is simply to produce a time varying longitudinal non-homogeneous field. It is the field which makes the signal grow. The use of a free space-charge wave to produce the pumping field imposes severe limitations with respect to the choice of beam parameters. The desire to obtain high gain entails the use of a space-charge field which may be so intense that detrimental second order effects, such as the generation of spurious signals by mixing, become hard to avoid.

It appears that if a pumping field of the correct waveform and velocity were externally imposed upon the beam by means of an extended slow-wave structure, the limitations inherent in the process of pumping by means of a space-charge wave would be avoided. Instead of designing the beam so that the velocity of the fast space-charge wave at pump frequency approaches that of a similar wave at signal frequency (*i.e.*, Louisell and Quate's factor a' close to unity) we would attempt to keep the velocity of the fast space-charge wave at pump frequency substantially lower (*i.e.*, $a'<1$). This would reduce the intensity with which the pump frequency space-charge wave is unavoidably generated. In fact it might be advantageous to make the velocity of the externally applied pumping field even higher than the optimum velocity for gain to further reduce the accompanying space-charge wave.

Presumably such a device could have high gain per unit length because the pump wave velocity could be optimum (rather than a compromise). Also, the device should be relatively free from spurious mixing products because only a relatively small residual space-charge wave need be generated.

The authors are indebted to Prof. H. Heffner and to James E. Monson of Stanford and to Dr. A. Ellett of Zenith for valuable discussions of the analog presented here.

G. Wade
Stanford University
Stanford, Calif.
R. Adler
Zenith Radio Corp.
Chicago, Ill.

A Tunable Maser Amplifier with Large Bandwidth*

This note describes a solid-state single-cavity X-band maser that has a 20-mc bandwidth at 10-db gain with a bath temperature of 4.2°K. Previous cavity masers[1] have been restricted to small bandwidths. The present system can be tuned from 8400 to 9700 mc. The performance of the maser is offered as further experimental support for the phonon saturation mechanism proposed previously.[2,3]

The maser crystal is ruby ($Al_2O_3 \cdot Cr_2O_3$), chromium being the paramagnetic ion. The chromium concentration is approximately 0.01 per cent. Maser action in ruby has been reported by Makhov and others.[4] The Cr^{+++} ion spin 3/2 system produces four energy levels in an applied magnetic field. For the 54°44′ polar orientation of the c axis, the

* Received by the IRE, August 5, 1958. This work was supported in part by the U. S. Army (Signal Corps), the U. S. Air Force (Office of Sci. Res., Air Res. and Dev. Command), and the U. S. Navy (Office of Naval Res.).

[1] A. L. McWhorter and J. W. Meyer, "Solid-state maser amplifier," *Phys. Rev.*, vol. 109, pp. 312–318; January 15, 1958.
[2] M. W. P. Strandberg, C. F. Davis, Jr., B. W. Faughnan, R. L. Kyhl, and G. J. Wolga, "Operation of a solid-state quantum-mechanical amplifier," *Phys. Rev.*, vol. 109, pp. 1988–1989; March 15, 1958.
[3] M. W. P. Strandberg, "Spin-lattice relaxation," *Phys. Rev.*, vol. 110, pp. 65–69; April 1, 1958.
[4] G. Makhov, C. Kikuchi, J. Lambe, and R. W. Terhune, "Maser action in ruby," *Phys. Rev.*, vol. 109, pp. 1399–1403; February 15, 1958.

1–3 and 2–4 transition frequencies are degenerate for all fields. The maser is operated in this orientation at fields of approximately 4000 gauss. The 1–3 and 2–4 transitions are saturated by pumping power near 23 kmc; population inversion is achieved between levels 2 and 3 with subsequent amplification at approximately 9100 mc.

A large ruby crystal (1 cm × 1 cm × ¾ cm) is placed in the short-circuited end of a 1-cm square waveguide. A moving plunger provides the other wall. Since the crystal dielectric constant is high,[5] at X-band the perturbed TE_{10} mode propagates in the crystal and is cut off in the rest of the waveguide. X-band fields are almost entirely confined to the crystal. Since the fields near the plunger are small, a Q_0 of 2000 is realized without plunger-wall contact. Coupling to the feeding K-band and X-band waveguides is furnished by the coupling slits shown in Fig. 1. To provide variable coupling and resulting gain and bandwidth control, the X-band waveguide is fitted with a sliding quarter-wavelength impedance transformer. A circulator is used in the signal circuit to give unidirectional gain and maximum gain-bandwidth. Plunger displacement tunes the TE_{10} resonance over a large frequency range. Maser operation is accomplished throughout this range by appropriately tuning the magnetic field and pumping frequencies as the cavity is being tuned.

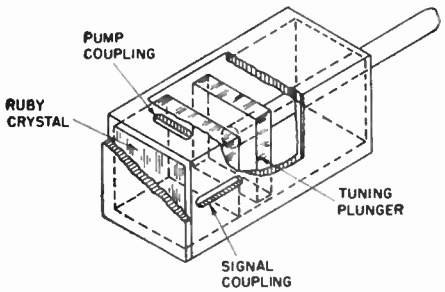

Fig. 1—Maser cavity.

This device has the unusual feature of complete maser action in the absence of cavity resonance at the pumping frequency. It is this characteristic that allows the amplifier to be operated at any frequency in the signal tuning range. If the maser is to be continuously tuned, operation cannot be restricted to those few frequencies at which the cavity is simultaneously resonant at the signal and pumping frequencies. We have observed that complete saturation can be achieved in the absence of a cavity resonance at the pumping frequency. Under these conditions, pumping power appears to be coupled to the crystal primarily by the fringing fields near the coupling hole.

The voltage gain-bandwidth product[6] was measured at representative frequencies in the tuning range, and is essentially constant at 43 mc with a bath temperature of 4.2°K. At 1.5°K, the product increases to approximately 65 mc. Magnetic absorption, observed in the absence of pumping power, yields a magnetic absorption Q of approximately 350. This value checks with expected absorption Q, as calculated from the known spin concentration. Furthermore, the absorption Q is essentially equal to the magnitude of the magnetic negative Q, as computed from the observed gain-bandwidth and cavity Q_0. At a small-signal gain of 11.5 db, the gain is constant for small-signal levels and is down by 3 db at 25 μw of input power. Since the negative and absorption magnetic Q's are approximately equal in magnitude, the effective input noise temperature of the crystal alone is approximately equal to the bath temperature, 4.2°K.[7] Furthermore, since the forward losses in the X-band circulator are 0.1 db, and the signal waveguide losses are small, the over-all effective input noise temperature is expected to be no higher than 20°K. This temperature and the saturating input signal power would give a dynamic range of 100 db, if a 6-mc bandwidth is assumed. The incident pumping power for saturation is approximately 15 mw when the cavity is nonresonant at the pump frequency and reduces to approximately 3 mw when the cavity is resonant. This reduction is the result of improved matching. In each case the gain-bandwidth is approximately the same. There is reason to believe that the crystal may require as little as 30 μw saturating power.

One reason for the small gain-bandwidths of previous solid-state masers is that small filling factors were used. Accepted theory specifies that the crystal should not extend beyond regions of large pumping rf magnetic field. Spins in small or zero pumping fields are expected to be absorptive at the signal frequency. However, the performance of our maser indicates that the cavity negative resistance is essentially independent of pumping-field configuration, since the gain-bandwidth is the same in the resonant and nonresonant cases. This, as well as the near equality of magnetic absorption and negative Q's, indicates that pump transitions are uniformly saturated throughout the crystal with nonuniform saturating fields. A possible explanation is offered by the phonon saturation mechanism that has recently been proposed.[2,3]

R. J. Morris
R. L. Kyhl
M. W. P. Strandberg
Dept. Elect. Eng., Phys., and Res. Lab. Electronics,
Mass. Inst. Tech.
Cambridge 39, Mass.

[5] $\epsilon/\epsilon_0 = 11.53$, parallel to c axis, semi color and 9.53, perpendicular.

[6] $(G^{1/2}-1)Bw = 2f_0/|Q_{neg}| =$ "voltage gain-bandwidth product" is nearly constant for high gains. Q_{neg} is the net negative cavity Q, including losses; f_0 is the operating frequency.

[7] $T_{amplifier} \approx (|Q_{neg}|/Q_{abs})T_{bath}$.

Four-Terminal Parametric Amplifier*

The purpose of this paper is to report some experimental results on a *four-terminal* parametric amplifier using nonlinear reactances. The amplifier (see Fig. 1) uses a lower-frequency pump and consists of three cascaded stages: 1) a down-converter which converts the incoming high-frequency signal (ω_s) into a low frequency "idling" signal (ω_d); 2) an amplifier which amplifies the idling signal ω_d; and 3) an up-converter which converts the amplified idler back into the amplified signal at ω_s. All of these stages are pumped with a common pump (ω_p), the frequency of which is lower than that of the signal. In the amplifier stage, the pump frequency may be multiplied through a multiplier (shown by a dotted box) to yield an effective pump frequency of $n\omega_p$. In this way, a lower noise factor is produced. Although the method employed here has some resemblance to that proposed by Hogan,[1] *et al.* there is, however, one striking difference. In the Hogan amplifier, regeneration is employed in the signal circuit so that the amplifier has inseparable input and output terminals. The amplifier discussed in this note has internal frequency isolation between the input and the output. Therefore, no circulators or isolators are needed.

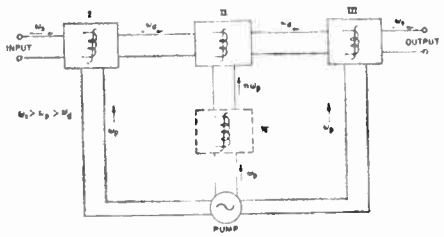

Fig. 1.

The over-all gain and noise factor of this amplifier have been calculated; they are

$$G = \frac{2\sqrt{\gamma/\alpha}}{1/\alpha + 1 - \beta/\alpha + \gamma/\alpha} \qquad (1)$$

$$F = 1 + (\beta/\alpha)\left(\frac{\omega_s}{(n+1)\omega_p - \omega_s}\right) + \left(\frac{\omega_s}{\omega_s - \omega_p}\right)1/\alpha + \gamma/\alpha \qquad (2)$$

where α, β, γ are, respectively, proportional to pumping powers entering the down-converter, the amplifier, and the up-converter.

A lumped-constant four-terminal parametric amplifier using germanium junction diodes has been built with a signal frequency of 214 mc and a pump frequency of 150 mc. The following results have been obtained:

Power gain = 8 db.
Band width = 0.25 mc.
Noise factor = 2.5 db.
Sensitivity = 114 dbm.
Pumping power = 100 mw.
Input-output isolation = 50 db.

The amplifier can be operated at linear gains as high as 30 db. The sensitivity at such gains is 120 dbm or better, which is beyond the small signal limit of any present standard signal generator. The noise factors at these gains are somewhat higher than 2.5 db.

* Received by the IRE September 26, 1958.

[1] C. L. Hogan, R. L. Jepsen, and P. H. Vartanian, "New type of ferromagnetic amplifier," *J. Appl. Phys.* vol. 29, pp. 422–423; March, 1958.

According to (2), lower noise factors can be realized by pumping the down-converter hard so that the pumping parameter α is made large. However, in order to operate at high gains, the ratio (β/α) must be in the order of unity by (1). Thus, at high gains, the noise factors are inferior to those at low gains because the frequency ratio

$$\left(\frac{\omega_s}{(n+1)\omega_p - \omega_s}\right),$$

will be the determining factor. These predictions agree well with experimental findings.

K. K. N. CHANG
RCA Labs.
Princeton, N. J.

Radio Observations of Jupiter*

A previous article[1] presented observations of radio radiation from Jupiter on 11 meters wavelength. Specifically, Figs. 5, 6 and 7 of that article show records of Jupiter emission on February 14, January 25, and January 20, 1956, respectively, while Figs. 8 and 9 present records and data obtained on February 2, 1956. No mention was made of the orientation of Jupiter during these observations, and the purpose of this note is to point out that all of the above observations occurred when the same emitting region on Jupiter was on or close to the central meridian of the planet (meridian toward the earth).

The observations were part of a series during which 11-meter Jupiter signals were recorded at Ohio State University on nine days between January 8 and February 26, 1956, and again on March 9, 1956. These occurrences of activity are summarized by the histogram in Fig. 1. The ordinate gives the number of occurrences and the abscissa the duration of the signals with respect to CMP (central meridian passage) of the Jovian longitude shown on the central meridian in the sketch (after Reese[2]) at the top of Fig. 1. In constructing the histogram, a rotation period for Jupiter of 9 hours, 55 minutes, and 30 seconds was assumed. This period is within about one second of the period which Carr[3] and Gallet[4] have shown to be associated with the source or sources of radio emission on the planet. This period is also nearly the same as for the South Tropical Disturbance.

The histogram suggests that the source of the radio emission observed at O.S.U.[1] is

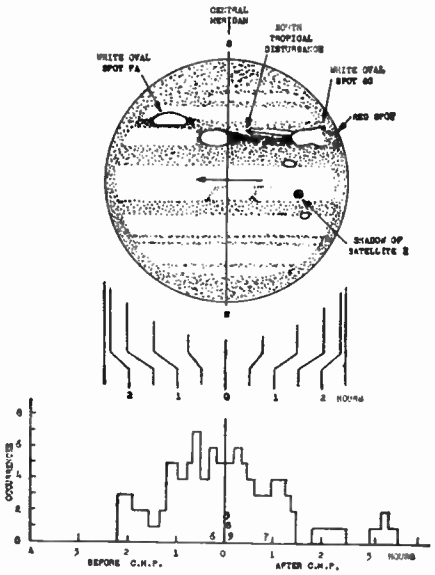

Fig. 1—Visual appearance of Jupiter at 0915 UT on January 1, 1956, after sketch by Reese, with histogram of occurrences of Jovian radio emission observed on 11 meter wavelength during the following two months. The south pole of the planet is up, as seen in an astronomical (inverting) telescope, and rotation is from right to left with the South Tropical Disturbance on or near the central meridian at the times of most occurrences of the Jovian radio emission.

on or close to the central meridian in the sketch in Fig. 1 and may be associated with the South Tropical Disturbance. Referring to the article mentioned,[1] the center of the active period in Fig. 5 is 3 minutes after CMP of the radio source, the center of the 4-minute active period in Fig. 6 is 14 minutes before CMP, the record of Fig. 7 is 56 minutes after CMP, all pulse groups of Fig. 8 are within 6 minutes of CMP, and the 0° point in Fig. 9 is 7 minutes after CMP of the source. Thus, all of the activity in the figures occurred close to the central meridian passage of what is presumed to be the same source of emission on Jupiter. The times before or after CMP of the active periods referred to in the figures are indicated by the numbers 5 through 9 in the histogram diagram of Fig. 1. Thus, the center of the active period in Fig. 5 is close to CMP (3 minutes after) as shown by the number 5 just to the right of the 0 line, while the active period of Fig. 6 is 14 minutes before CMP as shown by the number 6 to the left of the 0 line, etc.

JOHN D. KRAUS
Radio Observatory
Dept. of Elec. Eng.
Ohio State University
Columbus 10, Ohio

The Use of Beam Defocusing to Provide a Microwave Detector*

Ordinarily in devices using a long electron beam such as traveling-wave tubes, the defocusing action on the beam caused by the mutual repulsion of the electrons in the beam is considered detrimental to the operation of such devices. Hence, some scheme—sometimes simple, sometimes complicated—is usually employed to overcome this defocusing. In traveling-wave tubes, for example, focusing is necessary to confine the electron beam to a specified path so that electrical forces can act on the beam with maximum effectiveness while not permitting the beam to disperse and thus destroy the sought-for effect of these electrical forces. Most often the focusing scheme is a strong longitudinal magnetic field.

However, it is possible to utilize beam defocusing advantageously to provide a microwave detector. Mendel[1] has done this in a periodically focused TWT and has found the sensitivity of such a device to be comparable to that of a crystal diode. The purpose of this letter is to propose another method by which beam defocusing can provide detection action.

In an electron beam, the greater the current density of the beam, the stronger the defocusing forces. Thus, if a beam is density-modulated and then allowed to drift through a completely field-free space, the denser parts of the beam will disperse first. If now a cylindrical collector is placed around the beam in this space, the longitudinal distance along the collector at which the beam first strikes the collector will be a function of the initial density modulation of the beam. Further, if the collector is made of resistive material and the electrons which strike it are removed at one end of the collector, a voltage will be developed across the length of the collector as a function of the position at which the electrons strike the collector, since the total amount of resistance the electrons travel through is a function of the collector length they travel through. This voltage developed will thus be a function of the initial density modulation of the beam and detection action will result. In addition the functional relationship between detected voltage and initial modulation can be controlled by varying the resistance of the collector as a function of the distance along the length of the collector.

A similar action will take place if the beam is velocity modulated instead. In this case electrons with additional velocity will travel further down the resistive collector before striking it. The mechanism by which a voltage is developed across the length of the resistive collector is the same.

Preliminary experiments have shown that such detection action does indeed occur. By using a collector having a constant resistance per unit length it is found that a dc signal is developed across the length of the collector proportional to the square of the modulating signal. If the signal which modulated the beam is in turn modulated, the voltage across the collector will be a replica of the envelope of the beam-modulating signal.

The sensitivity of such a device appears to be comparable to that of a crystal diode, with the advantage of being a wideband device. Further advantages are an ability

* Received by the IRE, August 6, 1958.

[1] J. D. Kraus, "Planetary and solar radio emission at 11 meters wavelength," PROC. IRE, vol. 46, pp. 266–274; January, 1958.
[2] W. E. Fox, "Report on South Tropical Disturbance," *J. Brit. Astronom. Assn.*, vol. 66, pp. 124–125; March, 1956.
[3] T. D. Carr, A. G. Smith, R. Pepple, and C. H. Barrow, "18 mc observations of Jupiter in 1957," *Astrophys. J.*, vol. 127, pp. 274–283; March, 1958.
[4] R. M. Gallet, "The results of observations of Jupiter's radio emissions on 18 and 20 mc in 1956 and 1957" (abstract), IRE TRANS. ON ANTENNAS AND PROPAGATION, vol. AP-5, pp. 327–328; July, 1957.

* Received by the IRE, June 16, 1958.

[1] J. T. Mendel, "Microwave detector," PROC. IRE, vol. 44, pp. 503–508; April, 1956.

to handle a wide range in signal level without damage, and, as compared to traveling-wave tubes, less cost, less weight, and no requirement of any kind of focusing field.

P. S. Castro
J. S. Needle
Dept. Elec. Eng.
Northwestern University
Evanston, Ill.

Properties of Ion-Filled Waveguides*

The analysis carried out by Smullin and Chorney,[1] while correct for an unbounded medium filled with a uniform charge density of ions having a dc magnetic field along the z direction, cannot easily be extended to rectangular guides filled with the same medium, and having the dc magnetic field along the axis of the guide.

In fact, field solutions for the unbounded medium do not possess reflection symmetry along the x and y directions.[2,3] This means that it is not possible to construct a solution for the rectangular guide by simply assuming $\beta_x = l\pi/x_0$; $\beta_y = m\pi/y_0$ since the boundary conditions are not satisfied. This lack of reflection symmetry accounts for the difficulties encountered in the solution of the problem of a rectangular guide filled with a uniform charge density of ions or with ferrite and having a dc magnetic field along the axis. To our knowledge the exact solution of such a problem has not been given to date.

G. Barzilai
G. Gerosa
Istituto Elettrotecnico
Università di Roma
Rome, Italy
Istituto Superiore P.T.
Fondazione U. Bordoni
Rome, Italy

Authors' Comment[4]

The point made by Barzilai and Gerosa is perfectly correct. It is not possible to find simple TE or TM wave solutions for an ion filled waveguide, with a superimposed, axial magnetic field. The complexity of an exact solution of this problem is well illustrated in the paper by Suhl and Walker.[5] The difficulty that arises may be seen by examining the components of the electric field written for such a system in cylindrical coordinates

$$E_z = -\frac{j\beta_z\beta_r}{-\beta_r^2+k^2\left(1-\frac{\omega_p^2}{\omega^2}\right)} BJ_0(\beta_r r)e^{-j\beta_z z}$$

$$E_r = BJ_1(\beta_r' r)e^{-j\beta_z z}$$

$$E = j_\theta \frac{\omega_c}{\omega}\frac{\omega_p^2}{\omega^2-\omega_c^2} \cdot \frac{k^2}{-\beta_r^2-\beta_z^2+k^2\left(\frac{\omega^2-\omega_p^2-\omega_c^2}{\omega^2-\omega_c^2}\right)} BJ_1(\beta_r r)e^{-j\beta_z z}$$

where ω_c and ω_p are the ion plasma and cyclotron-frequencies, β_z and β_r are the axial and radial wave numbers, $k=\omega/c$, and B is a constant. It is clear that we cannot make E_z and E_θ vanish simultaneously on a conducting cylindrical boundary. However, $|E_\theta|$ differs from $|E_r|$ or $|E_z|$ by a factor of the order $|k^2/(\beta_r^2+\beta_z^2)|$. In our case, we consider ion natural frequencies of the order of megacycles per second, while "laboratory sized" waveguides have cutoff frequencies (corresponding to β_r) of kilomegacycles per second. Thus $|E_\theta/E_r|$ is of the order of 10^{-5} or 10^{-6}. If we let $E_\theta \approx 0$, this can be shown to be equivalent to making the electrostatic approximation, $\bar{E} = -\text{grad } V$, that we used in our letter. Our solutions, of course, are only good to within this approximation.[6,7]

Recent experiments by Gould and Trivelpiece have substantially verified the existence of the modes of propagation under discussion here.[8]

L. D. Smullin
P. Chorney
Dept. Elec. Eng.
and Res. Lab. of Electronics
Mass. Inst. Tech.
Cambridge, Mass.

* Received by the IRE, June 12, 1958.

[1] L. D. Smullin and P. Chorney, "Properties of ion filled waveguides," Proc. IRE, vol. 46, pp. 360–361; January, 1958.

[2] A. L. Mikaelian, *Radiotecknika*, vol. 10, p. 3; 1955.

[3] G. Barzilai and G. Gerosa, *Il Nuovo Cim.*, ser. 10, p. 685; 1958.

[4] Received by the IRE, June 24, 1958.

[5] H. Suhl and L. R. Walker, "Topics in guided-wave propagation through gyromagnetic media, Part I," *Bell Sys. Tech. J.*, vol. 23, pp. 579–659; May, 1954.

[6] L. D. Smullin and P. Chorney, "Wave propagation in ion plasma loaded waveguides," *Proc. Symp. on Electron Waveguides*, Polytechnic Inst. of Brooklyn, Brooklyn, N. Y., to be published.

[7] P. Chorney, "Electron-Stimulated Ion Oscillations," Res. Lab. Electronics, M.I.T. Cambridge, Mass., Tech. Rep. 277; May 26, 1958.

[8] R. W. Gould and A. W. Trivelpiece, "A new mode of wave propagation on electron beams," *Proc. Symp. on Electronic Waveguides*, to be published.

On the Usefulness of Transconductance as a Transistor Parameter*

The properties of a transistor, like those of any other amplifying device, may be described in terms of various kinds of parameter. The current gain seems to be in most common use at the present. While α, the common-base current gain, is often used, surely β (or call it what you will, but it seems a needless waste of writing to have a symbol with three or so subscripts to represent this quantity), the common-emitter current gain, should be preferred, since most transistors are used in the common-emitter configuration.[1] It may be that the preference for the current gain parameter arose in the days when the duality of transistors and vacuum tubes was being stressed, since the current gain is the dual of the amplification factor of a vacuum tube. If that is so, that reason has now disappeared, since it is now clear that, in general, the idea of duality has little to contribute to the solution of design problems.

In vacuum tube circuitry, actually, the tube parameter of most general use is not the amplification factor, but rather the transconductance. What is proposed here is that, as far as circuit design goes, transistors also may be usefully described in terms of their transconductance. This would make the design considerations for transistor circuits quite like those of tube circuits, at least formally. Such a similarity could be especially helpful to students, who are faced with the necessity of learning to deal with both devices at the same time. A book has already appeared which deals with both tubes and transistors on an equal footing;[2] the writer believes that anything helping to make design considerations for the two devices more nearly similar is sure to be helpful.

Another advantage to using transconductance as a parameter is seen when the behavior of the parameters with frequency is considered, and especially when the common approximate forms are used. The current gain β may be written, in this approximation, for the common-emitter configuration, as

$$\beta = \frac{\beta_0}{1+\frac{j\omega}{\omega_\beta}} \tag{1}$$

and the input impedance of the transistors as

$$z_i = \frac{r_i}{1+\frac{j\omega}{\omega_\beta}}. \tag{2}$$

β_0 is the current gain at low frequencies, r_i the input resistance at low frequencies, and ω_β the angular frequency at which the magnitude of β is 0.707 times its low-frequency value.

In the literature the relations in (1) and (2) are often given as[3]

$$\left.\begin{aligned} h_{21} &= \frac{\alpha_{b0}}{1-\alpha_{b0}} \frac{1}{1+\frac{j\omega}{(1-\alpha_{b0})\omega_{\alpha b}}} \\ h_{11} &= r_b' + \frac{r_e}{1-\alpha_{b0}} \frac{1}{1+\frac{j\omega}{(1-\alpha_{b0})\omega_{\alpha b}}} \end{aligned}\right\}. \tag{3}$$

Eqs. (1) and (2) are just simplifications of these relations, obtained by writing h_{21} as β and h_{11} as z_i, and defining

$$\left.\begin{aligned} \frac{\alpha_{b0}}{1-\alpha_{b0}} &= \beta_0 \\ (1-\alpha_{b0})\omega_{\alpha b} &= \frac{\omega_{\alpha b}}{\beta_0+1} = \omega_\beta \end{aligned}\right\}. \tag{4}$$

* Received by the IRE, July 14, 1958.

[1] H. L. Armstrong, "On the need for revision in transistor terminology and notation," to be published in Proc. IRE.

[2] K. R. Spangenberg, "Fundamentals of Electron Devices," McGraw-Hill Book Co., Inc., New York, N. Y.; 1957.

[3] R. F. Shea, "Transistor Circuit Engineering," John Wiley and Sons, Inc., New York, N. Y., p. 38, Table 2.2; 1957.

If r_b' is negligible, r_i is defined by

$$r_i = \frac{r_e}{1-\alpha_{bb}} = (\beta_0 + 1)r_e \qquad (5)$$

while if r_b' is not sufficiently negligible, an adequate approximation will be to define (neglecting the error in representing r_b')

$$r_i = r_b' + \frac{r_e}{1-\alpha_{bb}} \approx (\beta_0 + 1)\left(\frac{r_b'}{\beta_0 + 1} + r_e\right). \qquad (6)$$

It is apparent that the transconductance g_m is just given by

$$g_m = \frac{\beta}{z_i} = \frac{\beta_0}{r_i} \qquad (7)$$

i.e., in this approximation *the transconductance is independent of frequency.* Moreover, the input impedance z_i may be represented by a resistance r_i and a capacitance C_i in parallel, their magnitude being

$$\left.\begin{aligned} r_i &= r_i \\ C_i &= \frac{1}{r_i\omega_\beta} \end{aligned}\right\}. \qquad (8)$$

The remaining two transistor parameters, the output admittance or impedance and the internal feedback, could be treated similarly, but they are not required for the present discussion. It is apparent that, as far as the input and transconductance properties of the transistor are concerned, and to such an extent as the approximations used here are valid, it could be described by giving values of g_m, r_i, and C_i, just as a vacuum tube might be described by giving g_m, r_p, and the input or output capacitance (or both if they are equally important. Often, the sum of input and output capacitances is what is wanted).

It is in the design of cascaded stages that the utility of this representation becomes apparent. When tubes are being used, the problem is to couple from a tube of known transconductance and output conductance and capacitance (if the latter is important). But when the transistors are described in terms of their transconductance, input conductance and capacitance, and also output properties if the latter are not negligible, the data are of exactly the same kind as those for the tubes, although magnitudes may be much different. Thus the design procedure used with tubes may be applied directly to transistors, both for audio,[4] video,[5] and other types of amplifier.[6] In such problems as video amplifiers this seems especially convenient, in that one is dealing with relatively frequency-independent transconductance, conductance, and capacitance, instead of a frequency-dependent current gain.

The transconductance also has an advantage as a parameter when large signal operation is important, in that it is nearly independent of operating point over a considerable range. This is because the characteristic of collector current vs base voltage for most transistors approaches a straight asymptote; thus, the transconductance would just approach the value of the slope of this asymptote. It has already been pointed out that the current vs voltage characteristic of semiconductor diodes is of such a form,[7] being represented by

$$V = I\,\frac{R_B I + V_0}{I + I_N}. \qquad (9)$$

Another approximation to this, perhaps more convenient in calculation, is

$$I = \frac{V - V_0}{R_B} + \frac{V_0 I_N}{R_B\left(1 - \sqrt{\frac{I_N R_B}{V_0}}\right)V + R_B I_N} \qquad (10)$$

and either of these representations could be useful in dealing with many problems.

In summary, it is proposed that a representation of transistors in terms of transconductance, and input (and output, if necessary) conductance and capacitance, the design of transistor circuits could be made more nearly like that of tube circuits. The advantage, especially to students, of having the design of both kinds of stage performed similarly is obvious.

This stress on transconductance as a transistor parameter, it might also be mentioned, could serve to emphasize the viewpoint that both the transistor and the vacuum tube are really charge controlled devices, as has been recently pointed out.[8] The difference then is that the capacitance on which the charge is stored is much "leakier" for a typical transistor than for a typical vacuum tube.

While this discussion was being prepared, an article by Jochems, *et al.* has appeared,[9] in which it is shown experimentally how weak a function of frequency is the transconductance, in contrast to some of the other parameters.

H. L. Armstrong
Pacific Semiconductors, Inc.
Culver City, Calif.

[4] F. E. Terman, "Radio Engineering," McGraw-Hill Book Co., Inc., New York, N. Y., 3rd ed., section 6-3; 1947.
[5] *Ibid.*, section 6-5.
[6] *Ibid.*, section 7-1.
[7] H. L. Armstrong, "On the forward characteristics of semiconductor diodes," PROC. IRE, vol. 46, p. 361; January, 1958.
[8] J. J. Sparks and R. Beaufoy, "The junction transistor as a charge controlled device," PROC. IRE, vol. 45, pp. 1740–1742; December, 1957.
[9] P. J. W. Jochems, O. W. Memelink, and L. J. Tummers, "Construction and electrical properties of a germanium alloy-diffused transistor," PROC. IRE, vol. 46, pp. 1161–1165; June, 1958. Figs. 10–12 especially illustrate the point made here.

Short-Time Statistics of Tropospheric Radio Wave Propagation*

An experimental investigation of short-time statistics which characterize beyond-the-horizon tropospheric propagation is briefly summarized here. Specifically, information about the envelope amplitude probability distribution and period of stationarity was obtained.[1]

In these experiments, 915 mc continuous wave radio energy was transmitted by a 10 kw transmitter located at Bedford, Mass. The receiver was a triple-conversion, superheterodyne unit with a 3 kc bandwidth and 12 db noise figure, located at Schenectady, N. Y. The Bedford-Schenectady path length was 134 miles. Continuous paper records of the envelope of the received amplitude were obtained and these were sampled at intervals chosen so that successive sampled values were essentially independent. The values obtained over 30-second or one minute intervals were then grouped into statistical "samples," and these were the basic units for analysis. Six signal records, varying in length from twelve minutes to one hour, were thus obtained and analyzed.

The analysis of the data consisted of two statistical tests, an F test and a χ^2 goodness-of-fit test. Concerning stationarity, a sufficient condition for its violation was a change in the second absolute moment a_2 of the statistical population. It was determined that, assuming a Rayleigh distribution of amplitude r, the quantity

$$F = \frac{\overline{r_1^2}/(a_2)_1}{\overline{r_2^2}/(a_2)_2} \qquad (1)$$

is distributed as F with $\nu_1 = 2n_1$ and $\nu_2 = 2n_2$ degrees of freedom.[2] Here $\overline{r_1^2}$ and $\overline{r_2^2}$ are the mean square values of two samples:

$$\overline{r^2} = \frac{1}{n}\sum_{i=1}^{n}(r_i^2) \qquad (2)$$

$(a_2)_1$ and $(a_2)_2$ are the second absolute moments of their respective parent populations, and n_1 and n_2 are the number of values in the respective samples. It was also found that (1) yielded sufficient accuracy over a considerable range of approximate Rayleigh distributions. The standard F test[2] was then used to test the hypothesis that $(a_2)_1 = (a_2)_2$, with rejection implying a change in the distribution, or a violation of stationarity, between the times represented by the two samples.

The χ^2 goodness-of-fit test (see Cramer,[3] for example, for its development) was applied in the usual way to test the hypothesis that given data were drawn from a particular Rayleigh-distributed population.

As a result of the above analysis, it was concluded that the period of stationarity of the received signal was typically one to five minutes in length. The longest period noted was 19 minutes but this was exceptional, the next longest being eight minutes. The shortest period which could be detected was limited by the 30-second and one-minute grouping of samples.

Concerning the probability distribution, the conclusion was that the envelope ampli-

* Received by the IRE, June 27, 1958. The research reported here was supported by the Electronics Res. Dir. of the AF Cambridge Res. Center, Air Res. and Dev. Command, under Contract AF19(604)-1723.

[1] This work will be described in detail in "Short-Time Statistics of Tropospheric Radio Wave Propagation," GE Res. Lab. Rep., No. 58-RL-2030.
[2] P. G. Hoel, "Introduction to Mathematical Statistics," John Wiley and Sons, Inc., New York, N. Y., pp. 150–161; 1947.
[3] H. Cramer, "Mathematical Methods of Statistics," Princeton University Press, Princeton, N. J., pp. 416–441; 1946.

tude was frequently Rayleigh-distributed, as predicted for a scatter process. However, enough non-Rayleigh results were obtained to suggest other processes as important contributors on occasion. One of the six signal records tested almost exclusively non-Rayleigh. A surprising result, in view of many published statements that the distribution approaches the Gaussian over longer periods of time, was that the hypothesis of a Rayleigh distribution was accepted for an entire one-hour record in one instance.

The author is indebted to Dr. L. G. Abraham, Jr., and Dr. R. L. Shuey for their direction and counsel in connection with this work.

R. G. FINNEY
GE Res. Lab.
Schenectady, N. Y.

A Vector Method for the Evaluation of Derivatives of Phase, Gain, and Attenuation*

Vectors in the complex p plane are used commonly to evaluate geometrically the phase and gain of rational transfer functions. This note shows that vectors can also be employed to obtain the derivatives of phase, gain, and attenuation.

The transfer function

$$H(p) = A\frac{\prod_{i=1}^{M}(p-\bar{p}_i)}{\prod_{i=1}^{N}(p-p_i)} = A\frac{\prod_{i=1}^{M}\bar{P}_i}{\prod_{i=1}^{N}P_i} \quad (1)$$

with zeros at $\bar{p}_i=\bar{\sigma}_i+j\bar{\omega}_i (i=1,\cdots,M)$ and poles at $p_i=\sigma_i+j\omega_i (i=1,\cdots,N)$ is given, as indicated, by the product of M "zero" complex numbers (the $\bar{P}_i$) divided by the product of N "pole" complex numbers (the P_i). Geometrically the $\bar{P}_i$ and P_i are interpreted as vectors connecting p to the poles and zeros of $H(p)$. Fig. 1 presents a simple example with one zero at -1 and two poles at $-1\pm j$. The phase of H is

$$\angle H(p) = A + \sum_{i=1}^{M}\angle\bar{P}_i - \sum_{i=1}^{N}\angle P_i \quad (2)$$

and the gain of H is

$$|H(p)| = A\frac{\prod_{i=1}^{M}|\bar{P}_i|}{\prod_{i=1}^{N}|P_i|} \quad (3)$$

where $\angle\bar{P}_i$, $\angle P_i$, $|\bar{P}_i|$ and $|P_i|$ may be determined from a vector diagram such as that of Fig. 1.

We consider now the first derivative of $\angle H$ with respect to ω. From (2)

$$\frac{\partial\angle H}{\partial\omega} = \sum_{i=1}^{M}\frac{\partial\angle\bar{P}_i}{\partial\omega} - \sum_{i=1}^{N}\frac{\partial\angle P_i}{\partial\omega}.$$

* Received by the IRE, July 7, 1958.

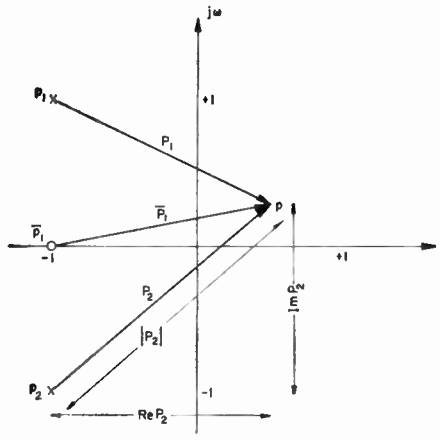

Fig. 1.

But

$$\angle P_i = \tan^{-1}\frac{\omega-\omega_i}{\sigma-\sigma_i},$$

so

$$\frac{\partial\angle H}{\partial\omega} = \sum_{i=1}^{M}\frac{(\sigma-\bar{\sigma}_i)}{(\sigma-\bar{\sigma}_i)^2+(\omega-\bar{\omega}_i)^2} - \sum_{i=1}^{N}\frac{(\sigma-\sigma_i)}{(\sigma-\sigma_i)^2+(\omega-\omega_i)^2}$$

which can be evaluated in terms of the vectors $\bar{P}_i$ and P_i by

$$\frac{\partial\angle H}{\partial\omega} = \sum_{i=1}^{M}\frac{\mathrm{Re}\,\bar{P}_i}{|\bar{P}_i|^2} - \sum_{i=1}^{N}\frac{\mathrm{Re}\,P_i}{|P_i|^2}. \quad (4)$$

Similarly,

$$\frac{\partial\angle H}{\partial\sigma} = -\sum_{i=1}^{M}\frac{(\omega-\bar{\omega}_i)}{(\omega-\omega_i)^2+(\sigma-\bar{\sigma}_i)^2} + \sum_{i=1}^{N}\frac{(\omega-\omega_i)}{(\omega-\omega_i)^2+(\sigma-\sigma_i)^2} = -\sum_{i=1}^{M}\frac{\mathrm{Im}\,\bar{P}_i}{|\bar{P}_i|^2} + \sum_{i=1}^{N}\frac{\mathrm{Im}\,P_i}{|P_i|^2}. \quad (5)$$

Higher derivatives may be obtained in like manner although the expressions become somewhat more complicated. For example,

$$\frac{\partial^2\angle H}{\partial\omega^2} = -\frac{\partial^2\angle H}{\partial\sigma^2} = -2\sum_{i=1}^{M}\frac{\mathrm{Re}\,\bar{P}_i\,\mathrm{Im}\,\bar{P}_i}{|\bar{P}_i|^4} + 2\sum_{i=1}^{N}\frac{\mathrm{Re}\,P_i\,\mathrm{Im}\,P_i}{|P_i|^4} \quad (6)$$

and

$$\frac{\partial^2\angle H}{\partial\omega\partial\sigma} = -\sum_{i=1}^{M}\frac{1}{|\bar{P}_i|^2} + \sum_{i=1}^{N}\frac{1}{|P_i|^2}. \quad (7)$$

From (3) the gain derivative with respect to ω is

$$\frac{\partial|H|}{\partial\omega} = \left[\sum_{i=1}^{M}\frac{\frac{\partial|\bar{P}_i|}{\partial\omega}}{|\bar{P}_i|} + \sum_{i=1}^{N}\frac{\frac{\partial|P_i|^{-1}}{\partial\omega}}{|P_i|^{-1}}\right]|H|.$$

Note that

$$|P_i| = \sqrt{(\sigma-\sigma_i)^2+(\omega-\omega_i)^2}$$

gives

$$\frac{\partial|H|}{\partial\omega} = \left[\sum_{i=1}^{M}\frac{(\omega-\bar{\omega}_i)}{(\sigma-\bar{\sigma}_i)^2+(\omega-\bar{\omega}_i)^2} - \sum_{i=1}^{N}\frac{(\omega-\omega_i)}{(\sigma-\sigma_i)^2+(\omega-\omega_i)^2}\right] = \left[\sum_{i=1}^{M}\frac{\mathrm{Im}\,\bar{P}_i}{|\bar{P}_i|^2} - \sum_{i=1}^{N}\frac{\mathrm{Im}\,P_i}{|P_i|^2}\right]|H| = -\frac{\partial\angle H}{\partial\sigma}|H|. \quad (8)$$

In the same way

$$\frac{\partial|H|}{\partial\sigma} = \left[\sum_{i=1}^{M}\frac{\mathrm{Re}\,\bar{P}_i}{|\bar{P}_i|^2} - \sum_{i=1}^{N}\frac{\mathrm{Re}\,P_i}{|P_i|^2}\right]|H| = \frac{\partial\angle H}{\partial\omega}|H|. \quad (9)$$

Finally, consider the derivative of attenuation with respect to logarithmic frequency $\ln\omega$. The attenuation is by (2)

$$\ln|H| = \ln A + \sum_{i=1}^{M}\ln|\bar{P}_i| - \sum_{i=1}^{N}\ln|P_i|.$$

Since

$$\frac{\partial\ln|P_i|}{\partial\ln\omega} = \frac{\partial\ln\sqrt{(\sigma-\sigma_i)^2+(\omega-\omega_i)^2}}{\partial\ln\omega} = \frac{1}{2}\frac{2(\omega-\omega_i)}{(\sigma-\sigma_i)^2+(\omega-\omega_i)^2}\frac{\partial\omega}{\partial\ln\omega} = \frac{(\omega-\omega_i)\omega}{(\sigma-\sigma_i)^2+(\omega-\omega_i)^2}$$

we have

$$\frac{\partial\ln|H|}{\partial\ln\omega} = \omega\left[\sum_{i=1}^{M}\frac{\mathrm{Im}\,\bar{P}}{|\bar{P}_i|^2} - \sum_{i=1}^{N}\frac{\mathrm{Im}\,P_i}{|P_i|^2}\right] = -\omega\frac{\partial<H}{\partial\sigma}. \quad (10)$$

To demonstrate the utility of one of the above formulations, let us evaluate the time delay of a Butterworth low-pass filter at $\omega=0$. Assuming that the cutoff frequency is ω_c and that the number of poles is N, the p_i are given by

$$p_i = \omega_c e^{j\alpha_i}, \quad i=1,\cdots,N \quad (11)$$

where

$$\alpha_i = \frac{\pi}{2}\left[1+\frac{1}{N}+\frac{2i}{N}\right] \quad (12)$$

(the zeros of H are all at $|p|=\infty$). The time delay at $\omega=0$ is given by

$$T = -\left.\frac{\partial<H}{\partial\omega}\right|_{\substack{\omega=0\\ \sigma=0}}.$$

Since all the P_i vectors to $p=0$ have the same length $|P_i|=\omega_c$ and the angles $=\alpha_i-\pi$ (see Fig. 2), application of (4) gives

$$T = \frac{1}{\omega_c^2}\sum_{i=1}^{N}\mathrm{Re}\,P_i = \frac{1}{\omega_c}\sum_{i=1}^{N}\cos\frac{\pi}{2}\left(-1-\frac{1}{N}+\frac{2i}{N}\right) = \frac{1}{\omega_c}\sum_{i=1}^{N}\sin\frac{\pi}{2}\left(\frac{2i-1}{N}\right). \quad (13)$$

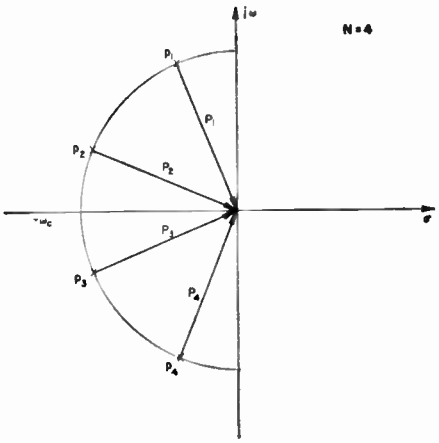

Fig. 2.

Well-known formulas for the summation of trigonometric series simplify (13) to

$$T = \frac{1}{\omega_r} \cdot \frac{1}{\sin \frac{\pi}{2N}}.$$

ELMER G. GILBERT
Dept. of Aeronautical Eng.
University of Michigan
Ann Arbor, Mich.

220-MC Radiowave Reception at 700–1000 Miles*

Within the past year, Booker and Gordon[1] have advanced a theory of radiowave scattering from stratospheric dielectric constant irregularities in order to explain the reception of UHF radiowaves beyond a distance of some 400–500 statute miles. They suggested that agreement be sought between their predictions and the actual values of path loss at such great distances by measuring the signal level vs distance in an aircraft at a wavelength near 3 meters.

As a continuation of our airborne investigations of long-distance 220-mc field strengths,[2] we have developed equipment and experimental techniques which permit measuring a path loss of approximately 280 db both on the ground and in the air; according to the Booker-Gordon estimates such a sensitivity should permit the detection of energy out to distances of some 850 statute miles at low altitudes.

A surface experiment was conducted prior to undertaking airborne measurements. During the month of February, 1958, field strengths were measured at a location in southwest Newfoundland near Stephenville at a surface distance close to 735 statute miles (~700 miles between average radio horizons) from our transmitting site at Scituate, just south of Boston, Mass. The measured median attenuation was 266 db ±5 db, a value in very good agreement with the Booker-Gordon estimate of some 260 db, considering that the measurements were taken during a cold weather period. There was little variation in the hourly median signal level over the two-week experiment duration; the slope of the cumulative distribution of these median values exhibited a $\sigma = 2$ db. Also, except for the presence of short meteor-induced signals, the general characteristics of signal behavior appeared much like those observed previously at shorter distances.

The first airborne measurement was made on March 18, 1958 at an altitude of 10,000 feet; our interest was confined to distances beyond 600 miles. The median path loss as a function of distance agreed rather closely both in absolute magnitude and slope with the Booker-Gordon estimates out to a surface distance of some 800–850 miles. For the short distance available beyond this region, however, we were surprised to find an indication that the field strength was decaying less rapidly with distance. Also, from about 750–800 miles out to the predetermined aircraft turn-around point just beyond 850 miles, careful examination of the data showed that a marked increase in short-time fading rate had taken place.

In view of the similarity between these field strength characteristics and those observed on the long-distance airborne Lincoln Laboratory-Cambridge Research Center measurements at 50 mc,[3] the possibility was raised that the fields beyond 800 miles were ionospheric in origin. Of immediate concern was the determination of whether these fields were persistent or, rather, whether they could be attributed to some unusual *E*-region condition occurring during the flight period.

Another flight measurement was conducted on April 15, 1958 at 6000 feet. This time the aircraft turn-around point was extended to 1000 miles and the flight was scheduled to reach this distance near noontime at the path midpoint, since it might be expected that the fields would be somewhat stronger at that time if they arrived via the *E* region.

Fig. 1 presents the measurement results of the two flights. In the latter case the signal was still being received at 1000 statute miles, where it was a very few db above the noise level. The indicated normal median path loss—assuming that the plane wave antenna gain was maintained—throughout the 800–1000 mile region is 275 db ±5 db.

Both the variation with distance and the fading rate offer strong evidence that we have measured 220-mc ionospheric scatter fields beyond 800 miles. Measurements now in progress along a 900-mile surface path between Scituate and a location near Argentia in southeastern Newfoundland leave no doubt about the persistence of the signal

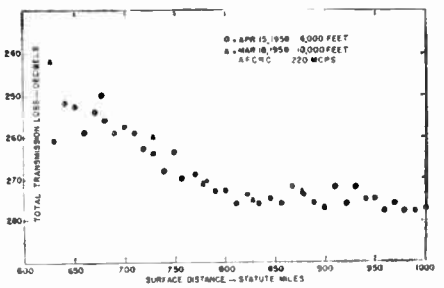

Fig. 1

level: it has remained consistently detectable for a period of three weeks at this writing.

The strength of these near-UHF ionospheric scatter fields is unexpectedly high. On the basis of the many 50-mc airborne measurements,[3] the median path loss at 1000 miles has been firmly established at close to 210 db for that frequency as deduced from data gathered on wide azimuth beamwidth (~60°) antennas. Fitting the median 28, 50, and 108-mc data points given in Fig. 19 of the paper by Bailey, Bateman, and Kirby[4] by their suggested function $1/(f^{A+Bf})$, a median path loss some 75 db greater than at 50 mc is predicted, *i.e.*, a total of 285 db, or 5 db lower than our measurement sensitivity. Alternatively, the theory of Villars and Weisskopf[5] predicts the relationship of f^{-11} for large f. This leads to a 280-db estimate for median path loss, *i.e.*, a signal-to-noise ratio of unity in our system.

Both of these estimates of path loss are made, however, under the assumption that our plane wave antenna gains are maintained; if allowance is made for an antenna-to-medium-coupling loss of our 27-db plane wave gain 4° azimuth beamwidth antenna under ionospheric scatter path conditions, the signal level might be anticipated to be perhaps 15–20 db below receiver noise.[6] We may therefore conclude that the path loss associated with the ionospheric scatter propagation mode is, very roughly, some 15 db less at 220 mc than that expected on the basis of lower frequency measurements.

It appears remarkable that the ionosphere *persistently* manifests its influence at this very high frequency—a frequency twice as high as has heretofore been demonstrated to exhibit characteristics of continuous ionospheric propagation.

The authors wish to express their appreciation to their colleagues at the Cambridge Research Center who were responsible for the actual experimental measurements: R. V. Barrett, J. Frazier, and T. Willson; to E. J. Martin for helpful discussions; and to the many military personnel associated with the entire program.

L. A. AMES
T. F. ROGERS
AF Cambridge Res. Ctr.
L. G. Hanscom Field
Bedford, Mass.

* Received by the IRE, August 5, 1958.

[1] H. G. Booker and W. E. Gordon, "The role of stratospheric scattering in radio communication," PROC. IRE, vol. 45, pp. 1223–1227; September, 1957.

[2] See, for example, L. A. Ames, P. Newman, and T. F. Rogers, "VHF tropospheric overwater measurements far beyond the radio horizon," PROC. IRE, vol. 43, pp. 1369–1373; October, 1955.
Also, T. F. Rogers, L. A. Ames, and E. J. Martin, "The possibility of extending air-ground UHF voice communications to distances far beyond the radio horizon," IRE TRANS. ON COMMUNICATION SYSTEMS, vol. CS-5, pp. 106–121; March, 1956.

[3] W. G. Abel, A. S. Orange, and T. F. Rogers, "VHF signal level measurements along a 2000 mile path," presented at URSI meeting, Washington, D. C.; April, 1958.

[4] D. K. Bailey, R. Bateman, and R. C. Kirby, "Radio Transmission at VHF by scattering and other processes in the lower ionosphere," PROC. IRE, vol. 43, pp. 1181–1230; October, 1955.

[5] F. Villars and V. F. Weisskopf, "The scattering of electromagnetic waves by turbulent atmospheric fluctuations," *Phys. Rev.*, vol. 94, pp. 232–240; April 15, 1954.

[6] Bailey, Bateman, and Kirby, *op. cit.*, pp. 1219–1220.

Numerical Analysis for Design of Electron Guns with Curved Electron Trajectories*

Recently, Cook[1] described a paper on the electrolytic tank for curved electron trajectories. This note describes a different approach to a similar problem, by numerical analysis using a digital computer. An *M*-type gun especially is considered, including space-charge effects for the dc conditions.

In a linear magnetron (Fig. 1) electrons reach the anode in curved paths when the dc magnetic field is below the cutoff value. These curves are not true cycloids due to space charge. When electrodes of suitable shapes and proper potentials are used, a strip of electron beam is formed, and the electrons are at rest on the finite width (along ξ in Fig. 2) cathode. In this beam the individual electron sees the identical electric field as if it were in the linear magnetron (Fig. 1).

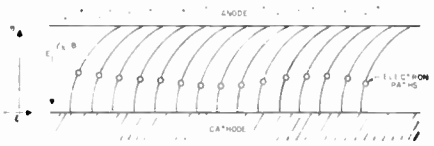

Fig. 1—Linear magnetron $B < B_{cutoff}$.

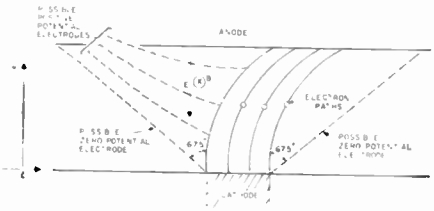

Fig. 2—Formation of a strip of electron beam from a linear magnetron $B < B_{cutoff}$.

Slater's works[2] on static linear magnetrons with space charge are modified a little because there is no returning electron stream from anode to cathode in the electron gun. Most of his notations are used without explanation, but some are defined differently below:

$\psi = \dfrac{\phi}{\phi_0}$ = normalized potential,

u = normalized y-direction electron velocity,

$\dfrac{\rho}{\rho_0}$ = normalized charge density,

$\xi = \dfrac{x}{y_0}$ = normalized x-direction displacement of electron,

$\eta = \dfrac{y}{y_0}$ = normalized y-direction displacement of electron,

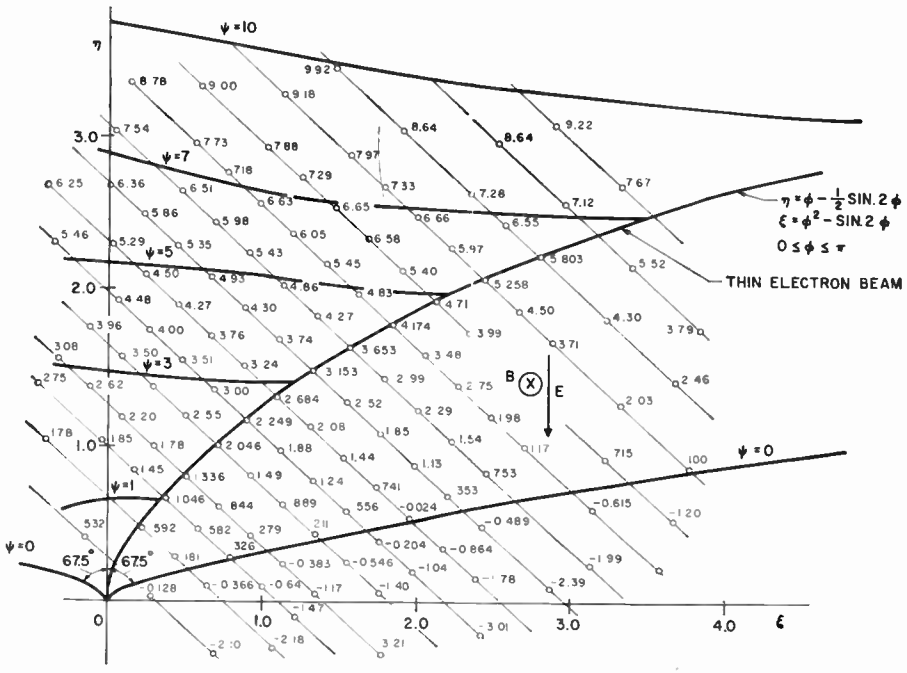

Fig. 3—"Crude" electrodes configurations from equipotential points by numerical analysis.

where

$y_0 = \dfrac{2eJ\,y}{m\bar{w}_c^{3}\epsilon_0}$ = fundamental distance.

$\phi_0 = \dfrac{2eJ^2y}{m\bar{w}_c^{4}\epsilon_0^{2}}$ = fundamental potential.

$\rho_0 = \dfrac{m\bar{w}_c^{2}\epsilon_0}{e}$ = Brillouin charge density in a linear magnetron.

Then the following equations for electron trajectory, potential, and velocities are derived in terms of electron transit angle ϕ, used as a parameter.

$$\psi = u^2 + \eta^2$$
$$\eta = \phi - \tfrac{1}{2}\sin^2\phi$$
$$\xi = \phi^2 - \sin^2\phi$$
$$u = \sin^2\phi$$
$$\frac{\rho}{\rho_0} = \frac{1}{2u}$$
$$1 - 2u = \cos\phi$$
$$2\phi = \omega_c\tau$$

where τ is the electron transit time.

As in the work of Slater, $\psi = \psi(\eta)$ is assumed inside the electron beam. ψ and its normal derivative are known on the electron beam edge $c = c(\xi, \eta)$. Thus Cauchy conditions are established on the boundary. Higher order partial derivatives are obtainable by the methods of characteristics of Riemann-Volterra.[3] As sketched in Fig. 2, the boundary is open and the Laplace equation under these circumstances has an "unstable" solution.[4] Studies made on propagation of errors using calculus of finite difference substantiated the statement about the instability of the solution of this problem.

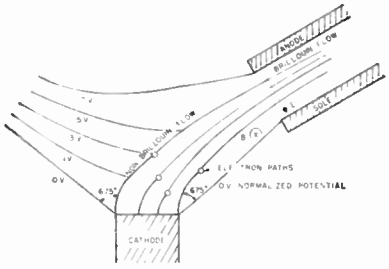

Fig. 4—Approximate picture of electron gun.

An attempt is made to calculate the potentials outside the beam by the two-dimensional Taylor series expansion in the "region" around the points right on the electron beam edge. This "region" is no longer restricted to the real vicinity of the points. This was done with a full awareness that only "approximate" or "crude" pictures of electrodes are possible by these calculations. The IBM 650 Computer was used, and third-order partial derivatives are included in computations for plotting of equipotentials. A few numerical examples illustrate the rate of convergence. (These examples are calculated up to and including fourth-order partial derivatives.)

Since $\psi = \psi(\eta)$ is inside the beam, and since there is no surface charge, the solutions of the Laplace equation outside the beam are the same for both the thick and thin beam case. Fig. 3 shows the "crude" electrode shapes of a thin beam case.

The possible application of this study would be the construction of an *M*-type gun, making a hole in the anode block so that the beam enters into the interaction region where a dc Brillouin flow is to be formed (Fig. 4). Notwithstanding "errors" committed in this numerical analysis, the digital computer provided sufficient preliminary information more easily than the analog computer does under the space-charge con-

* Received by the IRE, June 12, 1958. This work was done while the author was at the Microwave Res. Inst., Polytechnic Inst. of Brooklyn. The computations by the IBM 650 Computer were made possible by arrangement with Watson Scientific Computing Lab., IBM.

[1] E. J. Cook, "Electrolytic tank design of electron guns with curved electron trajectories," PROC. IRE, vol. 46, p. 497; February, 1958.

[2] J. C. Slater, "Microwave Electronics," D. Van Nostrand and Co., New York, N. Y., pp. 333–345; 1950.

[3] A. G. Webster, "Partial Differential Equations of Mathematical Physics," Dover Publications, Inc., New York, N. Y., ch. 6; 1955.

[4] P. M. Morse and H. Feshbach, "Methods of Theoretical Physics," McGraw-Hill Book Co., Inc., New York, N. Y., vol. 1, pp. 703, 706; 1953.

dition. These "crude" shapes of electrodes are now improved further for actual gun construction through the use of digital and analog computers.

Numerical Examples

Potentials at points outside of the electron beam are calculated by the "stretched" Taylor series from the potential ψ_0 at points right on the beam edge by

$$\psi_{(i)} = \psi_0 + \psi_1 h + \psi_2 h^2 + \psi_3 h^3 + \psi_4 h^4 + \cdots,$$

where ψ_1, ψ_2, ψ_3, and ψ_4 involve partial derivatives, and

$$h = i\Delta h \qquad \Delta h = 0.075$$

$$h^2 = (\Delta\xi)^2 + (\Delta\eta)^2,$$

in which $\Delta\xi$ is negative and $\Delta\eta$ is positive.

Numerical values are expressed by the Floating Point Mode, *i.e.*,

$$1234567850 = 0.12345678$$

$$1234567849 = 0.012345678$$

$$1234567851 = 1.2345678$$

For $\psi_0 = 1046355551$ at $\xi = 3885504050$, $\eta = 664083050$.

i	$\psi(i)$	$\psi_1 h$	$\psi_2 h^2$	$\psi_3 h^3$	$\psi_4 h^4$
1	1205108451	1620000050	3571189948	3171395047	−6981331345
3	1509343151	4860000050	3214070949	8562766448	−5654878547
5	1811081551	8100000050	8927974749	3964243849	−4363332148
7	2130908351	1134000051	1749883050	1087788550	−1676217849
9	2492088351	1458000051	2892663850	2311947050	−4580451549
11	2920567951	1782000051	4321139750	4221126850	−1022136750
13	3444973751	2106000051	6035310950	6967554650	−1993938150
15	4096613551	2430000051	8035177250	1070345851	−3534299150

For $\psi_0 = 4984916051$ at $\xi = 2291620851$, $\eta = 2021260251$.

i	$\psi(i)$	$\psi_1 h$	$\psi_2 h^2$	$\psi_3 h^3$	$\psi_4 h^4$
1	5252660051	2700000050	2280798548	2397441446	−7785395044
3	5775099251	8100000050	2052718649	647.3091847	−6306170146
5	6281379451	1350000051	5701996149	2996801848	−4865871947
7	6773249451	1890000051	1117591250	8223224048	−1869273548
9	7252756651	2430000051	1847446750	1747734749	−5107997748
11	7722247951	2970000051	2759766150	3190994449	−1139859749
13	8184368851	3510000051	3854549450	5267178649	−2223586749
15	8642063551	4050000051	5131796550	8091364849	−3941356149

Iwao Sugai
IBM Res. Center
Poughkeepsie, N. Y.

A Technique for Measuring High Antenna Field Strengths in a Very Small Region at 200 MC*

There is need to measure antenna field strengths of high intensities at almost point locations. This is especially true in modern anechoic chambers. These almost point locations may be in either the Fresnel or Fraunhofer zones of the field. It also is desirable to evaluate fields inside of various substances.

The usual meter for field strength measurements at this frequency possesses a resonant dipole that is too unwieldy for measuring conditions at a small region. Furthermore, the reading on the meter usually is rendered worthless by the penetration of the actual field or leakage field into the instrument since such a field is larger than that for which the instrument was intended.

A very simple shop substitute instrument can be fabricated, which can be calibrated against a standard field strength meter under conditions which do not vitiate the operation of the latter instrument. Some typical apparatus is described.

For pulse measurements, a very small loop or dipole feeds a calibrated shielded twinax transmission link which in turn operates into a calibrated attenuator and then to a balun, shielded envelope detector (a 50-ohm parallel resistor and series 1N54 rectifier) and a Tektronix visual display output device.

For continuous wave measurements, the detector is modified by adding a 0.01-μf parallel capacitor following the rectifier, and a series 330,000-ohm resistor after the capacitor where a Rubicon galvanometer (sensitivity 0.0006 μa/mm) serves as the output device along with an Ayrton shunt.

The detector assembly consisting of a balun, a particular detector, and output device is calibrated against a Stoddart Radio Interference and Field Intensity Meter, Model NM.A-5A, when these equipments are directly driven by an appropriate oscillator with very short cabling throughout in the absence of an electromagnetic field.

Since the transmission link and attenuator have standard calibrations (attenuating factors) as mentioned earlier in this substitute instrument, only the small loop or dipole remains to be calculated.

This can be done by first connecting the Stoddart resonant dipole (supplied with the formal instrument) to the substitute instrument when the resonant dipole is in the far field of some antenna. Then the small sampling dipole or loop replaces the original dipole and a new reading is taken at the same location. A ratio of readings gives the factor for the sampling probe. Of course, the substitute instrument could be calibrated in any known standard field of sufficiently high intensity.

The substitute instrument works very well in the far field of an antenna to be measured since points of zero electric field intensity can be found for the transmission link. In the near field, the amplitude of the various coordinate components of E vector (with dipole) and H vector (with loop) can be measured essentially at a point within the limit of field distortion caused by the transmission link. Free space power densities can be computed although, for most work, the field strengths are considered more meaningful.

When the sampling dipole or loop is immersed in a specimen, the calibration is not necessarily the same as when the sampling probe is in the air. By experimentally measuring the sampling antenna impedance both in the air and in the specimen, corrective constants can be applied to the air calibration when one knows the characteristics of the transmission link.

It is anticipated that this technique can be extended to higher frequencies.

F. P. Fischer
R. A. Neubauer
Y. T. Sarkees
Elec. Eng. Dept.
University of Buffalo
Buffalo, N. Y.

* Received by the IRE, August 7, 1958. This work is the result of a project sponsored by the Rome Air Dev. Ctr. under Contract No. AF30(602)-1639.

Intermediate Level Correction Factor to *P-N* Junction Forward Current*

When the divergence is taken of the separate hole and electron current densities $J_p = q\mu_p pE - qD_p \text{ grad } p$ and $J_n = q\mu_n nE + qD_n \text{ grad } n$ respectively, the equations

$$\text{div } J_p = q\mu_p(p \text{ div } E + E \cdot \text{grad } p) - qD_p\overline{V}^2 p \quad (1)$$

and

$$\text{div } J_n = q\mu_n(n \text{ div } E + E \cdot \text{grad } n) + qD_n\overline{V}^2 n \quad (2)$$

are obtained. When these equations are combined with

$$\text{div } (J_p + J_n) = 0 \quad (3)$$

which expresses the fact that the total current is solenoidal, div E can be eliminated and the equation

$$p\overline{V}^2 n + n\overline{V}^2 p + \frac{qE}{kT} \cdot (p \text{ grad } n - n \text{ grad } p) = U\left(\frac{D_p p + D_n n}{D_n D_p}\right) \quad (4)$$

where

$$U = -\frac{1}{q} \text{ div } J_p$$

can be obtained.

When determining the diffusion current in the n-region, of a forward-biassed p-n junction diode, Sah, Noyce and Shockley[1] wrote equation (4) as

* Received by the IRE, July 7, 1958.

[1] C. T. Sah, R. N. Noyce and W. Shockley, "Carrier generation and recombination in p-n junctions and p-n junction characteristics," Proc. IRE, vol. 45, pp. 1228–1243; September, 1957.

$$\overline{V}^2 p = U\left(\frac{D_p + D_n}{2D_pD_n}\right) \tag{5}$$

which has already been shown by Hoerni[2] to be valid only at high injection levels. [It is easily seen that (4) reduces to (5), when space charge neutrality is assumed so that

$$\left.\begin{array}{l}\text{grad } p = \text{grad } n \\ \overline{V}^2 p = \overline{V}^2 n\end{array}\right\} \tag{6}$$

and

$$p = n \ (\gg N_d)\,].$$

However, Hoerni does not mention the fact that in writing the low-level form of equation (4) as

$$\overline{V}^2 p = \frac{U}{D_p} \tag{7}$$

the term $-qE/kT$. grad p has been omitted from the left hand-side. This is justified if qE/kT grad $p \ll \overline{V}^2 p$, but it is not obvious and has to be shown.

If the values of E, dp/dx and d^2p/dx^2 at $x=0$ in the solution[1] given by Sah, *et al.*, are examined, the approximation is indeed found to be permissible. Nevertheless this is true only at *very low* levels. By considering the solution when p is of the same order as N_d, it is found that the term involving the field is comparable with the others in equation (4) and so cannot be neglected at intermediate levels.

A. W. Matz
Hivac Ltd.
South Ruislip, Eng.

[2] J. A. Hoerni, "Carrier mobilities at low injection levels," Proc. IRE, vol. 46, p. 502; February, 1958.

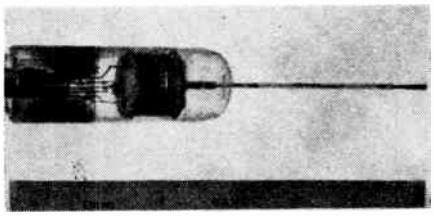

Fig. 1—An outside view of the mm amplifier tube (without metallic coating on the envelope for the helix).

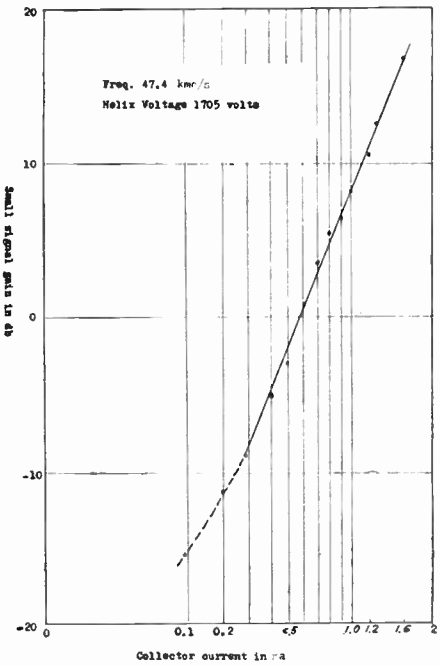

Fig. 2—Small signal gain vs collector current.

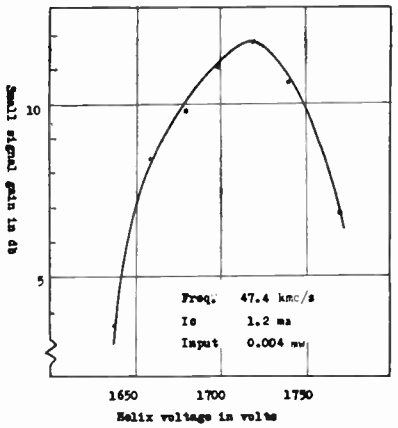

Fig. 3—Measured gain vs helix voltage.

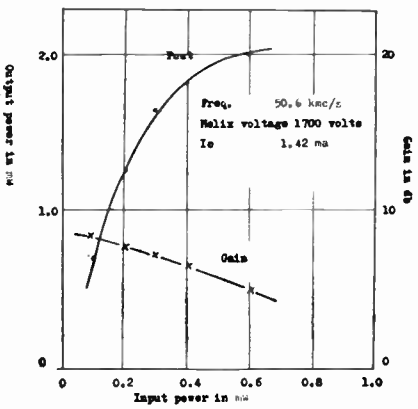

Fig. 4—Output power vs input power.

Helix-Type Traveling-Wave Amplifier for 48 KMC*

In succession to the previous paper[1] which reported on a helix-type traveling-wave tube for 24 kmc (kilomegacycles per second), some results obtained with a tube of the same type designed for 48 kmc band are presented here.

In order to get the maximum gain for a helix-type amplifier at 48 kmc, various dimensions and parameters relating to the helix are taken as shown below:

helix mean diameter	0.45 mm
helix wire diameter	0.05 mm
helix pitch	0.12 mm
helix length	40 mm
beam diameter	0.3 mm

The construction of the tube can be seen in Fig. 1. The helix is supported by four round quartz rods of 0.35 mm diameter and on the inner sides of these rods, graphite is coated for the suppression of oscillation. Both ends of these rods are inserted into the slots of the choke cylinders, which are connected to the antennas of the helix ends.

This construction of helix and quartz rods is supported by the outer glass envelope which was precisely made by a special technique (Japanese Patent No. 476,627) using town-gas flame, a high-frequency concentrator and an exhaust pump. The outer surface of this envelope is coated by a metallic foil, except for both antenna sections of the helix and the outer diameter of the envelope which is 2.0 mm; this length is experimentally decided from the cut-off frequencies of TE_{11} or TM_{01} circular waveguide mode, since the effective dielectric constant including glass envelope, quartz and helix is not known. It was found possible to arrange conditions so that only the helical mode is directly coupled with input and output rectangular waveguide through the envlope.

The tungsten helix is wound at pitch of 0.12 mm on a tensioned high-carbon rod of 0.4 mm diameter. After annealing, the rod is dissolved chemically The maximum error of this pitch is ± 3 per cent. In order to lower the cold-loss of the helix, the helix wire is polished electrolytically with the solution of caustic potash and cyanide potash. The measured cold-loss of the actual helix with supporting quartz rods (but without graphite) is about 30 db; with graphite coated rods the cold-loss is over 40 db.

For the electron gun, conventional Pierce type for parallel beam, with a specially constructed impregnate cathode of 0.3 mm diameter, are used.

The glass envelope around the gun is connected by town-gas flame with that for the helix using a precise jig inserted inside the envelope. As the inner radius of the helix is 0.20 mm and the beam radius is 0.15 mm, there remains maximum tolerance of only 0.05 mm, so the centering accuracy between two envelopes must be kept within ± 0.02 mm all over the length. This accuracy was assured by the measurement using the two-dimensional optical comparator and immersing the connected envelopes into the solvent, such as benzene, ethyl-alcohol, etc., whose dielectric constant is nearly equal to that of glass.

Test of operation was made by an equipment consisting of a QK-294 reflex klystron oscillator modulated at 400 cps, 1N 53 crystal detector and amplifier, standing-wave detector, rotational type attenuators and a bridge type power-meter employing a bolometer. A pole-piece type electromagnet is used for giving a uniform field of about 2700 gauss.

A curve of the measured small signal gain vs collector current (I_c, continuous operation) is shown in Fig. 2. The slope of this curve shows us that the gain is nearly proportional to $I_c^{1/3}$.

A curve of the measured gain vs beam voltage is shown in Fig. 3. The measured output of the continuous operation at the collector current 1.4 ma is given in Fig. 4.

* Received by the IRE, August 15, 1958.

[1] T. Miwa, J. Koyama, M. Mishima, and I. Yanaoka, "Helix-type traveling-wave tube for 24 Gc/s," *Le Vide*, no. 67, pp. 49–52; January–February, 1957.

As shown in the above figures, typical operating data are:

operating voltage	1,710 v
beam transmission efficiency	88 per cent
small signal gain at the collector current of 1.6 ma and input power of 0.004 mw	16.6 db
saturation power at the collector current of 1.4 ma and input power of 0.6 mw	2 mw

T. Miwa
M. Mishima
I. Yanaoka
Hyper-Frequency Res. Sec.
Electrical Communication Lab.
Nippon Telegraph and
Telephone Public Corp.
Musashino-Shi, Tokyo, Japan

Precision Phasemeter for Small Angles*

In conventional phasemeters, bistable circuits or similar devices are employed for the conversion of phase delays to dc voltages. Pulses derived from the positive going zero crossings of one wave are used to shift the bistable device from one equilibrium condition to the other. If, for instance, a so-called flip-flop circuit is employed, the zero crossing from one wave is employed to turn one of the tubes on and the zero crossing from the other wave is used to turn the tube off. The voltage across the load resistor of this tube consists of a series of pulses with a pulse repetition frequency equal to the frequency of the waves and with a pulse width proportional to the phase shift. This phase shift can be determined by measuring the average current of the integrated pulses. Fig. 1 shows the phase shift characteristic of such a device.

Now, if very small phase angles are to be measured, the supply voltages in the instrument have to be kept very stable—a condition which always exists if small dc potentials are to be measured. Besides, a region of uncertainty exists close to phase shift zero so that the instrument can hardly be employed for phase angles smaller than 0.1 degree.

The drawbacks can be avoided by an arrangement as shown in Fig. 2. As in any conventional phasemeter, the two waves A and B are passed through amplifiers G to limiters L and differentiators D. The pulses, however, are fed to the flip-flop through a commutator C. In addition, a delay line π with a phase shift of approximately 180 degrees is inserted ahead of one of the flip-flop tubes. The integrated output voltage, which has the form of a square wave with a frequency equal to the commutator switching rate, is passed to a synchronized rectifier S, driving

* Received by the IRE, July 23, 1958.

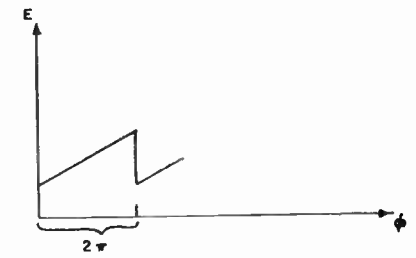

Fig. 1.

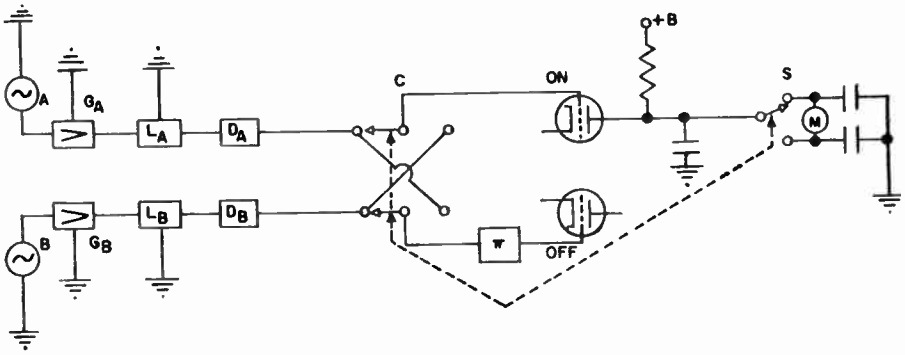

Fig. 2.

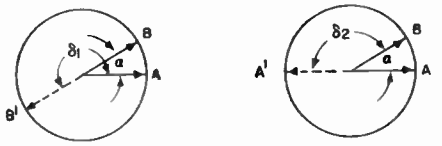

Fig. 3.

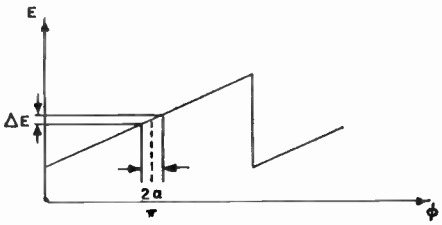

Fig. 4.

meter M. Commutator and synchronous rectifier are shown as mechanical devices—of course, it is possible to employ electronic switches instead.

The polar diagram in Fig. 3 explains the operation of the commutator and of the delay line. Voltage B is delayed behind A by a very small angle α which has to be measured. For the commutator in the left position, an additional phase shift of 180 degrees is introduced for voltage B, so that the integrated flip-flop output voltage corresponds to a delay of $\delta_1 = 180 + \alpha$. For the commutator in the right position, the additional phase shift is introduced for the A voltage so that the integrated voltage corresponds to $\delta_2 = 180 - \alpha$. In the first case, A turns the flip-flop on and B' turns it off. In the second case, B turns it on and A' turns it off. As shown in Fig. 4, the integrated flip-flop output voltage fluctuates at the switching rate by a value ΔE which corresponds to a phase shift of 2α.

Hence, it is only necessary to measure the amplitude of this square wave, and this is best accomplished by the use of a synchronized rectifier S as shown. The dc potentials of the flip-flop circuit are eliminated and noise can be made harmless by a long integration time in the synchronized rectifier.

The phase shift introduced by the delay line is not critical. It is only required that the operating point in Fig. 4 remains on a linear part of the phasemeter characteristic. In its simplest form, the delay line consists of a phase reversal transformer. The instrument has an excellent zero stability because no square wave at all is developed if α becomes zero. Transients produced by the commutator can be eliminated by making the closing time of the synchronized rectifier shorter than the closing time of the commutator.

Experiments showed that, using the new method, it is possible to build phasemeters with a full deflection sensitivity of 0.01 degree. This is important in the communication field and also for radar guidance instruments with high angular resolution.

H. P. Kalmus
A. L. Hedrich
Diamond Ordnance Fuze Labs.
Washington, D. C.

Beam Phasing in a Circular Array of Vertical Antennas*

The theory of steerable-beam antennas is a topic of considerable importance in view of the exponentially increasing rate of exchange of radio information in the civilized world. Due to mechanical limitations, the conventional rotatable Yagi array for high frequencies cannot be used at the medium and longer wavelengths. An interesting possibility for obtaining an azimuthally steerable radiation pattern is in the use of an appropriately phased circular array of uniformly spaced vertical monopoles. Phased-

* Received by the IRE, July 31, 1958.

ring aerial systems have previously been used for other purposes, the first being proposed by Chireix in a paper[1] published in 1936. Later work by Page[2] in 1948 extended the results of Chireix to concentric ring systems without modifying the non-directional azimuth pattern. Additional results were developed in a 1955 publication[3] by Tillman, Patton, Blakely and Schultz, who facilitated a choice between high and low radiation angles but did not elaborate on the omnidirectional azimuth pattern.

This communication concerns the development and mathematical exploration of an equation representing the composite radiation from a circular array of equally spaced isotropic sources whose excitations are phased sinusoidally with their peripheral disposition. The equation is in the form of a series of terms, each of which corresponds to a particular source on the circle. In the limit, as the number of sources increases without bound, the series reduces to Bessel's Integral. Of particular interest is the case in which the number of sources is large but finite. The functional behavior of the radiation equation is studied as the number of sources is varied. The divergence from the Bessel integral is graphically portrayed from numerical calculations.

Consider the circular array of identical, equally-spaced, isotropic sources illustrated in Fig. 1. Let n represent the number of sources, a the radius of the circle, θ the azimuth in the plane of the circle of the field point F from a selected reference diameter, r the radial distance from the center of the circle to F, ϕ_k the angular displacement of the kth source on the circle from the θ reference, ω the angular frequency of excitation, λ the radiation wavelength, α_k the phase lag angle of excitation of the kth source, and t the time. The field strength E at the point F may then be expressed as

$$E = R\sum_{k=1}^{n} I_k \frac{\cos\left(\omega t - \alpha_k - (2\pi/\lambda)\sqrt{r^2 + a^2 - 2ar\cos(\phi_k - \theta)}\right)}{\sqrt{r^2 + a^2 - 2ar\cos(\phi_k - \theta)}} \quad (1)$$

where R represents a radiation-resistance conversion factor for each of the n identical sources.

In the representative term of the above sum the radical may be replaced by r for use in the denominator and by $(r - a\cos(\phi_k - \theta))$ for use in the numerator when the field point is far removed from the circle ($r \gg a$). Then if the excitation currents and phase lag angles satisfy the uniform-amplitude, sinusoidal-phase distributions $I_k = I/N$ and $\alpha_k = (2\pi\alpha/\lambda)\cos\phi_k$ the above sum may be written as

$$E = \frac{RI}{nr}\sum_{k=1}^{n} \cos\left(\omega t - \frac{2\pi a}{\lambda}\cos\phi_k - \frac{2\pi}{\lambda}\left|r - a\cos(\phi_k - \theta)\right|\right). \quad (2)$$

Rearranging the trigonometric terms, letting E_0 represent the ratio RI/r, and substituting $\phi_k = 2\pi k/n$ gives

$$E = \frac{E_0}{n}\sum_{k=1}^{n} \cos\left(\left[\omega t - \frac{2\pi r}{\lambda}\right] + \frac{4\pi a}{\lambda}\sin\frac{\theta}{2}\sin\left[\frac{2\pi k}{n} - \frac{\theta}{2}\right]\right) \quad (3)$$

as the expression for the equatorial field strength induced by a beam-phased circular array of isotropic sources.

The foregoing radiation equation may be studied as a function of the azimuth angle θ in order to determine the beam shape of the radiation pattern. For all cases of practical interest the beam shape is adequately described by evaluating the function at azimuth angles which are integral multiples of half the angle between adjacent sources. The simplification resulting from the restriction that θ is a multiple of π/n is that the field strength is given by the formula

$$E = E_0 g(\theta)\cos\left(\omega t - \frac{2\pi r}{\lambda}\right)$$

where

$$g(\theta) = \frac{1}{n}\sum_{k=1}^{n} \cos\left(\frac{4\pi a}{\lambda}\sin\frac{\theta}{2}\cdot\sin\left[\frac{2\pi k}{n} - \frac{\theta}{2}\right]\right) \quad (4)$$

is the beam-shape function.

For large values of n the beam-shape is well-approximated by the Bessel[4] integral

$$\int_0^1 \cos(z\cos 2\pi u)\,du = J_0(z)$$

where

$$z = (4\pi a/\lambda)\sin\theta/2.$$

Thus

$$\lim_{n\to\infty} g(\theta) = J_0\left(\frac{4\pi a}{\lambda}\sin\frac{\theta}{2}\right) \quad (5)$$

represents the limiting beam-shape function. For intermediate and smaller values of n the beam-shape function $g(\theta)$ diverges from the limiting Bessel-integral form. The nature of this divergence is indicated by the numerical evaluations listed in Table I and the graphical illustrations in Figs. 2 and 3. These results show that for a circle radius of 0.6 λ, the divergence of the beam-shape function from its Bessel integral representation ($n = \infty$) is not serious until the number of radiating elements becomes fewer than 10. Similarly, for a circle of radius 1.6 λ, the divergence is not serious until the number of elements becomes fewer than 24.

TABLE I

BEAM FUNCTION $g(\theta)$ FOR $a = 0.6\ \lambda$

θ degree	$n=6$	$n=8$	$n=10$	$n=16$	$n=\infty$
0	1.00000	1.00000	1.00000	1.00000	1.00000
10	0.89488	0.89484	0.89486	0.89484	0.89491
20	0.61542	0.61523	0.61530	0.61521	0.61522
30	0.25195	0.25190	0.25187	0.25189	0.25195
40	−0.09188	−0.08717	−0.08686	−0.08684	−0.08675
50	−0.34374	−0.31806	−0.31664	−0.31662	−0.31662
60	−0.47569	−0.40464	−0.40189	−0.40198	−0.40198
70	−0.47887	−0.35428	−0.35581	−0.35667	−0.35566
80	−0.34203	−0.20343	−0.22467	−0.22633	−0.22635
90	−0.06518	−0.00941	−0.06486	−0.06485	−0.06489
100	0.30337	0.15354	0.07639	0.08423	0.08413
110	0.65753	0.21928	0.17875	0.19619	0.19614
120	0.87273	0.17435	0.25073	0.26456	0.26454
130	0.86594	0.08120	0.30854	0.29512	0.29510
140	0.64018	0.04475	0.34787	0.29941	0.29939
150	0.28171	0.13590	0.34425	0.28957	0.28958
160	−0.08291	0.33373	0.28831	0.27565	0.27573
170	−0.34325	0.53364	0.21417	0.26478	0.26481
180	−0.43636	0.61736	0.17976	0.26075	0.26075

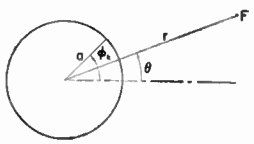

Fig. 1—Antenna and field geometry.

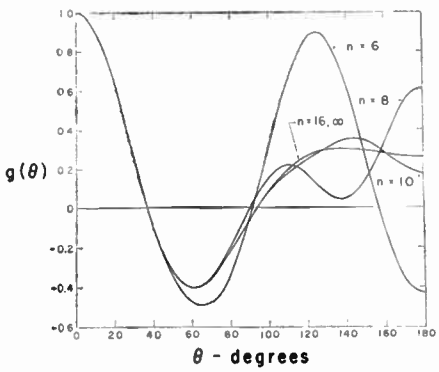

Fig. 2—Beam-shape functions for $a = 0.6\ \lambda$.

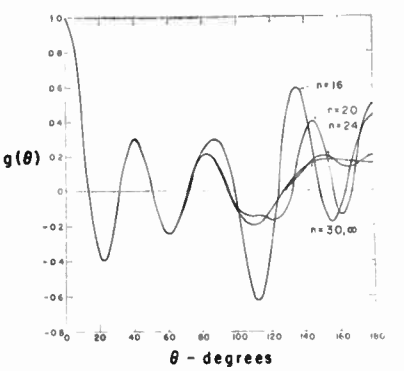

Fig. 3—Beam-shape functions for $a = 1.6\ \lambda$.

[1] H. Chireix, "Antennas à rayonnement zenithal reduit," *L'Onde Electrique*, vol. 15, pp. 440–456; July, 1936.

[2] H. Page, "Ring-aerial systems," *Wireless Engineer*, vol. 25, pp. 308–315; October, 1948.

[3] J. D. Tillman, W. T. Patton, C. E. Blakeley, and F. V. Schultz, "The use of a ring array as a skip range antenna," PROC. IRE, vol. 43, pp. 1655–1660; November, 1955.

[4] R. Courant and D. Hilbert, "Methods of Mathematical Physics," Interscience Publishers, New York, N. Y., vol. 1, 1953.

A simplified formula representing the equatorial field of a beam-phased circular array of equally spaced isotropic antennas has been developed, and the divergence of the actual beam-shape function from the simplified Bessel integral representation has been illustrated. Thus, observing the limitations of the simplified equation, it is possible to explore the fields due to a multiplicity of concentric beam-phased ring aerial systems. Extensions of this theory to specify the field above the plane of the antenna circle can also be made.

The writer wishes to thank Dr. Warren B. Boast, professor and head of the Department of Electrical Engineering, Iowa State College, for his encouragement of this study. The secretarial assistance of Mrs. Shirley Petersen is also gratefully appreciated.

VICTOR W. BOLIE
Dept. of Elec. Eng.
Iowa State Coll.
Ames, Ia.

Average Power of Impulsive Atmospheric Radio Noise*

The object of this letter is to provide an addendum to the papers on atmospheric noise interference to short and medium wave broadcasting.[1,2] Measured and estimated values of noise obtained by following the procedure described in the papers are directly useful for one service only, *viz.*, broadcasting. A method is described here to convert such data into forms useful for other services also.

During peak activity, the mechanism of radiation from tropical thunderstorms responsible for noise in the frequency range, 0.23–20 mc, appears to be as follows. A step in a leader stroke radiates an impulse. A train of such impulses arises from a stroke. A complete flash radiates as many such trains of impulses as there are stepped leaders. These facts are expected to form the basis for any analysis of the interfering effect of the noise to any service. Therefore, either the noise-field strength arising from a stroke or the noise-field strength from a complete flash will be required in the actual calculations. A generalized form of presentation of noise data is in terms of average power. In the particular case, the actual averaging has to be done for a) noise received from a stroke, and b) noise received from a complete flash. Now, suppose

E_s = rms noise-field strength corresponding to the average noise power received from a stroke, and

E_f = rms noise-field strength corresponding to the average noise power received from a complete flash.

Then, E_s and E_f are both scientifically justifiable generalized forms of expressing atmospheric radio noise. It is reasonable to suppose that they are likely to prove useful in analyzing the interfering effect of atmospheric radio noise to the different services. In the papers mentioned,[1,2] the quantity that is measured or estimated is E, the noise-field strength which is a measure of the interfering effect of atmospheric noise to broadcasting. The noise data given in terms of E can be converted to the corresponding data in terms of E_s or E_f. The necessary equations for the short and medium wave bands are given below.

For the Short-Wave Band, Viz., 2.5–20 Mc

From (7) and (9) in Aiya[1], it follows that

$$E_s = \frac{E_1}{\sqrt{2}} = \frac{E}{(1.414)\cdot(0.32)\cdot(0.85)} = (2.6)\cdot E. \quad (1)$$

In this band, noise arises from a flash which lasts 200 milliseconds and the flash has four stepped leaders, each of one millisecond duration. Therefore,

$$E_f = E_s\cdot\sqrt{4/200} = (0.37)\cdot E. \quad (2)$$

For the Medium Wave Band, Viz., 0.23–2.5 Mc

From (9) and (11) of Aiya[2], it follows that

$$E_s = \frac{E_1}{\sqrt{2}} = \frac{E}{(1.414)\cdot(0.19)\cdot(0.85)} = (4.4)\cdot E. \quad (3)$$

In this band, noise arises from a flash which lasts 200 milliseconds and the flash has mainly one stepped leader radiating for 2.1 milliseconds. Therefore,

$$E_f = E_s\cdot\sqrt{2.1/200} = (0.45)\cdot E. \quad (4)$$

The square root appears in (2) and (4) because we are averaging power.

A flash lasts 0.2 second. Suppose about 300 flashes follow each other successively for a minute and they contribute the same noise power at the place of observation. Then, the rms noise-field strength corresponding to a time average of received power, *i.e.*, averaging for a specific time like one minute, five minutes, etc., would be identical with E_f. Such a condition is approximately realized in Poona for distant source sky-wave noise at high frequencies.

Suppose we assume that conditions described in the last paragraph are approximately valid for all cases of received noise, and estimate noise levels on the basis of a time average of power. Then, it follows that we are attempting to estimate E_f. The extent to which the measured values would differ from the estimates would depend on the actual number of flashes contributing noise and on the variation in the noise power contributed from flash to flash. It would not be surprising if the measured values at a place differ from the estimates by factors up to ± 20 db.

Any attempt to evaluate E_f experimentally by a measurement corresponding to a time average of power is subject to the limitations indicated in the last paragraph. Further, it will include the average of noises arising from unwanted sources. Hence, it appears that the proper procedure for measuring E_f would be by measuring E and then deducing E_f by using (2) or (4).

When certain types of thunderstorms are building up, the noise received consists of a form of continuous noise on which are superposed impulses, bursts, etc. It is not improbable that atmospheric noise is received in this form quite often at certain places along certain latitudes. This problem is now under investigation.

S. V. CHANDRASHEKHAR AIYA
College of Engineering
Poona 5, India

* Received by the IRE, September 24, 1958.

[1] S. V. C. Aiya, "Atmospheric noise interference to short-wave broadcasting," PROC. IRE, vol. 46, pp. 580–589; March, 1958.

[2] S. V. C. Aiya, "Atmospheric noise interference to medium-wave broadcasting," PROC. IRE, vol. 46, pp. 1502–1509; August, 1958.

Efficiency of Frequency Measurements with an Atomic Clock*

Information theory can be used in measuring the efficiency with which a measurement (*e.g.*, of time) is taken. The method is related to the way in which the efficiency of a thermal engine is gauged by the second law of thermodynamics.

Brillouin[1] has shown that, if ΔS is the entropy increase in a measurement, and ΔI is the information gained by it, the following inequality holds:

$$\frac{\Delta I}{\Delta S} = \mathcal{E} \leq 1. \quad (1)$$

$\mathcal{E}$ is, therefore, a measure of the efficiency of an experiment in which an amount of entropy is traded for information. It turns out that for measurements such as frequency determination, we have

$$\Delta I = k \ln A. \quad (2)$$

Here, A, the accuracy of the experiment, is given by the interval in which we suspect the value to be, divided by the error left after the measurement has been performed. The reliability R is inversely proportional to the probability, P, that our measurement was false, since a spurious thermal-noise signal was mistaken for the signal. In a more accurate treatment R would appear in (2). This is the case, for example, in Woodward's treatment of radar measurements.[2] His exact treatment bears out the fact that, down to rather low $R(R \approx 2)$, (2) is essentially correct.

A high-efficiency frequency measurement can be carried out in the following manner. We build a lossless interaction space and place molecules in it that are ready to absorb the radiation of a frequency, $\omega_0 \pm \frac{1}{2}\Delta\omega$. All we know *a priori* is that $\omega_a < \omega_0 < \omega_b$. The interval (ω_a, ω_b) is now divided into n cells of width $\Delta\omega$. The measurement is carried out by sending a certain amount of radiation

* Received by the IRE, August 21, 1958. This work was supported in part by the U. S. Army Signal Corps, the U. S. Air Force Office of Scientific Research, Air Research and Development Command, and the U. S. Navy Office of Naval Research.

[1] L. Brillouin, "Science and Information Theory," Academic Press, Inc., New York, N. Y.; 1956.

[2] P. M. Woodward, "Probability and Information Theory, with Applications to Radar," McGraw-Hill Book Co., Inc., New York, N. Y.; 1953.

into the interaction space at each different frequency. The radiation will then be reflected back; therefore no energy has been used except at the resonant frequency at which the energy will be absorbed. Brillouin shows that the amount of energy that will be spent for a measurement of accuracy $A=n$ and reliability R is $\Delta E=kT\times\ln nR$. Thus, we find that our spectroscope operates with an efficiency

$$\mathcal{E}=\frac{\ln A}{\ln (nR)}=1\Big/\left(1+\frac{\ln R}{\ln n}\right). \quad (3)$$

This measurement would be hard to realize in its present form. Recovery of the energy, for example, would be difficult. We might imagine, say, that the power bounces back from the interaction space and is reflected from a moving wall and thus has a Doppler-shift frequency. But it is more practical to analyze an existing apparatus, such as the maser oscillator.[3] During the minimum response time of the maser, $\tau\approx 10^{-4}$ sec, we obtain a relative error $(\langle\Delta\omega_A^2\rangle)^{1/2}/\omega=10^{-10}$. If we divide the cavity Q by this number [the cavity passband represents our *a priori* interval (ω_b, ω_a)], we obtain $A=10^6$. The amount of entropy produced is given by $\Delta S=(P_0\times\tau)/T=300\ k$, with $P_0=nh\nu=1.4\times10^{-13}$ watt. Thus we obtain an efficiency $\mathcal{E}=0.01$. Our experiment is, therefore, very efficient. Why is it, nevertheless, not of optimum efficiency? Note that the wave train of 10^{-4}-sec duration has a "natural spectral width" $\Delta\omega_n\approx 2/\tau=2\times10^4$ cps. Our accuracy corresponds to a measurement with an error that is 1600 times smaller than $\Delta\omega_n/\omega_0$. This is possible since, in our experiment, the voltage signal-to-noise ratio r is large.[4] This allows us to decrease the statistical error of our measurement by a process that is analogous to repeating the measurement many times and taking the average result. (Systematic errors, however, will not be decreased.) But in this process a lot of redundant information is obtained, and it would have been more efficient to design the experiment from the outset so that it would give the result with the desired accuracy without averaging over many measurements.

In our case, if we want to obtain an atomic clock of nearly optimum efficiency, we must design a spectroscope with a sufficiently narrow natural spectral width.

Eq. (3) also illustrates the fact that an optimum design calls for a sacrifice in reliability. In an optimum-design experiment the phenomenon to be observed is not too well distinguished from the noise background. Thus it often happens that great difficulties are encountered in realizing an experiment designed for optimum precision.

MARTIN PETER†
M. W. P. STRANDBERG
Dept. of Phys.
and Res. Lab. of Electronics
Mass. Inst. Tech.
Cambridge, Mass.

[3] K. Shimoda, T. C. Wang, and C. H. Townes, "Further aspects of the theory of the maser," *Phys. Rev.*, vol. 102, p. 1308; June 1, 1956.

[4] M. W. P. Strandberg, H. R. Johnson, and J. R. Eshbach, "Apparatus for microwave spectroscopy," *Rev. Sci. Instr.*, vol. 25, p. 776; August, 1954.

† Now at Bell Telephone Labs., Inc., Murray Hill, N. J.

The Asymptotic Behavior of Ideal *M*-ary Systems*

Reiger's recent note,[1] which contains results on error probabilities for M-ary frequency-shift-keyed systems, calls to mind some closely related results I have obtained sporadically over the past five years; these are concerned with the asymptotic behavior of so-called ideal M-ary systems for large values of M.

In the type of system under consideration, one of M equiprobable, equi-energy, pairwise uncorrelated,[2] narrow-band waveforms is transmitted during each transmission interval into a channel which is disturbed solely by stationary, white, additive, Gaussian noise. On reception, the noisy received signal is passed into a parallel bank of M matched filters, one for each of the possible transmitted waveforms. The filter outputs are envelope detected, and these envelopes are sampled at the end of the reception interval. The waveform corresponding to the largest of these samples is then guessed by the receiver to have been the one transmitted. This system may be termed ideal in the following sense: the set of operations by which the receiver arrives at its guess is the one which, in the absence of subsequent error detection and/or correction information, affords the smallest possible probability of error for a noncoherent receiver.

The purpose of the present communication is to show that the system is ideal in the Shannon sense also; that is, for any given data rate less than the channel capacity, one can make the error probability as small as desired by choosing a large enough value of M.

To see this, let us first write down an expression for the information rate in natural logarithmic units (nits/sec):

$$H'=\frac{\ln M}{T}. \quad (1)$$

Here T is the length of each transmission interval, during which one of the M possible waveforms is sent.

Next, we set down the expression for the probability of error, P_e. In Reiger's notation:[3]

$$P_e=1-\int_{-\infty}^{\infty}p(y)\left[1-e^{-y^2/2}\right]^{M-1}dy \quad (2)$$

where

$$p(y)=\begin{cases}ye^{-(y^2+2\beta)/2}I_0(y\sqrt{2\beta}), & y\geq 0\\ 0 & y<0\end{cases} \quad (3)$$

and

$$\beta=\frac{E}{N_0}=\frac{PT}{N_0}. \quad (4)$$

E is the (common) energy of the M waveforms, P is the average transmitter power, and N_0 is the (single-ended) noise power density.

Now, it is easy to see either from (2) or from Reiger's (9) that for any finite M we can make $P_e\to 0$ by letting $T\to\infty$. However, note also that under these conditions the data rate, (1) goes to zero. What we really want to show is that under certain conditions we can make $P_e\to 0$ and still maintain a given nonzero H' by letting $M\to\infty$ and $T\to\infty$ together.

First, it will be convenient to make the change of variable $z=y-\sqrt{2\beta}$ in (2). Doing this, and noting from (1) and (4) that

$$\beta=\frac{P\ln M}{N_0H'}=\frac{\ln M}{r} \quad (5)$$

where we have set

$$r=\frac{N_0H'}{P} \quad (6)$$

we have

$$P_e=1-\int_{-\infty}^{\infty}p\left(z+\sqrt{\frac{2\ln M}{r}}\right)\left\{1-\exp\left[-\frac{1}{2}\left(z+\sqrt{\frac{2\ln M}{r}}\right)^2\right]\right\}^{M-1}dz. \quad (7)$$

In taking the limit of (7) as $M\to\infty$, we change the order of limiting and integration,[4] and note that for finite z

$$\begin{aligned}&\lim_{M\to\infty}\cdot\left\{1-\exp\left[-\frac{1}{2}\left(z+\sqrt{\frac{2\ln M}{r}}\right)^2\right]\right\}^{M-1}\\ &=\lim_{M\to\infty}\exp\left\{-M\exp\left[-\frac{\ln M}{r}\right]\right\}\\ &=\lim_{M\to\infty}\exp\left[-M^{(1-1/r)}\right]\\ &=\begin{cases}1 \text{ for } 0<r<1.\\ 0 \text{ for } r>1\end{cases}\end{aligned} \quad (8)$$

Further, we note that

$$p\left(z+\sqrt{\frac{2\ln M}{r}}\right)$$

tends toward a Gaussian distribution with zero mean and unity variance as $M\to\infty$,[5] so for infinite $|z|$ we have

$$\lim_{M\to\infty}p\left(z+\sqrt{\frac{2\ln M}{r}}\right)=0.$$

Using this result and (8) in (7), we have then

$$\lim_{M\to\infty}P_e=\begin{cases}0 \text{ for } 0<r<1.\\ 1 \text{ for } r>1\end{cases} \quad (9)$$

In order to give physical meaning to the parameter r, we refer to Shannon's channel

* Received by the IRE, August 22, 1958. This work was completed in two parts: the first at Lincoln Laboratory, M.I.T., Lexington, Mass., with the joint support of the U. S. Army, Navy, and Air Force; and the second at Hughes Aircraft Co., Culver City, Calif.

[1] S. Reiger, "Error rates in data transmission," PROC. IRE, vol. 46, pp. 919–920; May, 1958.

[2] The waveforms are pairwise uncorrelated in the sense meant here when the complex numbers $\int_0^T X_n(f)X_m^*(f)df$ are zero for all $m\neq n$, where $X_i(f)$ is the voltage-density spectrum of the ith waveform. These conditions are clearly met for any set of waveforms with nonoverlapping spectra. They are also satisfied in some special cases of overlapping spectra such as that of a set of rectangular sine wave pulses, all of duration T, the frequencies of which are separated by integral multiples of $1/T$. For further details see G. L. Turin, "Error probabilities for binary symmetric ideal reception through nonselective slow fading and noise," PROC. IRE, vol. 46, pp. 1603–1619; September, 1958.

[3] S. Reiger, *op. cit.* Note that (2) holds for any set of equiprobable, equi-energy, uncorrelated, narrow-band waveforms, Reiger's set of sine wave pulses being a special case.

[4] E. C. Titchmarsh, "The Theory of Functions," 2nd ed., Cambridge Univ. Press, p. 395; 1948.

[5] S. O. Rice, "Mathematical analysis of random noise," *Bell Sys. Tech. J.*, vol. 23, pp. 282–333; July, 1944, and vol. 24, pp. 46–157; January, 1945. See sec. 3.10.

capacity theorem for a Gaussian white noisy channel.[6] This says that the maximum rate of information transmission which can be attained with arbitrarily small error probability is, in natural logarithmic units,

$$C = W \ln\left(1 + \frac{P}{WN_0}\right) \tag{10}$$

where W is the channel bandwidth. Note that

$$C \leq \frac{P}{N_0} \tag{11}$$

so from (6) we have

$$r \leq \frac{H'}{C}. \tag{12}$$

Now, (9) tells us that we can make $P_e \to 0$ for $r = 1 - \epsilon$, where ϵ is any positive number less than unity. Further, from Shannon's theorem we know we must have $H' \leq C$ in order to be able to make $P_e \to 0$. Thus we can make $P_e \to 0$ for

$$1 - \epsilon \leq \frac{H'}{C} \leq 1 \tag{13}$$

for any $0 < \epsilon < 1$. That is, the system we have considered is asymptotically capable of error-free operation at any rate up to the theoretically maximum error-free rate: in the limit $M \to \infty$, $\ln M$ nits of information can be transmitted with no error in $T = (\ln M)/H'$ seconds when $H' < C$.

We may note two features of this asymptotic behavior. First, the bandwidth, W, of the system is, in the limit, infinite; this follows from the fact that the minimum bandwidth necessary to obtain M uncorrelated waveforms of duration $(\ln M)/H'$ is roughly $(H'/2)(M/\ln M)$, which becomes infinite as $M \to \infty$. Second, in the limit we have $T \to \infty$, so there is an infinitely long delay before the receiver makes its M-ary decision, at which time $\ln M$ nits of information become available all at once. On the other hand, one could maintain a finite bandwidth and obtain information gradually by sending the $\ln M$ nits as a *sequence* of, say, binary transmissions, with the receiver making a binary decision after *each* binary transmission. But this cannot be done without error; in fact, the probability that there will be an error in the reception of the $\ln M$ nits in this case approaches unity as $M \to \infty$ for *any* information rate, a markedly different asymptotic behavior from that of the M-ary system.

Since it is obviously impossible actually to obtain the asymptotic M-ary system behavior expressed by (9), it is of interest to determine how fast this behavior is approached for finite M (and hence finite T and W). The expression for P_e obtained from an evaluation of (2) is, using (6),[7]

$$P_e = \frac{1}{M^{(r+1)/r}} \sum_{k=2}^{M} (-1)^k \binom{M}{k} M^{1/kr}. \tag{14}$$

Curves of P_e vs $r^{-1} = P/H'N_0$ are shown in Fig. 1 for $M = 2, 4, 8, 16, 32, 64, 128$. We see from these that the system already exhibits

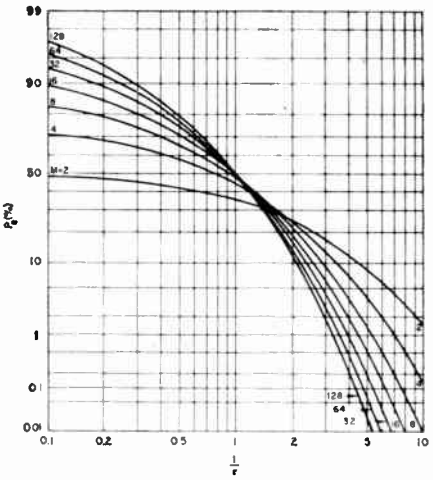

Fig. 1

the crossover behavior at $r = 1$ predicted by (9) for M greater than about 16.

As a final point it may be mentioned that the convergence of P_e to zero as $M \to \infty$ for any $H'/C < 1$ holds also for a system which utilizes coherent detection, since the error probability for coherent detection is bounded from above by that for noncoherent or envelope detection.[8]

I am indebted to the Mathematics Section, Systems Analysis Laboratory, Hughes Aircraft Company, and in particular to Virginia Stewart, for computing the curves of Fig. 1.

G. L. Turin
Hughes Res. Labs.
Culver City, Calif.

[8] This result for coherent detection can also be inferred from a generalization of an argument given by M. J. E. Golay, "Note on the theoretical efficiency of information reception with PPM," Proc. IRE, vol. 37, p. 1031; September, 1949. Golay shows that for N-position quantized PPM transmission with coherent detection and threshold decision circuits, $P_e \to 0$ as $N \to \infty$, provided that $H' < C$. Since this behavior holds for Golay's system which employs nonideal threshold decision, it must hold true *a fortiori* for the ideal system discussed here. The author wishes to thank Dr. R. Price for calling to his attention Golay's note.

Synchronous Magnetic Recorder and Delayed Feedback*

It interests me very much to note the paper by Hideo Saki on "Some studies on delayed feedback circuits"[1] with applications to signal to noise ratio (SNR) improvement, especially his remarks regarding the proposed application of magnetic recording; such a device for improving SNR, called the "synchronous magnetic recorder" (SMR), was made by me eight years ago[2] as has been followed by further work.[3]

The SMR utilizes the general principle of delayed feedback and is capable of performing many of the functions listed by Saki in in his paper. The instrument was originally intended for extracting weak nuclear magnetic resonance signals from noise. A number of systems for improving SNR have been set up by various investigators, and of these the SMR seems to be the earliest.

Essentially the SMR consists of a magnetic drum rotating synchronously with the signal; the signal, immersed in noise, is recorded in a close helix and reproduced by means of a long pick-up head, thus adding a large number of signals suitably delayed with respect to one another.

Details of the frequency characteristics, particularly its comb-like nature, are given in the above mentioned paper. I understand that the system is now being used to find the nature of nervous signals and is very much more flexible in operation than the system of synchronously commutated capacitors described by Le Page, Cahn and Brown,[4] Beard and Skomal,[5] and also by Dawson.[6]

A variety of continuously usable systems have also been designed. In addition to the delayed feedback inherent in the original SMR, additional feedback loops have been investigated with a view to getting purity in recording of sine waves, etc. Although in the electrical analogue of the delayed feedback system, loop gain has to be limited to prevent oscillations, etc., and there is an upper limit to the SNR improvement, the SMR is of variable Q and there is no such limit.

As a circuit element, it behaves as one with infinitely variable Q. (There is no loss of information once it is stored, so its effective Q may be treated as infinite. Information stored/lost per cycle $= Q$.) The two important innovations made in the SMR are use of a long pick up head and synchronization of signals with rotations. It was also realized that signal shapes will not be distorted. The signal power not only in the fundamental but also in the harmonics is utilized to full advantage. Because of the peculiar nature of the SMR, increase in SNR can be made very large. Thus the SNR improvement is not limited to 7.66 db. Full details and photographs illustrating the large SNR improvement obtained are given in my paper. It was also found that the noise-accompanying signal also acts as a suitable supersonic bias for magnetic recording.

One system for the employment of SMR principle in practice for signals received continuously is given in Fig. 1. This consists of a drum of special shape and rotating arm having three or four equally spaced recording heads. The pick up head covers the entire arc of the drum. Thus a certain definite part of the signal is integrated and the SNR improvement is dependent upon the length of time for which recording takes place. Many other types of mechanical and

* Received by the IRE, September 2, 1958.

[1] H. Seki, "Some studies on delayed feedback circuits," Proc. IRE, vol. 46, pp. 758–763; April, 1958.

[2] G. Suryan, "A new method of extracting weak nuclear magnetic resonance signals from noise," *Phys. Rev.*, vol. 80, p. 119; 1950.

[3] G. Suryan, "Synchronous magnetic recorder and its applications, Parts I and II," *J. Ind. Inst. Sci.*, vol. 35A, pp. 193 and 205.

[4] W. R. Le Page, C. R. Cahn and J. S. Brown, "Analysis of a comb filter using synchronously commutated capacitors," *Trans. AIEE*, vol. 72, pp. 63 68; March, 1953.

[5] C. I. Beard and E. N. Skomal, "RC memory commutator for signal to noise improvement," *Rev. Sci. Instr.*, vol. 24, pp. 276–280; 1953.

[6] G. D. Dawson, "A summation technique for the detection of small evoked potentials," *EEG Clin. Neurophysiol.*, vol. 6, pp. 65 84; 1954.

[6] C. E. Shannon, "The Mathematical Theory of Communication," Univ. of Illinois Press, Urbana, Ill., p. 67; 1949.

[7] Cf., *e.g.*, S. Reiger, *op. cit.*, (9).

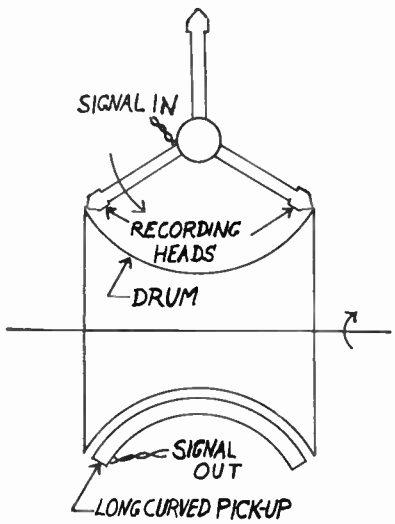

Fig. 1—Schematic diagram of continuously operable SMR. Note that all recording heads are excited by the same signal and that one recording head takes over as another leaves. Signals have to be in synchronism with drum rotation.

electrical layouts suitable for this purpose have been designed.

In addition to the feedback inherent in SNR, the effect of other feedback loops on recording and reproducing of waveforms have been investigated and further details will be published in due course.

My thanks are due to Professor R. S. Krishnan for his kind support of these investigations.

G. Suryan
Department of Physics
Indian Inst. of Sci.
Bangalore, India

Crossed Cylindrical Lens High Transconductance Gun*

A high transconductance gun, that is, a gun of high sensitivity, is described having a slit aperture in the control grid instead of the circular aperture used in conventional guns. No close spacings between cathode and control grid are required as in some other high transconductance guns. While modulating the cathode current, the variation of the accelerating field penetrating through the control grid aperture toward the cathode (in a plane perpendicular to the long axis of the slit) is of the same order as in the case of a circular aperture. For the same accelerating field at the cathode, a higher current flows in the case of a slit aperture, since electrons are drawn from a larger cathode area. Thus, an increased transconductance is obtained.

A line type crossover is formed. In order to obtain a circular spot on the screen, a cylindrical lens is introduced which is oriented perpendicularly to the cylindrical immersion lens formed by the slit aperture in the control grid. (It should be explained here that by cylindrical lenses are meant lenses which focus only in one direction, perpendicular to the lens axis.) A "lipped" cylindrical lens of the type described by Klemperer[1] was used. For final beam focusing on the tube screen, a conventional focusing lens with axial symmetry is used; in this particular case, a magnetic lens was employed.

The resolution of this type of gun increases with increasing transconductance, contrary to the situation in most other high transconductance guns. The reason for this is that the transconductance is determined by the ratio of width to length of the slit aperture in the control grid. When narrowing the slit, the transconductance increases while the spot size, determined by the width of the crossover, decreases. A further improvement in spot size results from reduced space charge repulsion.

Two types of undesirable ellipticity may be introduced during tube operation: deflection and modulation ellipticity. Deflection ellipticity occurs when the radius of the screen differs from the distance of the screen center to the plane of the deflection. This type of ellipticity can be overcome either by dynamic controls or by use of a system with a high depth of focus. Modulation ellipticity may be introduced because the crossover moves during modulation. To overcome this type of ellipticity, a crossed cylindrical lens system of good depth of focus was employed.

The experimental gun was of the triode type. The slit aperture in the control grid was 0.011 to 0.012 inch wide and about 0.120 inch long. The cathode-to-control grid distance was 0.005 inch with the cathode cold, a similar spacing as in conventional guns.

The characteristic of the gun is shown in Fig. 1. For 500 μa screen current, a drive voltage of about 8.5 volts was required. At 12 volts drive, 850 μa screen current was obtained. The current increases with the second power of drive voltage because the emitting area increases only in a single direction whereas, in a conventional gun where the 5/2 power law holds, the emitting area increases radially.

Resolution readings were taken with the Indian head resolution pattern. The maximum screen currents were determined at which the raster line structure in the focused resolution pattern became difficult to distinguish, *i.e.*, the resolution was considerably above 500×500 lines. At 7.3 kv screen voltage, this resulted at 500 μa screen current; at 10 kv, at 920 μa. Spot observations did not show any introduction of ellipticity during modulation. Traces of the pulsed beam on the screen at different currents are shown in Fig. 2. For large deflection angles, dynamic ellipticity and dynamic focusing control were required. The peak cathode loading in this type of gun is only about ⅓ of that in a conventional gun with an 0.025 inch diameter aperture in the control grid.

The experiments showed that a high resolution high transconductance gun can be built with relatively simple means. No close cathode-to-control grid spacings are required. A higher transconductance and higher resolution than in the experimental tube can be achieved without excessive cathode loading.

P. H. Gleichauf
General Electric Co.
Syracuse, N. Y.

* Received by the IRE, September 25, 1958.

[1] O. Klemperer, British Patent No. 574,056; December 19, 1945. Also see "Electron Optics," Cambridge University Press, Cambridge, Eng., pp. 295–300; 1953.

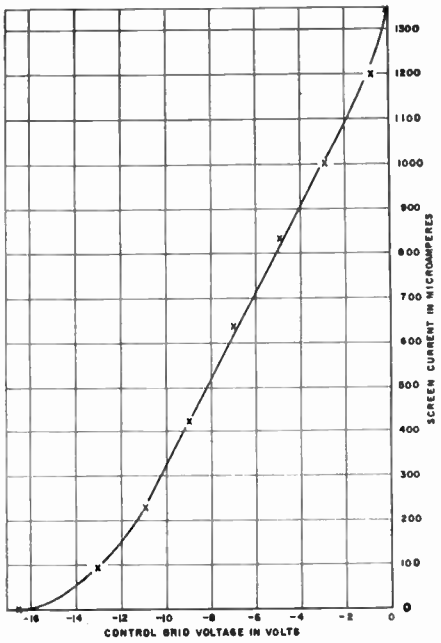

Fig. 1—Characteristics of crossed cylindrical lens high transconductance gun.

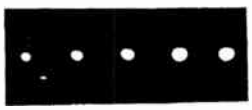

Fig. 2—Traces of pulsed beam on screen at 25, 50, 125, 500, and 1000 microamperes, respectively.

Observation of Transient Responses in RF Delay Lines, Filters, and Resonant Circuits*

As is well known, the sudden closing of a circuit containing a generator leads to a response which is the sum of the steady state solution and a transient. The transient is often the more important, and its proper evaluation must be made without the steady state term. Sabin[1] recently discussed theoretically and experimentally the use of pulsed oscillations to evaluate the transient response of transducers at low frequencies (≈40 kc). Essentially he used a sonar bridge to balance out the steady state response and leave only the transient.

* Received by the IRE, August 4, 1958.

[1] G. A. Sabin, "New technique for measuring transducer blocked impedance," *J. Acoustic Soc. of America*, v. 30, February, 1958.

The purpose of this note is to call attention to his method and extend the application to the megacycle region for RF delay lines, filters, and resonant circuits. In the former case it may be used directly to measure delay time. At these frequencies, an RF bridge may be used, but it should first be checked to ensure that the transient response of the bridge is negligible. However an alternate method was used.

The essential equipment consisted of a pulsed oscillator, such as the AUL PG-650, which has a balanced output, phase stability, and low harmonic distortion; a constant impedance 180 degree phase reversing switch; a calibrated attenuator; and a calibrated phase shifting network.[2] The fineness of control of the latter two will depend on the accuracy desired. The PG-650 has an available output of over 300 volts peak to peak into 93 ohms, which is sufficient to display the responses directly on a CRO. Under certain circumstances an amplifier is needed. The AUL WA-600 amplifier with 60 mc bandwidth and outputs either from the RF stage or a full-wave detector was used satisfactorily.

The equipment was set up as in Fig. 1. Where the test unit is of a different impedance than the attenuator, it may be necessary to add matching networks at each termination

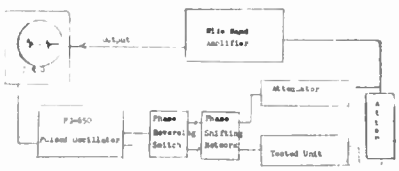

Fig. 1.

The pulser is set at the frequency of interest with a pulse length considerably longer than the transients. The attenuators are set to give equal amplitudes in each channel and then the phase adjusted to give complete cancellation at some point within the pulse. The attenuator and phase settings give the resistance and reactance of the transient impedance at that time. Figs. 2–8 illustrate the results.

The first series were taken at 6.6 mc with a 5.0 μsec pulse on an Advance Electronics variable delay line (Type 302) set at .32 μsec delay, but not properly terminated. Fig. 2 shows the pulse alone, and Fig. 3 the delayed pulse alone, with both transient and steady condition. Fig. 4 shows the transient residue after balancing out the steady state current and Fig. 5 the effect of reversing phase in one channel to double the CWRF signal. Note the nearly idential transients at the beginning and end of the pulse in Fig. 3.

The second series was taken at 9.1 mc with a delay of 0.55 μsec. Fig. 6 shows the input pulse alone and Fig. 7 the transient residues when the steady state current was balanced out after several microseconds. Due to the increase in frequency and delay time, several distinct reflections are evident. By adding 8 db attenuation, it was possible

Fig. 2—Direct pulse, 6.6 mc; delay, 0.5 μsec.

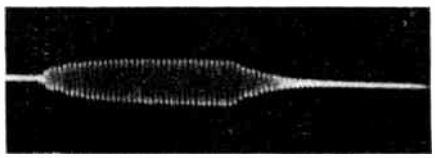

Fig. 3.—Delayed pulse, 6.6 mc; delay, 0.5 μsec.

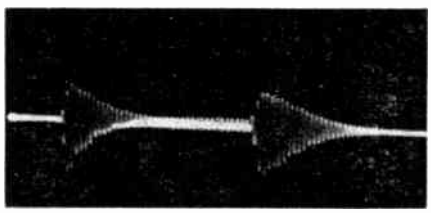

Fig. 4—Cancelled CW, 6.6 mc; delay, 0.5 μsec.

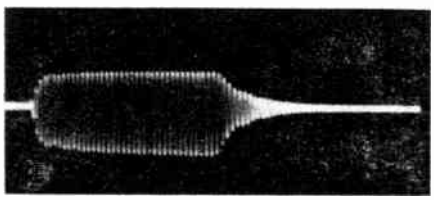

Fig. 5—Combined pulses, 6.6 mc; delay, 0.5, μsec.

Fig. 6—Direct pulse, 9.1 mc; delay, 0.55 μsec.

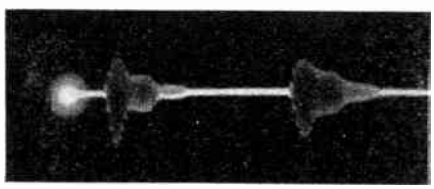

Fig. 7—Transient response, 9.1 mc; delay, 0.55 μsec.

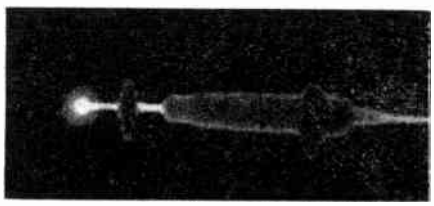

Fig. 8—Cancellation of first reflection, 9.1 mc; delay, 0.55 μsec.

to cancel the first echo entirely, as in Fig. 8, and get an exact measure of the delay time by counting the RF cycles in the first portion, where only the pulse traveling through the attenuator is received.

A great deal of difficulty may be experienced in getting a calibrated phase shifting network with a wide range and fine adjustment at the RF frequencies used. This may be avoided by using two pulsed oscillators triggered from the same source but having independent frequency, pulse length, and trigger delay controls; the transient condition can be cancelled out at any point as well as the CW part. If this is done at the end of the pulse, the transient frequency and phase may be obtained.

David L. Arenberg
Arenberg Ultrasonic Lab., Inc.
Boston, Mass.

[2] Arenberg Ultrasonic Laboratory Bulletin UE5(58); July, 1958.

Speed vs Circuit Power Dissipation in Flip-Flops*

The problem of determining the minimum power that may be dissipated by a transistor flip-flop, covering a set of given stability specifications, is one of general interest. Among the various significant considerations which determine the power level are: output power requirements, stability, temperature variations, and required speed of operation. An investigation illustrating the speed limitations as a function of circuit power dissipations is described below.

The circuits investigated are the emitter-coupled and the clamped base-return flip-flops illustrated in Figs. 1 and 2. These configurations are widely used and may be considered representative of transistor flip-flop designs.

The circuits employ silicon transistors to insure good temperature stability, and are based upon a design with specified dc stability with a specified constant collector output voltage swing of 2 volts.[1,2] The power dissipation, P_d, of each flip-flop is made a variable parameter by varying the current swing, ΔI_L, through the load resistor R_L. Experimentally it is found that P_d is approximately 15 milliwatts per ma of load current swing in both the emitter-coupled and base-return flip-flops. The flip-flops are triggered by turn-off trigger pulses applied through a suitable gating circuit to the base of the conducting transistor.

Essentially, the speed of operation of the flip-flops is limited by two parameters:

1) The time constant, T_f, associated with the collector current response
2) The time, T_K, required for the coupling capacitor C_K to recover after each change of state in the flip-flop.

The collector time constant T_f is related to the collector capacity and the effective load resistor, R_L', and therefore to the level of circuit power dissipation P_d, and is calculated from:[3]

* Received by the IRE, September 8, 1958.

[1] J. J. Suran, "Design of junction transistor flip-flops by driving-point impedance methods," 1957 IRE National Convention Record, pt. 2, pp. 142–147.

[2] J. J. Suran, "Transistor monostable multivibrators for pulse generation," Proc. IRE, vol. 46, pp. 1260–1271; June, 1958.

[3] J. W. Easley, "The effect of collector capacity on the transient response of junction transistors," IRE Trans. on Electron Devices, vol. ED-4, pp. 6–14; January, 1957.

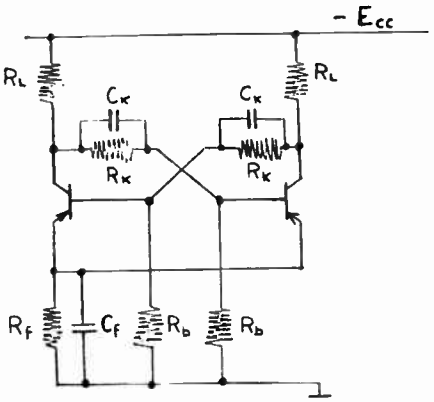

Fig. 1—Emitter-coupled flip-flop.

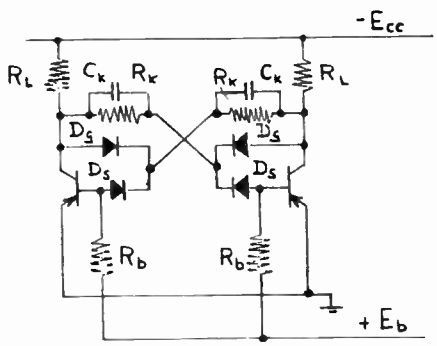

Fig. 2—Base-return flip-flop.

passed through the coupling networks. Measurements of flip-flops covering a wide range of circuit power dissipation values P_d show that the minimum value of T_K is related to the collector time constant T_f and is given approximately by:

$$(T_K/T_f) \approx 0.4. \tag{2}$$

Assuming that the maximum frequency of operation f_m of the flip-flop is

$$f_m \leq 1/(T_f + T_K) \tag{3}$$

and substituting (1) and (2) into (3) results in

$$f_m \leq 4.4 f\alpha_E/(1 + \omega_{\alpha E}\alpha_E R_L' C_C). \tag{4}$$

Close correspondence is found between the maximum frequency of operation measured experimentally and the frequency, f_m, calculated from (3).

Fig. 3 shows an experimental curve of the maximum frequency, f_m, vs circuit power dissipation, P_d, for both the emitter-coupled and base-return flip-flops. The transistor and circuit parameters, which limit the speed in several regions of power dissipation P_d are summarized below.

1) $P_d < 0.5$ milliwatts. In this region the current gain α_E decreases rapidly with decreasing power level and hence seriously limits the maximum operating frequency for a given set of circuit stability requirements.

2) 0.5 milliwatts $< P_d < 80$ milliwatts. In this power dissipation range the frequency limit f_m of (4) is determined by the collector capacitance-load resistance product, $R_L' C_C$.

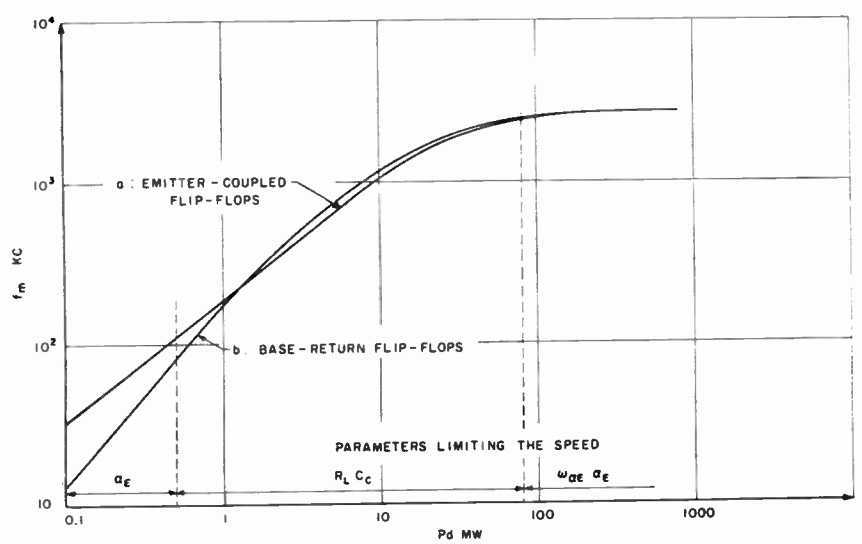

Fig. 3—Peak maximum operating frequency f_m vs power dissipation P_d for emitter-coupled and base-return flip-flops. $\Delta V_c = 2$ volts.

$$T_f = (1 + \omega_{\alpha E}\alpha_E R_L' C_C)/\omega_{\alpha E} \tag{1}$$

where R_L' is the parallel combination of R_L and R_b. It is apparent that T_f is independent of R_L', and hence of P_d, if the second term in the numerator of (1) is negligible.

The recovery time constant T_K of the coupling network can be calculated from circuit values and is proportional to the coupling capacitance C_K. For fast recovery, C_K and T_K must be as small as possible. However, if C_K is made too small, insufficient charge for reliable regeneration will be

3) $P_d > 80$ milliwatts. For larger power levels the second denominator term in (4) becomes negligible because R_L' becomes small. Therefore the frequency limit f_m is essentially independent of collector capacity and external circuit parameters and depends only on the gain-bandwidth product ($\omega_{\alpha E}\alpha_E$) of the transistors.

H. Raillard
J. J. Suran
General Electric Co.
Syracuse, N. Y.

A Generalization of the Exponential Transmission Line*

It is the purpose of this note to show that the exponential transmission line[1] and a line recently proposed as a broadband termination[2] are special cases of a general class of exponential lines. Furthermore, the solution of the non-uniform transmission line equations for this class may be expressed as a simple transformation of the solution for the ordinary exponential line.

A non-uniform transmission line is characterized by two functions, the distributed series impedance per unit length $Z(x)$, and the distributed shunt admittance per unit length $Y(x)$. Alternatively, the line may be described by its characteristic impedance $K(x)$

$$K(x) = \sqrt{Z(x)/Y(x)} \tag{1}$$

and by its propagation factor $\Gamma(x)$

$$\Gamma(x) = \sqrt{Z(x)\,Y(x)}. \tag{2}$$

The reciprocal of $\Gamma(x)$ will be called the phase-length.

The general exponential line is defined[3] by the condition that the fractional change in characteristic impedance per phase-length in the line is constant; *viz.*,

$$\frac{1}{\Gamma(x)}\frac{d \ln K(x)}{dx} = C \tag{3}$$

where C is an arbitrary complex constant. An equivalent form of this definition is

$$\frac{1}{Z(x)}\frac{dK}{dx} = C. \tag{4}$$

The steady state voltage V and current I in a transmission line are determined by

$$\frac{dV}{dx} = -IZ(x) \tag{5}$$

$$\frac{dI}{dx} = -V\Gamma(x). \tag{6}$$

It follows from (3) that for the class of exponential transmission lines, (5) and (6) may be expressed in the form

$$\frac{dV}{dx} = -I\Gamma(x)K(0)\exp\left[C\int_0^x dx\Gamma(x)\right] \tag{7}$$

$$\frac{dI}{dx} = \frac{-V\Gamma(x)}{K(0)}\exp\left[-C\int_0^x dx\Gamma(x)\right]. \tag{8}$$

It has been noted[4,5] that the change of variable from x to u, where

$$u = \frac{1}{\Gamma(0)}\int_0^x dx\Gamma(x) \tag{9}$$

reduces the problem with arbitrary propagation factor to one in which the propagation factor is constant. Specifically, it follows from (7), (8), and (9) that

* Received by the IRE, September 17, 1958.

[1] C. R. Burrows, *Bell. Syst. Tech. J.*, vol. 17, pp. 555–573; October, 1938.

[2] I. Jacobs, *Bell Syst. Tech. J.*, vol. 37, pp. 913–924; July, 1958.

[3] B. G. Kazansky, *Proc. IEE*, pt. C, vol. 105, pp. 126–138; March, 1958.

[4] C. O. Lund, *RCA Rev.*, vol. 11, pp. 133–142; March, 1950.

[5] E. F. Bolinder, "Fourier transforms in the theory of inhomogeneous transmission lines," *Trans. Roy. Inst. Technol.*, Stockholm, No. 48, 1; 1951.

$$\frac{dV}{du} = -IZ(0)\exp\left|C\Gamma(0)u\right| \quad (10)$$

$$\frac{dI}{du} = -VY(0)\exp\left|-C\Gamma(0)u\right| \quad (11)$$

which are the equations for the simple exponential transmission line, the solutions of which are well known.[1] Thus, for example, the voltage in the general exponential transmission line is given by

$$V(x) = A\exp\left[\left(\frac{C+C'}{2}\right)\int_0^x dx\Gamma(x)\right] + B\exp\left[\left(\frac{C-C'}{2}\right)\int_0^x dx\Gamma(x)\right] \quad (12)$$

where

$$C' = \sqrt{C^2+4}$$

and A and B are constants determined by the boundary conditions.

It is apparent from the above that when $\Gamma(x)$ is constant, the general exponential line reduces to the ordinary exponential line.

Another special case of physical interest is a non-uniform transmission line in which the distributed series impedance is constant; *e.g.*, a coaxial cable loaded with non-uniform dielectric. For $Z(x)=Z(0)$, it follows from (4) that the general exponential line is characterized by

$$K(x) = K(0)\left|1 + C\Gamma(0)x\right|. \quad (13)$$

Therefore, it follows from (1), (2), and (13) that the distributed shunt admittance is given by

$$Y(x) = \frac{Y(0)}{\left[1 + C\Gamma(0)x\right]^2}. \quad (14)$$

If $C\Gamma(0)$ is chosen to be a real negative number, $Y(x)$ is exactly of the form considered for a broad-band termination.[2] Consequently, that line is also a special case of the general exponential line.

The generalization discussed here was suggested to the author by W. J. Albersheim.

Ira Jacobs
Bell Telephone Labs., Inc.
Whippany, N. J.

Initial and Remanent Permeability Spectra of Yttrium Iron Garnet*

The unusually narrow ferromagnetic resonance line width observed in Yttrium Iron Garnet has been the subject of considerable study in an effort to obtain lower frequency operation of microwave devices which presently utilize ferrites. Somewhat less effort has been given to an experimental evaluation of the low field losses in YIG which also affect the low frequency utilization of these materials.

In an attempt to obtain more information on these losses, as well as to investigate the possibility of other low frequency applications of YIG, we have made a preliminary study of the initial complex permeability, $\mu=\mu'-j\mu''$, of polycrystalline YIG as a function of frequency.[1] Our results for the initial permeability spectrum at room temperature are shown in Fig. 1. As can be seen, the material exhibits a relaxation in the vicinity of 10 mc and a resonance in the region of 150 mc which is characterized by negative values of $\mu'-1$ in the microwave frequency region.

In analogy with the interpretation of magnetic spectra containing two dispersion regions given by Kittel[2] and independently by Rado and co-workers,[3] we can probably state that the low frequency relaxation is due to domain wall displacements while the higher frequency resonance is associated with domain rotation phenomena. This interpretation is also in agreement with the conclusions recently reported by Frackiewicz and Epstein[4] on the basis of similar measurements made by Westphal and East on another YIG material having a higher low frequency initial permeability than the material we measured. It is of interest to note that the higher static permeability observed in their material is also associated with a wall relaxation at a lower frequency and a rotation resonance at a somewhat higher frequency than was observed in the material we studied. The shift of the low frequency dispersion towards a smaller frequency with a higher static permeability is an argument that is often used for verifying the existence of rotation phenomena. However, the same situation can theoretically exist for a highly damped wall motion dispersion, and it is possible that this accounts for the difference between the frequency of the wall relaxation observed in our material and that reported for the higher permeability YIG.

In order to check the interpretation of these dispersion regions as wall motion and spin rotation, respectively, we measured the spectrum of the material in the remanent state as shown in Fig. 2. As discussed by Rado[3] one would expect a relatively large change in permeability between initial and remanent states if wall motion is present. However, the remanent and initial permeability should essentially be the same if domain rotation alone is responsible for the observed permeability. As can be seen in Fig. 2, the change in permeability between the initial and remanent state for the higher frequency resonance absorption is indeed smaller than the corresponding change observed for the lower frequency relaxation. Thus, the remanent spectrum appears to uphold our interpretation of the over-all magnetic spectrum; however, the change observed in μ between the initial and remanent states for the YIG in the region of the wall relaxation is certainly not as large as the change observed by Rado[3] in his measurements on the wall resonance in ferramic A.

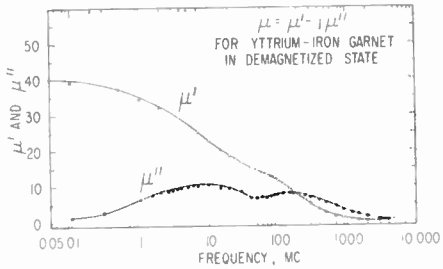

Fig. 1—Initial complex permeability spectrum for YIG at ambient temperature.

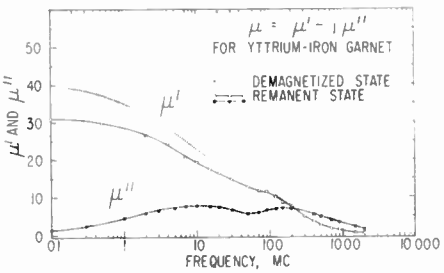

Fig. 2—Comparison of magnetic spectra for YIG in the initial and remanent states.

In any event, present efforts to improve the low frequency performance of garnets are in part directed towards decreasing the saturation magnetization, M_s, in order to decrease the frequency range over which losses in the demagnetized state occur. This procedure is in accord with Polder and Smit's[5] theory which attributes the broadness of the rotational resonance in ferrites to demagnetization effects due to domain walls and grain boundaries in the material. If we assume this theory is applicable to the high frequency resonance observed in the garnet, it does not immediately follow that it also describes the relaxation phenomena at lower frequency. It is probable that the present procedure of decreasing M_s is thus only affecting part of the low field loss observed in YIG.

R. D. Harrington
A. L. Rasmussen
Natl. Bureau of Standards
Boulder, Colo.

[5] D. Polder, J. Smit, "Resonance phenomena in ferrites," *Rev. Mod. Phys.*, vol. 25, pp. 89–90; January, 1953.

Millimicrosecond Microwave Ferrite Modulator*

This note describes a high-speed microwave ferrite modulator. Switching times of less than two millimicroseconds have been measured with this device. Switching speed was found to increase with applied magnetizing field. It was also observed that micro-

* Received by the IRE, September 25, 1958.

[1] The YIG material was obtained from Dr. D. M. Grimes, University of Michigan, Ann Arbor, Mich.

[2] C. Kittel, "Theory of magnetic dispersion in ferrites," *Phys. Rev.*, vol. 79, p. 214; July 1, 1950.

[3] G. T. Rado, R. W. Wright, and W. H. Emerson, "Ferromagnetism at very high frequencies. III. Two mechanisms of dispersion in a ferrite," *Phys. Rev.*, vol. 80, pp. 273–280; October 15, 1950.

[4] B. Frackiewicz, D. J. Epstein, "Magnetic Properties of yttrium-iron garnet," Lab. for Insulation Res., Mass. Inst. Tech., Cambridge, Mass., Prog. Rep. No. 23, p. 32; June, 1958.

* Received by the IRE, September 26, 1958. This work was supported by the Bureau of Ships under Contract NObsr 72717.

waves offer a convenient probe for measuring very rapid changes of magnetization in ferrites.

Enander[1] has described a ferromagnetic resonance isolator consisting of several toroidal pieces of ferrite surrounding a helical transmission line. The modulator shown in Fig. 1 is similar to this device, but the ferrite rings are placed inside the helix to reduce their size and the required magnetizing current. The helix is 0.75-inch long and has an inside diameter of 0.09 inch. The ferrite rings have an inside diameter of 0.05 inch, an outside diameter of 0.08 inch, and are 0.05 inch thick. A single straight wire along the axis of the helix carries the current that modulates the RF flow. Ferrite switches previously described in the literature used multi-turn coils to carry the modulating current; the greater inductance of such coils severely limits the rise time of current pulses and causes delay in pulse transmission. Le Craw[2] described such a switch and reported a switching time of 12 millimicroseconds. The design shown in Fig. 1 greatly reduces the inductance of the magnetizing circuit. The only appreciable time delay of this circuit is the propagation time of the RF wave along the short length of helix.

Fig. 1—Ferrite switch.

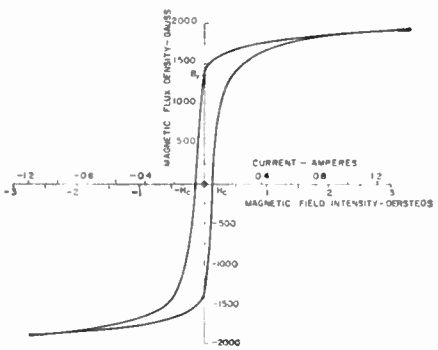

Fig. 2—Hysteresis curve of ferrites used in switch.

The ferrite used is a manganese-zinc composition; the hysteresis curve of this ferrite is shown in Fig. 2. The coercive force (H_c) is 0.14 oersted, and the remanence (B_r) is 1329 gauss. The dual horizontal scales indicate the amount of current required to produce the corresponding magnetic-field intensity at the mean diameter of the ferrite rings in the modulator.

The RF magnetic field within the helix is partially circularly polarized in all planes containing the axis of the helix. The magnetization of the ferrites is perpendicular to these planes. If the sense of this circular polarization is the same as that of the precession of the electron spins within the ferrites, the RF signal will be attenuated. The direction of applied field that gives this sense to the spin moments is termed the "back direction"; conversely, the opposite direction is the "forward direction." The RF wave is modulated by varying the magnetic field from one value to another in the back direction.

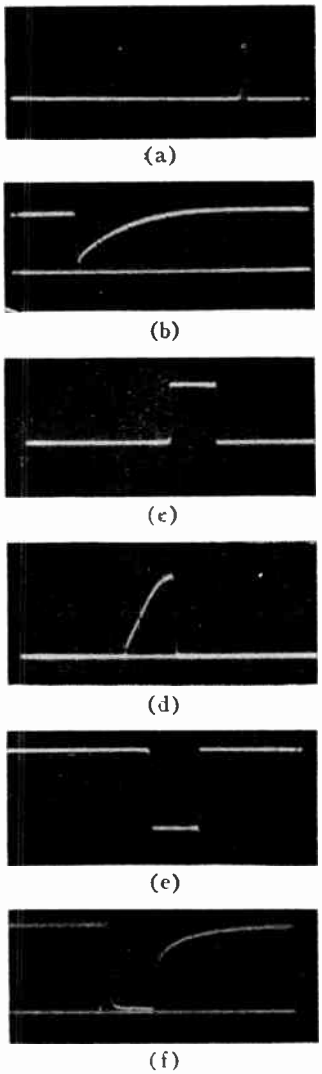

Fig. 3—Oscilloscope traces of modulating pulses and demodulated RF pulses.

Switching-time measurements were made for several values of applied magnetizing field; results are shown in Figs. 3 and 4. The ferrites were first saturated in the back direction (which is assumed to be the positive flux direction of Fig. 2), and a negative bias of 0.06 ampere, equal to the coercive force, was applied. A one-ampere pulse of 0.2 μsec duration [Fig. 3(a)] was then applied in the positive direction. The resulting RF output was demodulated and is shown in Fig. 3(b). In this figure, vertical distance above the reference trace indicates the magnitude of the transmitted RF power. The RF "switch-off," which is caused by the presence of the large applied field of the pulse, is many times faster than the subsequent "switch-on," which begins at the end of the pulse interval when the applied field returns to its previous value, $-H_c$. The cycle was then reversed, and a positive bias current of 0.94 ampere and a negative 2 μsec one-ampere pulse [Fig. 3(c)], were applied. Fig. 3(d) shows the long switch-on interval, followed by a short switch-off time. For the third experiment, a one-ampere 2 μsec positive pulse was applied after saturating the ferrites positively, so that the cycle started and ended at the remanent point, B_r. Figs. 3(e) and 3(f) show the applied pulse and the RF transmission response of the switch.

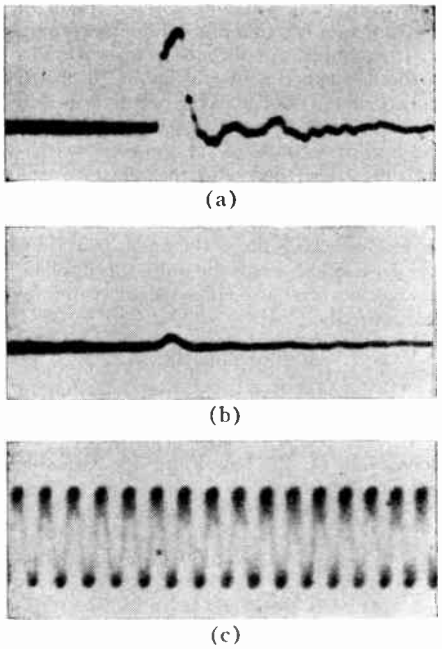

Fig. 4—Traces on a traveling-wave oscilloscope (a) Three-ampere modulating pulse. (b) Demodulated rf output pulse. (Baseline represents 35 db attenuation and pulse height represents transmission increase of 20 db.) (c) 250 megacycle timing wave.

It is seen that a large applied field is required to switch the RF power either on or off rapidly. As shown in Fig. 3(b), for example, the change in flux density for an applied field equal to the coercive force required almost four microseconds. On the other hand, the change caused by the large applied field of the pulse occurred in a small fraction of a microsecond. If it is desirable to switch both on and off very rapidly, the only feasible operating mode is one in which the applied field is at least moderately high at both the starting and ending points of the cycle.

The resonance characteristics of the particular ferrite material used are such that a 3100-megacycle signal is strongly attenuated with an applied positive magnetizing current of about one ampere, but increases in transmission by about 15 db when the current is increased to four amperes. Fig. 4(a) shows a three-ampere positive pulse which was applied on top of a one-ampere positive bias. Fig. 4(b) shows the resultant demodulated RF output pulse, and Fig. 4(c) shows a 250-megacycle sine wave for time-base comparison. The input pulse in this experiment was of sufficient duration to allow the transmission to rise to its maximum value. Rise and decay times of the RF pulse are less than two millimicroseconds each. The pictures shown in Fig. 4 were photographed

[1] B. N. Enander, "A new ferrite isolator," PROC. IRE, vol. 44, pp. 1421–1430; October, 1956.
[2] R. C. Le Craw, "High-Speed Magnetic Pulsing of Ferrites," *J. Appl. Phys.*, vol. 25, pp. 678–679; May, 1954.

from a traveling-wave oscilloscope having a rise time of a fraction of a millimicrosecond.

It should be noted that the insertion loss in the last experiment was about 20 db. In an experiment similar to the one described in Fig. 3(d), with a negative 0.06-ampere bias and a positive pulse of 2.4 amperes, switching time from the on to the off state was measured on the traveling-wave oscilloscope to be less than three millimicroseconds. Insertion loss was 8 db in the on state and increased to 53 db when the pulse was applied. It was not, of course, possible to switch on again rapidly.

ACKNOWLEDGMENT

The authors thank Dr. Irwin Gordon, of the RCA Laboratories, Princeton, N. J., for preparing the ferrites and for helpful discussions, and D. L. Thornburg for valuable technical assistance.

A. H. SOLOMON
F. STERZER
Radio Corp. of America
Princeton, N. J.

Digital-Analog Conversion with Cryotrons*

The recent development of the cryotron as a computer element by Buck[1] has led to many interesting applications. We would like to draw attention to the possible use of the cryotron as an active device in both analog-to-digital and digital-to-analog conversion equipment.

ANALOG-TO-DIGITAL CONVERSION

As is well known, the cryotron is similar to a gating relay in its operation. With a current less than the critical value flowing in the control winding, a current will pass through the gate. However, if a control current greater than critical is applied to the cryotron, the gate becomes resistive and no current flows (when shunted by a superconducting path). This operational mode may be used in an analog-to-digital converter. If the input is a voltage source, suitable means must be provided to allow operation as a current device, since only a time varying current input to the converter is considered.

In general, two steps are required in making the conversion. First, the input must be digitized. Second, this digitized information must be translated to a usable code. Two methods appear feasible for performing the first step in the conversion process. In the first method, n cryotrons are arranged such that the control winding of each cryotron is wound with a different pitch, the first having N/L turns per inch, the second, $2N/L$, and the third $3N/L$, and so forth. As the magnitude of the input current increases, the cryotron with the greatest pitch becomes resistive first, followed in turn by the next highest and so on. This gives an output of the form: zero out of n cryotrons

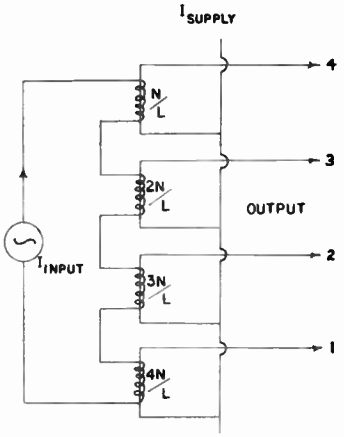

Fig. 1—Digitizing by means of series cryotrons with weighted pitches.

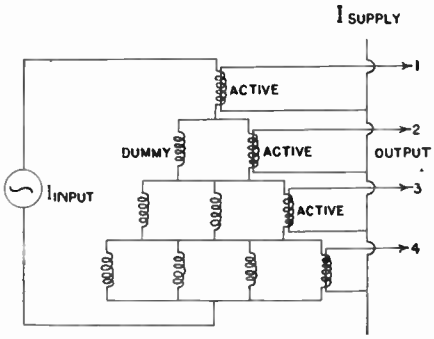

Fig. 2—Digitizing by means of current splitting. Dummy cryotrons are illustrated by a control winding with the gate wire omitted.

resistive, then one out of n resistive, until finally all n cryotrons are resistive. With this method n different types of cryotrons are required to give $n+1$ levels (Fig. 1).

The second method for performing this step in the conversion requires more cryotrons than the first; however all the cryotrons are of the same type. Here the digitizing function is performed by current division rather than by control windings of different pitches. The circuit takes the form shown in Fig. 2. The control windings of the cryotrons are always resistive. Therefore, the amount of current through each control winding is inversely proportional to the number in parallel. When the input current increases in magnitude the single cryotron will become resistive first, followed at known increments by each of the parallel sets. This method is somewhat wasteful of cryotrons, but has the advantage of simplicity. For $n+1$ levels, $(n)+(n-1)+(n-2)+\cdots+(1)$ cryotrons are required. If it is desired to minimize the number of cryotrons required, each of the parallel sets could be replaced by a single cryotron and equivalent impedances. For $n+1$ levels, n cryotrons and $n-1$ different equivalent impedances would be required.

The second step in the conversion process is easily performed using the matrix shown in Fig. 3. Here two types of cryotrons are employed. The first has a single control winding, the second, two control windings. The double control windings are connected so that their respective magnetic fields are in opposition. The cryotron is resistive if either of the control windings carry current, but

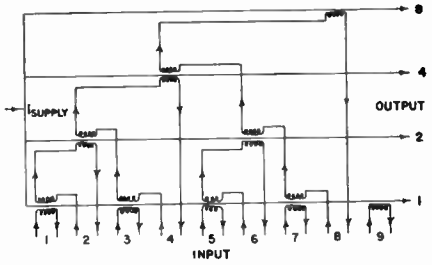

Fig. 3—Step code to binary code translating matrix using "Exclusive-Or" cryotrons. "Exclusive-Or" cryotrons are illustrated by double windings adjacent to the gate wire.

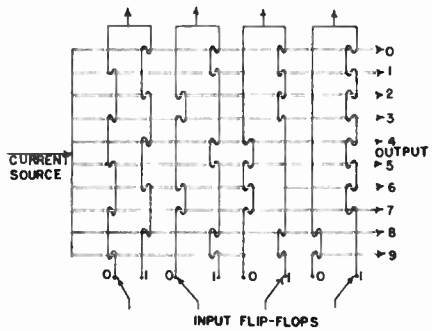

Fig. 4—Binary-to-step code translating matrix.

superconductive if neither or both of the control windings carry current. To insure proper operation it may be necessary to sample the input current. This is necessary since the digital code of the translator may not be of the Gray type.

DIGITAL-TO-ANALOG CONVERSION

Digital-to-analog conversion is also possible with cryotrons. In this case a two stage process may also be used, although it is not mandatory. Three conversion systems will be discussed. The first is a two-stage system, while the remaining two are single-stage systems. With the first method, we must translate from the binary machine code to the 1 out of n, 2 out of n, etc., step code. The second stage then converts this step code into an analog output.

Fig. 4 illustrates a possible matrix for accomplishing the translation to step code. The switches shown are the flip-flop outputs of the computer proper. The analog stage consists of n cryotrons with their gate windings in series. A well-regulated constant current source passes current through the cryotrons. When the gate windings are in the superconducting state, no voltage is developed across them. However, when one or more is switched to the resistive state, a proportional voltage results which is then amplified to usable values. The device is similar in operation to the catalog memory of Slade and McMahon.[2]

The second method is similar to the last stage of the two-stage system. However, it employs cryotrons with gate windings of calibrated resistances R, $2R$, $4R$, $8R$, etc., when in the resistive state. These weighted cryotrons are again connected in series as

* Received by the IRE, September 15, 1958.

[1] D. A. Buck, "The cryotron—a superconductive computer component," PROC. IRE, vol. 44, pp. 482–493; April, 1956.

[2] A. E. Slade and H. O. McMahon, "A cryotron catalog memory system," *Proc. Eastern Joint Computer Conf.*, pp. 115–120; December 10–12, 1956.

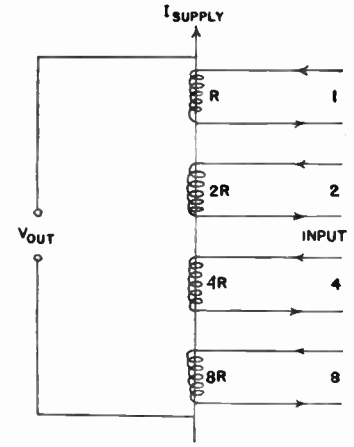

Fig. 5—Digital-to-analog converter using weighted resistance gates.

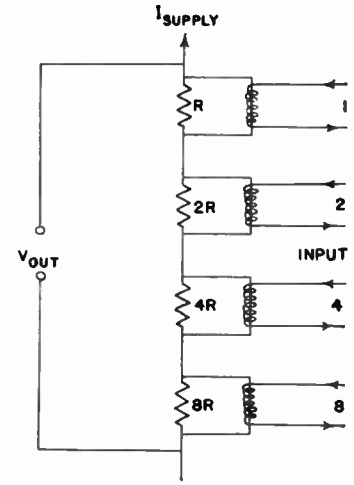

Fig. 6—Weighted resistor digital-to-analog converter.

shown in Fig. 5. The operation follows identically to that explained above. It should be noted that this system will operate only if a weighted machine code is used. Otherwise, we must revert back to the two stage device.

The final method merely uses the cryotron as a switch. The weighting necessary in the conversion from a binary code to an analog output is obtained by means of calibrated resistors (Fig. 6). Each of these resistors is paralleled with a cryotron. When a cryotron is in the superconducting state, no voltage appears across the parallel resistor. However, when the cryotron is in the resistive state, there is a voltage across the parallel combination of resistor and cryotron. It would be advantageous if the output voltage were independent of the cryotron parameters. This is possible if the largest resistance, in this case $8R$, is small in comparison with the resistance of a cryotron gate winding. To maintain accuracy it will probably be necessary to use cryotrons wound of resistive wire coated with superconducting material. As suggested by Buck,[1] this greatly increases the resistance of the cryotron when not in the superconducting state.

Switching Times

The switching time of a cryotron is inversely proportional to the amount by which the control field exceeds the critical field. For the digital-to-analog converter, this poses no problem since large drives can be employed. However, this is not the case for the analog-to-digital converter. Here the switching of the cryotrons must occur with applied fields only slightly larger than the control field. This puts a definite upper limit on the rate at which the input current can vary if the device is to operate properly.

Possible Applications

The most fruitful application of these converters is possibly as special-purpose devices for missiles and other one-shot, short-time applications, where the advantages of small size and weight, as well as strength and reliability, outweigh the acknowledged disadvantage of operation at liquid helium temperatures. In most cases, the liquid helium necessary could be provided by a small Dewar flask which would be ample for the short flight time. Of course, if large scale computers are designed using cryotrons as active elements, the above circuits would have obvious value as input-output devices.

The authors thank Prof. J. R. Singer, Electrical Engineering Division, University of California, for many invaluable discussions and suggestions concerning this project.

L. K. Wanlass
L. O. Hill
Electrical Eng. Div.
University of California
Berkeley, Calif.

Short Time Stability Measurements on Frequency Standards and the Notion of Resolution*

Despite recent interest in the subject of short time stability measurements, there seems to be some lack of common language among the different workers in the field. The following considerations are suggested.

There are two ways to measure frequency:

1) The measurement of phase accumulated within a time interval.
2) The use of a frequency discriminator.

The first method is used almost exclusively for all high precision RF measurements and we want, therefore, to restrict these considerations only to this case. Whatever the frequency measuring method is—a counter, the recording of a beat note, or a synchronous clock to compare time intervals—we actually always measure according to this principle.

Let $\Delta\phi$ be the accumulated phase difference between the oscillator being measured and the standard during an interval, Δt, Ω the measured frequency in radians per second, and Ω_0 the nominal frequency or the frequency of the standard with which we compare. Then we express the result of our frequency measurement as

$$R = \frac{\Omega - \Omega_0}{\Omega_0} = \frac{\Delta\Omega}{\Omega_0} = \frac{1}{\Omega_0}\frac{\Delta\phi}{\Delta t}. \quad (1)$$

Due to the very definition of frequency, there is no measurement of instantaneous frequency.[1] We always need a certain time interval to measure an average frequency during this interval. It is obvious that method 2), also suffers from this limitation because the more closely we want the definition of the "center" frequency, the longer the response time of the discriminator becomes.

Let $\delta\Delta\phi$ and $\delta\Delta t$ be the errors we make in the phase difference and in the time interval measurements, respectively. We can certainly assume these errors to be independent from each other.

The quantity defined (1) can be considered the fractional (dimensionless) rate of a clock employing the frequency, Ω, as basis, relative to the standard clock which uses Ω_0. The first order error in R due to our measurement errors therefore becomes:

$$\delta R = \frac{\partial R}{\partial \Delta\phi}\cdot\delta\Delta\phi + \frac{\partial R}{\partial \Delta t}\delta\Delta t, \text{ or} \quad (2)$$

$$\delta R = \frac{1}{\Omega_0}\left[\frac{1}{\Delta t}\delta\Delta\phi - \frac{\Delta\phi}{(\Delta t)^2}\delta\Delta t\right]. \quad (3)$$

The error, $\delta\Delta\phi$, can be caused by the presence of a phase modulation (hum) in the signal or can be due to random noise, both introduced by the measurement equipment. Let us assume here, for the sake of simplicity, that these effects enter with their maximum amount. Calling the modulation index, μ and the signal to noise power ratio S/N; one can show that:

$$\delta R = \frac{1}{\Omega_0\Delta t}\sqrt{\mu^2 + (S/N)^{-1} + \overline{(\Delta\Omega)^2}\overline{(\delta\Delta t)^2}}. \quad (4)$$

It is suggested that this quantity be defined as the *Resolution* of the frequency measurement, meaning the error we may expect to make in the determination of R due to phase modulation, noise, and errors in time interval measurement.

Let us consider the following examples: Observation frequency, $\Omega_0 = 2\pi\times 10^8$ rad/sec, time $\Delta t = 0.001$ sec, $\Delta f = 1$ kc/sec, $\delta\Delta t = 1$ μsec, $S/N = 30$ db, $\mu = 0.02$, then we get by (4):

$$\delta R = 6\times 10^{-8}.$$

This means that the measuring method does not allow the measurement of R to better than 6×10^{-8}.

If we measure R by means of a very slow beat note, then we may have: $f = 10^8$ cps, $\Delta t = 100$ sec, $\mu = 0.02$, $S/N = 30$ db, $\Delta\Omega$ $2\pi.10^{-2}$ rad/sec, $\delta\Delta t = 1$ sec. These values permit a resolution of measurement $R = 10^{-12}$.

Eq. (4) could also be used to establish minimum requirements for freedom from hum modulation and random noise if certain accuracy requirements have to be met.

Gernot M. R. Winkler
U. S. Army Signal Res. and Dev. Lab.
Fort Monmouth, N. J.

* Received by the IRE, September 24, 1958.

[1] Of course, there is a notion of instantaneous frequency. See B. Van der Pol, "The Fundamental Principles of Frequency Modulation," *J. IEE*, vol. 93, pt. 3, pp. 153–158; May, 1946. Also, "Frequency modulation," Proc. IRE, vol. 18, pp. 1194–1205; July, 1930.

Hall Effect in High Electric Fields*

The purpose of this letter is to discuss briefly some simple considerations which would appear to set an ultimate limit on the Hall voltage obtainable in any given semiconductor. It will also be shown that this limiting Hall voltage is different in different semiconductor materials; this results in an interesting "ordering" of the available semiconductors in terms of Hall effect sensitivity, which is remarkably different for high electric fields from that for modest ones.

To arrive directly at the fundamental point, consider the derivation of Hall voltage indicated in Fig. 1. We focus attention on the actual x component of electric field, E_x, rather than on the current flowing in the semiconductor bar. A simple calculation shows the Hall voltage to be

$$V_H = Wv_xB_z \qquad (1)$$

were v_x is the velocity resulting from the applied electric field E_x and B_z is the perpendicular magnetic field strength. This equation indicates that for a fixed geometry (fixed W) and fixed magnetic field (B_z), V_H will be maximized by maximizing v_x. We may therefore compare various semiconductors by comparing their v_x vs E_x curves. As is well known, these curves show two distinct regions: a low field region where v_x is directly proportional to E_x, and a high field region where v_x is independent of E_x. Typical log-log curves of v_x (electron velocity) vs E_x based on the best available data are given for several semiconductors in Fig. 2. The low field curves show the usual constant mobility relation, the value of v_x for $E_x=1$ being in fact μ.

The first conclusion to be drawn from these curves is that there is a maximum Hall voltage V_H which is determined by the terminal velocity of the carriers in the semiconductor. For a germanium sample with $W=1$ mm, $B_z=1$ gauss, maximum V_H is 6 mv. By comparison, the Hall voltage developed in a piece of 8-ohm-cm germanium with $W=1$ mm, $t=50$ microns, which is passing a current of 3.4 ma at room temperature is about 0.2 mv/gauss. This latter represents a typical value for Hall voltage. It is rather illuminating to observe that it is only 1/30th as large as it could be. One may therefore expect to increase the Hall output voltage considerably by achieving the velocity-limited condition.

Several advantages in addition to increased output voltage result from using the velocity-limited Hall effect. First, since terminal velocity is almost independent of temperature, the Hall voltage derived from it will also be reasonably insensitive to temperature variations. In a Hall effect flux-meter, this would be a decided advantage over the usual highly temperature sensitive Hall effect flux-meter which relies on the low field carrier mobility to produce carrier velocity.

Second, this velocity-limited Hall voltage is independent of the thickness of the semiconductor bar. This independence of maximum Hall voltage on thickness is rather illuminating since the normal Hall effect formula contains an explicit t dependence:

$$V_H = (R_HI_xB_z)/t.^1$$

This dependence is somewhat artificial, however, since the real effect of decreasing t is to increase carrier velocity for a given current, and as we have seen there is an ultimate limit beyond which this is a useless procedure.

The final conclusion to be made concerns the relation of the v_x vs E_x curves for different semiconductor materials shown in Fig. 2. For the low electric field case, it is clear that I_nSb is the best semiconductor of those shown for a Hall effect flux-meter, since it gives maximum velocity for a given electric field. For the high electric field case, however, I_nSb possesses no distinct advantage over germanium and is somewhat inferior to silicon from the point of view of Hall voltage developed. (Data on I_nSb are, however, still somewhat tentative.)

From the noise generation standpoint, of course, it may still be advantageous to use I_nSb at low fields, because the terminal velocity condition may be a noisy one. However, for a wide range measurement of magnetic fields, it should prove to be convenient to use silicon, which gives a greater output voltage, has generally superior temperature characteristics, and provides a range of resistivities which enables one to utilize the thickness-independent character of the limiting Hall voltage without using excessive currents.

Many of the conditions required for the velocity-limited Hall effect are found in the depletion layer of a back-biased p-n junction. In particular, the carriers move with terminal velocity but without simultaneously producing a large current. Unfortunately, rather high purity silicon material would have to be used to obtain the favorable ratio of the length of the depletion layer to its width, which is necessary for Hall effect measurements.[2]

J. F. Gibbons
Stanford University
Stanford, Calif.

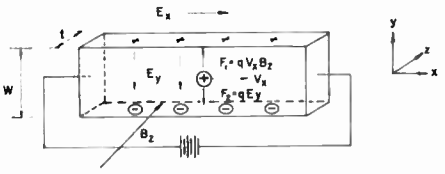

Fig. 1—Fundamental derivation of Hall voltage.

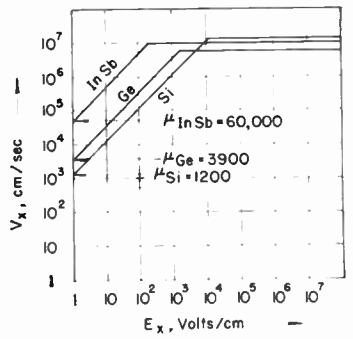

Fig. 2—V_x vs E_x curves for several semiconductors.

A Theorem on Lossy Nonreciprocal N-Port Junctions*

A recent problem concerned the realizability of a certain nonreciprocal junction. The matter was resolved by the theorem proved below. Special cases of the theorem can be found in the literature,[1,2] but the general result does not appear to have been stated previously.

Consider a linear passive n-port junction with all input and output impedances similarly normalized. Let the voltage transfer characteristics of the junction be represented by $AS=B$, where A and B are n-dimensional row vectors representing the inputs and outputs respectively, and S is an n by n scattering matrix.

From considerations based on the law of conservation of energy it is apparent that if a generator of unit available power is connected to the kth junction, and all ports are terminated in unit resistances, then the sum of the powers delivered to all the terminals is less than or equal to unity. This is equivalent to the mathematical statement that the rows of S are of length less than or equal to one. On the other hand, it is not obvious that there is an identical restriction on the length of the columns of such a nonreciprocal scattering matrix. That the restriction does hold is shown by the theorem below. In physical language, the theorem states that if a generator with unit available power is placed sequentially at each junction of a linear passive network, and all ports are terminated in unit resistances, then the sum of the powers delivered to the kth termination is less than or equal to unity.[3]

Notation: Capital letters will represent vectors and matrices; subscripted lower case letters will represent vector components or matrix elements. The transpose of a matrix S will be denoted by $\tilde{S}$, and * will be used for the operation of taking the complex conjugate. The length of a vector V is

* Received by the IRE, September 29, 1958. The work reported here was supported by the Office of Naval Research.

[1] Eq. 2 may be derived by multiplying (1) by $(nqt)/(nqt)$ and using the definition of R_h and I_x. From this manipulation it is clear that R_h also loses significance at high electric fields since R_hI_x/t is merely a complicated way of writing WV_x.

* Received by the IRE, October 15, 1958.

[1] H. J. Carlin, "Principles of gyrator networks," *Proc. Symp. Modern Advances in Microwave Techniques*, Polytechnic Inst. of Brooklyn, Brooklyn, N. Y., pp. 175–204; November 8–10, 1954.

[2] G. S. Heller, "Ferrites as microwave circuit elements," PROC. IRE, vol. 44, pp. 1386–1393; October, 1956.

[3] The word sequentially is essential. A magic T with one of the symmetrical ends terminated in a matched load has the property of yielding half-power at the other symmetrical end for excitation placed in either the E or the H-plane arm. It is, however, lossless if properly phased unit power is introduced simultaneously in both the E and the H-plane arms. Thus, for the two unit powers introduced sequentially, the sum of the powers realized at the third port is one, but for simultaneous introduction a power of two may be realized.

$$\sqrt{\sum_{i=1}^{n} v_i v_i^*}$$

The inner product $U \cdot V$ of two vectors is

$$\sum_{i=1}^{n} u_i v_i^*.$$

Theorem: The length of any column vector in S is less than or equal to unity.

Proof: By conservation of energy $A \cdot A \geq B \cdot B$, or in matrix notation, $A\tilde{A}^* \geq B\tilde{B}^* = AS\tilde{S}\tilde{A}^*$. Thus, $A(I - S\tilde{S}^*)\tilde{A}^* \geq 0$ for all vectors A, *i.e.*, the matrix $I - S\tilde{S}^*$ is nonnegative definite.

Consider first the lossless case $A(I - S\tilde{S}^*)\tilde{A}^* = 0$. As the equality must hold for all A, $S\tilde{S}^* = I$ or $\tilde{S}^* = S^{-1}$. The inverse commutes, and one finds $I = S\tilde{S}^* = SS^{-1} = S^{-1}S = \tilde{S}^*S$. The lengths of both the rows and the columns in the matrix S are unity.

The lossy case requires a bit of matrix algebra to reduce it to the lossless case. We first note that $S\tilde{S}^*$ is Hermitian, *i.e.*, $(\widetilde{S\tilde{S}^*})^* = S\tilde{S}^*$. For any Hermitian matrix there is a unitary matrix which diagonalizes it.[4] Let this matrix be U and consider $AU(I - S\tilde{S}^*)\tilde{U}^*\tilde{A}^*$. The value of this is greater than or equal to zero as AU is a permissible vector in our space and $\tilde{U}^*\tilde{A}^*$ is its conjugate transpose. That is, our statement that the combination $(I - S\tilde{S}^*)$ is nonnegative definite means that the inequality holds for any test vector and AU is just as suitable as A. Remembering that $U\tilde{U}^* = I$, one finds $A(I - US\tilde{S}^*\tilde{U}^*)\tilde{A}^* \geq 0$.

Let E be the matrix US. The columns in this matrix are of the same length as those in the original matrix S, for the squares of the column lengths of E are equal to diagonal elements of $\tilde{E}^*E = \tilde{S}^*\tilde{U}^*US = \tilde{S}^*S$.

As $E\tilde{E}^* = US\tilde{S}^*\tilde{U}^*$ is a diagonal matrix, the rows of E are orthogonal vectors. Moreover, the length of the rows in E are less than or equal to unity. (From above $A(I - E\tilde{E}^*)\tilde{A}^* \geq 0$. The test vector $A = (1, 0, 0, 0, \cdots)$ yields

$$1 - \sum_j e_{1j}e_{1j}^* \geq 0 \text{ or } \sum_j e_{1j}e_{1j}^* \leq 1, \text{ etc.}).^5$$

Finally, then, we consider the matrice F and G where F is derived from E by replacing any row of length zero with a row of unit length orthogonal to all other rows (the Gram-Schmidt orthogonalization process).[6] The matrix G is derived from F by normalization of all the rows to length one. (The normalization is done by dividing each row by its length, which before normalization was less than or equal to unity.) It is evident that the lengths of the columns cannot decrease in going from E to G so that the columns of S have lengths less than or equal to those of G. However, G is a lossless matrix, *i.e.*, $G\tilde{G}^* = I$. The proof for the lossless case shows that the columns in G have the same lengths as the rows, *i.e.*, unity. Therefore, the columns in S have lengths less than or equal to unity which was to be shown.

An example of the usefulness of the theorem is afforded by the analysis of an attempt to build a nonreciprocal receiving antenna having high gain in many directions by the use of n similar horns, each covering a sector and feeding into a common crystal. The connection may be regarded as an $n+1$ port linear junction without further specification. If it is assumed that equal voltage is to be transferred from each horn to the load, the theorem limits the maximum transfer coefficient to $1/\sqrt{n}$. The gain for a wave arriving from a single direction is thus reduced to $1/n$ of that which would be realized by a single horn. This is the result one would have got by reciprocity were it applicable.

L. Joseph
W. K. Saunders
Diamond Ordnance Fuze Labs.
Dept. of the Army
Washington 25, D. C.

[4] H. Margenau and G. M. Murphy, "The Mathematics of Physics and Chemistry," D. Van Nostrand and Co., Inc., Princeton, N. J., ch. 10, especially p. 331; 1956.

[5] The statement made in the third paragraph concerning the row vectors of S could be proved in a similar manner.

[6] Margenau and Murphy, *op. cit.*, p. 312.

Coaxial Line Isolators At and Below 1 KMC*

Pioneering work performed at Sperry in the field of nonreciprocal ferrite phenomena in coaxial transmission line was previously reported,[1-3] and this work enabled the design of extremely broad-band and compact ferrite isolators for operation over bandwidths of up to an octave or more anywhere in the 1.5 to 12.0 kmc frequency range. More recently an yttrium garnet isolator designed in a hybrid $3\frac{1}{8}$ inch diameter coaxial structure for operation in the UHF region has been described in the literature.[4] Effort at Sperry in this area has resulted in the design of compact low insertion loss—$\frac{7}{8}$ inch coaxial line isolators for use at both low and high average power levels. Techniques and materials used in attaining isolators exhibiting large attenuation ratios around and below 1 kmc plus operative 900–1300 and 730–800 mc isolators are described herein.

The 900–1300 mc isolator is designed in 46.3 ohm $\frac{7}{8}$ inch coaxial line, and utilizes the technique described by Duncan, *et al.*[1] The mode distorting dielectric is a low loss aluminum oxide ceramic, and the microwave ferromagnetic material used is an yttrium garnet whose density exceeds 5.0 gm/cm.[3] The isolator design, shown in cross section in Fig. 1(a) is such that the thin slabs of yttrium garnet are located flat against a metal insert in the outer coaxial line conductor. The metal insert can be made of soft iron to enable a reduction in magnet size, or a good heat conducting material to facilitate heat removal from the garnet when operation is at high power levels. A dc magnetic field is applied as shown in Fig. 1(a) perpendicular to the broad dimension of the garnet slabs. This garnet configuration and magnetic field orientation were selected in this case primarily from a heat dissipation viewpoint although additional considerations for low frequency operation would seem to dictate the selection of this combination. It will be shown later that this is not necessarily the condition which exists.

Using the above approach the high power isolator of Fig. 2 was derived. This unit exhibits a better than 10 db to 0.4 db reverse to forward wave attenuation ratio over the 900–1300 mc region, and a better than 10 db to 0.8 db attenuation ratio from 900–2700 mc (Fig. 3). It is capable of operation at power levels in excess of 400 watts cw when operating into a load VSWR of 2:1. Perhaps it is significant to note that at 1 kmc a re-

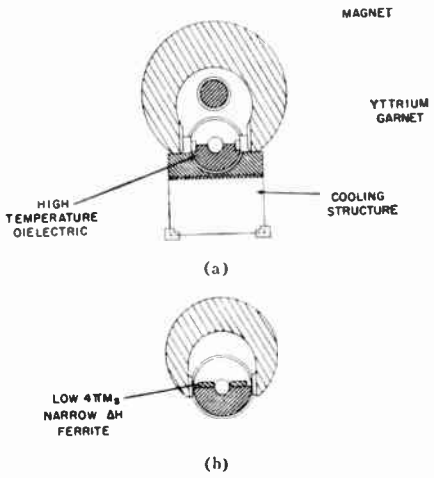

Fig. 1—Low frequency coaxial line isolator configurations.

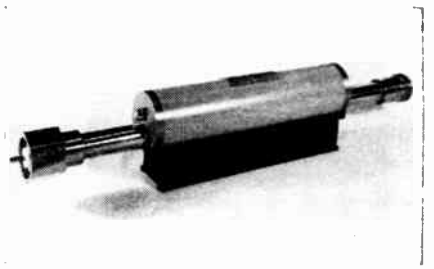

Fig. 2—Typical high-power low-frequency isolator.

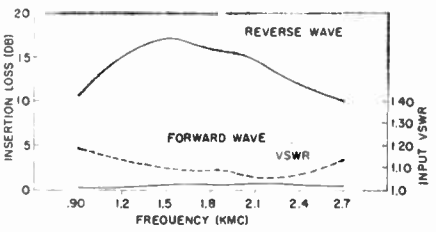

Fig. 3—Electrical performance of a high-power low-frequency yttrium garnet isolator.

* Received by the IRE, October 6, 1958.

[1] B. J. Duncan, L. Swern, K. Tomiyasu, and J. Hannwacker, "Design considerations for broadband ferrite coaxial line isolators," Proc. IRE, vol. 45, pp. 483–490; April, 1957.

[2] R. Mangiaracina and B. J. Duncan, "Nonreciprocal Ferrite Devices in TEM Mode Transmission Lines," presented at the Annual PGMTT meeting, New York, N. Y.; May 9–10, 1957.

[3] B. J. Duncan, L. Swern, and K. Tomiyasu, "Microwave magnetic field in dielectric loaded coaxial line," Proc. IRE, vol. 46, pp. 500–502; February, 1958.

[4] F. R. Morgenthaler and D. L. Fye, "Yttrium garnet UHF isolator," Proc. IRE, vol. 45, pp. 1551–1552; November 1957.

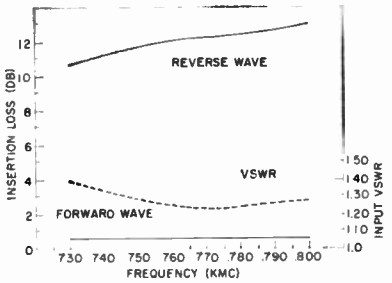

Fig. 4—Electrical performance of a low-power UHF ferrite isolator.

verse to forward wave attenuation ratio in excess of 50 db to 1 db is obtained. It is further significant to note that this same basic isolator design has been used to obtain a better than 10 db to 0.8 db reverse to forward wave attenuation ratio at frequencies to below 500 mc.

A low frequency isolator of equal or possibly more interest is one developed using the configuration of Fig. 1(b). As shown, thin slabs of microwave solid state materials with their broad dimension located flush against the dielectric flat faces, and magnetized parallel to their broad dimension, are used in this design. This solid state material configuration and magnetic field orientation when similarly used in most transmission line structures yields very low reverse to forward wave attenuation ratios, these ratios being so small at frequencies below *S* band as to prohibit its use when even the best of low zero field loss materials are available.

Isolators developed utilizing a low saturation magnetization (600 gauss) narrow resonance linewidth MgO-MnO-AlO-Fe_2O_3 ferrite have been made to consistently yield attenuation ratios of better than 10 db to 1 db even down to frequencies below 500 mc. One such isolator developed using this approach exhibits the electrical characteristics depicted in Fig. 4. As shown in the figure, a better than 10 db to 0.6 db reverse to forward wave attenuation ratio is obtained over the 730 to 800 mc range. This unit, which is basically a low-power design, weighs only two pounds and its physical size is only $1\frac{3}{4}$ by 2 by 15 inches.

One possible explanation of the origin of the outwardly unexpected large attenuation ratios involves a field displacement effect encountered in this structure [Fig. 1(b)]. With only the dielectric wedge in the coaxial line, it is reasonable to expect that practically all microwave energy propagated through this structure will be concentrated in the dielectric. In this case the forward (negative) wave sees a dielectric wedge with two thin-low microwave permeability-ferrite slabs which exhibit dielectric constants approximately equal to that of the dielectric wedge. Thus, this wave need not necessarily be grossly effected by the presence of the partially magnetized ferrite even though low field microwave losses are present.

However, a reverse (positive) wave sees ferrite slabs which, at resonance, exhibit high microwave permeabilities. Thus, the tendency here is to concentrate, if only weakly, or draw microwave energy into the ferrites. It is only reasonable to expect that under these conditions a large reverse wave loss is encountered in a relatively short length of ferrite material. It is, therefore, concluded that the large reverse to forward wave attenuation ratio attainable here is attributable to a field displacement effect put to use in the resonance region to minmize low field-forward wave loss and maximize resonance-reverse wave loss. Perhaps theoretical work already performed in the region away from resonance[5] when extended to the resonance region will establish the validity of this rather simple physical picture.

B. J. Duncan
G. F. Horner
Sperry Microwave Electronics Co.
Clearwater, Fla.

[5] K. J. Button, "Theory of Nonreciprocal Ferrite Phase Shifter in Dielectric Loaded Coaxial Line," Lincoln Labs., M.I.T., Cambridge, Mass., Tech. Rep. No. 176; March 7, 1958.

Comments Concerning the Possible Use of Gas Plasma in Thermoelectron Engines*

As suggested by Hatsopoulos and Kaye,[1] a high vacuum thermoelectron engine requires close spacing of electrodes in order to reduce the effect of electronic space charge. Theoretically, large spacing could be employed if the interelectrode space contained a gas plasma with substantially equal electron and positive ion space charge density. Such a plasma may be generated in a surprisingly easy manner in a simple tube structure by means of the circuit shown in Fig. 1.

The electrode arrangement used in the experimental work reported here was composed of an oxide coated cathode with a diameter of 0.15 cm concentric with an anode of 1.4 cm diameter. The length of the cathode and anode was 3.0 cm. The filling was xenon at a pressure of 2.7 millimeters of Hg.

Operation of the circuit was initiated by a single closing and opening of switch *S*. With the heater voltage considerably in excess of that normally employed in high vacuum operation of similar cathodes, an anode voltage waveform as shown in Fig. 2 was obtained. The frequency was in the neighborhood of several hundred cycles per second. Depending upon the value of the load resistor *R*, substantially constant currents in

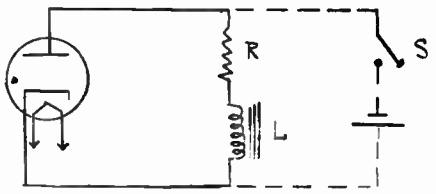

Fig. 1—Circuit diagram

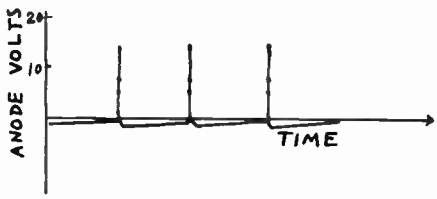

Fig. 2—Observed anode voltage.

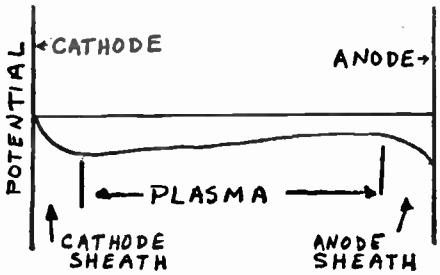

Fig. 3—Postulated potential distribution.

the range of 20 to 100 milliamperes were obtainable.

While a detailed discussion of transient conduction of current in similar tubes has been published previously,[2] reference to Figs. 2 and 3 indicates the principal considerations involved. Neglecting contact difference of potential, the postulated potential distribution within the tube during the negative anode potential time of Fig. 2 is shown in Fig. 3. Because of their thermal energy, electrons are able to pass over the potential energy barriers near the cathode and anode. When the plasma decays to the point where the random electron current is unable to supply the required anode current, the anode voltage rises rapidly (due to the $L(di/dt)$ in the external circuit) to the ionization potential of the gas. As a result, an active arc is initiated; and the plasma is regenerated in a very short fraction of a cycle.

Besides ordinary thermal losses, energy is obviously required in this arrangement for the ionization of the plasma. It is not known if careful design consideration would yield efficiencies in the range reported by Hatsopoulos and Kaye.

J. C. Schuder
Harrison Dept. of Surgical Res.
University of Pennsylvania
Philadelphia 4, Pa.

* Received by the IRE, October 6, 1958.

[1] G. N. Hatsopoulos and J. Kaye, "Analysis and experimental results of a diode configuration of a novel thermoelectron engine," Proc. IRE, vol. 46, pp. 1574–1579; September, 1958.

[2] J. C. Schuder, "The transient conduction of current in a hot-cathode gas diode," *Proc. Nat. Electronics Conf.*, vol. 9, pp. 626–634; 1953.

Contributors

F. A. BRAND

Frank A. Brand (M'58) was born in Brooklyn, N. Y. on June 26, 1924. He attended Hofstra College, Hempstead, N. Y., from 1946 to 1948 and the Polytechnic Institute of Brooklyn, Brooklyn, N. Y., receiving the B.S. degree in physics in 1950 and the M.S. degree in physics in 1958.

Mr. Brand joined the U. S. Army Signal Research and Development Laboratory, Fort Monmouth, N. J. in 1950 as a research physicist and has since been engaged in research and development activities concerned with electron devices and semiconductor physics. Since 1956, he has been Deputy Chief of the Solid-State Devices Branch, U. S. Army Signal Research and Development Laboratory at Fort Monmouth. For the past year Mr. Brand has been teaching in the Electronic Engineering Department of Monmouth College, West Long Branch, N. J.

❖

M. CHODOROW

Marvin Chodorow (A'43–SM'47–F'54) was born on July 16, 1913, in Buffalo, N. Y. He received the B.A. degree in physics from the University of Buffalo in 1934, and the Ph.D. degree from the Massachusetts Institute of Technology in 1939.

During 1940, he was a research associate at Pennsylvania State College. Dr. Chodorow was an instructor of physics at the College of the City of New York from 1941 to 1943, when he became associated with the Sperry Gyroscope Co. as a senior project engineer. He remained at Sperry until 1947, when he joined the physics department of Stanford University, where he is now professor of applied physics and electrical engineering. In 1957 he was appointed acting director of the Microwave Laboratory.

Dr. Chodorow is a member of the American Physical Society and Sigma Xi.

❖

Hewitt D. Crane (SM'56) was born on April 27, 1927 in Jersey City, N. J. He received the B.S. degree in electrical engineering from Columbia University, New York, N. Y., in 1947.

H. D. CRANE

His main interest has been in the field of computers. He spent two years on the IBM, SSEC computer, and for four years worked at the Institute for Advanced Study in Princeton, N. J., where he designed the input-output system and a magnetic drum memory for the IAS computer. The following year he joined the magnetics group at RCA Laboratories, Princeton, where he worked on magnetic memory and logic circuits.

At present he is with the Computer Techniques Laboratory at Stanford Research Institute, Menlo Park, Calif., where his main activity is in connection with magnetic devices and circuits.

Mr. Crane is a member of Tau Beta Pi.

❖

E. I. DOUCETTE

E. I. Doucette was born May 21, 1929, in Edinboro, Pa. He received the B.S. and M.S. degrees from Texas College of Arts and Industries in 1953 and the Ph.D. degree from Pennsylvania State University in 1955.

After spending two years in the U. S. Navy as an instructor of mathematics and electronics, Dr. Doucette was associated with Nueces Research Laboratories and Columbia-Southern Chemical Corporation, Corpus Christi, Tex., where he did fundamental work in high-temperature combustion processes, heavy chemical reactions, organic synthesis, and analytical instrumentation.

Since joining Bell Telephone Laboratories, Murray Hill, N. J., he has studied the fundamental properties and deposition of pyrolytic carbon films. He is currently supervising a group in the design and development of new solid-state components.

Dr. Doucette is a member of the American Physical Society, American Chemical Society, and the Electrochemical Society.

❖

Eugene G. Fubini (A'36–SM'46–F'54) was born in Italy on April 19, 1913. He received the Ph.D. degree from the University of Rome, Italy, in 1933.

From 1936 to 1938 Dr. Fubini was engaged in ultra-high-frequency measurements for the National Electric Institute of Italy. Before World War II he also worked for Columbia Broadcasting System, Inc., in the general engineering department, short-wave division, as acting engineer for the installation of VHF links. During 1943 and 1944 Dr. Fubini was a research associate at the Radio Research Laboratory of Harvard University, a technical observer in countermeasure work with the United States Army and Navy in Italy, Corsica, and Africa, and with the United States Air Force in charge of operational analysis, Radar Countermeasures Section, of the Eighth Air Force in England.

E. G. FUBINI

Dr. Fubini joined Airborne Instruments Laboratory, Mineola, N. Y., in 1945. As supervising engineer of the Special Devices Section, he guided work on the development of multidirectional antennas, multiple frequency-selective receivers, information-handling circuits, an automatic Smith Chart impedance plotter, unusual subminiaturization of receivers, microwave slip rings, faired-in antennas, automatic direction-finder systems, and multicouplers. He became co-director of the Research and Engineering Division of AIL in 1955.

❖

S. K. GHANDHI

Sorab K. Ghandhi (S'49–A'52–SM'56) was born on January 1, 1928, in Allahabad, India. He received the B.Sc. (E.E. and M.E.) degree from the Benares Hindu University in 1947. He was a recipient of the J. N. Tata Scholarship in 1947, and obtained the M.S. and Ph.D. degrees in 1948 and 1951, respectively, both from the University of Illinois, Urbana. During the years 1948 to 1950, he held a fellowship in the Graduate School of this University.

Since 1951 he has been a member of the Advanced Circuits Component Department of the Electronics Laboratory, General Electric Company, Syracuse, N. Y. where he has worked in the field of circuit theory and applications of solid-state devices.

Dr. Ghandhi is a co-author of "Transistor Circuit Engineering" and "Principles of Transistor Circuits." He is a member of Eta Kappa Nu, Pi Mu Epsilon, and Phi Kappa Phi.

Edward L. Ginzton (S'39–A'40–SM'46–F'51) was born in Russia on December 27, 1915, and came to the United States in 1929. He received the B.S. degree in electrical engineering in 1936, and the M.S. degree in 1937 from the University of California. He then received the E.E. degree in 1938, and the Ph.D. degree in 1940 from Stanford University.

E. L. GINZTON

Dr. Ginzton is now a professor of applied physics and electrical engineering at Stanford, and is the Director of the Stanford Microwave Laboratory. He has written many papers in the field of electronics and microwave physics, and his text on microwave measurements has recently been published. He is the sole or joint holder of approximately 50 patents on various microwave devices and circuits. Dr. Ginzton has been a member of the Board of Directors of Varian Associates, Inc., Palo Alto, Calif., since that company's organization in 1948.

He is a member of Sigma Xi, Tau Beta Pi, and Eta Kappa Nu. In 1958 he was the recipient of the Morris Leibmann Award presented by the IRE.

❖

E. A. Guillemin (A'41–SM'48–F'49) was born in Milwaukee, Wis., on May 8, 1898. He received the B.S. degree in electrical engineering in 1922 from the University of Wisconsin at Madison and the S.M. degree in electrical engineering in 1924 from Massachusetts Institute of Technology, Cambridge, Mass. In 1926, he received the doctor's degree from the University of Munich, Germany, on the Saltonstall Traveling Fellowship. He returned to M.I.T. as an instructor, becoming assistant professor in 1928, associate professor in 1936, and professor of electrical communications in 1944.

E. A. GUILLEMIN

In 1940, he was appointed consultant to the Microwave Committee of the NDRC. In this capacity he devoted approximately half of his time to consultation with various groups in the Radiation Laboratory, M.I.T., on problems dealing with the design of electrical networks for special applications. In 1941, Dr. Guillemin took over the administrative responsibilities of the Communications Option, Department of Electrical Engineering, at M.I.T.

In 1948, Dr. Guillemin was awarded the President's Certificate of Merit for his outstanding wartime contributions. He is particularly known for two volumes, "Communications Networks," and a reference entitled, "The Mathematics of Circuit Analysis."

He is a Fellow of the AIEE and a member of the ASEE.

❖

Weldon H. Jackson (S'53–A'55–M'55) was born in India on September 14, 1920. During World War II he served with the United States Navy as a student and staff member at the Radio Materiel School. In 1946 he joined the Underwater Ordnance Department of the Naval Ordnance Test Station in Pasadena, Calif., where he was engaged in the design of instrumentation for test facilities.

W. H. JACKSON

Mr. Jackson received the A.A. degree in 1952 from Pasadena City College, and the B.S.E.E. degree from the California Institute of Technology, Pasadena, in 1954.

A member of the technical staff of Bell Telephone Laboratories since 1954, he has participated in the Communications Development Training Program and has worked in the design of components for submarine cables. More recently, his responsibility has been in the design and development of semiconductor devices.

Mr. Jackson is a member of the AIEE and of Tau Beta Pi.

❖

John H. Jasberg (S'42–A'45–M'55) was born in Telluride, Colo. on November 3, 1917. He received the B.S.E.E. degree from the University of Idaho, Moscow, in 1943. From 1943 to 1946, he was a research associate at the Radio Research Laboratory at Harvard University. From 1946 until 1948 he was a graduate student at Stanford University and a research assistant in the Stanford Microwave Laboratory. Since 1948 he has been a research associate at the Microwave Laboratory, working mainly on problems pertaining to high-power klystrons.

J. H. JASBERG

Mr. Jasberg is a member of Sigma Xi and Sigma Tau.

❖

B. Kazan (A'40–SM'55) was born in New York, N. Y., on May 8, 1917. He received the B.S. degree in physics from the California Institute of Technology, Pasadena, Calif., in 1938 and the M.A. degree in physics from Columbia University, New York, in 1940.

He joined the Signal Corps Engineering Laboratories in 1940 and was engaged in early experimental work with radar equipment. From 1944 to 1950, he was Chief of the Special Purpose Tube Section at the Evans Signal Laboratory, where he was responsible for development and application engineering of traveling-wave tubes, klystrons, storage tubes, and transistor devices. From 1951 to 1958 he was engaged in research on television tubes and display devices at the RCA Laboratories. Since July, 1958 he has been associated with the Hughes Research Laboratories, Culver City, Calif., as Head of the Display Panel Section.

B. KAZAN

Mr. Kazan is a member of the American Physical Society, Sigma Xi, and Tau Beta Pi.

❖

Jean V. Lebacqz (M'46–SM'55) was born in Tilff, Belgium, on July 30, 1911. He received the Bachelor's degree in electrical and mechanical engineering in 1933, from the University of Brussels, Belgium, and the E.E. and Ph.D. degrees in 1934 and 1935, respectively, from Stanford University, Stanford, Calif.

J. V. LEBACQZ

From 1939 to 1946, he was an instructor and assistant professor at the University of California in Berkeley and was on leave of absence to the MIT Radiation Laboratory in Cambridge, Mass., from 1943 to 1946. From 1946 to 1951, he was assistant professor of electrical engineering at The Johns Hopkins University, Baltimore, Md. Since then Dr. Lebacqz has been at Stanford University, where he is presently a senior research associate in the Microwave Laboratory. He has been responsible for the development of high-power tunable klystron amplifiers for radar application and the development of high-power traveling-wave tubes.

Dr. Lebacqz is a member of Eta Kappa Nu and Sigma Xi.

❖

Wesley G. Matthei (M'56) was born in Jamaica, N. J., on September 11, 1927. After a brief tour with the U. S. Navy from 1945 to 1946, he entered Hofstra College, Hempstead, N. Y. in 1947. He then transferred in 1948, to the Polytechnic Institute of Brooklyn, Brooklyn, N. Y., where he received the B.S. degree in physics

in 1950. Since that time he has continued graduate work at the Polytechnic Institute of Brooklyn.

W. G. MATTHEI

From 1950 to 1952, he served in the U. S. Army, where he worked on research problems in thermionics at Evans Signal Laboratory in Belmar, N. J. Since that time he has worked on various research and development problems in the field of solid-state devices. At present he is in charge of the Device Research Section of the Solid-State Devices Branch of the U. S. Army Signal Research and Development Laboratory.

Mr. Matthei is a member of the American Physical Society and the American Association for the Advancement of Science.

❖

Theodore S. Saad (A'45–SM'54) was born at West Roxbury, Mass., on September 13, 1920. He received the B.S. degree in electrical engineering in 1941 from the Massachusetts Institute of Technology, Cambridge, Mass.

T. S. SAAD

He has worked at the MIT Radiation Laboratory from 1942 through 1945, and at Submarine Signal Co. from 1945 until March of 1949. From 1949 through 1953, he was vice president and chief engineer of Microwave Development Laboratories. He spent the next year at Sylvania in Woburn, Mass., as a microwave specialist. In early 1955, he was a co-founder of Sage Laboratories, Wellesley, Mass., where he is presently employed.

Mr. Saad is a co-founder of *The Microwave Journal* and chairman of the National Administrative Committee of PGMTT.

❖

Herbert J. Shaw (M'55) was born in Seattle, Wash., on June 2, 1918. He received the B.S. degree from the University of Washington, Seattle, in 1941, and the M.A. and Ph.D. degrees in 1942 and 1948, respectively, from Stanford University, Stanford, Calif.

H. J. SHAW

In 1941 he was a test engineer at the General Electric Co. in Schenectady, N. Y. Since then he has been at Stanford University, where he is presently a senior research associate in the Microwave Laboratory and a research associate in the physics department. He is engaged in research in microwave tubes and microwave physics.

Dr. Shaw is a member of Tau Beta Pi and Sigma Xi.

❖

H. A. Stone, Jr. (SM'56) was born in New York, N. Y., on July 7, 1909. He received the B.S. degree in physics from Yale University, New Haven, Conn., in 1933.

H. A. STONE

Mr. Stone joined the Bell Telephone Laboratories in 1936. Until 1953 he was engaged in the design of inductors. From 1953 to 1958 he was components development engineer at Bell Telephone Laboratories in charge of an organization devoted to the development of inductors, capacitors, and resistors. In 1958, he was appointed director of component development.

Mr. Stone is a member of AIEE.

❖

W. Norris Tuttle (A'26–SM'46–F'49) was born in New York, N. Y., on March 29, 1902. He received the A.B. and S.M. degrees in physics and electrical communication in 1924 and 1926, respectively, from Harvard University, which also awarded him the Ph.D. degree in 1929.

After a year of teaching at Harvard, Dr. Tuttle joined General Radio Company, West Concord, Mass., where he has worked ever since, except for three years spent as Consultant in Operations Research for the Eighth and Twentieth Air Forces. At General Radio he has engaged in research on equipment for measuring modulation and distortion and for measuring vacuum-tube characteristics, on vacuum-tube voltmeters, wave-filter design, parallel-T null circuits, servo circuits, motor speed controls and rectifier test methods.

W. N. TUTTLE

Dr. Tuttle is now Engineering Consultant for General Radio Company, Consultant in Operations Analysis, U. S. Air Force, and a member of the IRE editorial board.

❖

R. M. Warner, Jr., was born in Barberton, Ohio, on March 21, 1922. He received the B.S. degree in physics from Carnegie Institute of Technology, Pittsburgh, Pa., in 1947, and the M.S. and Ph.D. degrees in physics from Case Institute of Technology, Cleveland, Ohio, in 1950 and 1952. His special field of graduate work was nuclear physics.

R. M. WARNER, JR.

Dr. Warner spent 40 months in the Army Signal Corps, serving as radio officer during World War II in both overseas theaters.

He served as physics instructor at both Carnegie Tech and Case Institute, and also worked for two years in the Pittsburgh Plate Glass and Corning Glass Works Research Laboratories. Since 1952 he has been engaged in semiconductor device development at Bell Telephone Laboratories.

He is a member of the American Physical Society, the American Association for the Advancement of Science, Sigma Xi, Tau Beta Pi, and Phi Kappa Phi.

Scanning the Transactions

Will *R*, *L*, and *C* become outmoded concepts? While this may seem to be utterly fanciful thinking, it is a kind of contemplation of the future which should not be disregarded. It is prompted by a serious appraisal of the impact that solid-state electronics may have on the future development of circuits and components. It is notable than in the last two years authorities have repeatedly called attention to the concept of the solid-state circuit, a three-dimensional combination of different types of solid-state materials by which several circuits and devices are merged into a single solid within which currents are transmitted and controlled in the same manner as by arrays of conventional circuits and components. It is pointed out that *R*, *L*, and *C* are mathematical concepts and may in time disappear, since the flow of current in circuits of the future may be controlled by interrelated electrostatic, electromagnetic, and possibly other force fields. As a matter of fact, the trend toward merging circuit and device is already evident in the microwave tube. (P. S. Darnell, "History, present status, and future development of electronic components," IRE TRANS. ON COMPONENT PARTS, September, 1958.)

Magnetic recording of bat cries offers an interesting example of a frequency translation technique that is finding use in a wide variety of scientific fields. The technique consists of recording of phenomenon of interest on magnetic tape and then playing it back at a much higher or lower speed in order to study and analyze the recorded events more easily. The photograph below[1] shows an oscillograph of the frequency modulated ultrasonic cry of a bat. By recording the bat cry on

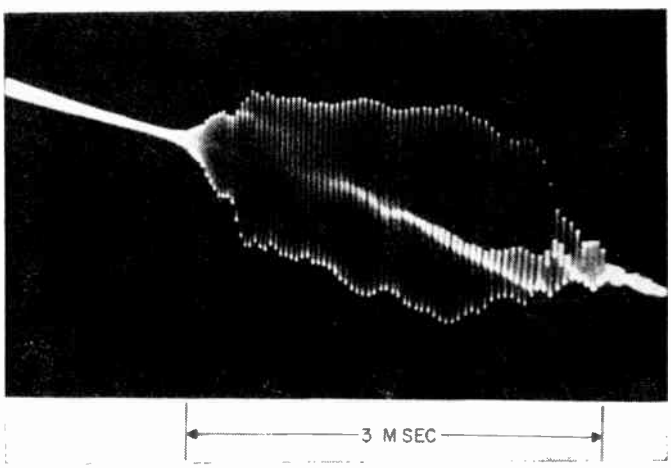

magnetic tape and employing a tape speed reduction of 10 or 20 to 1, the pulses emitted by the bat were transformed into a startling auditory display, and a frequency analysis was carried out conveniently. Moreover, the spacing between pulses, which changes markedly as the bat approaches an obstacle or his prey, could then be measured with a simple stop-watch rather than by electronic timing circuits operating in the ultrasonic frequency range.[2] Other applications of this recording technique may be found in the analysis of mechanical vibrations, pressure fluctuations in wind tunnels, and atmospheric turbulence, to name a few. (F. M. Wiener, "Time and frequency scaling in magnetic recording," IRE TRANS. ON AUDIO, July–August, 1958.)

The progress of progress. We have become so used to miraculous progress in this electronic-nuclear-jet-missile age that it is sometimes difficult to realize how far and how fast we have come. Here is one interesting yardstick of what has been accomplished in the field of propulsion: The engine of Lindberg's "Spirit of St. Louis" would not be powerful enough to energize the starting device on a modern jet engine. (V. I. Weihe, "Navigation and power," IRE TRANS. ON AERONAUTICAL AND NAVIGATIONAL ELECTRONICS, September, 1958.)

Automatic landing of aircraft has moved a step closer to reality with the development of an automatic ground controlled approach system (AGCA) which takes over control of the plane ten miles out and flies it to a release point 2000 feet from touchdown, where the pilot resumes command for a visual landing. At the release point the plane is about 100 feet off the ground, within 30 feet of the ideal glide path, and within 50 feet of the runway centerline. With present nonautomatic GCA systems, landings must be spaced at least two minutes apart. However, the increasing density of air traffic plus the influx of jet planes with their high rates of fuel consumption will soon require that the interval between landings be reduced to as low as 30 seconds. The AGCA system is designed to automatically control six aircraft simultaneously and should come close to meeting the 30-second goal. Although still under test, AGCA shows promise of meeting the stringent demands of the jet age. (R. M. Brooks and W. F. Hoy, "Engineering evaluation of an automatic ground controlled approach system," 1958 IRE NATIONAL CONVENTION RECORD, Part 5.)

Mortality rates and life spans have become as important to electronics as they are to the insurance business. Indeed, a sizeable number of engineers have become actuaries of a sort, collecting and analyzing data on equipment failures and calculating the life probabilities of many types of components. Predicting the life of a piece of equipment is an important but complicated business which involves considering the failure rates of a large variety of components which are interconnected in a complex array. As a matter of general interest we are listing below the results of a recent study to show how various members of the component family stack up against one another as to reliability, and to point out the wide range of failure rates the designer must contend with—nearly 400 to one.

Component	*Failure Rate (%/1000 Hours*
Vacuum tubes	3.4
Motors, dynamotors	2.3
Transistors (estimated)	1.0
Switches	0.7
Relays	0.5
Diodes	0.45
Transformers, inductors, filters	0.4
RF coils	0.15
Connectors	0.07
Capacitors	0.06
Resistors	0.009

(R. L. Vander Hamm, "Component part failure rate analysis for prediction of equipment mean life," 1958 IRE NATIONAL CONVENTION RECORD, Part 6.)

The airborne computer has taken over the cockpit, or so it would seem. One of the latest models to be developed, an all-transistor job, performs all of the following functions for the pilot: dead-reckoning navigation, inertial navigation, Doppler navigation, aircraft control (autopilot), management of fuel consumption, control of various weapon systems, and

[1] From a private communication, D. R. Griffin, Harvard University.

[2] D. R. Griffin, "Listening in the Dark," Yale Univ. Press, New Haven, Conn.; 1958.

self-checking and diagnosis of computer faults. This important new member of the crew weighs about 160 pounds and occupies 3 cubic feet, but subsequent models are expected to have only one-quarter this weight and one-third the volume. (G. L. Hollander, "Transac C-1100: Transistorized computers for airborne and mobile system," IRE TRANS. ON AERONAUTICAL AND NAVIGATIONAL ELECTRONICS, September, 1958).

Spurious radiation is a problem that is not confined only to broadcast and communication services in the middle ranges of the frequency spectrum. The development of pulse radar transmitters of exceedingly high power has created serious problems in the microwave portion of the spectrum. Radar transmitters have been found to radiate relatively large power at spurious frequencies far removed from their own operating frequencies in frequency bands assigned to other radar and communication equipment. Eliminating this cause of interference has been an especially ticklish problem, because these radars transmit a peak power of the same order of magnitude as the breakdown power limit of the waveguide, and exceeding the limit of existing types of waveguide filters that might be utilized to suppress the undesired radiation. A new type of high-power waveguide filter has now been developed which can handle substantially increased amounts of power without incurring serious corona and arcing breakdowns. Thus, a seemingly specialized advance in one component promises to have far-reaching impact on the performance and operating capability of many systems throughout an important segment of the frequency spectrum. (J. H. Vogelman, "High-power microwave filters," IRE TRANS. ON MICROWAVE THEORY AND TECHNIQUES, October, 1958.)

Books

Basic Feedback Control System Design, by C. J. Savant, Jr.

Published (1958) by McGraw-Hill Book Co., 330 W. 42 St., N. Y. 36, N. Y. 350 pages+57 appendix pages+7 index pages+xvi pages. Illus. 9¼×6¼. $9.50.

Feedback control theory is presented in a clear and concise manner, with an emphasis on the root locus approach. Unfortunately, however, the author badly slights the frequency-response approach, although he does present some of the basic frequency-response tools. His justification for this slight appears to be based upon his general thesis that "the root locus method is most convenient for rapid analysis." There are many who would strongly dispute this, and the examples given in the book using the root locus analysis do not appear to offer much substantiation for the author's conclusion.

The book contains two well-written chapters on servomechanism components, including potentiometers, synchros, servomotors, tachometers, gyros, and a variety of other transducers. The various components are described and a number of practical design considerations involving these components are discussed.

Because of the clear and concise method of presentation and the discussion of practical hardware considerations, the book represents a rather good textbook for a basic course in feedback control, provided that the instructor supplements the weakness of the book in the area of frequency-response analysis.

GEORGE A. BIERNSON
Sylvania Electronic Systems
Waltham 54, Mass.

Foundations of Information Theory, by Amiel Feinstein

Published (1958) by McGraw-Hill Book Co., Inc., 330 W. 42 St., N. Y. 36, N. Y. 131 pages+1 index page+3 bibliography pages+x pages. 9¼×6¼. $6.50.

This book is intended to provide an up-to-date, reasonably complete, concise and rigorous exposition of recent activity in the mathematical aspects of information theory. The main mathematical tool used is the theory of probability of finite systems, of measure, and of the Lebesque integral. It is not the author's intention to discuss the problems arising in evolving hardware suggested by his theoretical results.

After two introductory chapters concerned with the properties of the H function, the topics subsequently considered are the properties of the discrete channel without and with memory, and the semicontinuous channel without memory. The last chapter is concerned with the practically important binary symmetric channel, for which such things are considered as the probability of error corresponding to random coding, and parity check symbol codes. About fifty references to recent important work in this field are mentioned. The book is recommended especially for those concerned with the mathematical aspects of information theory.

M. J. DITORO
Polytechnic Research and Development Co.
Brooklyn, N. Y.

Wave Propagation and Antennas, by G. B. Welch

Published (1958) by D. Van Nostrand Co., Inc., 120 Alexander St., Princeton, N. J. 248 pages+5 index pages+2 bibliography pages+viii pages. Illus. 9¼×6¼. $5.75.

This book is an elementary text whose purpose is well expressed by the following quotation from its preface: "Written primarily for readers who are presumed to be familiar with general physics, trigonometry, and a little analytic geometry, this text is designed to provide in general a background knowledge of electromagnetic wave propagation and in particular an understanding of the fundamental principles of antennas."

Chapters 1–6 are essentially devoted to a review of elementary physical optics, in which the concepts more familiar to the beginning student concerning light are related to similar ideas involving radio frequencies. Chapter 7 briefly describes the ionosphere. Chapters 8 and 9 deal with descriptive material relevant to antenna fundamentals and directional systems. A survey of transmission phenomena over the radio spectrum comprises Chapter 10. The text closes with Chapter 11, on waveguides.

The book is apparently written for presentation of this material to the general student. It is at too elementary a level to be of value to engineering and physics students with serious interest in either wave propagation or antennas.

A. H. WAYNICK
Pennsylvania State University
University Park, Pa.

Magnetic Recording Techniques, by W. Earl Stewart

Published (1958) by McGraw-Hill Book Co., Inc., 330 W. 42 St., N. Y. 36, N. Y. 202 pages+4 index pages+ix pages+66 appendix pages. Illus. 9¼×6¼. $8.50.

Unlike some of the texts dealing with magnetic recording, this one gives preference to the treatment of fundamentals rather than to the detailed description of commercial equipment.

The first chapter gives a general introduction to the magnetic recording process, including the theory of dc and ac bias, effect of bias on frequency response and distortion, boundary-displacement recording, and equalization in magnetic recording.

The second deals with the magnetic recording media. The author goes somewhat deeper than has been customary into the descriptions of the composition of magnetic coating, methods of coating, magnetic inks, and typewriter-ribbon-ink. The phenomenon of "print-through," the effects of time and temperature, the erase process, erase heads, and bulk erasing are covered.

In the third chapter the reproducing process is described. Gap loss, contour effect, azimuth misalignment loss, frequency loss, and spacing loss are explained, and playback equalization is treated. The electron-beam

head and other flux-responsive heads are described, and mention is made of special-purpose heads.

Chapter four is devoted to mechanisms, chapter five contains a review of fundamental electromagnetics, and chapter six covers definitions and standards pertinent to magnetic recording.

The end of the book is devoted to reprints of papers on magnetic recording theory by Axon, Begun, Camras, Daniels and others. These provide a more advanced treatment for those who wish to go further in the study of magnetic recording.

The book is well illustrated and indexed. Each chapter includes an extensive bibliography. It could well be used as an upper-class level supplementary college text and as a valuable addition to the reference library.

BENJAMIN B. BAUER
CBS Labs.
Stamford, Conn.

Conductance Curve Design Manual, by K. A. Pullen, Jr.

Published (1958) by John F. Rider, Inc., 116 W. 14 St., N. Y. 11, N. Y. 22 pages+1 index page+2 bibliography pages+xiv pages. 73 Figs. 8½×11. $4.25.

This volume, published in loose-leaf form, summarizes and brings up to date Dr. Pullen's numerous papers and reports on the use of conductance curves in the design of tube circuits.

For some reason that is not made clear, the author appears to have a phobia for the concept of tube amplification factor, and one searches his book in vain for the usual symbol, μ. In showing families of tube characteristics he prefers, for example, to plot curves of plate conductance, g_p, along with the transconductance, g_m, and the static currents. Thus, in computing the gain of a simple resistance-coupled triode amplifier, one substitutes data from the curves into the expression

$$K = \frac{e_p}{e_g} = \frac{-g_m R_L}{1 + g_p R_L},$$

where the term on the right is more familiarly written $\mu R_L/(r_p+R_L)$. The reader is not specifically warned against using what one might here call the classic concepts—$\mu = g_m/g_p = g_m r_p$—but he is not told that it is often convenient to use them.

Dr. Pullen has worked hard during the past ten or more years to convince the engineering profession that his system for displaying and employing tube characteristics greatly simplifies circuit design procedures and yields more precise results. For this labor he is entitled to much credit. On the basis of the new volume, however, this reviewer is strongly of the opinion that tube manufacturers and most engineers will not be eager to adopt the g-curve scheme as preferred practice, if for no other reason than that our present concepts, now more than forty years old, are rather solidly entrenched.

GEORGE D. O'NEILL
Sylvania Electric Products Inc.
Bayside, N. Y.

Vacuum-Tube and Semiconductor Electronics, by Jacob Millman

Published (1958) by McGraw-Hill Book Co., Inc., 330 W. 42 St., N. Y. 36, N. Y. 526 pages+26 appendix pages+12 index pages+77 problems pages+ix pages. Illus. 9¼×6¼. $10.00.

This book has been written for use as a text for third and fourth year electrical engineering students. In the tradition of the author's previous volume ("Electronics" by J. Millman and S. Seely, McGraw-Hill Book Co., Inc., 1951) it develops electronic engineering from the fundamentals of physical processes. The text draws heavily on the earlier volume, and essentially brings it up to date by adding semiconductor devices to the area of vacuum and gas tubes previously covered.

The author first develops the physics of electron behavior in vacuum, solids, and gases in a very readable fashion. A high degree of accuracy is maintained despite the elementary fashion with which such subjects must be treated to get them all into a single text. This exposition of the fundamentals flows smoothly into a discussion of the operating principles of electron devices. Linear equivalent circuits are developed and discussed for diodes, tubes, and transistors. Approximately the last half of the book is devoted to circuit applications where rectifiers, voltage amplifiers, power amplifiers, feedback amplifiers, oscillators, and power supplies are covered. Throughout the book, good example problems are worked out and at the end some 600 problems for the student are given.

The treatment of transistors is well organized and up to date and abundant pertinent references are given at the end of each chapter. The text should give students a balanced, over-all view of present day electronics. This reviewer (who has a vested interest) looks forward to electrical engineers who will have used Professor Millman's text and who will, therefore, start their work with more than a nodding acquaintance with semiconductors.

W. M. WEBSTER
Semiconductor and Materials Div.
RCA
Somerville, N. J.

Abstracts of IRE Transactions

These issues of TRANSACTIONS have recently been published, and are now available from the Institute of Radio Engineers, Inc., 1 East 79th Street, New York 21, N. Y. at the prices indicated. The contents of each issue and, where available, abstracts of technical papers are given on the following pages.

Sponsoring Group	Publication	Group Members	IRE Members	Non-Members*
Aeronautical and Navigational Electronics	Vol. ANE-5, No. 3	$0.90	$1.35	$2.70
Audio	Vol. AU-6, No. 4	0.30	0.45	0.90
Automatic Control	PGAC-6	1.05	1.60	3.15
Component Parts	Vol. CP-5, No. 3	1.15	1.75	3.45
Component Parts	Vol. CP-5, No. 4	0.70	1.05	2.10
Microwave Theory and Techniques	Vol. MTT-6, No. 4	2.50	3.75	7.50

* Libraries and colleges may purchase copies at IRE Member rates.

Aeronautical and Navigational Electronics

Vol. ANE-5, No. 3, September, 1958

Navigation and Power—Vernon I. Weihe (p. 140)

The history of navigation is described briefly, with particular attention to the rapid progress that has taken place since 1940. The problems still to be solved are outlined, and possible directions of future progress in navigation are discussed. The challenge for the future is highlighted by the observation that it is significant that in one hundred and twenty years, mankind has passed the "oats, sonic and thermal barriers," and now is in a position to discuss openly the ultimate speed barrier of all physical matter.

The Display and Use of Navigational Intelligence—A. M. A. Majendie (p. 142)

For future navigation systems the major problems in development will be as much concerned with the presentation and use of data as with its provision. The relationship between a stated operational requirement and the means developed to meet it are discussed on this basis.

The nature of different types of navigational intelligence are considered, and a distinction is drawn between control and monitoring functions.

The navigational task is analyzed, and different types of associated displays are examined. Safety considerations call for a degree of redundancy in a complete system, and the importance of avoiding dependence on a single navigational technique is emphasized.

The Development of Operational Requirements for Civil Avionic Systems—David S. Little (p. 149)

This paper reviews some of the earlier developments of civil avionic equipment design specifications, and describes how the U. S. Flag Air Carriers now arrive at procurement specifications, and how they determine their current operational needs. The responsibilities and activities of ATA, ARINC, AEEC, and RTCA are described and related to the development and coordination of such specifications.

Applying Computers to Air Traffic Control—Howard S. Stokes (p. 152)

The present manual system of air traffic control is described briefly to provide background material for the reader who is not familiar with existing practice. Then follows an outline of the plans for modernization of our national airways system as set forth in the Curtis Report. The body of this paper deals with the plans of Airways Modernization Board for applying computers to air traffic control in its five-year Phase II program.

Transac C-1100: Transistorized Computers for Airborne and Mobile Systems—Gerhard L. Hollander (p. 159)

A pilot's job has become so complex that he must rely increasingly on support from automatic aids for such functions as aircraft stabilization, navigation, cruise control, and landing. The Transac® C-1100 series digital control computers are designed to handle these functions in a single computer for commercial and military aircraft. The C-1100 computers are entirely transistorized for small size and utmost reliability. While their modular structure allows variations in many features for different applications, the computers are characterized by high precision, typically one part in 10^8, and fast operation, typically 60,000 additions per second. The general-purpose stored-program organization allows the C-1100 to be shared by various tasks during flight, and enables the same computer to execute a large variety of operations merely by changing the program. A powerful system of internal and external decisions permits the computer to respond to both the en-route instructions by the pilot and to conditions of the system as sensed in one of the 64 data channels.

A representative problem involving dead-reckoning and VOR-TAC navigation, automatic control of the aircraft, and fuel management illustrates how the computer is programmed. The functional and physical description should provide the reader with enough background to consider the computer in terms of his own application.

Audio

Vol. AU-6, No. 4, July–August, 1958

Time and Frequency Scaling in Magnetic Recording—Francis M. Wiener (p. 81)

An electrical signal recorded on magnetic tape can be relatively easily transposed in frequency by reproducing it at a tape speed different from the tape speed at which it was originally recorded. Transposition into the audio-frequency range is most frequently employed for convenience because of the ready availability of indicating and analyzing equipment in that frequency range. Examples where this technique has been helpful are cited.

Loudspeakers and Negative Impedance—Richard E. Werner (p. 83)

A direct radiator moving coil loudspeaker driven by an amplifier whose output impedance approaches the negative of the blocked voice-coil impedance can be made to exhibit extended low-frequency response with reduced distortion. The results are not to be confused with the effects of a negative resistance source. In a typical case, neutralization of 70 per cent of the blocked voice-coil impedance completely damps the cone resonance, as well as substantially reducing the nonlinear distortion below resonance. When the amplifier is compensated for the falling radiation resistance at low frequencies, uniform output can be obtained to any arbitrary low frequency, limited only by the ultimate power-handling capability of the amplifier and speaker. In this system, no additional amplifier power is required at frequencies down to the speaker resonance; additional power is required below that point.

Automatic Control

PGAC-6, December, 1958

Feedback System Testing—Charles F. White (p. 79)

An analog method of servo system performance testing applicable to experimental analysis and system development and to go—no-go production and maintenance testing has been devised. For a servo system with a forward transfer function G_{ou} and a feedback transfer function G_{ou} the loop actuating signal equals the loop input signal divided by $1+G_{ou}G_{ou}$. The loop actuating signal becomes exactly equal to a test signal if the test signal is multiplied by the factor $1+G_{ou}G_{ou}$ before application to the servo system. The difference between the loop actuating signal of the closed-loop servo system and the arbitrary test signal is continuously zero for the system exactly meeting the specification $G_{ou}G_{ou}$ function simulated in the signal generator. Sinusoidal testing methods are most effective with the servo system loop open. Transient testing (single-event time-domain input) is usually performed on servo systems with the loop closed. The analog method described, as distinguished from transient and sinusoidal methods, uses *time*-domain signals (a step-function signal generator input is found suitable) to obtain *frequency*-domain parameters in a method effectively making an *open-loop test of a closed-loop servo system.*

The $1+G_{ou}G_{ou}$ signal generator is conveniently realized using an analog computer of the operational amplifier type. An alternative mechanization of the signal generator uses only passive elements. Nonlinear as well as linear servo systems may be tested by the method.

Single-integrator, angle-tracking, and range-tracking servo systems have been analyzed. The range-tracking transfer function was employed in an analog computer experiment. Recordings of both the loop actuating signal and the difference between the loop actuating signal and the signal generator input were made for 0, ±6 db, and ±12 db departures from correct gain and for 0, ±1, and ±2 octave departures from correct corner frequency. A study of these recordings revealed potentialities for control of adaptive servo systems.

Considerations in Phase Shifting—M. G. Rekoff, Jr. (p. 89)

The problem of phase shifting is investigated from an ideal viewpoint. The different possibilities of obtaining quadrature voltages at the terminals of an ac servomotor with static impedance elements, connected to the reference winding, are discussed together with the limiting restrictions for each. Formulas for specifying elements of the phase shifting impedance are given in terms of motor constants for several of the more common impedance configurations.

Analysis of Gyro Orientation—Arthur Mayer (p. 93)

The frequency response of a gyro-stabilized platform is limited by the gyros. For the most effective suppression of instability with a minimum sacrifice in bandwidth, it is necessary to orient single-degree-of-freedom gyros in a certain way. Methods of orientation are discussed in this paper.

A Survey of Adaptive Control Systems—J. A. Aseltine, A. R. Mancini, and C. W. Sarture (p. 102)

The various criteria upon which self-optimizing systems have been based are reviewed, and the operation of each type of system is discussed. A new system which is self-optimizing with respect to a measure of impulse response is described, and experimental results are presented.

Stability of Forced Oscillations in Nonlinear Feedback Systems—Ze'ev Bonenn (p. 109)

It has been known for a considerable time that non-linear systems may exhibit multivalued response under external periodic excitation. The stability of these forced oscillations has been extensively investigated for second-order systems and a general criterion for their stability was found. Stability of higher order systems was investigated by means of the incremental describing function. This function must be calculated for every case of interest. In this paper the general criterion formerly derived for second-order systems is extended to higher order systems. Thus it is not necessary to make a special stability investigation in every case.

A Selective Bibliography on Sampled Data Systems—Peter R. Stromer (p. 112)

References have been compiled on the synthesis and analysis of sampling servo systems

as differentiated from continuous servo systems. No attempt has been made to cover material before 1955 except where particular references have been cited by various authors repeatedly, indicating "classic" references in this comparatively new area of feedback control system literature. Items are listed alphabetically by author.

Component Parts

Vol. CP-5, No. 3, September, 1958

History, Present Status, and Future Developments of Electronic Components—Paul S. Darnell (p. 124)

The character of the factors involved in the development of the older kinds of electronic components during the past several decades is examined by considering a few typical components. It is seen that advances in performance capabilities have occurred mainly as a consequence of incremental improvements in materials and processes and not as a result of radically new technology. The extent to which further significant advances may be realized from continued effort along traditional lines is questioned. Attention is called to the rapidly growing area of knowledge in solid-state physics and electronics associated with the development of new solid-state devices during the past decade. It is suggested that the most rapid and significant progress may be made by applying the findings of modern research in physics, chemistry, and electronics to the development of new concepts in devices and methods for accomplishing the electrical functions of the older varieties of component parts.

Intermetallic Semiconductors—Henry T. Minden (p. 129)

The intermetallic semiconductors indium antimonide, indium arsenide, indium phosphide, gallium arsenide, cadmium telluride, mercuric telluride, and bismuth telluride are discussed. Methods of synthesis, purification and single crystal growth are described. Interesting properties of these compounds are examined, and some of their applications listed.

Size Reduction of Airborne Transformers—Ray E. Lee (p. 142)

It is important that transformers for airborne applications be as small as possible. The volume and weight of transformers can be reduced by simplifying the design, and by using better application practices and closer mechanical tolerances. The size can also be reduced by increasing the frequency, current density, coil space factor, or flux density in the transformer. Figs. 1 and 2 show how loss and heat density of the transformer are increased as the size is reduced. Greater heat density can be used if the transformer has improved thermal conductivity, or higher temperature insulation. Performance of a sample transformer using built-in thermal conductors demonstrates the advantage of this system of removing heat. Another sample design using silicone insulation shows how high-temperature materials can be used to reduce size.

By using these techniques, it is possible to reduce greatly the size of transformers. To get best results, all the factors affecting size should be considered in order to select an optimum arrangement.

Component Parts

Vol. CP-5, No. 4, December, 1958

Current Noise and Nonlinearity in Carbon Resistors—T. R. Williams and J. B. Thomas (p. 151)

The relationship between nonlinearity and current noise in carbon resistors is investigated. Results are given for seven different groups of resistors, and they show that there is a correlation between the nonlinearity of a resistor and its current noise: in general, noisy resistors are more nonlinear than quiet ones. The character of the relationship varies considerably among the types tested, and it depends on the construction of the resistor.

Character of Insulator Surface Leakage at High Humidity—S. W. Chaikin and F. M. Church (p. 153)

Dissipation of leakage power in the surface film of water on an insulator at high humidity is thought to cause the observed improvement in surface resistance by elevating the temperature and evaporating part of the water. Surface resistance of a printed circuit test pattern varied from 0.3 to over 3000 megohms in response to the magnitude of electrical potential applied (5 to 400 volts) and the cleanliness of the sample.

In addition to such gradual changes, oscilloscopic observation revealed transient changes, possibly arising from sudden shifting of current paths from one area to another in the surface film of water. Contamination produced transient reductions in resistance as great as 50 per cent. With clean samples, less pronounced and less frequent variations in resistance were observed.

Microwave Theory and Techniques

Vol. MTT-6, No. 4, October, 1958

General Treatment of Klystron Resonant Cavities—Kazuo Fujisawa (p. 344)

Klystron resonant cavities are treated for general cases and their equivalent circuits are theoretically determined, which allows a fairly accurate estimate of resonant properties. It is shown that a reentrant cavity is expressed as a low-frequency series LCR_{se} circuit or a shunt LCR_{sh} circuit, taking L as the inductance of a toroidal coil with one turn and with a cross section the same as the cavity, C as the gap capacitance plus the equivalent capacitance of the cavity, and R_{se} or R_{sh} as the equivalent series or shunt resistance of the cavity at resonance. The introduction of the equivalent cavity capacitance has proved to be very effective.

The formulas derived here enable one to calculate the resonant frequency within an error of a few per cent and the shunt resistance and the Q within an error of several tenths of a per cent in most cases, and thus should prove to be very useful to the designer of microwave circuits.

A Unified Discussion of High-Q Waveguide Filter Design Theory—Henry J. Riblet (p. 359)

For the general design of conventional, high-Q, direct-coupled waveguide filters to be based on the frequency behavior of a classical ladder network prototype, it is necessary and sufficient that the reflecting elements of the filter be replaceable by admittance inverters and that the lengths of transmission line be replaceable by resonant elements. The error due to the latter assumption is of the order of twice the square of the percentage bandwidth measured in guide wavelengths, and the classical synthesis problem is a limiting case of a solvable transmission line problem. In this limit, an exact equivalence is established between the design of a direct-coupled filter and the design of a quarter-wave-coupled filter based on the same ladder network prototype. Design formulas for equal ripple and maximally flat performance are given for the VSWR's of the reflecting elements in terms of dimensionless quantities. Detailed comparison of previous formulas is made.

An Analysis of a Broad-Band Coaxial Hybrid Ring—V. J. Albanese and W. P. Peyser (p. 369)

This paper describes a broad-band coaxial hybrid ring which has excellent isolation and balance characteristics. The ring differs from the conventional hybrid in that the fourth arm has a series-type balun feed and is positioned so that a plane of symmetry exists through two of the arms. Isolation between these arms and balance between the output arms are theoretically independent of frequency. The admittance and VSWR of the input arms are computed by bisecting the ring about the plane of symmetry and employing standard Smith Chart techniques. Corresponding experimental data are included. A comparison is made with the conventional coaxial hybrid ring.

Some Notes on the Optimum Design of Stepped Transmission-Line Transformers—L. Solymar (p. 374)

This paper describes an optimum design of monotonic stepped transmission-line transformers when the reflection coefficient and the bandwidth ratio are prescribed. For the analysis, discontinuity capacitances and reflection interactions are neglected and the validity of the conclusions is therefore restricted to small steps. The analysis is applicable to a multistep transmission line of which the quarter-wave transformer is a special case. In particular, it is shown that if the number of steps is increased from three to five a larger bandwidth may be obtained, but it is not possible to reduce the over-all length in this manner. For a given bandwidth, the shortest taper is always a stepped transmission line and never a continuous one.

Microwave Semiconductor Switching Techniques—R. V. Garver, E. G. Spencer, and M. A. Harper (p. 378)

This paper describes new microwave techniques employing the properties of N-type germanium diode switches. For applications requiring very high isolations, multiple switches are added in tandem. With proper spacing, they form antiresonant cavity circuits. In this case the isolations and insertion losses in db are directly additive. A switch is described which is normally ON and is pulsed OFF. Finally, details are given of a switch in a hybrid-tee configuration in which switching isolations of 50 db are obtained with an insertion loss of 0.7 db.

Microwave Q Measurements in the Presence of Coupling Losses—E. L. Ginzton (p. 383)

In the use of the impedance (Q-circle)

method of measuring the cavity Q values, the presence of losses in the coupling network (between the cavity and the available external terminals) is usually neglected. If appreciable losses are present this simplification is not justified, and its use can lead to significant errors.

The losses in any coupling network can be described by means of an equivalent canonical circuit containing a series and a shunt resistor. The losses due to the series element are immediately apparent from the character of the impedance locus when plotted on a Smith Chart and can be corrected for an "apparent" Q value. However, unless the shunt loss can be determined by a separate calibration of the coupling network, the apparent Q value will be ambiguous because the shunt losses occurring in the coupling network are not distinguishable from those in the cavity proper.

Methods for using the impedance data for determining the Q values are given on the assumption that the coupling network parameters can be found. It is also pointed out that due to the presence of coupling losses the loaded and external Q values are no longer uniquely defined, but their meaning depends upon the application of interest. Formulas relating these to the coupling network parameters are given.

The Excitation of a Dielectric Rod by a Cylindrical Waveguide—C. M. Angulo and W. S. C. Chang (p. 389)

This paper is a theoretical analysis of the excitation of the lowest circular symmetric TM surface wave along an infinite circular dielectric rod by a metallic cylindrical waveguide coaxial with the rod. The asymptotic expressions for all the fields are obtained by means of the Wiener-Hopf method. The expressions for the total average power transmitted to the surface wave, the total average power reflected, and the total power radiated, per unit incident power, are derived and computed for $\epsilon = 2.49$ for various radii of the dielectric rod.

An Investigation of the Properties of Germanium Mixer Crystals at Low Temperatures—L. K. Anderson and A. Hendry (p. 393)

Experimental determinations of the noise temperature ratio, IF resistance, and conversion loss of 1N263 germanium mixer diodes operated in an X-band receiver are presented as a function of mixer temperature for the range -196°C to 27°C. No improvement in receiver noise factor was obtained by cooling the mixer to -196°C; however an improvement of 0.3 to 0.6 db was observed by cooling to a temperature in the region -100°C to -50°C. The exact value of the improvement and the optimum temperature depends on the individual crystal, as well as on dc bias and local oscillator drive.

The Multiple Branch Waveguide Coupler—John Reed (p. 398)

A multiple branch directional coupler is discussed for rectangular waveguide applications for series junctions. A design method is developed which is valid for any coupling ratio and any number of branch lines with perfect match and directivity. The frequency response of this type coupler is calculated with the aid of a digital computer.

Coupled-Transmission-Line Directional Couplers—J. K. Shimizu and E. M. T. Jones (p. 403)

Formulas are presented for the design of coupled-transmission-line directional couplers that are rigorous for any value of coupling. Two basic types are treated in detail; the simplest is one-quarter wavelength long at the center of its frequency band, while the other is three-quarter wavelength long. The quarter-wavelength type can be used over an octave of frequencies with approximately constant coupling, while the three-quarter-wavelength type can be used equally well over more than two octaves. For example, a -3-db coupler of the first type has a variation of ± 0.3 db over a 2:1 band while the second type has the same variation over a 4.5:1 band. Theoretically both types should have infinite directivity at all frequencies. The experimental results for models of these directional couplers have been found to conform very closely to the theoretical coupling functions, while the directivity, although usually good, is limited by discontinuity effects and constructional tolerances.

Design of a Full Waveguide Bandwidth High-Power Isolator—B. J. Duncan and B. Vafiades (p. 411)

An analysis of the microwave fields in rectangular waveguide indicates that circular polarization of the H-vector components exists at two planes only and the location of these planes is frequency dependent. Also, an examination of Kittel's theory reveals that resonance in ferrites can be made to occur at different frequencies for a constant value of dc magnetic biasing field provided the ferrites are characterized by different values of saturation magnetization. These two effects have been used concurrently in the design of an X-band waveguide isolator for operation over a 45 per cent bandwidth, and at high power levels. The theory underlying the design of this isolator is presented. Included is a treatment of the parameters which affect the isolator design. Finally, an operative isolator is described and its experimental characteristics are reported.

Correction to "A Simple Artificial Anisotropic Dielectric Medium"—Robert E. Collin (p. 414)

Wide-Band Microwave Transmission Measuring System—J. B. Linker, Jr., and H. H. Grimm (p. 415)

A relatively broad-band balanced microwave measurement system has been built using a traveling-wave tube amplifier which permits automatic phase and amplitude transmission measurements to be made simultaneously as a function of frequency over the frequency range 8.7 kmc–9.6 kmc. A phase accuracy of ± 1 degree can be achieved for a change of attenuation in the unknown of 24 db. Loss measurements can be made with an accuracy of ± 2 per cent. The bridge is built largely of commercially available components and can be easily duplicated. The basic technique is compatible with additional broad-banding efforts as improved components become available, and it will eventually be applicable to all microwave frequencies.

A Method for Measuring the Directivity of Directional Couplers—G. E. Schafer and R. W. Beatty (p. 419)

This method of measuring directivity requires the measurement of the ratio of powers delivered to the side arm when the normal input arm is connected alternately to an adjustable sliding termination and a sliding short circuit. The short circuit is phased to yield maximum and minimum responses and the amplitudes are averaged. Two techniques of adjusting the termination may be used. One procedure requires zero reflection from the termination. The other procedure requires adjustment for a null at the detector and then measurement of the maximum response due to changing the phase of the termination. The inherent errors of the method are analyzed and found to be within the limits -0.01 to 0.00 db in a specific example.

Development of a High-Power L-Band Resonance Isolator—E. O. Schulz-DuBois, G. J. Wheeler, and M. H. Sirvetz (p. 423)

Waveguide resonance absorption isolators have been developed for use under high peak and average power conditions at L band. Two ferrite materials, one a nickel aluminate ferrite, the other a nickel cobalt ferrite, were developed for this purpose. The characteristics of isolators using these two materials are described.

High-Power Microwave Filters—Joseph H. Vogelman (p. 429)

In order to obtain filters capable of handling very high power, the use of radial lines and uniform line discontinuities was investigated as the most promising approach. In this connection, it was necessary to consider the equivalent circuit and interaction for H-type radial line mated at each end to uniform TE_{10} waveguide for taper angles of 45°. It was found that the equivalent circuit was valid for taper angles of 45°, and that for engineering design purposes the interaction could be neglected. The author utilized the 45° tapers and the uniform lines to design a high-power microwave filter capable of handling 700 kw at 10 pounds pressure in 0.900 by 0.400 ID waveguide. The design procedure for a multielement filter is described utilizing a partly graphical approach.

A Method of Calculating the Characteristic Impedance of a Strip Transmission Line to a Given Degree of Accuracy—Rudolf G. de Buda (p. 440)

The calculation of the characteristic impedance of the strip transmission line TEM-mode can be reduced to the solution of a two-dimensional potential equation with the strip cross section determining the boundary conditions.

Usually this potential equation is solved by conformal mapping, but only the most simple shapes permit exact mapping. Approximations may require considerable work and their accuracy is uncertain.

This paper describes an alternative numerical method which is particularly suitable for boundaries consisting of any number of straight lines and right angles.

It is based on relaxation methods, but by using also variational principles it derives an approximate value for the impedance, and an upper and lower bound with a difference as small as desirable.

Ferrite Line Width Measurements in a Cross-Guide Coupler—Donald C. Stinson (p. 446)

Theoretical and experimental results are presented to show that the line width and the g factor of a spherical ferrite sample can be measured in a cross-guide coupler. The method is much easier to instrument than the usual cavity method and the measurements are much easier to perform. Experimental verification with a cavity perturbation system indicates that the measured quantities are sufficiently accurate for most purposes.

Applications of Directional Filters for Multiplexing Systems—Franklin S. Coale (p. 450)

The design of microwave multiplexing systems for frequency channelization of a broadband microwave spectrum is complicated by problems such as off-resonance mismatch and mutual interaction between adjacent filters. By employing directional filters as basic building blocks, it is possible to construct multiplexing filters with a perfect input match since the input VSWR of a directional filter is theoretically unity both at resonance and off-resonance. Less insertion loss of a manifold may be obtained by the use of directional filters than with conventional band-pass filters. Curves giving the predicted response of a manifold containing n elements are presented for single-tuned and double-tuned directional filters. An asymmetrical response shape is obtained which has a midband insertion loss related to the separation of adjacent channels.

An experimental model consisting of a five-channel multiplexer has been constructed utilizing double-tuned-circular-waveguide directional filters.

Abstracts and References

Compiled by the Radio Research Organization of the Department of Scientific and Industrial Research, London, England, and Published by Arrangement with that Department and the *Electronic and Radio Engineer*, incorporating *Wireless Engineer*, London, England

NOTE: The Institute of Radio Engineers does not have available copes of the publications mentioned in these papers, nor does it have reprints of the articles abstracted. Correspondence regarding these articles and requests for their procurement should be addressed to the individual publications, not to the IRE.

The number in heavy type at the upper left of each Abstract is its Universal Decimal Classification number. The number in heavy type at the top right is the serial number of the abstract. D.C. numbers marked with a dagger (†) must be regarded as provisional.

U.D.C. NUMBERS

Extensions and changes in U.D.C. numbers published in P.E. Notes, up to and including P.E. Note 609, will be introduced in Abstracts and References where applicable, notably the subdivisions of 621.372.8 waveguides published in P.E. Note 594. U.D.C. publications are obtainable from The International Federation for Documentation, Willem Witsenplein 6, The Hague, Netherlands, or from The British Standards Institution, 2 Park Street, London, W.1, England.

The Index to the Abstracts and References published in the PROC. IRE from February, 1957 through January, 1958 is published by the PROC. IRE, May, 1958, Part II. It is also published by *Electronic and Radio engineer*, incorporating *Wireless Engineer*, and included in the March, 1957 issue of that journal. Included with the Index is a selected list of journals scanned for abstracting with publishers' addresses.

ACOUSTICS AND AUDIO FREQUENCIES

534.15:538.56 3663

Proposed Massless Remote Vibration Pickup—C. Stewart. (*J. Acoust. Soc. Amer.*, vol. 30, pp. 644–645; July, 1958.) The method proposed is to transmit a narrow beam of microwave energy to the vibrating surface and detect the resulting phase modulation in the reflected wave. It is estimated that displacement sensitivities below a micron could be obtained using a 20-kw klystron transmitter. The method is also applicable to soil impedance measurements.

534.2 3664

Propagation of Plane Waves of Finite Amplitude—Z. A. Gol'dberg. (*Akust. Zh.*, vol. 3, pp. 322–328; October–December, 1957.) A discontinuity criterion is given for propagation in a viscous thermally conducting medium, and absorption coefficient formulas are derived.

534.2–14 3665

Diffraction and Radiation of Acoustic Waves in Liquids and Gases: Part 1—M. D. Khaskind. (*Akust. Zh.*, vol. 3, pp. 348–359; October–December, 1957.) General theory of hydrodynamic forces.

534.2–14:534.5 3666

The Phenomenon of Amplitude Modulation in Acoustic Combination Waves—G. D. Mikhailov. (*Akust. Zh.*, vol. 3, pp. 376–378; October–December, 1957.) Extension of theoretical treatment noted earlier (1 of 1957) and a note of experimental results obtained using a quartz transducer operating simultaneously at 1.0 and 1.5 mc.

534.2–8:541.135 3667

Effect of Pressure on Ultrasonic Relaxation in Electrolytes—E. H. Carnevale and T. A. Litovitz. (*J. Acoust. Soc. Amer.*, vol. 30, pp. 610–613; July, 1958.) Measurements of ultrasonic absorption and velocity, made on aqueous solutions of ammonia at pressures up to 2030 kg/cm², show that the absorption decreases and the relaxation frequency increases as pressure is raised.

534.231 3668

Axially Symmetric Acoustic Streaming at a Resonator—P. N. Kubanskiĭ. (*Akust. Zh.*, vol. 3, pp. 337–341; October–December, 1957.)

534.231–8:534.26 3669

Diffraction Effects in the Ultrasonic Field of a Piston Source—R. Bass. (*J. Acoust. Soc. Amer.*, vol. 30, pp. 602–605; July, 1958.) A new formula representing apparent attenuation due to diffraction is developed, using the relation defined by Williams (1546 of 1951). Results of measurements made at 1 and 3 mc using a pulse technique confirm the theory qualitatively.

534.26+621.396.812.3 3670

Influence of the Directivity of a Receiving Unit on the Average Intensity of a Signal Received as a Result of Scattering—V. A. Zverev. (*Akust. Zh.*, vol. 3, pp. 329–336; October–December, 1957.) A general expression is derived for the average intensity as a function of scattering angle, and its application to particular cases is noted, including that of a highly directional receiver.

534.6+621.317.3.029.6 3671

Experiments on cm Waves in Analogy with Acoustic Techniques made in Göttingen—E. Meyer. (*J. Acoust. Soc. Amer.*, vol. 30, pp. 624–632; July, 1958.) Measurement techniques in the two fields are compared, with particular emphasis on the use of reverberation chambers. The design and performance of absorbing structures of both resonant and nonresonant types are discussed.

534.613 3672

Torques due to Acoustical Radiation Pressure—G. Maidanik. (*J. Acoust. Soc. Amer.*, vol. 30, pp. 620–623; July, 1958.) A general expression is derived and applied to plane waves incident in an arbitrary direction and to "rigid" plane disks of arbitrary shape.

534.613 3673

Acoustic Radiation Force—H. Olsen, H. Wergeland, and P. J. Westervelt. (*J. Acoust. Soc. Amer.*, vol. 30, pp. 633–634; July, 1958.) Supplementary notes to 2316 of 1957 (Westervelt) and 1611 of 1958 (Olsen *et al.*) are given, including a formula for the force on an arbitrary scatterer, which is derived without making any assumptions about the scatterer.

534.84:621.396.712.3 3674

The Large Auditorium of the Hessischer Rundfunk—H. Schreiber. (*Rundfunktech. Mitt.*, vol. 2, pp. 29–34; February, 1958.) Details of the acoustic design and treatment of the hall are given, as well as a description of the lighting system and control-room equipment.

534.861 3675

Analysis and Measurement of Programme Levels—(*BBC Eng. Div. Monographs*, no. 16, pp. 5–31; March, 1958.)

Part 1—Investigation of Extreme Values of Sound Pressure—D. E. L. Shorter and W. I. Manson, pp. 5–14. Correction, no. 20, p. 23; August, 1958.

Part 2—A Description of an Optical Instrument for Monitoring Sound Signals—E. R. Wigan, pp. 15–31.

534.88 3676

Electronic Sector Scanning—D. G. Tucker, V. G. Welsby, and R. Kendell. (*J. Brit. IRE*, vol. 18, pp. 465–484; August, 1958.) A method is described of providing a rapid scan of an acoustic beam over a sector many times the beam width. The output of each element of a linear array or transducer is changed in frequency by a double-balanced modulator so that phase is retained. The outputs are then combined in a delay line, the ends of which are connected to a double-beam oscillograph giving bearing information over a sector for a continuous frequency sweep. The design of the modulators, delay line, and the choice of sector width are discussed together with display arrangements.

621.395.614:534.6–8 3677

Miniature Piezoelectric Ultrasonic Receivers—E. V. Romanenko. (*Akust. Zh.*, vol. 3, pp. 342–347; October–December, 1957.) Description of the manufacture and calibration of small $BaTiO_3$ receivers with a 0.2-mm detector element. Sensitivity is 0.004–0.007 μV/b over a frequency range of 1–10 mc.

ANTENNAS AND TRANSMISSION LINES

621.372.2 3678

Miniature Delay Lines—R. Gerharz. (*Electronic Radio Eng.*, vol. 35, pp. 371–373; October, 1958.) The construction, which is described briefly, allows lines weighing 50 g and having a volume of 80 cm^3 to be made. Propagation constants for seven experimental lines varied from 0.64 to 0.84. Pulse frequencies from about 5 to 39 mc were obtained.

621.372.2+621.372.8]:537.226 3679

Diffraction of Surface Waves by a Semi-infinite Dielectric Slab—C. M. Angulo. (IRE TRANS. ON ANTENNAS AND PROPAGATION, vol. AP-5, pp. 100–109; January, 1957. Abstract, PROC. IRE, vol. 45, p. 716; May, 1957.)

621.372.8:621.396.65 3680

Microwave Aspects of Waveguides for Long-Distance Transmission—A. E. Karbowiak. (*Proc. IEE*, pt. C, vol. 105, pp. 360–369; September, 1958.) Problems associated with long-range communication systems are discussed, and the circular waveguide excited in the H_{01} mode is shown to be most suitable. The problem of unintentional bends due to ground contours, etc., is analyzed in detail and design criteria are established in terms of the surface impedance. Practical methods for obtaining the desired impedance are considered including the use of surface dielectric coatings and helical waveguides.

621.372.8.001.2 3681

Normal-Modes Methods for Boundary-Excited Waveguides—J. Van Bladel. (*Z. angew. Math. Phys.*, vol. 9a, pp. 193–202; July 25, 1958.)

621.372.821 3682

Shielded Coupled-Strip Transmission Line—S. B. Cohn. (IRE TRANS. ON MICROWAVE THEORY AND TECHNIQUES, vol. MTT-3, pp. 29–38; October, 1955. Abstract, PROC. IRE, vol. 44, p. 276; February, 1956.)

621.372.823 3683

Effect of Ellipticity on Dominant-Mode Axial Ratio in Nominally Circular Waveguides—P. I. Sandsmark. (IRE TRANS. ON MICROWAVE THEORY AND TECHNIQUES, vol. MTT-3, pp. 15–20; October, 1955. Abstract, PROC. IRE, vol. 44, p. 276; February, 1956.)

621.372.825 3684

The Design of Ridged Waveguides—S. Hopper. (IRE TRANS. ON MICROWAVE THEORY AND TECHNIQUES, vol. MTT-3, pp. 20–29; October, 1955.) Practical design curves for single and double-ridged waveguides are given.

621.372.831.25 3685

Step-Twist Waveguide Components—H. A. Wheeler and H. Schwiebert. (IRE TRANS. ON MICROWAVE THEORY AND TECHNIQUES, vol. MTT-3, pp. 44–52; October, 1955. Abstract, PROC. IRE, vol. 44, p. 276; February, 1956.)

621.372.832.43 3686

Intrinsic Directional Coupler using Elliptical Coupling Apertures—J. Figanier and E. A. Ash. (*Proc. IEE*, pt. C, vol. 105, pp. 432–437; September, 1958.) A coupler with a single elliptical hole in the broad face of a rectangular waveguide is analyzed. A filter coupler using two such apertures is also examined. See also 1065 of 1958 (Coale).

621.396.67 3687

A Generalized Form of the Aerial Reciprocity Theorem—J. Brown. (*Proc. IEE*, pt. C, vol. 105, pp. 472–475; September, 1958.) "The reciprocity theorem which relates the transmission and reception properties of an aerial is extended to give information on the phase and amplitude of the signal received by the aerial for an incident plane wave of any polarization. The paper includes a rigorous proof based on the Lorentz reciprocity theorem for electromagnetic fields." See 3689 below.

621.396.67:621.315.668.2 3688

Steel Masts and Towers for the Danish Radio and Television Broadcasting Systems—I. G. Hannemann, B. J. Rambøll, and I. Mogensen. (*Teleteknik, Copenhagen, English Ed.*, vol. 2, no. 1, pp. 1–12; 1958.) Revised and extended version of 1736 of 1952 (Hannemann and Rambøll).

621.396.67.012.12 3689

A Theoretical Analysis of some Errors in Aerial Measurements—J. Brown. (*Proc. IEE*, pt. C, vol. 105, pp. 343–351; September, 1958.) The reciprocity theorem is used to derive an expression for the power received by one antenna as a result of transmission from a second similar antenna at any distance from the first. Under conditions of antenna measurements the size of the receiving antenna can influence the errors in measured radiation patterns and power gains. The errors differ from those predicted by diffraction theory.

621.396.674.3.011.21 3690

Measured Self-Impedance of a Dipole Antenna near a Conducting Cylinder of Elliptical Cross-Section—T. Y. Wong. (*Can. J. Phys.*, vol. 36, pp. 855–857; July, 1958.)

621.396.677:523.164 3691

A New Type of Pencil Beam Aerial for Radio Astronomy—J. H. Blythe. (*Mon. Not. R. Astr. Soc.*, vol. 117, no. 6, pp. 644–651; 1957.) In the interferometric technique described, a long narrow aperture and a small moving antenna are used at 38 mc, and phase-switch records obtained at a number of different spacings are combined to give an effective beamwidth of 2.2°. Limitations are discussed. For results see 3792 below.

621.396.677.3 3692

Optimum Stacking Spacing in Antenna Arrays—H. W. Kasper, (*QST*, vol. 42, pp. 40–43; April, 1958.) Principles are outlined and general design information given in graphical form, relating spacing to source beamwidth.

621.396.677.5 3693

Loop Antenna Measurements—P. A. Kennedy. (IRE TRANS. ON ANTENNAS AND PROPAGATION, vol. AP-4, pp. 610–618; Abstract, PROC. IRE, vol. 45, p. 571; April, 1957.)

621.396.677.6:621.396.93 3694

The Effect of Mutual Impedance on the Spacing Error of an Eight-Element Adcock—Travers. (See 3828.)

621.396.677.71 3695

Circularly Polarized Slot Radiators—A. J. Simmons. (IRE TRANS. ON ANTENNAS AND PROPAGATION, vol. AP-5, pp. 31–36; January, 1957. Abstract, PROC. IRE, vol. 45, p. 715; May, 1957.)

621.396.677.71 3696

Radiation Characteristics with Power Gain for Slots on a Sphere—Y. Mushiake and R. E. Webster. (IRE TRANS. ON ANTENNAS AND PROPAGATION, vol. AP-5, pp. 47–55; January, 1957. Abstract, PROC. IRE, vol. 45, p. 715; May, 1957.)

621.396.677.71 3697

Cylindrical Radio Waves—S. Sensiper. (IRE TRANS. ON ANTENNAS AND PROPAGATION, vol. AP-5, pp. 56–70; January, 1957. Abstract, PROC. IRE, vol. 45, p. 715; May, 1957.)

621.396.677.73 3698

Circularly Polarized Biconical Horns—C. Goatley and F. D. Green. (IRE TRANS. ON ANTENNAS AND PROPAGATION, vol. AP-4, pp. 592–596; October, 1957. Abstract, PROC. IRE, vol. 45, p. 570; April, 1957.)

621.396.677.8 3699

Phase Centres of Microwave Antennas—D. Carter. (IRE TRANS. ON ANTENNAS AND PROPAGATION, vol. AP-4, pp. 597–600; October, 1956. Abstract, PROC. IRE, vol. 45, p. 570; April, 1957.)

621.396.677.83.095 3700

Radiation by Disks and Conical Structure—A. Leitner and C. P. Wells. (IRE TRANS. ON ANTENNAS AND PROPAGATION, vol. AP-4, pp. 637–640; October, 1956. Abstract, PROC. IRE, vol. 45, p. 571; April, 1957.)

621.396.677.833.2 3701

The Image Method of Beam Shaping—P. T. Hutchison. (IRE TRANS. ON ANTENNAS AND PROPAGATION, vol. AP-4, pp. 604–609; October, 1956. Abstract, PROC. IRE, vol. 45, pp. 570–571; April, 1957.)

621.396.677.85 3702

Measured Phase Distribution in the Image Space of a Microwave Lens—G. W. Farnell. (*Can. J. Phys.*, vol. 36, pp. 935–943; July, 1958.) Contours of constant phase at 3.2 cm λ are shown for a solid-dielectric aberration-free lens; extra detail is given near certain phase singularities which occur. Agreement is obtained with scalar diffraction theory. See also 29 of 1958 (Bachynski and Bekefi).

621.396.677.85 3703

A Design Procedure for Dielectric Microwave Lenses of Large Aperture Ratio and Large Scanning Angle—F. S. Holt and A. Mayer. (IRE TRANS. ON ANTENNAS AND PROPAGATION, vol. AP-5, pp. 25–30; January, 1957. Abstract, PROC. IRE, vol. 45, p. 715; May, 1957.)

621.396.677.85:537.226 3704

The Fields Associated with an Interface between Free Space and an Artificial Dielectric—J. Brown and J. S. Seeley. (*Proc. IEE*, pt. C, vol. 105, pp. 465–471; September, 1958.) An approximate solution is obtained for the metal-strip dielectric in terms of evanescent waves inside the dielectric and in free space. Measured values for an equivalent circuit agree with the calculated values. See also 1367 of 1955 (Brown and Jackson).

AUTOMATIC COMPUTERS

681.142 3705

Short-Cut Multiplication and Division in Automatic Binary Digital Computers—M. Lehman. (*Proc. IEE*, pt. B, vol. 105, pp. 496–504; September, 1958.) A modified short-cut process is proposed and the application of such procedures to restoring or nonrestoring division techniques is discussed.

681.142 3706

A Full Binary Adder employing Two Negative-Resistance Diodes—J. W. Horton and A. G. Anderson. (*IBM J. Res. and Dev.*, vol. 2, pp. 223–231; July, 1958.) This adder provides outputs which are virtually in coincidence with the input signal. A full adder is described using positive-gap diodes of the type described by Reeves and Cooke (3772 of 1955) which operate with 20-mμs pulses.

681.142 3707

TRADIC: the First Phase—J. R. Harris. (*Bell Lab. Rec.*, vol. 36, pp. 330–334; September, 1958.) A general report is given of the equipment which was designed and built to test the feasibility of airborne digital computers using transistors.

681.142 3708
An Analogue-Computer Study of the Transient Behaviour and Stability Characteristics of Serial-Type Digital Data Systems—O. I. Elgerd. (*Commun. and Electronics*, no. 37, pp. 358–366; July, 1958.) The transient characteristics of sampled-data computer systems incorporating a holding circuit are examined, with particular emphasis on the transient response to a standard input step-function.

681.142 3709
Transistorized Analogue—Digital Converter—W. B. Towles. (*Electronics*, vol. 31, pp. 90–93; August 1, 1958.) The analog /digital converter described has a power consumption of less than 4 w, and codes input signals up to 5 v at a maximum sampling rate of 5000 inputs with errors not exceeding 0.5; the output is at the rate of 100,000 digits. The volume of the unit is 160 in^3.

681.142 3710
A Direct-Reading Printed-Circuit Commutator for Analogue-to-Digital Data Conversion—C. A. Walton. (*IBM J. Res. and Dev.*, vol. 2, pp. 178–192; July, 1958.) The disk-type commutator described supplies the digital signal required for output equipment operation without the need for supplementary coding or additional translation circuitry to remove ambiguities.

681.142:621–52 3711
Function Tables in Digital Control Computers—E. J. Schubert. (*Commun. and Electronics*, no. 37, pp. 316–319; July, 1958.) Stored function tables, with appropriate interpolation techniques, can be used with advantage in digital control computers where there are limitations on space and computing time, *e.g.*, the control loop of servo systems.

681.142:621.318.134:621.318.57 3712
A Load-Sharing Matrix Switch—G. Constantine, Jr. (*IBM J. Res. and Dev.*, vol. 2, pp. 205–211; July, 1958.) A matrix-switch winding pattern has been developed which allows the power from several pulse generators to be combined in a single high-power pulse to drive a computer core-type storage system. This pulse may be directed into one of a group of outputs; an example with 16 outputs is given.

CIRCUITS AND CIRCUIT ELEMENTS

621.3.049–181.4:621.318.5 3713
Miniaturization Design Techniques—J. S. Zimmer. (*Electronic Equip. Eng.*, vol. 6, pp. 37–38; July, 1958.) The construction of an em relay is described as an example.

621.3.049.75 3714
Reliable Printed Wiring without Hole Pads—G. F. Leyonmark. (*Electronic Equip. Eng.*, vol. 6, pp. 43–45; July, 1958.) A "plated-hole" technique is described.

621.314.2:621.372.45 3715
An Electronic Transformer—T. G. Clark. (*Electronic Eng.*, vol. 30, pp. 545–548; September, 1958.) The anode-follower circuit is used as a transformer in a cable system where signals are distributed from a master generator to a number of separate displays. The load on the source is negligible, the voltage transformation is independent of the impedance transformation, both being controllable, the cable may be matched if necessary, and the system bandwidth is inversely proportional to the cable length.

621.316.825 3716
Large-Signal Behaviour of Directly Heated Thermistors—S. Ekelöf, N. Björk, and R. Davidson. (*Acta polyt., Stockholm*, no. 216, 31 pp.; 1957. *Chalmers tek. Högsk. Handl.*, no. 185; 1957.) Part 3 of a study of thermistor circuits. Part 1: 3481 of 1954 (Ekelöf and Kilulberg); Part 2: *Chalmers tek. Högsk. Handl.*, no. 169 (Björk and Davidson); 1955.

621.316.825:621.375.4 3717
Temperature Compensating Networks—H. D. Polishuk. (*Electronic Radio Eng.*, vol. 35, pp. 373–377; October, 1958.) "A generalized analytical design procedure is proposed for the realization of two typical temperature-compensating bias networks, employing thermistors, for class-B push-pull transistor amplifiers. A set of simple relations is derived for evaluating the network component values, and restrictions are indicated on the choice of appropriate thermistors."

621.318.4 3718
The Spherical Coil as an Inductor, Shield, or Antenna—H. A. Wheeler. (PROC. IRE, vol. 46, pp. 1595–1602; September, 1958.) The coil is a single-layer winding of constant axial pitch on a spherical surface. Its properties can be expressed by simple formulas, and can be used to evaluate the shielding effect of a closed nonmagnetic metal shell. Resonance effects are studied.

621.318.435 3719
Applications of Nonlinear Magnetics—H. F. Storm. (*Commun. and Electronics*, no. 37, pp. 380–388; July, 1958.) It is shown how saturable-core reactors may be used in such applications as counters, timers, voltage and current references, frequency multipliers, firing circuits for thyratrons and ignitrons, pulse-shaping circuits for magnetrons, rectifying circuits, bistable flip-flops, frequency detectors, and square-wave oscillators; 82 references.

621.318.57 3720
Minimization of Components in Electronic Switching Circuits—T. J. Beatson. (*Commun. and Electronics*, no. 37, pp. 283–291; July, 1958. Discussion.) The details are given of a method which uses Boolean functions to design switching circuits using minimum number of diodes or transistors.

621.318.57 3721
Some Comments on Minimum Triggering Signals—J. L. Dautremont, Jr. (PROC. IRE, vol. 46, pp. 1654–1655; September, 1958.) A theorem on the energy transfer characteristics of a linear network is proved. See also 1994 of 1958 (Beattie).

621.372:621.376.3 3722
The Response of a Network to a Frequency-Modulated Input Voltage—J. W. Head and C. G. Mayo. (*Proc. IEE*, Pt. C., vol. 105, pp. 509–512; September, 1958.) Mathematical treatment illustrating the relative simplicity of the method of operational calculus.

621.372.011.1 3723
An Exact Theory of *N*-Component Steady-State Operators for Linear Circuits—A. J. O. Cruickshank. (*Proc. IEE*, Pt. C, vol. 105, pp. 513–518; September, 1958.) See also 1997 of 1958.

621.372.2 3724
Unstable Linear Systems and the Minimum Phase Condition—P. E. Pfeiffer. (*J. Franklin Inst.*, vol. 265, pp. 291–301; April, 1958.) The relations between transfer functions for unstable systems and the class of minimum-phase transfer functions are examined.

621.372.41:621.318.424 3725
The Limits of the Regions of Stability of the Normal State in certain Ferroresonant Circuits—M. Panet. (*Compt. Rend. Acad. Sci., Paris*, vol. 246, pp. 85–87; January 6, 1958.) The unequal voltage distribution between the two identical resonance circuits referred to in 1350 of 1958 is explained by periodic variations in coil inductance.

621.372.45 3726
Multi-gain Representation for a Single-Valued Nonlinearity with Several Inputs, and the Evaluation of their Equivalent Gains by a Cursor Method—M. J. Somerville and D. P. Atherton. (*Proc. IEE*, pt. C, vol. 105, pp. 537–549; September, 1958.)

621.372.5 3727
Radio Engineering Use of the Cayley-Klein Model of Three-Dimensional Hyperbolic Space—E. F. Bolinder. (PROC. IRE, vol. 46, pp. 1650–1651; September, 1958.) Applications to the solution of network problems are outlined. See also 3768 of 1957.

621.372.5 3728
Some Optimum Four-Terminal Networks having Given Input and Output Shunt Capacitances—O. P. D. Cutteridge. (*Proc. IEE*, pt. C, vol. 105, pp. 398–403; September, 1958.)

621.372.5:621.376.23:621.396.822 3729
Optimum Network Functions for the Sampling of Signals in Noise—H. S. Heaps and M. R. McKay. (*Proc. IEE*, pt. C, vol. 105, pp. 438–443; September, 1958. Discussion, p. 443.) Transfer functions are calculated for networks which maximize a) the ratio between the average amplitude of n successive samples of the output signal and the rms output noise, and b) a continuous sample of the output.

621.372.57 3730
Active Band-Pass Filter has Sharp Cut-Off—J. R. MacDonald. (*Electronics*, vol. 31, pp. 84–87; August 15, 1958.) An adjustable, RC AF filter having Butterworth attenuation characteristics and 42 db/octave cutoff slope is described. Outputs of 50 volts rms can be obtained without appreciable harmonic distortion. The dynamic range exceeds 100 db.

621.373.4.072.9 3731
On the Discrimination of a Synchronized Oscillator against Interference Accompanying the Synchronizing Signal—R. Spence and A. R. Boothroyd. (*Proc. IEE*, pt. C, vol. 105, pp. 519–526; September, 1958.) The response of the oscillator to an interfering signal is investigated when the interference component of the oscillator output is small. The response is found to be linear, and the discrimination is expressed analytically. The experimental results are in good agreement with theory.

621.373.43 3732
Simplified Design of Pulse-Forming Networks—K. H. Recorr. (*Electronics*, vol. 31, p. 94; August 1, 1958.) The network consists of a five-section capacitive circuit and a single-layer continuously-wound tapped solenoid.

621.373.52:621.318.57 3733
Designing Transistor Circuits—Switching Dynamics—R. B. Hurley. (*Electronic Equip. Eng.*, vol. 6, pp. 30–34; July, 1958.) Equivalent-circuit data for determining over-all response time are tabulated for basic transistor switches with an applied input step for the underdriven condition. The overdriven case is also considered. See also 2667 of 1958.

621.373.52:621.395.43 3734
Transistor Pulse Generators for Time-Division Multiplex—K. W. Cattermole. (*Proc. IEE*, pt. B, vol. 105, pp. 471–479; September, 1958. Discussion, pp. 479–482.) "Point-contact transistor circuits to generate pulses in the microsecond range are described, together with means of frequency-dividing and interlacing pulse trains and their application to time-division operation of telephone transmission and switching systems."

621.374.32 3735
Build-Up of Large Signals with Elimination of Reflections in Magnetostrictive Storage Lines by means of Multicoil Transducers—D. Maeder. (*Helv. phys. Acta*, vol. 30, pp. 347–352; August 15, 1957. In German, with English summary.) An ultrasonic storage delay line using 12 transducer coils and a stainless-steel wire 18 m long has a capacity of 300 decimal places. See 69 of 1958.

621.375.1012 3736
Amplifier Delay Charts—J. B. Harrington. (*Electronics*, vol. 31, pp. 88–90; August 15, 1958.) The time delay in various types of amplifiers due to the network phase shift can be determined from the series of charts given, if the amplifier bandwidth and number of stages are known.

621.375.13:621-52 3737
Relating the Nyquist Plot to the Root-Locus Plot—W. G. Johnston. (*J. Electronics Control*, vol. 5, pp. 89–96; July, 1958.)

621.375.3:621.318.57:621.314.7 3738
High-Efficiency Push-Pull Magnetic Amplifiers with Transistors as Switched Rectifiers—A. G. Milnes. (*Commun. and Electronics*, no. 37, pp. 327–330; July, 1958. Discussion, pp. 330–331.) Various circuits are considered in which the efficiencies exceed 50 per cent. They are particularly suitable where the available power supply is limited.

621.375.4:538.632 3739
A Simple Transistor Amplifier for Energizing a Hall Multiplier—D. J. Lloyd. (*Electronic Eng.*, vol. 30, pp. 560–561; September, 1958.)

621.375.4.018.7 3740
Nonlinear Distortion in Transistor Amplifiers at Low Signal Levels and Low Frequencies—N. I. Meyer. (*Proc. IEE*, pt. C, vol. 105, pp. 550–552; September, 1958.) Discussion on 2392 of 1957.

621.375.4.029.5:621.397.6 3741
Transistor Video Amplifiers—P. H. Helsdon. (*Marconi Rev.*, vol. 21, no. 129, pp. 56–75; 2nd quarter, 1958.) The principles of design of iterated video amplifiers using transistors are discussed in terms of a simplified hybrid-π equivalent circuit. The design and performance of an experimental television video distribution amplifier are described.

621.375.9:538.569.4 3742
Polarization of a Molecular Beam by an Alternating Field with Variable Amplitude and Phase—Lyubimov and Khokhlov. (See 3781.)

621.375.9:538.569.4 3743
Nonlinear Effects of the Interaction of Resonance Fields in the Molecular Generator and Amplifier—V. M. Kontorovich and A. M. Prokhorov. (*Zh. eksp. teor. Fiz.*, vol. 33, pp. 1428–1430; December, 1957.) Analysis of a molecular oscillator with an auxiliary field [see 402 of 1956 (Basov and Prokhorov)], based on the polarizability of a quantum system situated in two resonance fields. Such a system can operate at two frequencies which depend on the amplitude as well as the frequency of the auxiliary field.

621.375.9:538.569.4.029.6 3744
Susceptibility of the Three-Level Maser—A. M. Clogston. (*Phys. Chem. Solids*, vol. 4, no. 4, pp. 271–277; 1958.) The susceptibility presented to a radiation field of frequency $(E_3-E_2)/h$ by the paramagnetic material is calculated. The effect of the cavity reaction at the frequency $(E_2-E_1)/h$ is conisdered. The line shape is shown to be drastically altered for large-amplitude driving fields.

621.375.9:538.569.4.029.6:621.396.822 3745
Noise in Maser Amplifiers—Theory and Experiment—J. P. Gordon and L. D. White. (Proc. IRE, vol. 46, pp. 1588–1594; September, 1958.) The theoretical treatment is based on an equivalent microwave circuit. The effective input noise temperature of a reflection-type NH_3 beam maser was found experimentally to be 80°K, which is in agreement with theory. An upper limit of 20° K for the "beam temperature" was deduced. See also 737 of 1958.

621.375.9.029.6:538.569.4:538.221 3746
Quantum Analogue of the Ferromagnetic Microwave Amplifier—H. Suhl. (*Phys. Chem. Solids*, vol. 4, No. 4, pp. 278–282; 1958.) "Certain resemblances between the modes of operation of the three-level maser and the ferromagnetic microwave amplifier are shown to be superficial by constructing a quantum-mechanical model of the latter device. It is shown that while establishment of a negative temperature for two levels is essential in the three-level maser, it is inessential in the analogue of the ferromagnetic amplifier, which in essence depends only on the time-varying part of the density matrix." See also 3076 of 1957.

621.375.9.029.6:538.569.4:538.221 3747
Phase Dependence of a Ferromagnetic Microwave Amplifier—W. L. Whirry and F. B. Wang. (Proc. IRE, vol. 46, pp. 1657–1658; September, 1958.) The phase-dependent operation of an amplifier using polycrystalline yttrium garnet is shown experimentally.

621.375.9.029.6:621.372.413 3748
Minimum Noise Figure of a Parametric Amplifier—H. Heffner and G. Wade. (*J. Appl. Phys.*, vol. 29, p. 1262; August, 1958.) With the aid of a circulator the noise figure may be made to approach the minimum value ω_p/ω_2 where ω_p is the pumping and ω_2 the output frequency.

621.375.9.029.63:621.3.011.23 3749
A Low-Noise Nonlinear-Reactance Travelling-Wave Amplifier—R. S. Engelbrecht. (Proc. IRE, vol. 46, p. 1655; September, 1958.) Results obtained with an experimental model for 380 mc using nonlinear capacitances are given. See also 2035 of 1958 (Tien and Suhl).

621.376.223 3750
A Rectifier Modulator with Stable Low Carrier-Leak—E. Hands. (*Proc. IEE*, pt. C., vol. 105, pp. 381–390; September, 1958.) The action of a constant-current ring modulator in which the input transformer is replaced by high-impedance tube circuits is analyzed in detail. The theoretical analysis is confirmed experimentally using a 3-kc carrier frequency. Stable carrier—leak levels more than 90 db below the carrier current from each source are possible.

621.376.5:621.372.632 3751
Pulse Modulation Transmitted through a Linearly Modulated Transit-Time Device—V. Met. (Proc. IRE, vol. 46, pp. 1656–1657; September, 1958.) A discussion of basic principles with reference to the serrodyne device [1366 of 1957 (Cumming)], and their application to frequency shifting, computers, pulse duplexing and a multiple reflex-pulse amplifier.

GENERAL PHYSICS

53.081.6 3752
New Physical Constants from Dimensional Analysis—A. T. Gresky. (*J. Franklin Inst.*, vol. 265, pp. 85–95; February, 1958.) Three quantities are formulated which represent constants of astronomy and classical mechanics and of submicroscopic physics, and which correlate phenomena in electromagnetic, quantum and classical physics.

530.112:530.12:531.18 3753
The Special Theory of Relativity and the Ether—A. Metz. (*Compt. rend. Acad. Sci., Paris*, vol. 245, pp. 2197–2198; December 16, 1957.) Datzeff's theory (1381 of 1958) is held to be quite untenable.

530.12:535.13 3754
Spherically Symmetric Solution of the General Relativity Equations taking the Tensor of Born-Infeld Electromagnetic Theory as Energy-Momentum Tensor—J. Lameau. (*Compt. rend. Acad. Sci., Paris*, vol. 245, pp. 2208–2210; December 15, 1957.)

537.122 3755
Theoretical Problem Posed by an Extended Model of the Electron and the Proton—E. J. Sternglass. (*Compt. rend. Acad. Sci., Paris*, vol. 246, pp. 1386–1389; March 3, 1958.) Arguments about the stability and relativistic properties of elementary particles taken as extended sources of em fields are considered.

537.311.1 3756
The Physical Interpretation of Mean Free Path and the Integral Method—P. J. Price. (*IBM J. Res. and Dev.*, vol. 2, pp. 200–203; July, 1958.) An extension of previous theoretical work on electron transport in solids. See 90 of 1958 and *IBM J. Res. and Dev.*, vol. 1, pp. 239–248; July, 1957.

537.311.1 3757
Generalization of the Variation Principle in the Theory of Electrical Conductivity—V. Glaser and B. Jakšić. (*Nuovo Cim.*, vol. 7, pp. 259–262; January 16, 1958. In English.)

537.311.62 3758
Theory of the Anomalous Skin Effect in Normal and Superconducting Metals—D. C. Mattis and J. Bardeen. (*Phys. Rev.*, vol. 111, pp. 412–417; July 15, 1958.) The current density in a normal metal in which the electric field varies over a mean free path is derived from a quantum approach in which use is made of the density matrix in the presence of scattering centers but in the absence of the field. The method is applied to superconductors.

537.311.62:538.63 3759
Anomalous Skin Effect in a Magnetic Field—D. C. Mattis and G. Dresselhaus. (*Phys. Rev.*, vol. 111, pp. 403–411; July 15, 1958.) A classical and quantum mechanical derivation of cyclotron resonance in metals is given. The quantum derivation yields the same result as the classical calculation except in the limit of low quantum numbers or high magnetic fields.

537.52 3760
Noise and Electron Temperatures of some Cold-Cathode Argon Discharges—E. W. Collings. (*J. Appl. Phys.*, vol. 29, pp. 1215–1219; August, 1958.) Noise temperatures at 3 kmc are compared with the corresponding electron temperatures for the positive columns of some cold-cathode discharges in A; they are found to be in close agreement. The discharges give reproducible results and are recommended for use as noise standards.

537.525:538.69 3761
The Townsend Discharge in a Coaxial Diode with Axial Magnetic Field—P. A. Redhead. (*Can. J. Phys.*, vol. 36, pp. 255–270; March, 1958.) An approximate theory of the striking characteristics of coaxial cylinders in an axial magnetic field, taking into account the effects of elastic collisions of the electrons. Measurements in the pressure range 10^{-3}–10^{-9} mm Hg are in general agreement with the theory.

537.533 3762
The Fresnel Biprism in Electron Optics; Influence of the Size of the Source; Effect of a Periodic Voltage Applied to the Wire of the Biprism—J. Faget, J. Ferré, and C. Fert. (*Compt. rend. Acad. Sci., Paris*, vol. 246, pp. 1404–1407; March 3, 1958.) See 1393 of 1957 (Faget and Fert).

537.533.7:538.561 3763
Contribution to the Theory of Transition Radiation—G. M. Garibyan. (*Zh. Eksp. Teor. Fiz.*, vol. 33, pp. 1403–1410; December, 1957.) The transition radiation and Cherenkov radiation produced when a charged particle moves in succession through two media of different dielectric and magnetic properties are considered. The cases in which one medium is a vacuum are discussed in detail. See also 3829 of 1957 (Pafomov).

537.56 3764
Apparatus for Producing Plasma Beams—E. R. Harrison and R. H. Dawton. (*J. Electronics Control*, vol. 5, pp. 29–32; July, 1958.) A brief account is given of simple apparatus and experiments conducted with it.

537.56 3765
Effect of Electron Exchange on the Dispersion Relation of Plasma Oscillations—H. Kanazawa and S. Tani. (*Progr. Theoret. Phys. (Kyoto)*, vol. 19, pp. 153–158; February, 1958.) The dispersion relation is derived from a canonical transformation slightly different from that of Bohm and Pines (1375 of 1954). A correction factor is introduced for electron exchange effects but agreement between theory and experiment is not thereby improved.

537.581 3766
Model for the Surface Potential Barrier and the Periodic Deviations in the Schottky Effect—P. H. Cutler and J. J. Gibbons. (*Phys. Rev.*, vol. 111, pp. 394–402; July 15, 1958.) The model is based on the quantum-mechanical calculation by Bardeen (*ibid.*, vol. 49, pp. 653–663; May 1, 1936) on the form of the potential at the surface of a sodium-like metal and the analysis of Sachs and Dexter (*J. Appl. Phys.*, vol. 21, pp. 1304–1308; December, 1950) on the quantum limits of the image-face theory. The periodic deviations are recalculated and results compared with previous theory and experiment.

538.114 3767
Remarks on Spin-Wave Theory for the Ferromagnetic Exchange Problem—I. Mannari. (*Progr. Theor. Phys.*, vol. 19, pp. 201–213; February, 1958.) A theory is developed which is essentially equivalent to the Bloch-Bethe-Van Kranendonk formalism [see 2025 of 1956 (Van Kranendonk)]. Thermodynamic properties below the Curie point are fully treated.

538.311:621.318.4 3768
The Production of very Homogeneous Axially Symmetric Magnetic Fields—H. Primas and H. H. Günthard. (*Helv. Phys. Acta*, vol. 30, pp. 331–346; August 15, 1957. In German.) Inhomogeneity in the magnetic field between two pole pieces is due to irregularity in the pole piece and to boundary effects which may be reduced by "current shims" in the form of compensating coils.

538.312 3769
Electromagnetic Energy Transfer—P. Hammond. (*Proc. IEE*, pt. C, vol. 105, no. 8, pp. 352–358; September, 1958. Discussion, p. 359.) "Methods of calculating and measuring the flow of electromagnetic energy are compared and contrasted. The differences between the low-frequency and high-frequency approaches to energy flow problems are discussed and suggestions are made to ease the difficulties in the way of students and teachers faced with these apparently irreconcilable differences."

538.56.029.6:538.615 3770
Microwave Zeeman Effect and Theory of Complex Spectra—F. R. Innes and C. W. Ufford. (*Phys. Rev.*, vol. 111, pp. 194–202; July 1, 1958.)

538.566:535.32 3771
Dispersion—(*Wireless World*, vol. 64, pp. 502–506; October, 1958.) The effect is discussed in terms of group and phase velocities, and applied to waveguides, cables, circuits and the ionosphere.

538.566:535.42]+534.26 3772
The Effect of Fluctuations on the Diffraction Patterns of a Focusing System—L. A. Chernov. (*Akust. Zh.*, vol. 3, pp. 360–365; October–December, 1957.) General formulas are derived for the average distribution of intensity and the distribution of fluctuations in a diffraction pattern when fluctuations are present in the incident wave. Limiting cases of large and small fluctuations are considered.

538.566:535.42 3773
Transmission Characteristics of Inclined Wire Gratings—O. J. Snow. (IRE TRANS. ON ANTENNAS AND PROPAGATION, Oct. 1956, vol. AP-4, No. 4, pp. 650–654. Abstract, PROC. IRE, vol. 45, p. 571; April, 1957.)

538.566:535.42 3774
On Resonance in Infinite Gratings of Cylinders—S. N. Karp and J. Radlow. (IRE TRANS. ON ANTENNAS AND PROPAGATION, vol. AP-4, pp. 654–661; October, 1956. Abstract, PROC. IRE, vol. 45, p. 571; April, 1957.)

538.566:[535.43+535.312 3775
On Scattering and Reflection of Electromagnetic Waves by Rough Surfaces—V. Twersky. (IRE TRANS. ON ANTENNAS AND PROPAGATION, vol. AP-5, pp. 81–90; January, 1957. Abstract, PROC. IRE, vol. 45, p. 716; May, 1957.)

538.566.029.6:535.42 3776
Diffraction of Microwaves by Tandem Slits—L. R. Alldredge. (IRE TRANS. ON ANTENNAS AND PROPAGATION, vol. AP-4, pp. 640–649; October, 1956. Abstract, PROC. IRE, vol. 45, p. 571; April, 1957.)

538.569:539.2 3777
Induced and Spontaneous Emission in a Coherent Field—I. R. Senitzky. (*Phys. Rev.*, vol. 111, pp. 3–11; July 1, 1958.) The resonant interaction between a coherently oscillating radiation field and a number of similar atomic systems coupled to the field through their electric dipole moments is analyzed quantum-mechanically. Distinction is drawn between coherent and incoherent parts of the energy. Terms corresponding to induced and spontaneous emission are identified, and it is shown that the latter includes both coherent and incoherent components. Special situations related to masers and to the coherence of spontaneous radiation are discussed.

538.569.4 3778
Theory of Cyclotron Resonance—E. A. Kaner. (*Zh. Eksp. Teor. Fiz.*, vol. 33, pp. 1472–1476; December, 1957.) Treatment of cyclotron resonance in a metal in an inclined magnetic field and in a parallel magnetic field with arbitrary electron reflection.

538.569.4 3779
Theory of Cyclotron Resonance in Metals—E. A. Kaner and M. Ya. Azbel'. (*Zh. Eksp. Teor. Fiz.*, vol. 33, pp. 1461–1471; December, 1957.) An investigation of the influence of field strength and temperature on the surface impedance of a metal in RF and constant magnetic fields parallel to the surface.

538.569.4:537.311.62 3780
The Skin Effect and Ferromagnetic Resonance—V. L. Gurevich. (*Zh. Eksp. Teor. Fiz.*, vol. 33, pp. 1497–1504; December, 1957.) Mathematical analysis of normal and anomalous skin effect in metals under conditions of ferromagnetic resonance.

538.569.4:621.375.9 3781
Polarization of a Molecular Beam by an Alternating Field with Variable Amplitude and Phase—G. P. Lyubimov and R. V. Khokhlov. (*Zh. Eksp. Teor. Fiz.*, vol. 33, pp. 1396–1402; December, 1957.) Equations are derived and an exact solution is given for the case when the frequency of the applied field is the same as that of the molecular transition. Approximate solutions are obtained for slow and rapid variations in the amplitude and frequency of the field during the time of transit of the molecular beam through the resonator cavity.

538.569.4.029.6 3782
Measurement of Microwave Absorption in Binary Gaseous Mixtures—G. Boudouris and D. Ilias. (*Compt Rend. Acad. Sci., Paris*, vol. 246; pp. 1407–1410; March 3, 1958.)

538.569.4.029.6 3783
Absorption and Refraction of some Polar Gases as a Function of Pressure at Microwave Frequencies—A. Battaglia, F. Bruin, and A. Gozzini. (*Nuovo Cim.*, vol. 7, pp. 87–94; January 1, 1958. In English.)

538.569.4.029.6:535.33.08 3784
Optical Detection of Hyperfine Transitions of Caesium Atoms—F. Diamand, J. M. Legendre, and T. Skalinski. (*Compt. rend. Acad. Sci., Paris*, vol. 246, pp. 90–92; January 6, 1958.) Report of measurements made at frequencies of 9205.3 mc and 9179.8 mc to detect hyperfine Zeeman transitions in Cs.

538.569.4.029.6:535.343.4 3785
Microwave Apparatus for the Measurement of the Refraction, Dispersion and Absorption of Gases at Relatively High Pressure—A. Battaglia, F. Bruin, and A. Gozzini. (*Nuovo Cim.*, vol. 7, pp. 1–9; January 1, 1958. In English.)

538.569.4.039.64/.65:535.343.4 3786
A Microwave Spectrometer for the Study of Free Radicals—I. R. Hurle and T. M. Sugden. (*J. Sci. Instr.*, vol. 35, pp. 319–323; September, 1958.) Description of apparatus suitable for the study of short-lived molecules in the gas phase, and operating in the frequency range 20–70 kmc.

538.569.4.08 3787
Micromodulator—a Device for Measuring the Intensities of Microwave Absorption Lines—R. D. Mattuck and M. W. P. Strandberg. (*Rev. Sci. Instr.*, vol. 29, pp. 717–721; August, 1958.) By means of a small electromagnet and power supply, a free electron resonance is utilized to provide a standard comparison line at any frequency up to 40 kmc.

GEOPHYSICAL AND EXTRATERRESTRIAL PHENOMENA

523.15 3788
On Force-Free Magnetic Fields—S. Chandrasekhar and L. Woltjer. (*Proc. Nat. Acad. Sci.*, vol. 44, pp. 285–289; April 15, 1958.) The assumption that the Lorentz force vanishes in cosmic magnetic fields which occur in regions of low density is discussed.

523.164 3789
Observations of Discrete Radio Sources at a Frequency of 500 Mc/s—R. G. Conway.

(*Mon. Not. R. Astr. Soc.*, vol. 117, no. 6, pp. 692–697; 1957.) An interferometer system with long integration times is used to determine the flux densities of eleven sources relative to Cygnus A.

523.164 3790

The Spectra of Radio Stars—G. R. Whitfield. (*Mon. Not. R. Astr. Soc.*, vol. 117, no. 6, pp. 680–691; 1957.) By considering all available measurements on the flux density of Cassiopeia A, it is concluded that its spectrum obeys a simple power law. Using this law, the spectra and spectral indices of 31 radio stars are derived, including Cygnus A, Virgo A and Taurus A.

523.164 3791

On the Nature of the Cygnus-X Radio Source as derived from Observations in the Continuum and at the Hydrogen-Line Frequency—R. D. Davies. (*Mon. Not. R. Astr. Soc.*, vol. 117, pp. 663–679; 1957.)

523.164 3792

Results of a Survey of Galactic Radiation at 38 Mc/s—J. H. Blythe. (*Mon. Not. R. Astr. Soc.*, vol. 117, no. 6, pp. 652–662; 1957.) The results, covering most of the sky north of $-20°$, are presented in the form of a contour map together with a list of reliably observed sources and HII regions with their features.

523.164:621.396.677 3793

A New Type of Pencil—Beam Aerial for Radio Astronomy—Blythe. (See 3691.)

523.164:621.396.677.3 3794

A Theoretical Study of Errors in Radio-Interferometer-Type Measurements Attributable to Inhomogeneities of the Medium—G. J. Simmons. (IRE TRANS. ON TELEMETRY AND REMOTE CONTROL, vol. TRC-3, pp. 2–5; December, 1957. PROC. IRE, vol. 46, p. 805; April, 1958.)

523.164.32 3795

Duration and Bandwidth of Short-Lived Transients in Solar Noise—T. de Groot. (*Nature, London*, vol. 181, pp. 1676–1677; June 14, 1958.) Histograms of single-frequency measurements made at 400 mc and a table of results for a two-channel receiver covering the band 394–406 mc are given. See also 439 of 1958.

523.5:621.396.11 3796

The Variation of Ionization along a Meteor Trail—J. S. Greenhow and E. L. Neufeld. (*Mon. Not. R. Astr. Soc.*, vol. 117, no. 4, pp. 359–369; 1957.) Results are described of investigations, using two spaced receivers to observe radio echoes from faint meteor trails. The mean ionization curve is much shorter than that predicted by present theory and the rise to maximum electron density more rapid than expected.

523.5:621.396.822 3797

Radio Noise from Meteors—G. S. Hawkins (*Nature, London*, vol. 181, p. 1610; June 7, 1958.) A note of attempts made in the United States to detect meteor noise at frequencies of 1 c, 30 mc, 218 mc and 475 mc. No emission from meteors was detected. It is concluded that the efficiency of conversion of the kinetic energy of meteors to radio energy is less than 10^{-16} per unit bandwidth.

523.5:621.396.96 3798

Analysis of Meteoric Body Doppler Radar Records taken during a Geminid Shower Period—M. S. Rao. (*Can. J. Phys.*, vol. 36, pp. 840–854; July, 1958.) The prevailing-wind speed in the 80–100-km region has been determined using a CW Doppler radar and three-station pulsed radars operating simultaneously at about 30 mc. The body Doppler frequency and its fluctuations indicate a wind speed of 54 m and a turbulence scale of about 1 km on the night of December 10–11, 1948.

523.745:523.165 3799

A Cosmic-Ray Increase Related to Solar Activity—J. Katzman. (*Can. J. Phys.*, vol. 36, pp. 807–814; July, 1958.) A large increase in cosmic-ray activity, measured with telescopes of small solid angle, was observed to accompany a sustained increase in the F_2 layer critical frequency during the period September, 1956, to February, 1957.

523.75:535.334 3800

Temperatures and Electron Densities in Flares as derived from Spectroscopic Data—J. T. Jefferies. (*Mon. Not. R. Astr. Soc.*, vol. 117, no. 5, pp. 493–504; 1957.)

523.752 3801

Type IV Emissions and the Origin of Cosmic Rays Associated with Chromospheric Eruptions—A. Boischot and J. F. Denisse. (*Compt. rend. Acad. Sci., Paris*, vol. 245, pp. 2194–2197; December 16, 1957.) See also 2437 of 1957 (Boischot).

550.38 3802

The Origin and Maintenance of Geomagnetism, its Secular Variation and its Inversions—A. Dauvillier. (*Compt. rend. Acad. Sci., Paris*, vol. 246, pp. 1354–1356; March 3, 1958.)

550.389.2:629.19 3803

Orbital Behaviour of Earth Satellites—R. E. Roberson. (*J. Franklin Inst.*, vol. 264, pp. 181–202, 269–285; September and October, 1957.) Sources of perturbation are considered with particular attention to the effect of the oblateness of the earth, for which an analysis is developed, and recent contributions are reviewed.

550.389.2:629.19 3804

Radio Doppler Measurements on the Russian Satellites at the National Standards Laboratory—G. J. A. Cassidy. (*Proc. IRE, Aust.*, vol. 19, No. 3, pp. 105–109; March, 1958.) From observations made on the 40-mc transmission at one station, values for the period and other orbit parameters were deduced using simple methods.

550.389.2:629.19 3805

Sputnik I's Last Days in Orbit—J. D. Kraus and E. E. Dreese. (PROC. IRE, vol. 46, pp. 1580–1587; September, 1958.) The satellite was tracked by using a CW reflection technique [see 1724 of 1958 (Kraus)], and was found to break up in a complex manner over a period of days. Possible break-up mechanisms are suggested.

550.389.2:629.19 3806

Effect of Air Drag on the Orbit of the Russian Earth Satellite 1957β: Comparison of Theory and Observation—D. G. King-Hele and D. C. M. Leslie. (*Nature, London*, vol. 181, pp. 1761–1763; June 28, 1958.)

550.389.2:629.19 3807

Measurement of Cosmic Radiation on the Sputnik—S. N. Vernov, N. L. Grigorov, Yu. I. Logachev, and A. E. Chudakov. (*Dokl. Akad. Nauk S.S.S.R.*, vol. 120, pp. 1231–1233; June 25, 1958.) Preliminary results obtained by means of two independent recording instruments located in the second artificial earth satellite are shown graphically. A 3-min 50 per cent increase in intensity was recorded on November 7, 1957, above latitude 58°N.

550.389.2:629.19 3808

Radio Scintillations of Satellite 1958α—O. B. Slee. (*Nature, London*, vol. 181, pp. 1610–1612; June 7, 1958.) Graphical recordings of the 108-mc signal from satellite 1958α are reproduced. The scintillations observed are correlated with scintillations of cosmic RF sources recording during the same period. Results indicate that the ionospheric irregularities responsible for the scintillations must lie below 350 km. Corresponding recordings from satellite 1958α show significantly less scintillation activity at perigee (185 km) than on preceding and following days.

550.389.2:629.19:551.510.535 3809

Some Effects of the Fine Structure of the Ionosphere on Transmission Received from the Russian Earth Satellite 1958δ—F. A. Kitchen and W. R. R. Joy. (*Nature, London*, vol. 181, pp. 1759–1761; June 28, 1958.) Anomalies in Doppler observations of the satellite are discussed. It appears practicable to make a detailed study of the lower boundary of the F region by an analysis of Doppler frequency discontinuities in conjunction with accurately known orbit parameters.

550.389.2:629.19:551.510.535 3810

On the Results of the Electron-Concentration Determinations in the External Region of the Ionosphere Made on the Basis of Radio Signals from the First Sputnik—Ya. L. Al'pert, F. F. Dobryakova, E. F. Chudesenko and B. S. Shapiro. (*Dokl. Akad. Nauk S.S.S.R.*, vol. 120, pp. 743–746; June 1, 1958.) Brief description of the method of observation of 40-mc radio signals from the satellite to determine the exact time of its "rising" and "setting." Calculated values of electron density range from 1.8×10^6 electrons/cm^3 at 320 km to 10^2 electrons/cm^3 at 3050 km.

551.510.535 3811

Rocket Measurements of Electron Concentration in the Ionosphere by means of an Ultra-Short-Wave Dispersion Interferometer—K. I. Gringauz. (*Dokl. Akad. Nauk S.S.S.R.*, vol. 120, pp. 1234–1237; June 21, 1958.) Investigations have been carried out since 1954 at heights up to 473 km using rockets equipped with transmitters operating at 48 and 144 mc. Signals were recorded at the ground by two different oscillographic methods. Results indicate that the true height of F-layer reflections is 50–150 km lower than the effective height recorded by an ionospheric sounder.

551.510.535 3812

Apparent Saturation in F_2 Layer—T. W. Bennington. (*Wireless World*, vol. 64, pp. 472–473; October, 1958.) At sunspot numbers near 100, there is a departure from the linear relation with F_2-layer critical frequency which is attributed to a combination of high sunspot numbers and local summer daytime conditions.

551.510.535 3813

Horizontal Ionospheric Drifts in the F_2 Region at Equatorial Latitudes—B. R. Rao and E. B. Rao. (*Nature, London*, vol. 181, pp. 1612–1613; June 7, 1958.) Systematic measurements of F_2 drift made at Waltair, India, by the spaced-receiver method from February, 1956, to January, 1958, are analyzed. The 24-h E-W component (80–90 m) is invariably higher than the N-S component (65–75 m). The prediction of phase reversal of F_2 drift at a latitude of 35 °is confirmed. See also 2090 of July (Purslow) and 3818 below.

551.510.535:523.72 3814

Similarities in the Characteristics of Solar Radiation at λ 10.7 cm and in the Far Ultraviolet—O. M. Minnis and G. H. Bazzard. (*Nature, London*, vol. 181, p. 1796; June 28, 1958.) Values of the activity index Ch_E, based on E-layer data for Slough, have been correlated for a ten-year period with the monthly mean value Φ of solar RF noise flux meas-

ured at Ottawa. The close correlation found ($r_{max}=0.99$), and results of an analysis of eclipse data [3437 of 1958 (Minnis)], support the conclusion of Denisse and Kundu (1758 of 1957).

551.510.535:550.385 3815
Equatorial Spread-F and Magnetic Activity—A. J. Lyon, N. J. Skinner, and R. W. Wright. (*Nature, London*, vol. 181, pp. 1724–1725; June 21, 1958.) Analysis of data for Ibadan, Nigeria, for the years 1956 and 1957 shows that the incidence of spread-F on international quiet days is higher than that on international disturbed days.

551.510.535:621.396.11 3816
Diurnal Variation of Deviative Absorption in the F_2 Region of the Ionosphere—S. K. Sherma. (*Indian J. Phys.*, vol. 32, pp. 297–298; June, 1958.) Note of absorption measurements near the critical frequency. Daytime reduction of deviative absorption is ascribed to thermal expansion of the F_2 layer.

551.510.535:621.396.11 3817
Anomalous Variation of Total Absorption of Radio Waves Reflected from the F_2 Region of the Ionosphere around Midday—S. K. Sharma. (*Proc. Phys. Soc.*, vol. 71, pp. 1007–1010; June 1, 1958.) Observations made at Banaras, using frequencies higher than F_1-layer critical frequency, show two maxima, one before and the other after local noon. The first maximum has been attributed to thermal expansion of the F_2 region, the effect of which is normally observed before midday; the second coincides with the usual maximum of total absorption observed at lower frequencies after midday.

551.510.535:621.396.812.3 3818
Investigation of Horizontal Drifts in the E Region of the Ionosphere in Relation to Random Fading of Radio Waves—B. R. Rao and M. S. Rao. (*J. Brit. IRE*, vol. 18, pp. 493–495; August, 1958.) Measurements of E-region wind velocities V and frequency of fading N were made at 2.3 and 2.8 mc. The linear relation $V=1.86\ N\lambda$, which is in agreement with theory, is deduced.

551.594.223 3819
Ball Lightning and Thermonuclear Reaction—A. Dauvillier. (*Compt. rend. Acad. Sci., Paris*, vol. 245, pp. 2155–2156; December 16, 1957.) It is suggested that ball lightning is formed by radiocarbon 14 due to the action on atmospheric nitrogen of thermal neutrons liberated by lightning discharges. See also 2957 of 1955 (Kapitsa).

551.594.5 3820
Height Distribution of the Red Auroral Line in Polar Aurorae—L. Harang. (*Geofys. Publ.*, vol. 20, 9 pp., January, 1958.) Luminosity curves along vertical cross-sections of auroral forms recorded by means of a photoelectric photometer are analyzed.

551.594.5:621.396.96 3821
Some Observations of Aurora using a Low-Power Frequency-Modulated Radar—C. Collins. (*Can. J. Phys.*, vol. 36, pp. 926–934; July, 1958.) An experimental CW radar is described which provides information on range and radial motion of auroral echoes. A histogram of the range distribution of echoes from reflecting areas north of Ottawa shows a maximum at 650–750 km.

551.594.6 3822
Polarization of Atmospherics—F. Horner: S. R. Khastgir. (*Nature, London*, vol. 181, pp. 1678–1680; June 14, 1958.) Comment on 2420 of 1958 and author's reply.

551.594.6 3823
"Whistlers" in the Antarctic—L. H. Martin. (*Nature, London*, vol. 181, pp. 1796–1797; June 28, 1958.) Observations made from April 15–30, 1958, at Scott Base showed considerable activity including "bonks," "tweeks," long and short whistlers and periods of strong "sferics," but no dawn chorus. It is probable that the whistlers are propagated from lower-latitude regions, first along the appropriate magnetic flux line, and then by ionospheric reflection.

551.594.6:621.3.087.4/.5 3824
Automatic Recorder of the Waveforms of Atmospherics—B. A. P. Tantry. (*Indian J. Phys.*, vol. 32, pp. 267–275; June, 1958.) Description, with circuit diagrams, of component units of film-type recording equipment in operation since 1952 and of similar design to that described earlier [679 of 1952 (Clarke and Mortimer)].

523.164 3825
The Exploration of Space by Radio [Book Review]—R. H. Brown and A. C. B. Lovell. Publishers: Chapman and Hall, London, Eng., 107 pp.; 1957. (*Nature, London*, vol. 181, pp. 1562–1563; June 7, 1958.) A detailed review of different branches of the subject.

LOCATION AND AIDS TO NAVIGATION

534.88 3826
Electronic Sector Scanning—Tucker, Welsby, and Kendell. (See 3676.)

621.396.93:621.396.677.6 3827
The Effect of Mutual Impedance on the Spacing Error of an Eight-Element Adcock—D. N. Travers. (IRE TRANS. ON ANTENNAS AND PROPAGATION, vol. AP-5, pp. 36–39; January, 1957. Abstract, PROC. IRE, vol. 45, p. 715; May, 1957.) See also 1423 of 1956.

621.396.93(083.71) 3828
IRE Standards on Radio Aids to Navigation: Definitions of Terms, 1954—(PROC. IRE, vol. 46, p. 1645; September, 1958.) A correction to standard 54 IRE 12.S1 (1350 of 1955).

621.396.933 3829
Radio Navigation and Pilotage Facilities of the Danish Aircraft Control Area—K. Svenningsen. (*Teleteknik, Copenhagen, English Ed.*, vol. 2, pp. 12–22; English version of 1668 of 1955.

621.396.933.2 3830
Recording Techniques for H.F. Direction Finding—C. W. McLeish. (*Electronic Radio Eng.*, vol. 35, pp. 386–390; October, 1958.) Methods are described for reducing the information given by DF equipment to a form which can be easily assimilated. The alternatives discussed are pen-recording of bearing/time and the photographic reproduction of the bearing/amplitude distribution functions. In both cases, records can be produced simultaneously from two direction finders, which facilitates comparisons.

621.396.96 3831
Investigation of Extended Over-Water Ranges of Low-Sited Radar—F. A. Sabransky. (*J. Met.*, vol. 15, pp. 303–308; June, 1958.) The increase in range of radars due to surface-based superrefractive layers has been studied to verify predictions of extended coverage.

621.396.96:621.396.11 3832
A Study of Radar Elevation-Angle Errors due to Atmospheric Refraction—B. M. Fannin and K. H. Jehn. (IRE TRANS. ON ANTENNAS AND PROPAGATION, vol. AP-5, pp. 71–77; January, 1957. Abstract, PROC. IRE, vol. 45, pp. 715–716; May, 1957.)

621.396.96:621.396.822 3833
A Proposed Technique for the Improvement of Range Determination with Noise Radar—H. Hochstadt. (PROC. IRE, vol. 46, p. 1652; September, 1958.) Comment on paper by R. Bourret, vol. 45, p. 1744; December, 1957.)

621.396.962.3.029.65 3834
8-mm High-Definition Radar—J. Verstraten and J. M. G. Seppen. (*Tijdschr. ned. Radiogenoot.*, vol. 23, pp. 17–32; January, 1958.) The information capacity of an 8-mm-λ pulsed system is considered and a description is given of equipment and operational results.

621.396.969.34:621.396.933.2 3835
Radar Beacon System Performance—S. Thaler and D. L. Ashcroft. (IRE TRANS. ON AERONAUTICAL AND NATIGATIONAL ELECTRONICS, vol. ANE-4, pp. 65–71; June, 1957.) A system of ground radar beacon interrogators and airborne beacon transponders in a circular area of approximately 200 miles radius is considered with special reference to undesirable mutual interactions.

MATERIALS AND SUBSIDIARY TECHNIQUES

53:061.6(494) 3836
Report of the Meeting of the Swiss Physical Society—(*Helv. Phys. Acta*, vol. 30, pp. 221–296; August 15, 1957.) The text is given of the following papers included among those read at a meeting held at Brunnen on May 4–5, 1957.

a) A Relation between the Structure of Semiconductors and Atomic Properties—E. Mooser and W. B. Pearson (pp. 222–223, in German).

b) Magnetic Susceptibility of Liquid Selenium and Tellurium—G. Busch and O. Vogt (pp. 224–227, in German).

c) Hall Effect of Bismuth as a Function of Magnetic Induction—R. Jaggi (pp. 228–230, in German).

d) Critical Magnetic Fields of Superconducting Vanadium—G. Busch and J. Müller (pp. 230–233, in German).

e) Hall Effect in Fe_3Al Alloy—J. P. Jan (pp. 233–235, in French).

f) Photoconductivity of Zinc Oxide with Ohmic and Blocking Contacts—H. J. Gerritsen, W. Ruppel, and A. Rose (pp. 235–238, in German).

g) Maximum Performance of Photoconductors—A. Rose (pp. 242–244). See also 768 of 1956.

h) Blackening of ZnS and CdS Single Crystals by Light—W. J. Merz (pp. 244–246, in German).

i) A New Type of Radio Spectrograph for the Observation of Electron Resonance in the Region of Metric and Decimetric Waves—J. P. Borel and C. Manus (pp. 254–257, in French).

j) Stability of NH_3 Frequency Standards—J. Bonanomi, J. De Prins, J. Herrmann, and P. Kartaschoff (pp. 288–290, in French).

k) High-Resolution Microwave Spectrograph—J. Bonanomi, J. De Prins, J. Herrmann, and P. Kartaschoff (pp. 290–292, in German).

l) A High-Frequency Ion Source with Low Power Requirements—M. Bloom, A. Rytz, and H. Staub (pp. 292–296, in German).

531.788.7 3837
Operation of an Inverted-Magnetron Gauge in the Pressure Range 10^{-3} to 10^{-12} mm Hg—J. P. Hobson and P. A. Redhead. (*Can. J. Phys.*, vol. 36, pp. 271–288.) Description of a cold-cathode ionization gauge with axial magnetic field and radial electric field. See also 3761 above.

535.215 3838
On the Theory of Photoemission—P. Gorlich and H. Hora. (*Optik, Stuttgart*, vol. 15, pp. 116–126; February–March, 1958.) The dis-

tinction between two different types of photoemission from metals is clarified. Phenomenological theory for Cs_3Sb is applied to measured photoemission in the far ultraviolet region; close agreement is found and generalizations of the principle are discussed. See also 798 of 1958 (Methfessel).

535.215 3839
Optical Absorption and Photoemission of Barium and Strontium Oxides, Sulphides, Selenides, and Tellurides—R. J. Zollweg. (*Phys. Rev.*, vol. 111, pp. 113–119; July 1, 1958.) Considerable structure is observed at the intrinsic optical absorption edge of annealed films of BaO, BaS, BaSe, BaTe, SrO, SrS, SrSe and SrTe at −160°C. An estimate is made from photoemission measurements of the energy separation between the top of the valence band and the vacuum level.

535.215 3840
Optical Transmission and Photoconductive and Photovoltaic Effects in Activated and Unactivated Single Crystals of ZnS—G. Cheroff and S. P. Keller. (*Phys. Rev.*, vol. 111, pp. 98–102; July 1, 1958.)

535.215:546.482.21:537.312.8 3841
Magnetoresistance Effect in Cadmium Sulphide—S. Tanaka and T. Masumi. (*J. Phys. Soc. Japan*, vol. 13, p. 314; March, 1958.)

535.37 3842
Radiationless Recombination in Phosphors—L. Bess. (*Phys. Rev.*, vol. 111, pp. 129–132; July 1, 1958.) "An Auger-type process is proposed for a possible means of nonradiative annihilation of free holes at electron traps in phosphors. A rough calculation is made of the cross section for the process, and some of the consequences are considered qualitatively."

535.37 3843
Two Kinds of Manganese Luminescence Centers in the Cadmium-Lithium Orthosilicate Phase—V. V. Osiko. (*Dokl. Akad. Nauk S.S.S.R.*, vol. 121, pp. 507–510; July 21, 1958.) Investigation showed a luminescence spectrum with two maxima in the wavelength regions 514 and 615 mμ and varying with the molarity ratio of CdO/Li_2O.

535.37:537.226 3844
Two Distinct Types of Photodielectric Effect in Cadmium Sulphide—R. Freymann, E. Grillot, M. Hagene, and J. Le Bot. (*Compt. rend. Acad. Sci., Paris*, vol. 245, pp. 2261–2264; December 16, 1957.) CdS when pure or activated with Ag or Cu shows an unusual type of absorption when illuminated at 4°K and then heated in darkness to about 250°K.

535.37:546.41−31:535.215 3845
Photoconductivity of Calcium Oxide—J. Janin and L. Cotton. (*Compt. rend. Acad. Sci., Paris*, vol. 246, pp. 1536–1538; March 10, 1958.) The photoconductivity induced by irradiation at certain wavelengths in pure CaO and CaO activated by Pb, Mn, (Pb+Mn) and (Pb+Sm) has been investigated experimentally using voltages up to 210 volts. See also 729 of 1955 (Crozet and Janin).

535.37:546.472.21 3846
Radiative Energy Transfer in ZnS—R. E. Halsted, E. F. Apple, and J. S. Prener. (*Phys. Rev. Lett.*, vol. 1, pp. 134–136; August 15, 1958.) Absorption and emission spectra are identified with specific impurities, and support an explanation in terms of hole transitions.

535.37:546.472.21 3847
Exhaustion Barriers in Zinc Sulphide—G. F. Alfrey and K. N. R. Taylor. (*Helv. Phys. Acta*, vol. 30, pp. 206–208; July 1, 1957.) "The nature of the exhaustion barrier at a metallic contact to a ZnS crystal is considered in the light of the evidence of electroluminescence and of the effect of electric fields on the scintillations produced by alpha particles. The evidence suggests that the donor states whose depletion gives rise to the barrier are concentrated at a single energy level, rather than distributed through the forbidden band." See also 781 of 1956.

535.376:537.226 3848
Electroluminescence from the Surface Layer of $BaTiO_3$, $SrTiO_3$, and Associated Materials—G. G. Harman. (*Phys. Rev.*, vol. 111, pp. 27–33; July 1, 1958.) It is shown that light emission resulting from HF excitation is due to a high RF field across a thin surface barrier. An efficiency of the order of 10^{-6} per cent was obtained. A model involving field emission from the metal electrode into the crystal surface layer is proposed.

537.226/.228.2:546.431.824−31 3849
Inquiry into the Electrostriction Equation of Barium Titanate Ceramic—K. Masuzawa, Y. Tomita, and T. Yamaguchi. (*Rep. Elect. Commun. Lab., Japan*, vol. 6, pp. 105–108; April, 1958.) The relation between the applied polarization and strain in a $BaTiO_3$ ceramic is investigated.

537.226/.228.1:546.431.824−31 3850
Elastic and Piezoelectric Coefficients of Single-Crystal Barium Titanate—D. Berlincourt and H. Jaffe. (*Phys. Rev.*, vol. 111, pp. 143–148; July 1, 1958.) Mechanical resonance and antiresonance frequencies were measured at temperatures from −50°C to +150°C. A complete set of elastic, piezoelectric and dielectric constants of the tetragonal modification at 25°C is obtained. The elastic compliances show deviation from cubic symmetry. Measurements in the orthorhombic state show longitudinal compliance four times higher than in the tetragonal state.

537.226/.227:538.569.4 3851
Paramagnetic Resonance of Fe^{3+} in $SrTiO_3$ Single Crystals—K. A. Müller. (*Helv. Phys. Acta*, vol. 31, pp. 173–204; June 2, 1958. In German.) 58 references.

537.226:621.319.2 3852
On the Making of Electrets and Measurement of the Changes of Dielectric Constant of a Polarized Electret-Forming Material with Time—T. C. Bhadra. (*Indian J. Phys.*, vol. 32, pp. 281–296; June, 1958.) More detailed account of measurements reported earlier [3627 of 1955 (Chatterjee and Bhadra)].

537.226:621.396.677.85 3853
The Fields Associated with an Interface between Free Space and an Artificial Dielectric—Brown and Seeley. (See 3704.)

537.227 3854
Ferroelectricity in Diglycine Nitrate $(NH_2CH_2COOH)_2HNO_3$—R. Pepinsky, K. Vedam, S. Hoshino and Y. Okaya. (*Phys. Rev.*, vol. 111, pp. 430–432; July 15, 1958.)

537.227 3855
Ferroelectric Properties of Glycine Sulphate—L. Taurel, E. Pourel, and F. Thomassin. (*Compt. rend. Acad. Sci., Paris*, vol. 246, pp. 70–72; January 6, 1958.) See also 1105 of 1957 (Matthias *et al.*).

537.227 3856
Ferroelectricity of $NaNH_4$-Tartrate—Y. Takagi and Y. Makita. (*J. Phys. Soc. Japan*, vol. 13, pp. 272–277; March, 1958.) Below the transition point, 109°K, a crystal plate shows domain structure if viewed under a polarizing microscope parallel to the *b* axis; shearing stress will reverse the polarization. The spontaneous value is 0.21 μC/cm² at 92°K, and is probably constant below the transition temperature.

537.227:546.431.824−31:621.318.57 3857
Ultrasonic Measurement of Polarization Switching Processes in Barium Titanate Single Crystal—K. Husimi and K. Kataoka. (*J. Appl. Phys.*, vol. 29, pp. 1247–1251; August, 1958.) A nondestructive piezoelectric method for studying the polarization of ferroelectric crystals is applied to study polarization switching in $BaTiO_3$ single crystals. Three polarization processes are believed to exist, one of these being very slow. Switching-time results are considered in the light of the above experiments. See also 147 of 1958 (Zen'iti *et al.*).

537.227:621.318.57 3858
Polarization Reversal in Triglycine Sulphate Crystal—K. Zen'iti, K. Husimi, and K. Kataoka. (*J. Phys. Soc. Japan*, vol. 13, p. 661; June, 1958.)

537.311.3:534.23:538.6 3859
Acoustomagnetoelectric Effects in Metal and Semiconductor Filaments—G. G. E. Low. (*Proc. Phys. Soc.*, vol. 71, pp. 965–972; June 1, 1958.) The interaction of a magnetic field and a compressional acoustic wave, traveling in a conducting medium, is considered. Assuming charge neutrality, expressions for the electric current densities and fields in filamentary specimens are derived, and applied in particular to semiconductors. Second-order effects are discussed.

537.311.3:537.534.9 3860
Application of the Ion Bombardment Cleaning Method to Titanium, Germanium, Silicon and Nickel as Determined by Low-Energy Electron Diffraction—H. E. Farnsworth, R. E. Schlier, T. H. George, and R. M. Burger. (*J. Appl. Phys.*, vol. 29, pp. 1150–1161; August, 1958.)

537.311.33 3861
Carrier Mobilities in InP, GaAs, and AlSb—F. J. Reid and R. K. Willardson. (*J. Electronics Control*, vol. 5, pp. 54–61; July, 1958.) Measurements of carrier mobilities in single crystals have been made as a function of impurity concentration and temperature. Scattering of charge carriers at 300°K suggests lattice mobilities of 11,500 cm²/v for electrons in GaAs, 6600 cm²/v for electrons in InP and 450 cm²/v for holes in AlSb.

537.311.33 3862
Effect of Electron-Electron Scattering on Hall Mobility of Electrons in *n* Semiconductors—M. S. Sodha and P. C. Eastman. (*Progr. Theor. Phys.*, vol. 19, pp. 344–346; March, 1958.) A Hall-mobility/drift-mobility ratio of 1.18 is obtained if account is taken of electron-electron scattering.

537.311.33 3863
Recombination at Two-Level Traps in Semiconductors—M. Bernard. (*J. Electronics Control*, vol. 5, pp. 15–18; July, 1958. In French.) The statistics of recombination of excess carriers is examined in the case of a flaw common to two nonindependent levels in the forbidden energy gap. Two examples given refer to carrier lifetime with low-level injection, and carrier generation rate in the space-charge zone of a *p-n* junction. See also 2124 of 1958 (Sah and Shockley).

537.311.33 3864
The Electrical Conductivity of *p*-Type Semiconductors in the Case of Chemisorption of Atoms and Radicals—I. A. Miasnikov (*Dokl. Akad. Nauk S.S.S.R.*, vol. 120, pp. 1298–1301; June 21, 1958.) Experimental investigation of the effect of chemisorption on

the conductivity of ZnO or TiO_2 in the presence of H_2, N_2 or alcoholic vapours.

537.311.33 3865
Electrical Conduction via Slow Surface States on Semiconductors—H. Statz and G. A. deMars—(*Phys. Rev.*, vol. 111, pp. 169–182; July 1, 1958.) Steady-state and transient conductance of inversion layers created by acetone vapor on silicon *n-p-n* bars were investigated. The interpretation gives strong evidence that the charge in the outer surface states can move in an electric field. The mobility of the charge is of the order of 10^{-3}cm²/v for thick films and becomes progressively smaller for thinner films. It is found that inversion layers created by mobile charges may be unstable for certain applied voltages.

537.311.33 3866
Preventing Conductivity Fluctuations during Growth of a Semiconducting Crystal—W. G. Pfann, J. N. Hobstetter, and G. S. Indig. (*J. Appl. Phys.*, vol. 29, pp. 1238–1240; August, 1958.) Fluctuations in the electrical conductivity of an extrinsic semiconductor can be eliminated by adding to the melt a critical concentration of a suitable donor or acceptor.

537.311.33:53.08:536.62 3867
Construction of a Microcalorimeter for Investigations on Semiconductors—D. Blet-Talbot. (*Compt. rend Acad. Sci., Paris*, vol. 245, pp. 2224–2227; December 11, 1957.) Theoretically determined values of sensitivity and time constant of the calorimeter are respectively 0.24 μv/μw and 11s.

537.311.33:541.135:621.375.9 3868
Amplification in an Electrolyte—(*Engr., London*, vol. 185, p. 696; May 30, 1958.) Note on an experimental device described by J. F. Dewald which consists of a hexagonal rod-shaped crystal of pure ZnO immersed in a highly conducting electrolyte. Gains exceeding 15db at kc have been obtained.

537.311.33:546.26–1 3869
Electronic Structure and Diamagnetism of Graphite—S. Mase. (*J. Phys. Soc. Japan*, vol. 13, pp. 563–573; June, 1958.)

537.311.33:[546.28+546.289 3870
Radiation Damage in Ge and Si Detected by Carrier Lifetime Changes: Damage Thresholds—J. J. Loferski and P. Rappaport. (*Phys. Rev.*, vol. 111, pp. 432–439; July 15, 1958.) Minority carrier lifetime, τ, is shown to be more sensitive by a factor of 10^4 to radiation-induced defects than the conductivity. Both direct measurements of τ and evaluation of dependent parameters are described. The thresholds for production of Frenkel defects were found. Analysis shows how the radiation-induced energy levels and the relative minority-carrier capture cross sections can be determined experimentally. Comparisons are made with theory.

537.311.33:546.28 3871
Temperature Dependence of Carrier Lifetime in Silicon—D. J. Sandiford. (*Proc. Phys. Soc.*, vol. 71, pp. 1002–1006; June 1, 1958.) Experimental results and theory may be reconciled on the assumption that the capture probabilities of the recombination centers are temperature dependent, and that the energy levels of the centers lie 0.45 ± 0.05 ev above the valence band.

537.311.33:546.28 3872
Absorption Spectrum of Bismuth-Doped Silicon—H. J. Hrostowski and R. H. Kaiser. (*Phys. Chem. Solids*, vol. 4, no. 4, pp. 315–317.)

537.311.33:546.28 3873
Work Function and Sorption Properties of Silicon Crystals—J. A. Dillon, Jr, and H. E. Farnsworth. (*J. Appl. Phys.*, vol. 29, pp. 1195–1202; August, 1958.) The work functions of Si single crystals were found for various samples of floating-zone and nonfloating-zone Si. Differences are noted between radiation-quenched and annealed specimens. The effects of exposure to oxygen, hydrogen, and nitrogen, and of heating in high vacuum were measured.

537.311.33:[546.28+546.289]:538.63 3874
Interpretation of Magnetoconductivity in *n*-Type Germanium and Silicon—R. W. Keyes. (*Phys. Rev.*, vol. 111, pp. 34–35; July 1, 1958.) The phenomenological magnetoconductance coefficients of a cubic crystal are expressed in terms of the single-valley magnetoconductance constants, for energy bands consisting of [111] or [100] valleys. The "symmetry conditions" for magnetoconductance are found to depend on the vanishing in the principal axis directions of the longitudinal magnetoconductance coefficients of a single valley.

537.311.33:546.289 3875
Electrical Properties of Clean Germanium Surfaces—G. A. Barnes and P. C. Banbury. (*Proc. Phys. Soc.*, vol. 71, pp. 1020–1021; June 1, 1958.) A preliminary report is given of studies of field effect and photoconductance using a technique in which specimens, electrodes and fracturing equipment are contained in envelopes under pressures of the order of 10^{-10}mm Hg.

537.311.33:546.289 3876
Dislocation Etch Pits in Germanium—W. Bardsley, R. L. Bell and B. W. Straughan. (*J. Electronics Control*, vol. 5, pp. 19–28; July, 1958.) From an examination of the shape of CP4 etch pits on (111) faces, azimuth but not declination of a dislocation line may be derived. Observations of azimuth and trace direction have been used to identify the direction of dislocation lines in some crystals.

537.311.33:546.289 3877
Low-Level Absorption in Germanium—T. S. Moss and T. D. H. Hawkins. (*Phys. Rev. Lett.*, vol. 1, pp. 129–130; August 15, 1958.) Absorption coefficients as low as 10^{-5}cm^{-1} were observed at photon energy levels down to 0.56 ev.

537.311.33:546.289 3878
Absorption of Light by Electron-Hole Pairs Liberated by the Photoelectric Effect in a Single Crystal of Germanium—F. Desvignes. (*Compt. rend. Acad. Sci. Paris*, vol. 246, pp. 1824–1827; March 24, 1958.) A beam of light of wavelength above the photoelectric threshold and of constant intensity impinges directly on a slab of Ge which is also obliquely illuminated by a modulated beam of light from another source. The transmission factor of the material is correspondingly modulated.

537.311.33:546.289 3879
Nonradiative Recombination of Electrons at Impurity Centers in *n*-Type Germanium—V. A. Kovarskii. (*Zh. Eksp. Teor. Fiz.*, vol. 33, pp. 1445–1453; December, 1957.) Theoretical treatment of nonradiative recombination at liquid-helium temperatures. The interaction between an electron and acoustic vibrations of the lattice is taken into account by successive diagonalization of the orignal Hamiltonian by a unitary transformation. See *e.g.*, 3557 of 1955 (Kubo and Toyozawa).

537.311.33:546.289 3880
Precipitation of Cu in Ge: Part 2—Supersaturation Effects—A. G. Tweet. (*Phys. Rev.*, vol. 111, pp. 57–66; July 1, 1958.) Further investigation of precipitation rates indicating the occurrence of nucleation at sites other than dislocations. See 3191 of 1957.

537.311.33:546.289 3881
Precipitation of Cu in Ge: Part 3—Quench Effects in Nearly Perfect Crystals—A. G. Tweet. (*Phys. Rev.*, vol. 111, pp. 67–71; July 1, 1958.) Part 2: 3880 above.

537.311.33:546.289 3882
Measurement of Germanium Surface States by Pulsed Channel Effect—G. Rupprecht. (*Phys. Rev.*, vol. 111, pp. 75–81; July 1, 1958.) Densities, cross sections, and activation energies of several fast Ge surface states are inferred from low-temperature conductivity relaxations in a thin diffused surface layer. The results indicate the exstence of an electron trap 0.24 ev from the conduction band and two hole traps 0.17 ev and 0.22 ev from the valence band.

537.311.33:546.289 3883
Anisotropy of Hot Electrons in *n*-Type Germanium—W. Sasaki, M. Shibuya, and K. Mizuguchi. (*J. Phys. Soc. Japan*, vol. 13, pp. 456–460; May, 1958.) The EMF perpendicular to the current flow in *n*-type Ge has been measured and compared with theoretical values. This effect is attributed to anisotropic conduction due to ellipsoidal energy surfaces.

537.311.33:546.289:535.215 3884
Large-Signal Surface Photovoltage Studies with Germanium—E. O. Johnson. (*Phys. Rev.*, vol. 111, pp. 153–166; July 1, 1958.) The studies were carried out over a wide range of excess-carrier densities. Ambient-induced inversion and accumulation layer surfaces were studied on *p*-type and *n*-type Ge. The results agree with the theory that considers the surface space charge, but neglects charge changes in fast surface states.

537.311.33:545.289:538.63 3885
Phonon-Drag Thermomagnetic Effects in *n*-Type Germanium: Part 1—General Survey—C. Herring, T. H. Geballe, and J. E. Kunzler. (*Phys. Rev.*, vol. 111, pp. 36–57; July 1, 1958.) Experimental investigation of the Nernst field and thermoelectric power for single-crystal *n*-type Ge over a wide range of temperature, for various orientations and with fields up to 18,000 G. Both effects are dominated by "phonon drag" at low temperatures. The results can be explained by a model which assigns to each ellipsoidal energy shell in crystal-momentum space an anisotropic phonon-drag Peltier tensor with principal components in the high—and low—mass directions.

537.311.33:546.289.221 3886
Electrical and Optical Properties of GeS—T. Yabumoto. (*J. Phys. Soc. Japan*, vol. 13, pp. 559–562; June, 1958.) GeS was purified by recrystallization in an atmosphere of ammonia gas. Measurements were made of dark conductivity, optical absorption, photoconductivity and thermoelectric force.

537.311.33:546.3–1′289′28 3887
Mobility of Electrons in Germanium-Silicon Alloys—M. Glicksman. (*Phys. Rev.*, vol. 111, pp. 125–128; July 1, 1958.) The scattering of electrons in the alloys (with compositions varying from 0 to 30 atomic per cent Si) includes a contribution from scattering by the disorder present which depends on the composition as $[\alpha(1-\alpha)]^{-1}$ where α is the mole-fraction of the minority component. The disorder scattering mobility varies as $T^{-0.8}$.

537.311.33:546.482.21 3888
Ohmic Probe Contacts to CdS Crystals—V. T. Sihvonen and D. R. Boyd. (*J. Appl. Phys.*, vol. 29, pp. 1143–1145; August, 1958.) Wire probe contacts are found to be diodic upon first touching CdS, but can be permanently changed from diodic to ohmic by the passage of a moderately intense electric current

pulse. This result was obtained for ten metals, and it is postulated that the current pulse punctures the exhaustion barrier thereby permitting electrons to tunnel more freely and in greater numbers. See also 3197 of 1957 (Walker and Lambert).

537.311.33:546.49.241 3889
Electrical Properties of Mercury Telluride—R. O. Carlson. (*Phys. Rev.*, vol. 111, pp. 476–478; July 15, 1958.) Preparation of polycrystalline samples is described. The compound has a band gap of ~0.02 ev and a large mobility ratio. The magneto-Hall effect suggests a complicated conduction band. Zn acts as a donor impurity and Cu as an acceptor impurity.

537.311.33:546.681.19 3890
Effective Mass of Electrons in Gallium Arsenide—L. C. Barcus, A. Perlmutter, and J. Callaway. (*Phys. Rev.*, vol. 111, pp. 167–168; July 1, 1958.) "The effective mass of electrons in a simple of *n*-type gallium arsenide has been measured by determining the reflectivity in the infrared. The value obtained, $(0.043 \pm 0.005)m_0$, supports the hypothesis that the minimum of the conduction band is at the center of the Brillouin zone."

537.311.33:546.681.19 3891
Optical Absorption in *p*-Type Gallium Arsenide—R. Braunstein and L. Magid. (*Phys. Rev.*, vol. 11, pp. 480–481; July 15, 1958.) A number of absorption bands have been observed on the low-energy side of the intrinsic absorption edge. The main features of the spectra can be explained in terms of hole transitions between different branches of the valence band.

537.311.33:546.682.19 3892
Temperature Dependence of Optical Absorption in *p*-Type Indium Arsenide—F. Matossi and F. Stern. (*Phys. Rev.*, vol. 111, pp. 472–475; July 15, 1958.) Observed and calculated absorption characteristics are compared. The position and magnitude of the absorption peak change approximately as predicted using a model in which absorption is attributed to transitions between the light- and heavy-hole bands.

537.311.33:546.873.241:536.21 3893
Heat Conduction in Bismuth Telluride—H. J. Goldsmid. (*Proc. Phys. Soc.*, vol. 72, pp. 17–26; July 1, 1958.) The calculated electronic component of the thermal conductivity, for *p*-type material, agrees with experimental results, assuming the lattice thermal conductivity to be independent of the electrical conductivity. Agreement has also been obtained for non-halogen-doped *n*-type Bi_2Te_3, but not for halogen-doped material, due to the high effective scattering cross section, for phonons, of the halogen atoms. See also 2449 of 1956.

537.311.33:546.873.241:537.324 3894
The Performance of Bismuth Telluride Thermojunctions—H. J. Goldsmid, A. R. Sheard, and D. A. Wright. (*Brit. J. Appl. Phys.*, vol. 9, pp. 365–370; September, 1958.) The thermoelectric properties of *n*-type and *p*-type thermojunctions have been measured between 150° and 300°K, and a figure-of-merit calculated. This is highest for material with a conductivity of $1000\Omega^{-1}$ cm^{-1} with current parallel to the cleavage planes.

537.311.33:548.32 3895
The Isomorphism of Type $A^{III}B^{V}$ Compounds—W. Köster and W. Ulrich. (*Z. Metallkde*, vol. 49, pp. 365–367; July, 1958.)

537.311.33:548.5 3896
Floating Crucible Technique for Growing Uniformly Doped Crystals—W. F. Leverton. (*J. Appl. Phys.*, vol. 29, pp. 1241–1244; August, 1958.) A simple modification of the Czochralski technique permits the growing of large Ge single crystals of uniform resistivity. Each crystal is grown from an inner crucible floating in the Ge melt; the liquid volume in this crucible is constant and the impurity concentration gradient is eliminated. The application of the technique to the growing of uniform Si crystals is discussed.

537.311.33.621.396.822 3897
Semiconductor Noise as a Queuing Problem—D. A. Bell. (*Proc. Phys. Soc.*, vol. 72, pp. 27–32; July 1, 1958.) A power spectrum whose intensity appears to increase without limit as the frequency is decreased can be explained by considering the rate at which carriers leave the conduction band to be the result of a queuing problem rather than a relaxation problem. See also 818 of 1956.

538.22 3898
A Thermodynamic Theory of "Weak" Ferromagnetism of Antiferromagnetics—I. Dzyaloshinsky. (*Phys. Chem. Solids*, vol. 4, pp. 241–255; 1958.) English version of 2475 of 1958.

538.22 3899
Measurement of the Magnetothermal Effect of MnAs—A. J. P. Meyer and P. Taglang. (*Compt. rend. Acad. Sci., Paris*, vol. 246, pp. 1820–1822; March 24, 1958.) Measurements made on powdered material in a field of 26, 250 Oe at temperatures from 20° to 180°C are shown graphically.

538.22:538.569.4 3900
Absorption Lines in the Antiferromagnetic States of $MnCl_2 \cdot 4H^2O$ and $MnBr_2 \cdot 4H_2O$—I. Tsujikawa. (*J. Phys. Soc. Japan*, vol. 13, pp. 315–316; March, 1958.)

538.221 3901
A Ferromagnetic Dynamical Equation—H. B. Callen. (*Phys. Chem. Solids*, vol. 4, no. 4, pp. 256–270; 1958.) A general form of ferromagnetic dynamical equation with three parameters having definite quantum-mechanical significance is discussed. An explicit rotational dynamical equation is obtained for a special case, and may serve to explain qualitatively certain observed size and shape effects.

538.221 3902
Magnetization Mechanism and Domain Structure of Multidomain Particles—H. Amar. (*Phys. Rev.*, vol. 111, pp. 149–153; July 1, 1958.) "The free energy of a two-domain cube of iron is considered with and without an applied magnetic field. It is shown that the two-domain configuration may exist only beyond a critical size (200Å), that the wall characteristics are size-dependent and that their values are substantially different from the values assumed in bulk material."

538.221 3903
A Semi-empirical Equation for the Initial Susceptibility of Homogeneous Ferromagnetic Alloys—E. W. Lee and R. C. Jackson. (*Proc. Phys. Soc.*, vol. 72, pp. 130–134; July 1, 1958.)

538.221 3904
The Approach to Saturation as $1/H^2$ for Polycrystalline Ferromagnetic Materials—H. Danan. (*Compt. rend. Acad. Sci., Paris*, vol. 246, pp. 1822–1824; March 24, 1958.)

538.221 3905
Investigation of the Variation of the Magnetization of Pure Polycrystalline Iron and Nickel near Saturation Point—H. Danan. (*Compt. rend. Acad Sci., Paris*, vol. 246, pp. 73–76; January 6, 1958.)

538.221 3906
Measurement of the Gyromagnetic Ratio of Very Pure Nickel—A. J. P. Meyer. (*Compt. rend. Acad. Sci., Paris*, vol. 246, pp. 1517–1519; March 10, 1958.)

538.221:539.23 3907
Thin Ferromagnetic Layers. Magnetic Properties deduced from Investigations of the Conductivity of Thin Layers of Nickel—A. Colombani and G. Goureaux. (*Compt. rend. Acad. Sci., Paris*, vol. 246, pp. 1979–1983; March 31, 1958.)

538.221:621.318.124 3908
Effects of some Additionals for the Magnetic Properties of Ba and Sr Oxide Magnets—H. Kojima. (*Sci. Rep. Res. Inst. Tohoku Univ., ser. A*, vol. 10, pp. 175–182; April, 1958.)

538.221:621.318.13.017.31 3909
Eddy-Current Losses in Thin Ferromagnetic Sheets—E. W. Lee. (*Proc. IEE*, pt. C., vol. 105, pp. 337–342; September, 1958.) In very weak fields, observed eddy-current losses are greater than those theoretically predicted. It is suggested that the classical calcu ation of eddy-current loss is invalid when the distance between domain walls becomes comparable with the sheet thickness. See also 508 of 1957 (Aspden).

538.221:621.318.134 3910
Elementary Domains on the {100} Planes of Nickel Ferrite Crystals and on the (0001) Plane of Barium Ferrite Crystals—M. Paulus. (*Compt. rend. Acad. Sci., Paris*, vol. 245, pp. 2227–2230; December 16, 1957.) Photographs of powder patterns are shown and discussed. See also 3210 of 1957 (Pearson).

538.221:621.318.134 3911
Phase Equilibria in the Ferrite Region of the System Manganese-Iron-Oxygen—M. W. Shafer. (*IBM J. Res. and Dev.*, vol. 2, pp. 193–199; July, 1958.)

538.221:621.318.134 3912
Galvanomagnetic Properties of Manganese Ferrite—K. P. Belov and E. V. Talalaeva. (*Zh. Eksp. Teor. Fiz.*, vol. 33, pp. 1517–1519; December, 1957.)

538.221:621.318.134 3913
A Richter-Type Magnetic Loss in Yttrium-Iron Garnet—H. Sekizawa, S. Iida, and T. Miyadai. (*J. Phys. Soc. Japan*, vol. 13, p. 658; June, 1958.) A magnetic loss observed in ferrites containing ferrous ions is attributed to electron diffusion. A similar loss has been observed in Y-Fe garnet. The peak-loss frequency varies with temperature and peaks do not appear after heating in air to 380°C.

538.221:621.318.57 3914
Effect of a Transverse Field on Switching Rates of Magnetic Memory Cores—T. D. Rossing and S. M. Rubens. (*J. Appl. Phys.*, vol. 29, pp. 1245–1247; August, 1958.) A transverse magnetic field applied at the same time as a remagnetizing pulse facilitates the magnetization of a ferromagnetic material, and provides an improved method of writing into a magnetic-core storage system.

621.315.61:537.529 3915
Dielectric Breakdown in Solids—J. J. O'Dwyer. (*Advances in Phys.*, vol. 7, pp. 349–394; July, 1958.) Various theories of breakdown in dielectric solids are reviewed and compared with the results of experimental work. Over 40 references.

621.315.616.9 3916
New Protectants for Polyethylene—F. H. Winslow. (*Bell Lab. Rec.*, vol. 36, pp. 319–322; September, 1958.) A combination of carbon black and sulphur compounds offers the best protection against oxidation by heat and light.

621.315.616.96:537.311.31:621.372.56.029.6 3917

Casting Lossy Microwave Parts in Resin aids Design Work—A. Staniforth and K. A. Steele. (*Can. Electronics Eng.*, vol. 2, pp. 16–20; May, 1958.) Attenuation characteristics of iron-powder filler in casting resins are shown. The use of this material for lossy microwave components in transmission lines is noted.

621.318.1 3918

Materials used in Radio and Electric Engineering: Part 5—Magnetic Materials—(*J. Brit. IRE*, vol. 18, pp. 449–464; August, 1958.) A survey including tabulated information of properties and applications of different types, together with British standards and over 50 references. For earlier parts see 1419 of 1955, and 501 and 2828 of 1956.

MATHEMATICS

517.949 3919

Contribution on the Method of Difference Equations—J. Hersch. (*Z. angew. Math. Phys.*, vol. 9a, pp. 129–180; July 25, 1958. In French.) Detailed treatment of linear difference equations and certain of their applications noted earlier (975 and 1623 of 1957).

518.5:517.512.2 3920

A Calculator for Numerical Fourier Synthesis—V. Timbrell. (*J. Sci. Instr.*, vol. 35, pp. 313–318; September, 1958.) A method of Fourier synthesis using a mechanical calculator is ten times faster than customary methods using three-figure tables, and accuracy is about the same. An instrument of simple construction for handling 15 harmonics is described.

519.2:621.396.822 3921

A Systematic Approach to a Class of Problems in the Theory of Noise and Other Random Phenomena—(IRE TRANS. ON INFORMATION THEORY, vol. IT-3, pp. 32–43; March, 1957. Abstract, PROC. IRE, vol. 45, p. 1165; August, 1957.)

Part 1—D. A. Darling and A. J. F. Siegert (pp. 32–37).

Part 2—Examples—A. J. F. Siegert (pp. 38–43).

519.283:621.391 3922

Linear Least-Squares Smoothing and Prediction, with Applications—S. Darlington. (*Bell Sys. Tech. J.*, vol. 37, pp. 1221–1294; September, 1958.) Techniques, based on concepts in circuit theory, are developed explicitly for time series which are continuous and statistically stationary. Functions of time are replaced by functions of frequency representing their transforms. Mathematical complications are avoided by restricting statistical ensembles to those which have rational power spectra. General techniques are developed for specific problems including signal detection, diversity reception and network synthesis.

MEASUREMENTS AND TEST GEAR

621.3.018.41(083.74):529.786:525.35 3923

Frequency of Caesium in terms of Ephemeris Time—W. Markowitz, R. G. Hall, L. Essen, and J. V. L. Parry. (*Phys. Rev. Lett.*, vol. 1, pp. 105–107; August 1, 1958.) Description of the conversion of the frequency of Cs resonance, based on the second of U.T.2, to the frequency expressed in terms of ephemeris time, using observations of the moon. See also 3195 of 1958.

621.317.3.029.6+534.6 3924

Experiments on cm Waves in Analogy with Acoustic Techniques made in Göttingen—Meyer. (See 3671.)

621.317.33 3925

Dynamic-Conductance Meter—M. R. Barber and A. G. Bogle. (*Electronic Radio Eng.*, vol. 35, pp. 392–394; October, 1958.) The instrument gives a direct indication of the dynamic conductance of a resonant circuit at frequencies up to 1.5 mc. It makes use of the properties of a transitron-connected pentode.

621.317.34 3926

Measurement of Impedance and Attenuation of a Cable through an Arbitrary Loss-Free Junction—J. Allison and F. A. Benson. *Proc. IEE*, pt. B, vol. 105, pp. 487–495; September, 1958.) Various methods are discussed and their usefulness and accuracy compared.

621.317.342 3927

How to Measure Midfrequency Phase Shift—A. Nirenburg. (*Electronics*, vol. 31, pp. 46–47; August 29, 1958.) A comparison method for the range 5–50 mc, using double mixing and a CR oscilloscope, is described.

621.317.373.029.64 3928

Phase-Shift at Microwave Frequencies—M. H. N. Potok. (*Electronic Radio Eng.*, vol. 35, pp. 382–386; October, 1958.) "Phase-shift through waveguide arbitrary lossless networks can be measured by the application of the nodal shift method. Measurements on filters in the 4-kmc/s range agree well with calculations."

621.317.443:621.318.5 3929

A Permeameter Controller for Magnetic Measurements—M. J. Swan. (*J. Sci. Instr.*, vol. 35, pp. 344–346; September, 1958.) Description of a semi-automatic system for the cyclical switching of the main and compensating magnetization currents of the N.P.L. permeameter, using relay-operated mercury switches.

621.317.62 3930

Measurement of Magnetization Curves in High Pulsed Magnetic Fields—I. S. Jacobs and P. E. Lawrence. (*Rev. Sci. Instr.*, vol. 29, pp. 713–714; August, 1958.)

621.317.7 3931

Scientific Electrical Measuring Instruments—F. C. Widdis. (*Proc. IEE*, pt. B, vol. 105, pp. 415–424; September, 1958.) A progress review. The types of apparatus discussed include semiconductor and nuclear devices, ac bridges, electronic instruments and apparatus for measuring nonelectrical quantities; 77 references.

621.317.7 3932

Industrial Electrical Measuring Instruments—F. R. Axworthy. (*Proc. IEE*, pt. B, vol. 105, pp. 404–414; September, 1958.) A review of the progress made in design, construction and measuring techniques; 41 references.

621.317.7:721.396.82 3933

Radio Interference: Part 4—Measuring Equipment—Macpherson. (See 3964.)

621.317.725:621.385 3934

Automatic Range Selector for Electronic Voltmeter—M. Hoberman. (*Electronics*, vol. 31, pp. 84–85; August 1, 1958.)

621.317.761 3935

High-Precision Frequency Meter with Linear Response—G. Giralt. (*Compt. rend. Acad. Sci., Paris*, vol. 246, pp. 77–79; January 6, 1958.) The apparatus which includes a relaxation oscillator [see 983 of 1958 (Lagasse *et al.*)] can be used as frequency meter and discriminator. It has been applied to measure frequencies between 42.5 and 52.5 c.

OTHER APPLICATIONS OF RADIO AND ELECTRONICS

612.14:621.375.4 3936

Transistor Unit monitors Blood Pressure—O. Z. Roy and J. R. Charbonneau. (*Electronics*, vol. 31, pp. 82–83; August 15, 1958.)

621.362:621.385.2 3937

Analysis and Experimental Results of a Diode Configuration of a Novel Thermoelectron Engine—Hatsopoulos and Kaye. (See 4024.)

621.384.622.2 3938

On Traveling-Wave Electron Accelerators Incorporating their Source of High-Frequency Energy—R. Warnecke, H. Leboutet and G. Vincent. (*Compt. rend. Acad. Sci., Paris*, vol. 246, pp. 1399–1401; March 3, 1958.) Two designs of linear electron accelerator are outlined in which the delay line is common to both electron accelerator and HF generator. The latter can be a carcinatron, or a traveling-wave amplifier operating as an oscillator by virtue of the reaction across the circuit.

621.384.622.2 3939

A New Type of Linear Electron Accelerator Incorporating a High-Frequency Generator—H. Leboutet, G. Vincent, and R. Warnecke. (*Compt. rend. Acad. Sci., Paris*, vol. 246, pp. 1519–1522; March 10, 1958.) The properties of periodic delay lines and their application to the apparatus outlined in 3938 above are considered, and details of the apparatus are given.

621.385.833 3940

Asymmetric Electron Lenses—P. Durandeau, C. Fert, and P. Tardieu. (*Compt. rend. Acad. Sci., Paris*, vol. 246, pp. 79–81; January 6, 1958.) See also 3621 of 1957 (Durandeau and Fert).

621.385.833 3941

An Unconventional Electron Lens—G. D. Archard. (*Proc. Phys. Soc.*, vol. 72, pp. 135–137; July 1, 1958.) Methods of removing spherical aberration are discussed, and a new electrode arrangement proposed for this purpose is analyzed.

621.385.833 3942

The Electron-Optical Action of an Annular Aperture Lens—L. A. Harris. (PROC. IRE, vol. 46, pp. 1655–1656; September, 1958.)

621.385.833 3943

Optical Properties of a Doublet formed by Two Strongly Convergent Magnetic Lenses—A. Septier. (*Compt. rend. Acad. Sci., Paris*, vol. 246, pp. 1835–1838; March 24, 1958.)

621.385.833 3944

The Electron Microscopy of Crystal Lattices—J. W. Menter. (*Advances in Phys.*, vol. 7, pp. 299–348, July, 1958; 29 plates.) A review of the present development of the electron microscope and of direct and indirect methods of studying molecular detail and crystal lattices. Over 100 references.

621.385.833 3945

Use of a Strong-Focusing Doublet in Electron Microscopy—A. Septier. (*Compt. rend. Acad. Sci., Paris*, vol. 246, pp. 1938–1985; March 31, 1958.)

621.387.4:621.374.32 3946

Analysis of Pulse Pile-Up Effects in a Pulse-Counting System—R. H. Frazier. (*J. Franklin Inst.*, vol. 264, pp. 203–233; September, 1957.) An analysis of the rate of spurious counts due to background radiation.

621.385.833+537.533.72 3947

Electron Microscopy: Proceedings of the Stockholm Conference, September 1956 [Book Review]—F. S. Sjöstrand and J. Rhodin, ed. Publishers: Almqvist and Wiksell, Stockholm, Sweden, and Academic Press, New York, N. Y., 355 pp.; 1957. 85 Sw. kr. (*Nature, London*, vol. 181, pp. 1626–1627; June 14, 1958.)

PROPAGATION OF WAVES

621.396.11 3948
Line-of-Sight Wave Propagation in a Randomly Inhomogeneous Medium—B. M. Fannin. (IRE TRANS. ON ANTENNAS AND PROPAGATION, vol. AP-4, pp. 661–665; October, 1956. Abstract, PROC. IRE, vol. 45, p. 571; April, 1957.)

621.396.11 3949
The Use of Equivalent Secondary Sources in the Theory of Ground-Wave Propagation over an Inhomogenous Earth—Z. Godziński. (*Proc. IEE*, pt. C, vol. 105, pp. 448–464; September, 1958.) The actual field is shown to be the superposition of the fields generated by the primary source and by secondary sources distributed along the path. The analysis is discussed in detail when the paths may be regarded as plane, and when they extend into the diffraction zone. The influence of ground conductivity at transmitting and receiving sites is also discussed; 31 references.

621.396.11 3950
Ray Theory vs Normal-Mode Theory in Wave Propagation Problems—L. G. McCracken. (IRE TRANS. ON ANTENNAS AND PROPAGATION, vol. AP-5, pp. 137–140; January, 1957. Abstract, PROC. IRE, vol. 45, p. 716; May, 1957.)

621.396.11 3951
Universal Curves for the Vertical Polarization Reflection Coefficient—G. P. Ohman. (IRE TRANS. ON ANTENNAS AND PROPAGATION, vol. AP-5, pp. 140–142; January, 1957. Abstract, PROC. IRE, vol. 45, p. 716; May, 1957.)

621.396.11:551.510.535 3952
[Communications on] 28 Mc/s (10.7 m) between Spain and Argentine and Uruguay—R. Gea Sacasa. (*Rev. Telecomunicación, Madrid*, vol. 12, pp. 16–24; March, 1958.) Critical comparison of I.F.R.B. predictions with those obtained by Gea's method, on the basis of amateur reception reports.

621.396.11.029.6 3953
Theory of the Scintillation Fading of Microwaves—O. Tukizi. (IRE TRANS. ON ANTENNAS AND PROPAGATION, vol. AP-5, pp. 130–136; January, 1957. Abstract, PROC. IRE, vol. 45, p. 716; May, 1957.)

621.396.11.029.6 3954
Refraction Anomalies in Airborne Propagation—M. S. Wong. (PROC. IRE, vol. 46, pp. 1628–1638; September, 1958.) The anomalies are investigated by analog computation of ray tracings, using a differential analyzer. Results are used to explain large spatial field variations and radio ducting, and comparisons with field-strength data are made. Radar angular and range errors under certain conditions are deduced.

621.396.11.029.62 3955
Reflection of an Electromagnetic Wave by an Atmospheric Layer presenting a Variation of Refractive Index—F. du Castel, P. Misme, and J. Voge. (*Compt. rend. Acad. Sci., Paris*, vol. 246, pp. 1838–1840; March 24, 1958.) The calculations given in 3956 below may be generalized by an analysis applicable to any layer with a variation having a Fourier transform.

621.396.11.029.62 3956
Contribution of Partial Atmospheric Reflections to the Explanation of the Field Received at Great Distances—F. du Castel and P. Misme. (*Compt. rend. Acad. Sci., Paris*, vol. 246, pp. 82–84; January 6, 1958.) Attenuation at 1 mλ relative to transmission in free space has been calculated for distances of 200–600 km on the assumption that the atmosphere has randomly distributed reflecting strata.

621.396.11.029.64 3957
Diffraction by Smooth Cylindrical Mountains—H. E. J. Neugebauer and M. P. Bachynski. (PROC. IRE, vol. 46, pp. 1619–1627; September, 1958.) A new Fresnel theory is compared with the results of model experiments at K-band frequencies. Other theories are also discussed.

RECEPTION

621.376.23 3958
Automatic Bias Control for a Threshold Detector—J. Dugundji and E. Ackerlind. (IRE TRANS. ON INFORMATION THEORY, vol. IT-3, pp. 65–70; Abstract, PROC. IRE, vol. 45, pp. 1165–1166; August, 1957.)

621.376.23:621.396.822 3959
The Output Signal-to-Noise Ratio of Correlation Detectors—P. E. Green, Jr. (IRE TRANS. ON INFORMATION THEORY, vol. IT-3, pp. 10–18; March, 1957. Abstract, PROC. IRE, vol. 45, p. 1165; August, 1957.)

621.376.23:621.396.822:621.372.5 3960
Optimum Network Functions for the Sampling of Signals in Noise—Heaps and McKay. (See 3729.)

621.396.621.5–519 3961
Stable Receiving Circuits for Remote Control—S. J. Neshyba and F. E. Brooks, Jr. (*Electronics*, vol. 31, pp. 74–76; August 1, 1958.) "Analysis of single-stage superregenerative receivers employed in remote-controlled applications shows that with self-quenching circuits, optimum performance is obtained when the receiver is in a weak oscillatory state and an incoming signal causes oscillation every third quench cycle. Vacuum-tubes exhibit low sensitivity to impulse noise, wide dynamic range and high gain."

621.396.81/.82 3962
Error Probabilities for Binary Symmetric Ideal Reception through Nonselective Slow Fading and Noise—G. L. Turin. (PROC. IRE, vol. 46, pp. 1603–1619; September, 1958.) A theoretical treatment of the selection by an ideal receiver of one of two waveforms transmitted through a channel, subject to fading and contaminated by Gaussian noise. Conclusions relating to system design are applied to binary frequency-shift keyed systems.

621.396.812.3+534.26 3963
Influence of the Directivity of a Receiving Unit on the Average Intensity of a Signal Received as a result of Scattering—Zverev. (See 3670.)

621.396.82:621.317.7 3964
Radio Interference: Part 4—Measuring Equipment—A. Macpherson. (*P.O. Elect. Eng. J.*, vol. 51, pt. 2, pp. 115–119; July, 1958.) The general principles and technical requirements of an interference measuring set are discussed and brief descriptions are given of apparatus in use. Part 3: 3624 of 1958 (Dilworth).

STATIONS AND COMMUNICATION SYSTEMS

621.376.53:621.395.4 3965
Efficiency and Reciprocity in Pulse-Amplitude Modulation—(*Proc. IEE*, pt. B., vol. 105, pp. 449 470; September, 1958. Discussion, pp. 479–482.)

Part 1—Principles—K. W. Cattermole (pp. 449–462).

Part 2—Testing and Applications—J. C. Price (pp. 463–470).

A method of converting a LF signal into a modulated pulse train and back again, with low power loss, provides multiple communication on a two-wire basis without amplifiers. Theoretical and practical aspects are discussed; transmission with an over-all loss of about 2 db can be achieved.

621.376.55 3966
A Study of the Pulse-Phase-Modulation Installation—R. Kaenel, H. Pfyffer, and H. E. Weber. (*Tech. Mitt. PTT*, vol. 36, pp. 1–12; January 1, 1958.) A comparison of the PPM system with other modulation systems, and a description of a model installation for four telephony channels.

621.391 3967
On the Estimation in the Presence of Noise of the Impulse Response of a Random, Linear Filter—G. L. Turin. (IRE TRANS. ON INFORMATION THEORY, vol. IT-3, pp. 5–10; March, 1957. Abstract, PROC. IRE, vol. 45, p. 1165; August, 1957.)

621.391 3968
On the Capacity of a Noisy Continuous Channel—S. Muroga. (IRE TRANS. ON INFORMATION THEORY, vol. IT-3, pp. 44–51; March, 1957. Abstract, PROC. IRE, vol. 45, p. 1165; August, 1957.)

621.391 3969
Merit Criteria for Communication Systems—A. Hauptschein and L. S. Schwartz. (IRE TRANS. ON INFORMATION THEORY, vol. IT-3, pp. 52–55; March, 1957. Abstract, PROC. IRE, vol. 45, p. 1165; August, 1957.)

621.391:621.376.56 3970
Noise-Reducing Codes for Pulse-Code Modulation—J. E. Flood. (*Proc. IEE*, pt. C, vol. 105, pp. 391–397; September, 1958. Discussion, p. 397.) A discussion of methods of improving the signal/noise ratio of PCM systems by making the more significant digits less liable to error than the less significant ones. Systems using pulses of varying height and length are compared.

621.391:621.376.56 3971
The Rate of Transmission of Information in Pulse-Code-Modulation Systems—A. R. Billings. (*Proc. IEE*, pt. C, vol. 105, pp. 444–447; September, 1958.) A general expression is derived for the maximum rate of communication of information when the interfering noise has a Gaussian amplitude distribution. The cases of binary and tertiary coding are dealt with in detail.

621.391(083.7) 3972
IRE Standards on Information Theory: Definitions of Terms, 1958—(PROC. IRE, vol. 46, pp. 1646–1648; September, 1958.) Standard 58 IRE 11.S1.

621.395.4:621.318.5 3973
Selective Signalling and Switching for the SAGE System—H. J. Michael. (*Bell Lab. Rec.*, vol. 36, pp. 335–339; September, 1958.) An outline of the telephone circuits within the system.

621.395.4:621.318.5 3974
Automatic Line-Switching for L3 Carriers—E. C. Thompson. (*Bell Lab. Rec.*, vol. 36, pp. 340–343; September, 1958.) Techniques are outlined for by-passing faulty sections of line.

621.395.4:621.318.57 3975
Experimental Electronic Telephone Switching System—(*Bell Sys. Tech. J.*, vol. 37, pp. 1091–1220; September, 1958.) The system described in the following papers includes a stored program, a network employing gas-diode crosspoints, time-division common control and large-capacity photographic and barrier-grid valve storage systems.

a) An Experimental Switching System using New Electronic Techniques—A. E. Joel, Jr. (pp. 1091–1124).

b) Semiconductor Circuit Design Philosophy for the Central Control of an Electronic Switching System—B. J. Yokelson, W. B. Cagle, and M. D. Underwood (pp. 1125–1160).

c) Fundamental Concepts in the Design of the Flying-Spot Store—C. W. Hoover, Jr., R. E. Staehler, and R. W. Ketchledge (pp. 1161–1194).

d) A High-Speed Barrier-Grid Store—T. S. Greenwood and R. E. Staehler (pp. 1195–1220).

621.395.43:621.373.52 3976
Transistor Pulse Generators for Time-Division Multiplex—Cattermole. (See 3734.)

621.396.3:621.396.43:523.5 3977
Meteor Bursts provide Communications Path—B. M. Sifford and W. R. Vincent. (*Electronics*, vol. 31, pp. 42–45; August 29, 1958.) Details are given of the equipment used in the radio link previously described [1549 of 1958 (Vincent *et al.*)].

621.396.3:621.396.43:523.5 3978
Storage Capacity in Meteor-Burst Communication Systems—W. A. Helbig. (PROC. IRE, vol. 46, pp. 1649–1650; September, 1958.) A method differing from that of Campbell (907 of 1958) is used to derive the storage capacity.

621.396.41 3979
Multichannel U.H.F. Radio Telephone Equipment—J. Fieguth. (*Proc. IRE, Aust.*, vol. 19, pp. 43–53; February, 1958.) Recently developed FM equipment, operating in the 900-mc band, is described. It can be used for up to 36 telephone channels, and performance figures shows that CCIF standards are met.

621.396.65:621.372.8 3980
Microwave Aspects of Waveguides for Long-Distance Transmission—Karbowiak. (See 3680.)

621.396.712.2/.3 3981
The B.B.C.'s Mark II Mobile Studio and Control Room for the Sound Broadcasting Service—L. E. H. O'Neill. (*BBC Eng. Div. Monographs*, no. 20, pp. 5–23; August, 1958.)

621.396.712.3:534.84 3982
The Large Auditorium of the Hessischer Rundfunk—Schreiber. (See 3674.)

621.396.933.42 3983
Single-Sideband Aircraft Communication—G. L. Grisdale. (*Wireless World*, vol. 64, pp. 460–465; October, 1958.) SSB and SB systems are compared with reference to long-distance aeronautical communications, and the advantages of the former are described together with the technical problems involved in its introduction to civil air routes.

SUBSIDIARY APPARATUS

621–526 3984
Transistors Reduce Relay Servo Size—S. Shenfeld. (*Electronics*, vol. 31, pp. 73–75; August 15, 1958.)

621.311.6.072.2:621.314.6 3985
New Type Constant-Voltage Rectifier—Y. Imamizu, M. Take, and Y. Suzuki. (*Rep. Elect. Commun. Lab., Japan*, vol. 6, pp. 116–129; April, 1958.) A constant-voltage supply for use as a floating-battery power source is described; its output rating is 50v at 150a.

621.316.542.2:621.398 3986
A High-Speed Rotary Switch and some Applications—M. Lowenberg. (*Electronic Eng.*, vol. 30, pp. 524–527; September, 1958.) The general requirements of high-speed switches are discussed with particular reference to applications in information sampling systems. Details and applications of a rotary switch permitting rotational speeds of up to 200 rev/minute are described.

621.316.721/.722:621.314.7 3987
The Principle of Stabilization of Constant-Impedance Devices and its Application to a Transistor Power Supply—É. Cassignol. (*Compt. rend. Acad. Sci., Paris*, vol. 246, pp. 1401–1404; March 3, 1958.) The useful operating range of a shunt-type voltage regulator is expressed in terms of a utilization coefficient. General relations derived are applied to a two-transistor circuit of the type described earlier [3642 of November (Cassignol and Giralt)] particularly suitable for stabilization of valve heater supplies.

TELEVISION AND PHOTOTELEGRAPHY

621.397.5 3988
Australian Television—(*Proc. IRE, Aust.*, vol. 19, pp. 122–124; March, 1958.) Definition of the revised technical standards issued on November 4, 1957.

621.397.5:623 3989
Military Uses of Television—*J. Soc. Mot. Pict. Telev. Eng.*, vol. 67, pp. 441–479; July, 1958.) The test is given of 10 papers, most of which were read at the Convention of the Society of Motion Picture and Television Engineers held in Philadelphia, October, 1957.

a) Pickup-Tube Performance with Slow Scanning Rates.—C. T. Shelton and H. W. Stewart (pp. 441–451).

b) Development of the Thin Cathode-Ray Tube.—W. R. Aiken (pp. 452 455). See also 977 of March.

c) Development and Applications of Transparent Cathode-Ray Screens.—C. Feldman (pp. 455–460).

d) Television for Parade Control and Field Exercises.—H. Dakin, F. L. Martin, P. A. J. Bue and J. R. Smith (pp. 461–463).

e) Technical and Production Problems in Military Television Recordings.—N. Gray (pp. 463–464).

f) Army Television Research and Development.—W. A. Huber and R. B. Le Vino (pp. 465–469).

g) Television for Use under Rugged Environmental Conditions.—J. P. Day and F. R. Pike (pp. 470–472).

h) Television Viewing of Rocket Engine Tests.—J. P. Mitchell (pp. 473 474).

i) Some Aspects of the Application of Television to the Tracking of Guided Missiles.—H. L. Roberts (pp. 475–477).

j) Airborne Closed-Loop Television System.—A. F. Flacco (pp. 477–479).

621.397.6 3990
Efficiency-Diode Scanning Circuits—K. G. Beauchamp. (*Electronic Eng.*, vol. 30, pp. 490–497, 549–556; August and September, 1958.) Various types of efficiency-diode circuit are examined theoretically, and the influence of tube characteristics on the series circuit is investigated for various operating modes. Both tube and saturated-reactor methods of controlling scan linearity are described and a "differential method" of controlling scan width is outlined. A complete scanning circuit with provision for deriving the ehт supply for the CR tube is given.

621.397.6:621.314.7 3991
The Application of Transistors in Video-Frequency Techniques—H. Fix. (*Rundfunktech. Mitt.*, vol. 2, pp. 10–17; February, 1958.) Circuit and performance details of portable television camera equipment incorporating transistors are given.

621.397.6:621.396.65:621.317.799 3992
A Pulse-and-Bar Waveform Generator for Testing Television Links—I. F. Macdiarmid and B. Phillips. (*Proc. IEE*, pt. B, vol. 105, pp. 440–448; September, 1958.) Details are given of the design of a test-signal generator which, at the line-frequency repetition rate, produces a composite waveform consisting of a sine-squared pulse, a smoothed-bar pulse and a normal line-synchronizing pulse.

621.397.611:522.2 3993
Television Camera with Prolonged Storage Time for Televising Objects of Low Light Intensity particularly for Use in Television Astronomy—P. Piepereit. (*Rundfunktech. Mitt.*, vol. 2, pp. 18–19; February, 1958.) Modifications to an image-orthicon circuit for increasing its photosensitivity and avoiding flicker are described.

621.397.611.2 3994
Transmission Characteristics of the Image-Orthicon Television Camera Tube at Extremely High Photocurrents—R. Theile and F. Pilz. (*Rundfunktech. Mitt.*, vol. 2, pp. 1–9; February, 1958.) See also 603 of 1958. Good picture quality can be obtained with very high photocurrents and low storage time.

621.397.611.2 3995
The Influence of the Optical System of a Television Camera on the Frequency Response Characteristic of a Television System—D. Frenzel. (*Rundfunktech. Mitt.*, vol. 2, pp. 20–28; February, 1958.)

621.397.62:621.396.665 3996
A.G.C. for Television Receivers—R. H. Skinner. (*Wireless World*, vol. 64, pp. 486–490; October, 1958.) Two methods are described, using bias volts derived from the video signal at the grid of the synchronizing-pulse separator, and delay volts for the RF stage from the contrast control.

621.397.621.2:535.623 3997
Colour Selection with the Chromotron Tube—L. W. Allen. (*Radio-Electronics*, vol. 29, pp. 115 118; April, 1958.) The principle of operation and the circuitry of the single-gun three-color Lawrence tube are described.

621.397.7 3998
B.B.C. Television Centre—(*Wireless World*, vol. 64, pp. 484–485; October, 1958.) Description, with perspective drawings and photographs, of the layout and special features of the White City center due to be completed in 1961.

621.397.8 3999
The Relation between Picture Size, Viewing Distance and Picture Quality—L. C. Jesty. (*Proc. IEE*, pt. B, vol. 105, pp. 425–434; September, 1958. Discussion, pp. 435–439.) A description of experiments to determine the preferred viewing distance for a number of different types and sizes of picture with different bandwidths, including 405-line and 625-line monochrome and 405-line color television. The use of spot-wobble techniques are also investigated.

621.397.8 4000
Performance of U.H.F. and V.H.F. Transmitting and Receiving Equipment—W. J. Morlock and W. O. Swinyard—(*Elect. Eng., New York*, vol. 77, pp. 226–231; March, 1958.) Survey of the problems investigated by Panels 1 and 2 of TASO [see 3259 of 1958 (Town)] to assist the F.C.C. in making frequency allocations.

621.397.8:621.396.822 4001
Visibility of Noise on Television Pictures—R. Fatehchand. (*Nature, London*, vol. 181, p. 1797; June 28, 1958.) Note of an experiment demonstrating the increased visibility of

"quasi-triangular" noise (power per unit bandwidth increasing with frequency) when a sinusoidal signal is applied with it to the grid of a video amplifier.

621.397.82 4002
Nonlinear Distortion in Television Transmission Lines—J. Müller. (*Arch. elekt. Übertragung*, vol. 11, pp. 485–494; December, 1957.) Frequency-dependent nonlinear distortion in program lines and FM radio links is discussed with particular regard to the effect on the video signal and picture quality. Oscillograms obtained in measurements on a 4 kmc radio link are given.

TUBES AND THERMIONICS

621.314.63 4003
Analysis of Current Flow in a Planar Junction Diode at a High Forward Bias—A. K. Jonscher. (*J. Electronics Control*, vol. 5, pp. 1–14; July, 1958.) Using planar geometry, the general case of an asymmetric *p-n*-type diode is analyzed, the impurity concentrations and widths on both sides being arbitrary. With certain assumptions, the current/voltage relation is $I^{\frac{1}{2}}=S(V-V_0)$, where S is expressed in terms of the physical parameters of the junction and V_0 is the equilibrium potential.

621.314.63:621.317.3 4004
Crystal Rectifiers in Measurement Technique—H. Wucherer. (*Arch. tech. Messen*, no. 265, pp. 41–44; February, 1958.) Equivalent circuits and rectifier characteristics are summarized.

621.314.7 4005
A New Method of Voltage and Power Amplification at High Frequencies—S. Teszner. (*Compt. rend. Acad. Sci., Paris*, vol. 246, pp. 72–73; January 6, 1958.) A note on the construction, characteristics and theory of the tecnetron. See 3657 of 1958 (Aisberg).

621.314.7:621.397.6 4006
The Application of Transistors in Video-Frequency Techniques—Fix. (See 3991.)

621.314.7 4007
Variation with Temperature of the Cut-Off Frequency of Junction Transistors in the Common-Emitter Connection—R. Birebent and R. Morelière. (*Compt. rend. Acad. Sci., Paris*, vol. 246, pp. 909–911; February 10, 1958.) Diffusion-type *p-n-p* junction transistors subjected to temperature variations in the range −20°C to +30°C showed a regular diminution of cutoff frequency with increase of temperature.

621.314.7 4008
The Measurement of the Operating Temperature of Transistors—H. Bencking. (*Arch. elekt. Übertragung*, vol. 11, pp. 504–508; December, 1957.) The operation of the equipment described is based on the measurement of collector current with emitter and base terminals short-circuited.

621.314.7 4009
On Understanding Transistors—K. C. Johnson. (*Wireless World*, vol. 64, pp. 429–443, 497–501; September and October, 1958.) LF and HF equivalent circuits, for junction transistors, are developed by comparison with the ideal thermionic tube. Semiconductor theory is included.

621.383.2 4010
On the Random Character of Photon Absorption—E. Baumgardt. (*Compt. rend. Acad. Sci., Paris*, vol. 245, pp. 2236–2238; December 16, 1957.) The random character of the absorption of photons by a SbCs photocathode is demonstrated experimentally.

621.385.029.6 4011
International Congress on Microwave Valves—(*Le Vide*, vol. 12, pp. 229–370; July/August, 1957.) A further selection of papers presented at the Congress (See also 639 of 1958), including the following:

a) Microwave Triode B-26 for 4000-mc Operation—Y. Nakamura, T. Miwa, and Y. Hasegawa (pp. 230–246, in French and English).

b) A Magnetron Controlled by a Symmetrically Coupled TE_{011}-Mode Cavity—J. Feinstein and R. J. Collier (pp. 247–254, in French and English).

c) Magnetron: 8 mm, 40 kW, 12 W—R. Juillerat and A. Regeffe (pp. 255–260).

d) The Problem of Designing "Turbators" (Magnetrons) for Communication Equipment—H. Paul (pp. 261–268, in French and German).

e) Reflex Klystron with a Wide Mechanical Tuning Range for the Millimetre Region—E. D. Naumenko (pp. 269–272, in French and English).

f) High-Power Travelling-Wave Valves Types O and M: Amplifiers and Oscillators—P. Guenard and O. Doehler (pp. 273–277).

g) Some New Circuits for High-Power Travelling-Wave Valves—M. Chodorow and R. A. Craig (pp. 278–283, in French and English). See 3698 of 1957.

h) Development of Travelling-Wave Amplifier Valves at Federal Telecommunication Laboratories—A. G. Clavier, O. Boychenko and R. W. Wilmarth (pp. 284–293, in French and English).

i) Travelling-Wave Valves Types 4W85 and 4W86 used in the Microwave Link Tokyo-Osaka—S. Hayashi, K. Sato, D. Kobayashi, and H. Nishio (pp. 294–300, in French and English).

j) High-Gain and Medium-Power Travelling-Wave Valve Type ECL-1140—K. Sato, D. Kobayashi, S. Hamada, and Y. Uji (pp. 301–307, in French and English).

k) Very-Low-Noise Travelling-Wave Valve—E. W. Kinaman and M. Magid (pp. 308–317, in French and English).

l) Millimetre Carcinotrons—J. Laborderie, G. Vincent, and T. Yeou (pp. 318–326).

m) Contribution to the Design of Permanent Magnets with particular reference to Magnet Shapes for Travelling-Wave Valves—L. Brück (pp. 327–335, in French and German).

n) Ion Discharge Tubes in Microwave Techniques—J. Lecorguillier (pp. 336–340).

o) Oscillography and Beam Analysis at Microwave Frequencies—H. Von Foerster, E. W. Ernst, O. T. Purl, and M. Weinstein (pp. 341–351, in French and English).

p) Technology of the Millimetre Region—H. Piatti (pp. 352–355).

q) Research and Development of Microwave Valves in Japan—Y. Koike and Y. Nakamura (pp. 356–370, in French and English).

621.385.029.6 4012
Shunt Impedance of Klystron Cavities—E. L. Ginzton and E. J. Nalos. (IRE TRANS. ON MICROWAVE THEORY AND TECHNIQUES, vol. MTT-3, pp. 4–7; October, 1955. Abstract, PROC. IRE, vol. 44, p. 275; February, 1956.)

621.385.029.6 4013
A.C. Operation of Magnetrons for Coherent Operation—W. Schmidt. (*Elektronische Rundschau*, vol. 12, pp. 12–14; January, 1958.) The use of ac voltage supplies instead of dc is discussed and the relative advantages are tabulated.

621.385.029.6 4014
Focusing in High-Voltage Beam-Type Electron Devices—S. V. Yadavalli. (*J. Electronics Control*, vol. 5, no. 1, pp. 65–87; July, 1958.) The paraxial electron trajectory equation, applicable at relativistic speeds, including the effects of self-magnetic field and space-charge of the beam, is derived. The equation is applied to problems of beam spreading, e.s. and magnetic lenses, Brillouin flow, and beam stability. Results are discussed in detail and practical applications are indicated.

621.385.029.6 4015
Analysis of Travelling-Wave Tubes with Tapered Velocity Parameter—D. V. Geppert. (PROC. IRE, vol. 46, p. 1658; September, 1958.)

621.385.029.6 4016
Interaction within the Attenuator of a High-Power T.W.T.—D. E. T. F. Ashby, T. D. Cockhill, A. F. Hassell, and R. O. Jenkins. (*J. Electronics Control*, vol. 5, pp. 62–64; July, 1958.) An account is given of an unsuccessful attempt to cause interaction to take place in the attenuator of a traveling-wave valve at normal beam voltages. The method used was to vary the phase velocity in the two sections of the attenuator by varying the pitch of the helix. Conclusions are drawn.

621.385.029.6:621.3.032.53:666.1.037.5 4017
Sealed-In Connections with Improved Surfaces for Microwave Valves—W. Düsing. (*Telefunken Ztg.*, vol. 30, pp. 264–269; December, 1957. English summary, pp. 288–289.) Improved high-frequency conductivity and other advantages are obtained using disk-shaped connectors of Fe-Ni alloy which are silver-plated over a thin layer of gold and sealed with lead glass. The resulting improvement in the performance of disk-seal triodes is shown graphically.

621.385.032.21 4018
A Cathode Test Utilizing Noise Measurements—W. Dahlke and F. Dlouhy. (PROC. IRE, vol. 46, pp. 1639–1645; September, 1958.) Shot-noise effects are used as a sensitive measure of cathode quality. Test equipment and procedure are described.

621.385.032.213.13 4019
The Conductivity of Oxide Cathodes: Part 5—Functional Structure of the Cathode—G. H. Metson. (*Proc. IEE*, pt. C, vol. 105, pp. 374–380; September, 1958.) The cathode is considered as a thin-film emitter covered by a porous oxide matrix. The thin-film emitter determines the total available emission, and the self-generated electron density within the matrix determines the potential rise between emitter and electron-exit boundary. See 2274 of 1958.

621.385.032.26:537.533 4020
Large Perturbations in Electron Beams from Shielded and Immersed Guns—T. S. Chen. (*J. Electronics Control*, vol. 4, pp. 523–538; June, 1958.) "Large perturbations in cylindrical beams from magnetically shielded and immersed guns are calculated by numerical integration of the electron dynamic equations. Contours of a particular beam from both types of electron gun are given, and the calculated contours in the shielded gun are compared with the experimental results obtained by Lawson (3790 of 1955). By the use of reduced variables, universal beam contours are prepared for determination of the profiles of other beams. The limit of applicability of the small-perturbation theory used in analysis of electron beams is evaluated."

621.385.1 4021
A Perturbation Analysis of the Equations for Electrostatic Space-Charge Flow and its Application to the Production of Hollow Beams from a Toroidal Cathode—P. T. Kirstein. (*J. Electronics Control*, vol. 5, pp. 33–53; July, 1958.)

621.385.1 4022
Grid Current in Electron Tubes—E. Fairstein. (*Rev. Sci. Instr.*, vol. 29, pp. 524–526; June, 1958.) In modern low-power receiving tubes grid current is mainly due to photoelectric emission from the grid, caused by soft X rays produced at the plate. A simple formula is given for predicting this current from the operating conditions.

621.385.2:537.533 4023
Magnetic Constriction in Simple Diodes—B. Meltzer. (*Nature, London*, vol. 181, pp. 1332–1333; May 10, 1958.) A note on the restriction which must be placed on cathode size for parallel flow to be approximately realizable. The ratio of radius to anode/cathode spacing must be considerably less than 29, 5.6 and 1.1 for diodes in which the maximum kinetic energy of the electrons is respectively one tenth, equal to and ten times their rest energy. See also 3037 of 1958.

621.385.2:621.362 4024
Analysis and Experimental Results of a Diode Configuration of a Novel Thermoelectron Engine—G. N. Hatsopoulos and J. Kaye. (PROC. IRE, vol. 46, pp. 1574–1579; September, 1958.) The engine is designed to convert heat into electrical work without use of moving mechanical parts. It depends on the transfer of electrons emitted with high initial velocity from a hot cathode to an anode, against a potential barrier. An efficiency of 12 per cent has been achieved in a model made to investigate the principles of operation. See also 3592 of 1958.

621.385.3.029.63 4025
Energy Balance in Disk-Seal Oscillators at Ultra High Frequencies—M. R. Gavin and L. J. Herbst. (*Brit. J. Appl. Phys.*, vol. 9, pp. 377–380; September, 1958.) Measurements on Type CV273 disk-seal triodes in the range 500–2000 mc showed that the input dc power could be accounted for by the ac output power and dissipation at the electrodes.

621.385.4:621.397.621 4026
Improving the Deflection Amplifier—C. Droppa. (*Electronic Ind.*, vol. 17, pp. 76–79; May, 1958.) A new Type-6FH6 tube has been developed for the horizontal-deflection amplifier in television receivers. The grid wires are supported at constant tension at exactly 90° to the vertical.

621.385.832 4027
The Optimum Design of Electrostatically Deflected Cathode-Ray Tubes—H. Moss. (*J. Brit. IRE*, vol. 18, pp. 485–491; August, 1958.) For a given spot size and beam current it is shown that defocusing is a minimum and deflection sensitivity is a maximum when a) the electron gun is short so that the deflectors are mounted as far as possible from the screen, and b) the deflectors are as large and sensitive as possible.

621.385.832 4028
Electron-Beam Tubes as Information Carriers—F. Schröter. (*Telefunken Ztg.*, vol. 30, pp. 251–263; December, 1957. English summary, p. 288.) Several electron-beam devices are described including deflection amplifiers, and storage-type and writing tubes.

621.387:621.396.822.029.63 4029
Helix-Coupled Gas-Tube Noise Sources—K. W. F. Steward. (*Marconi Rev.*, vol. 21, pp. 43–55; 2nd quarter, 1958.) Design data are presented for noise sources in the frequency-range 300–1450 mc using the Type CV1881 gas discharge tube. Curves are given for the input voltage SWR and insertion loss as functions of frequency.

MISCELLANEOUS

061.3:[621.38/.39+681.142] 4030
Second Electronics Convention in Israel—(*Bull. Res. Counc. Israel*, vol. 6C, pp. 77–83; November, 1957.) Summaries of papers presented at the convention held at Rehovot, June 16–17, 1957.

061.4:621.396 4031
Farnborough, 1958—(*Wireless World*, vol. 64, pp. 491–494; October, 1958.) Review of aviation electronics at the S.B.A.C. exhibition.

061.6:621.396 4032
The Radio Research Station, Slough—(*Nature, London*, vol. 181, pp. 1642–1643; June 14, 1958.) A summary of the program of research in progress at the time of the open days, May 20–21, 1958. See also 4086 of 1957.

621.3–71 4033
Liquid Cooling of Electronic Equipment—E. N. Shaw. (*Electronic Eng.*, vol. 30, pp. 516–523; September, 1958.) Experimental results are analyzed showing the effectiveness of liquid cooling applied to miniaturized equipment. Built-in heat exchangers can remove 95 per cent of the heat developed inside a pressurized container. See also 2311 of 1957.